


For Reference

NOT TO BE TAKEN FROM THIS ROOM

Ex LIBRIS
UNIVERSITATIS
ALBERTAENSIS





Digitized by the Internet Archive
in 2023 with funding from
University of Alberta Library

<https://archive.org/details/Brown1983>

T H E U N I V E R S I T Y O F A L B E R T A

RELEASE FORM

NAME OF AUTHOR DAVID WAYNE BROWN

TITLE OF THESIS ANALYTICAL APPLICATIONS OF SPIN-ECHO
FOURIER TRANSFORM NUCLEAR MAGNETIC
RESONANCE SPECTROSCOPY

DEGREE FOR WHICH THESIS WAS PRESENTED Ph.D.

YEAR THIS DEGREE GRANTED 1983

Permission is hereby granted to THE UNIVERSITY OF ALBERTA LIBRARY to reproduce single copies of this thesis and to lend or sell such copies for private, scholarly or scientific research purposes only.

The author reserves other publication rights, and neither the thesis nor extensive extracts from it may be printed or otherwise reproduced without the author's written permission.

THE UNIVERSITY OF ALBERTA

ANALYTICAL APPLICATIONS OF SPIN-ECHO FOURIER TRANSFORM
NUCLEAR MAGNETIC RESONANCE SPECTROSCOPY

by



DAVID WAYNE BROWN

A THESIS

SUBMITTED TO THE FACULTY OF GRADUATE STUDIES AND RESEARCH
IN PARTIAL FULFILMENT OF THE REQUIREMENTS FOR THE DEGREE
OF DOCTOR OF PHILOSOPHY

IN

ANALYTICAL CHEMISTRY

DEPARTMENT OF CHEMISTRY

EDMONTON, ALBERTA

FALL, 1983

THE UNIVERSITY OF ALBERTA
FACULTY OF GRADUATE STUDIES AND RESEARCH

The undersigned certify that they have read, and
recommend to the Faculty of Graduate Studies and Research, for
acceptance, a thesis entitled ANALYTICAL APPLICATIONS OF
SPIN-ECHO FOURIER TRANSFORM NUCLEAR MAGNETIC RESONANCE
SPECTROSCOPY
submitted by DAVID WAYNE BROWN
in partial fulfilment of the requirements for the degree of
DOCTOR of PHILOSOPHY

To Barb

ABSTRACT

Several analytical applications of the spin-echo Fourier transform nuclear magnetic resonance (NMR) experiment are investigated in this work. The spin-echo pulse sequence:

$$90^\circ - \tau_2 - 180^\circ - \tau_2 - \text{Acquisition}$$

employs two pulses, 90° and 180° , and two equal delay periods, τ_2 , following which a free induction decay (FID) is collected in digital form. The FID is Fourier transformed to generate a frequency domain spectrum. The resonances in spin-echo spectra are subject to several phenomena during the τ_2 delays. Resonances for multiplets undergo phase modulation effects caused by spin-spin coupling to other nuclei. All resonances in spin-echo spectra decay due to spin-spin (T_2) relaxation during the delay periods.

The phase modulation of multiplets has been utilized to devise methods for simplifying and assigning ^{13}C NMR spectra. With these methods, resonances can be assigned to carbon types (C, CH, CH_2 or CH_3) and subspectra containing only resonances from C and CH_2 or CH and CH_3 carbons can be generated. Also, two means of measuring

one-bond ^{13}C - ^1H coupling constants are developed. All the methods are based on the intensity modulation of ^1H decoupled, ^{13}C singlets which result from broadband ^1H decoupling during acquisition.

The effects of T_2 relaxation acting on the various nuclei in a sample to different extents give rise to differential T_2 relaxation. This can be used to provide resolution enhancement in spin-echo NMR spectra. To characterize this application, the T_2 relaxation times for the protons of a number of varying molecular weight compounds are measured using the spin-echo technique. Using the demonstrated differential T_2 relaxation behavior, it is possible to eliminate the resonances for the larger molecules in spin-echo spectra. This is used to monitor the purity of protein solutions with respect to small molecules.

Methods of quantitating compounds in complex samples from the intensities of their resonances in spin-echo spectra are developed. The occurrence of differential T_2 relaxation makes simple relative intensity comparisons invalid. The application of two general methods; i) standard addition experiments, and ii) the use of proportionality constants to calculate comparable resonance intensities, is demonstrated for samples of human erythrocytes. A more specific measurement technique

is developed for measuring glutathione (GSH) levels in intact red blood cells based on the reaction of GSH with t-butylhydroperoxide catalyzed by the enzyme GSH-peroxidase. The titration of the GSH is followed by noting the intensity changes in successive spin-echo spectra.

The applications described show the versatility of the spin-echo NMR experiment for the measurement of qualitative and quantitative analytical data. In some cases, the information obtained is difficult or impossible to obtain by other means. In others, the results are obtained in a noninvasive and nondestructive manner on intact cellular systems.

ACKNOWLEDGEMENTS

My sincere thanks go to Dr. D.L. Rabenstein for his guidance, inspiration and patience throughout the course of this research.

I am also grateful to all the members of the research group, past and present, for their helpful discussions and advice and especially for their cooperation in providing blood samples for portions of this work. My thanks also go to other friends, my family and particularly my wife for their patience and support during my studies.

Thanks are also due to Miss A. Wiseman for her competent efforts in typing this thesis.

Financial support from the National Sciences and Engineering Research Council of Canada, the Alberta Heritage Foundation for Medical Research and the University of Alberta is gratefully acknowledged.

TABLE OF CONTENTS

List of Tables.....	xii
List of Figures.....	xv

CHAPTER	PAGE
I. INTRODUCTION.....	1
A. Pulsed FT NMR.....	3
B. The Spin-Echo Experiment.....	10
C. Features of the Spin-Echo Experiment.....	19
D. Overview.....	39
II. EXPERIMENTAL.....	42
A. Chemicals.....	42
B. Solution Preparation.....	43
1. Standardization of Glutathione Solutions.....	43
2. Standardization of t-Butylhydroperoxide Solutions.....	46
3. Other Solutions.....	48
C. Instrumentation.....	49
1. pH Measurements.....	49
2. Optical Measurements.....	50
3. NMR Measurements.....	50
D. Dialysis Measurements.....	53
E. Erythrocyte Pretreatment.....	54

CHAPTER	PAGE
F. DTNB Method for Glutathione Determination in Erythrocytes.....	56
G. Calculations.....	58
III. SIMPLIFICATION AND ASSIGNMENT OF ^{13}C SPECTRA AND MEASUREMENT OF ^{13}C - ^1H COUPLING CONSTANTS BY SPIN-ECHO TECHNIQUES.....	59
A. Introduction.....	59
B. Intensity Modulation of Singlets in Spin-Decoupled Spin-Echo Spectra.....	65
C. Determination of ^1H - ^1H Coupling Constants from Intensity Modulated Spin-Echo Spectra.....	72
D. Phase and Intensity Modulation in ^{13}C Spectra.....	76
E. Assignment of Carbon Types.....	87
F. Generation of Subspectra.....	98
G. Measurement of ^{13}C - ^1H Coupling Constants..	106
H. Discussion.....	112
IV. DIFFERENTIAL SPIN-SPIN RELAXATION OF ^1H NUCLEI ON COMPOUNDS OF VARYING MOLECULAR WEIGHT.....	122
A. Introduction.....	122
B. T2 Studies on a Series of Compounds of Increasing Molecular Weight.....	126
C. Monitoring of Small Molecules in Protein Solutions.....	164

CHAPTER	PAGE
V. METHODS FOR OBTAINING QUANTITATIVE INFORMATION	
FROM SPIN-ECHO NMR SPECTRA.....	181
A. Introduction.....	181
B. Spectral Digitization and Accurate In-	
tensity Data.....	184
C. NMR Intensity Data.....	186
D. The NMR Standard Addition Experiment.....	193
E. Proportionality Constants in Concentration	
Determinations by NMR.....	217
F. Discussion.....	225
VI. DETERMINATION OF GLUTATHIONE IN ERYTHROCYTES BY	
TITRATION WITH t-BUTYLHYDROPEROXIDE.....	227
A. Introduction.....	227
B. The NMR Titration Procedure.....	234
C. Hemolyzed Red Blood Cells.....	240
D. Whole Red Blood Cells.....	246
E. Reaction of GSSG with Hemoglobin.....	252
F. Discussion.....	256

BIBLIOGRAPHY	266

LIST OF TABLES

TABLE	PAGE
1. Carbon types and ^{13}C chemical shifts for cholesterol.....	61
2. Phase modulation frequencies for components of various multiplet types.....	67
3. Equations describing the intensity modulation of decoupled singlets for various multiplet types -- $I = I_0 \exp(-2\tau_2/T_2^*)\chi$	71
4. Three-bond ^1H - ^1H coupling constants for various compounds.....	75
5. Equations describing the intensity modulation of ^1H decoupled, ^{13}C singlets -- $I = I_0 \exp(-2\tau_2/T_2^*)\chi$	85
6. Representative one-bond ^{13}C - ^1H coupling constants for various carbon hybridization states.....	91
7. One-bond ^{13}C - ^1H coupling constants of cholesterol.....	108
8. T_2 relaxation times measured for the methylene protons of a series of glycine peptides.....	129
9. pK_a values measured for a series of glycine peptides.....	144

TABLE	PAGE
10. T_2 relaxation times measured for higher molecular weight compounds.....	157
11. Preparation of solutions for construction of an NMR calibration curve.....	189
12. Volume axis intercepts for the singlet of diethylsuccinate in NMR standard addition experiments.....	202
13. Volume axis intercepts for the triplet of diethylsuccinate in NMR standard addition experiments.....	203
14. Volume axis intercepts for the quartet of diethylsuccinate in NMR standard addition experiments.....	204
15. Determinations of T_1 and T_2 relaxation times for diethylsuccinate and 1,4-dioxane before and after standard addition experiments.....	207
16. Concentrations of compounds in hemolyzed erythrocytes from Donor I determined by replicate NMR standard addition experiments on the same blood sample.....	211
17. Concentrations of compounds in hemolyzed erythrocytes determined by standard addition measurements.....	213

TABLE	PAGE
18. Concentrations of compounds in hemolyzed erythrocytes from Donor I determined by NMR standard addition experiments on a blood sample after successive washes with saline D ₂ O.....	215
19. Determinations of T ₁ and T ₂ relaxation times on hemolyzed erythrocyte samples before and after standard addition experiments.....	216
20. T ₂ relaxation times for compounds in intact erythrocytes.....	219
21. Concentrations of compounds in intact erythrocytes determined using proportionality constants and intensity measurements based on peak areas.....	223
22. Concentrations of compounds in intact erythrocytes determined using proportionality constants and intensity measurements based on peak heights.....	224
23. Glutathione levels in hemolyzed erythrocytes...	243
24. Glutathione levels in intact erythrocytes.....	251

LIST OF FIGURES

FIGURE		PAGE
1.	The behavior of spin $1/2$ nuclei in a magnetic field, B_0 . (A) A single nuclear magnetic moment, μ , precessing about B_0 . (B) Conversion to the rotating frame in which μ is stationary in $x'-y'$ plane. (C) Many μ in sample; spin $+1/2$ nuclei above the $x'-y'$ plane and spin $-1/2$ nuclei below. (D) Vector summation of the individual μ giving rise to a net macroscopic magnetization, M_0	4
2.	The rotation of the magnetization from along the z' axis into the $x'-y'$ plane by the application of an RF field, B_1 , directed along the x' axis.....	6
3.	The spin-echo experiment. (A) The behavior of the magnetization during the experiment. (B) The spin-echo pulse sequence.....	11
4.	The Carr-Purcell modification of the spin-echo experiment showing the cumulative effect of missetting the 180° pulse by α	15
5.	The Carr-Purcell-Meiboom-Gill modification of the spin-echo experiment showing how misset 180° pulses are compensated on even numbered echoes.....	17

FIGURE	PAGE
6. Signals resulting from Fourier transformation of magnetization located along the positive and negative x' and y' axes at acquisition.....	20
7. Decay of the magnetization in the x' - y' plane with time as a function of the spin-spin (T_2) relaxation time. Lines A to E correspond to T_2 values of 2, 1, 0.5, 0.2 and 0.1 seconds, respectively.....	22
8. 400 MHz NMR spectra of red blood cells which had been washed with saline D_2O . (A) Single pulse spectrum. (B) Spin-echo spectrum with $\tau_2 = 0.06$ second. Reproduced with permission from reference 15.....	24
9. The energy level diagram for the case of two homonuclear spin-spin coupled nuclei before and after the application of a nonselective 180° pulse.....	26
10. The behavior of the two components of the magnetization for a homonuclear coupled doublet during the spin-echo experiment.....	28
11. The phase modulation behavior of the components of a doublet as τ_2 varies. The top portion of the figure shows the orientation of the components of the magnetization at acquisition while the bottom	

- portion shows the signal resulting upon
Fourier transformation..... 29
12. The phase modulation behavior of the
components of a triplet as τ_2 varies. The
top portion of the figure shows the
orientation of the components of the
magnetization at acquisition while the bottom
portion shows the signal resulting upon
Fourier transformation..... 30
13. The phase modulation behavior of the
components of a quartet as τ_2 varies. The
top portion of the figure shows the
orientation of the components of the
magnetization at acquisition while the bottom
portion shows the signal resulting upon
Fourier transformation..... 31
14. The energy level diagram for the case of two
heteronuclear spin-spin coupled nuclei before
and after the application of a 180° pulse to
the X nuclear species. The bottom portion of
the figure is a representation of the
magnetization of the X nuclear species in the
 $x'-y'$ plane before and after the 180°
pulse. The component of the magnetization
which was precessing slower before the pulse

is still precessing slower after the pulse and that precessing faster before the pulse is still precessing faster after the pulse.....	34
15. The ^{13}C spin-echo pulse sequence with (A) the gated decoupling technique and (B) the spin- flip decoupler sequence.....	36
16. The behavior of the magnetization for a ^{13}C doublet due to coupling to a methine proton during the ^{13}C spin-echo experiment using (A) the gated decoupling sequence and (B) the spin-flip method.....	37
17. The high field portion of the (A) broadband ^1H decoupled, (B) single frequency off- resonance decoupled and (C) fully coupled 100.6 MHz ^{13}C spectra of cholesterol.....	60
18. The observation and decoupling pulse sequences for the generation of intensity modulated, decoupled singlets in ^1H spectra. The 90° and 180° pulses of the observation channel are broadband while the decoupler irradiation is applied over a narrow frequency range centered at the resonance frequency of the ^1H nuclei coupled to the nuclei under observation.....	68

19. The intensity modulation behavior of the decoupled, ^1H singlet resulting from coupling to a methine proton at various τ_2 delay times. The top portion of the figure shows the orientation of the two components of the magnetization at acquisition while the bottom portion shows the decoupled singlet which results upon Fourier transformation..... 69
20. Fits of intensity versus τ_2 data sets for the intensity modulated, decoupled singlets resulting from the CH_3 (triplet) and CH_2 (quartet) protons of ethanol. The solid lines are the non-linear least-squares results derived by using the equations in Table 3 to fit the experimental data..... 74
21. The ^{13}C spin-echo pulse sequence (top) with various ^1H decoupler schemes, A to H..... 77
22. Vector representations of the magnetization from a methine carbon during the spin-echo pulse sequence with (A) broadband decoupling during both evolution periods, (B) no decoupling, (C) broadband decoupling during the first evolution period and (D) a 180° ^1H pulse applied simultaneously with the 180° ^{13}C pulse. The magnetization is in the $x'-y'$

- plane of a coordinate system rotating at a frequency midway between the two precessional frequencies of a coupled methine carbon..... 79
23. Vector representations of the magnetization from quaternary, methine, methylene and methyl carbons following the ^{13}C spin-echo pulse sequence in Figure 21 with decoupler scheme E or F. The diagrams show the magnetization of the start of acquisition as a function of the length of the delay time..... 82
24. Calculated intensities, neglecting T_2^* relaxation, of quaternary, methine, methylene and methyl carbon resonances in spin-echo spectra measured with decoupler scheme E in Figure 21 as a function of the length of the delay time..... 86
25. The high field portion of the ^{13}C spin-echo spectra of cholesterol measured with decoupler scheme E in Figure 21. (A) was measured with $\tau_2 = 0.008$ second, (B) is the difference spectrum obtained by subtracting the FID collected with $\tau_2 = 0.0032$ second from that collected with $\tau_2 = 0.0048$ second and (C) was measured with $\tau_2 = 0.004$ second.... 92

26. The intensity of ^1H decoupled, ^{13}C singlets resulting from a spin-echo experiment with $\tau_2 = 0.008$ second and decoupler scheme E of Figure 21 as a function of $^1J_{^{13}\text{C}-^1\text{H}}$ for the various carbon types..... 95
27. The intensity of ^1H decoupled, ^{13}C singlets for quaternary (C) and methylene (CH_2) carbons measured by a spin-echo experiment with $\tau_2 = 0.004$ second and decoupler scheme E of Figure 21 as a function of $^1J_{^{13}\text{C}-^1\text{H}}$ 96
28. The intensity of ^1H decoupled, ^{13}C singlets for methine (CH) and methyl (CH_3) carbons measured by a spin-echo difference experiment, conducted by subtracting the FID measured at $\tau_2 = 0.0032$ second from the FID measured at $\tau_2 = 0.0048$ second using decoupler scheme E of Figure 21, as a function of $^1J_{^{13}\text{C}-^1\text{H}}$ 97
29. Subspectra containing (A) resonances from methine and methyl carbons and (B) quaternary and methylene carbons. (B) was obtained by addition of two spin-echo FIDs measured with $\tau_2 = 0.008$ second and decoupler schemes A and E of Figure 21. (A) was obtained by subtracting the FID measured with decoupler scheme A from that measured with scheme E..... 100

30. The high field portion of (A) the fully coupled subspectrum for the methine and methyl carbons, (B) the fully coupled subspectrum for the quaternary and methylene carbons and (C) the fully coupled spectrum of cholesterol..... 102
31. The intensities of resonances in subspectra measured by addition of two spin-echo FIDs with $\tau_2 = 0.008$ second and decoupler schemes A and E of Figure 21 as a function of $^1J_{13C-1H}$ for the various carbon types..... 104
32. The intensities of resonances in subspectra generated by the subtraction of an FID obtained with $\tau_2 = 0.008$ second and decoupler scheme A of Figure 21 from an FID obtained with $\tau_2 = 0.008$ second and decoupler scheme E as a function of $^1J_{13C-1H}$ for the various carbon types..... 105
33. The singlets obtained with decoupling scheme E in Figure 21 for the methine carbon at 56.38 ppm (top), the methylene carbon at 37.40 ppm (middle) and the methyl carbon at 18.78 ppm (bottom) as a function of the length of the delay interval. The smooth curves are predicted with the parameters

FIGURE	PAGE
obtained from the non-linear least-squares fits of the data to the equations in Table 5...	110
34. The relationship between τ_C and $f(\tau_C)^{-1}$ (see text) for protons at a resonance frequency of 360 MHz. At $\omega_0\tau_C = 1$, $\tau_C = 2.78 \times 10^{-9}$ second.....	125
35. A series of spin-echo spectra at various τ_2 delay times for diglycine from which T_2 relaxation times can be evaluated.....	130
36. A plot of intensity versus τ_2 delay time, normalized to one at a τ_2 delay of zero, for the methylene protons of glycine. The solid curve was calculated using the T_2 value in Table 8.....	131
37. Plots of intensity versus τ_2 delay time, normalized to one at a τ_2 delay of zero, for the methylene protons of diglycine. The solid curves were calculated using the T_2 values in Table 8. (A)ⓐ is for the methylene protons nearest the terminal amino end of the molecule. (B)ⓑ is for the methylene protons nearest the terminal carboxylate end.....	132
38. Plots of intensity versus τ_2 delay time, normalized to one at a τ_2 delay of zero, for the methylene protons of triglycine. The	

solid curves were calculated using the T_2 values in Table 8. (A)◻, (B)⊙ and (C)▲ represent the two equivalent methylene protons of each glycine residue from the N-terminal to the C-terminal end of the molecule. The resonances giving rise to (A) and (C) were coincident in the NMR spectra..... 133

39. Plots of intensity versus τ_2 delay time, normalized to one at a τ_2 delay of zero, for the methylene protons of tetraglycine. The solid curves were calculated using the T_2 values in Table 8. (A)◻, (B)⊙, (C)▲ and (D)+ represent the two equivalent methylene protons of each glycine residue from the N-terminal to the C-terminal end of the molecule..... 134

40. Plots of intensity versus τ_2 delay time, normalized to one at a τ_2 delay of zero, for the methylene protons of pentaglycine. The solid curves were calculated using the T_2 values in Table 8. (A)◻, (B)⊙, (C)▲, (D)+ and (E)Y represent the two equivalent methylene protons of each glycine residue from the N-terminal to the C-terminal end of the molecule..... 135

41. Plots of intensity versus τ_2 delay time, normalized to one at a τ_2 delay of zero, for the methylene protons of hexaglycine. The solid curves were calculated using the T_2 values in Table 8. (A)◻, (B)⊙, (C)▲, (D)+, (E)Y and (F)X represent the two equivalent methylene protons of each glycine residue from the N-terminal to the C-terminal end of the molecule..... 136
42. Plots of chemical shift versus pH* for the methylene protons of diglycine. (A) is for the methylene protons nearest the terminal amino end of the molecule. (B) is for the methylene protons nearest the terminal carboxylate end..... 138
43. Plots of chemical shift versus pH* for the methylene protons of triglycine. (A) to (C) represent the two equivalent methylene protons of each glycine residue from the N-terminal to the C-terminal end of the molecule..... 139
44. Plots of chemical shift versus pH* for the methylene protons of tetraglycine. (A) to (D) represent the two equivalent methylene protons of each glycine residue from the N-

	terminal to the C-terminal end of the molecule.....	140
45.	Plots of chemical shift versus pH* for the methylene protons of pentaglycine. (A) to (E) represent the two equivalent methylene protons of each glycine residue from the N-terminal to the C-terminal end of the molecule.....	141
46.	Plots of chemical shift versus pH* for the methylene protons of hexaglycine. (A) to (F) represent the two equivalent methylene protons of each glycine residue from the N-terminal to the C-terminal end of the molecule.....	142
47.	360 MHz single-pulse NMR spectrum of a 2 mM solution of lysozyme. The sharp resonance at 1.91 ppm is due to acetate present as an impurity while the resonance at 1.24 ppm is due to t-butanol added as a chemical shift reference.....	150
48.	A plot of intensity versus τ_2 delay time, normalized to one at a τ_2 delay of zero, for the imidazole proton on carbon 2 of the histidine residue in position 6 of angiotensin II. The solid curve was calculated using the T_2 value in Table 10.....	151

49. Plots of intensity versus τ_2 delay time, normalized to one at a τ_2 delay of zero, for the imidazole protons on carbon 2 of the histidine residues in positions 6 and 9 of angiotensin I. The solid curves were calculated using the T_2 values in Table 10. Curve 1 is for the histidine in position 6 and curve 2 for that in position 9..... 152
50. Plots of intensity versus τ_2 delay time, normalized to one at a τ_2 delay of zero, for several chemical shifts in the spectrum of trypsin inhibitor. The solid curves were calculated using the T_2 values in Table 10. Curves 1□, 2○, 3▲ and 4+ are for 7.88, 7.58, 3.81 and 1.64 ppm, respectively..... 153
51. Plots of intensity versus τ_2 delay time, normalized to one at a τ_2 delay of zero, for several chemical shifts in the spectrum of lysozyme. The solid curves were calculated using the T_2 values in Table 10. Curves 1□, 2○, 3▲, 4+ and 5Y are for 7.21, 6.98, 4.28, 3.12 and 1.04 ppm, respectively..... 154
52. Plots of intensity versus τ_2 delay time, normalized to one at a τ_2 delay of zero, for several chemical shifts in the spectrum of

- bovine serum albumin. The solid curves were calculated using the T_2 values in Table 10. Curves 1 \square , 2 \circ , 3 Δ and 4+ are for 6.79, 4.03, 1.69 and 0.93 ppm, respectively..... 155
53. Plots of intensity versus τ_2 delay time, normalized to one at a τ_2 delay of zero, for several chemical shifts in the spectrum of hemoglobin. The solid curves were calculated using the T_2 values in Table 10. Curves 1 \square , 2 \circ and 3 Δ are for the non-histidine region at 4.10, 1.16 and 0.76 ppm, respectively. Curves 4+, 5Y and 6X are for the histidine region at 8.01, 7.78 and 6.90 ppm, respectively..... 156
54. A plot of the average T_2 relaxation times for each of the compounds discussed in Figures 36 to 41 and Figures 48 to 53 versus their molecular weights. The straight line results from a linear least-squares fit to the points, excluding glycine (upper left), and has a correlation coefficient of -0.9853..... 160
55. The calculated intensity versus τ_2 behavior during the spin-echo experiment for several compounds using the average T_2 values for each compound plotted in Figure 54. Curves 1

- to 6 correspond to glycine, tetraglycine, angiotensin II, trypsin inhibitor, lysozyme and hemoglobin, respectively..... 161
56. The single-pulse spectrum (A) and spin-echo spectra measured at various τ_2 delay times (B to D) for a 2 mM solution of both tetraglycine and lysozyme..... 163
57. Single-pulse spectra of a solution of 0.003 M bovine serum albumin (A) before dialysis and (B) after 5 dialyses against saline D₂O..... 166
58. Spin-echo spectra ($\tau_2 = 0.06$ second) of a solution of 0.003 M bovine serum albumin after successive dialyses against saline D₂O..... 167
59. Spin-echo spectra ($\tau_2 = 0.06$ second) of successive dialysis media against which a 0.003 M solution of bovine serum albumin was dialyzed.. 168
60. Single-pulse spectra ($\tau_2 = 0.06$ second) of a solution of hemolyzed red blood cells (A) before dialysis and (B) after 5 dialyses against saline D₂O..... 172
61. Spin-echo spectra ($\tau_2 = 0.06$ second) of a solution of hemolyzed red blood cells after successive dialyses against saline D₂O..... 173
62. Spin-echo spectra ($\tau_2 = 0.06$ second) of successive dialysis media against which a

FIGURE	PAGE
<p>solution of hemolyzed red blood cells was dialyzed.....</p>	175
<p>63. A portion of the spin-echo spectra ($\tau_2 = 0.06$ second) of hemolyzed red blood cells (A) after 5 dialyses against saline D₂O and (B) the same sample after the addition of glycine to raise the concentration by 0.1 mM. The glycine resonance is located at 3.54 ppm.....</p>	176
<p>64. Spin-echo spectra ($\tau_2 = 0.06$ second) of intact erythrocytes after successive washings with twice the volume of saline D₂O.....</p>	178
<p>65. Single-pulse FT NMR spectra collected for a single resonance with a $W_{1/2}$ of 5 Hz using a spectral window of 4000 Hz at various length FIDs ranging from 1K to 32K of data points. Note the improvement in the definition of the peak shape in the longer FIDs.....</p>	187
<p>66. A single-pulse spectrum of a D₂O solution containing 4 mM GSH and 2 mM dimethylamine (DMA). The DMA resonance is located at 2.66 ppm. The other resonances, g1 to g4 and g6, belong to GSH. The g5 resonance of GSH is further downfield near the HDO peak.....</p>	190
<p>67. Plots of peak heights and peak areas for the g1 resonance of GSH, normalized to the DMA</p>	

resonance present as an internal standard, as a function of the GSH concentration. The solid lines represent linear least-squares fits of the experimental data..... 192

68. Calculated standard addition plots for an experiment where compound is added to raise the concentration by 25% of the initial value with each increment until the initial concentration is tripled. Line A is the linear least-squares fit of the calculated points for the case of no change in the T_2 relaxation time over the course of the standard addition experiment. Lines B and C are linear least-squares fits of the points for a 20% linear decrease in T_2 and a 20% linear increase in T_2 , respectively, from the beginning to the end of the experiment..... 196

69. A single-pulse NMR spectrum of diethylsuccinate and 1,4-dioxane in $CDCl_3$. The resonance at 3.75 ppm is due to 1,4-dioxane and that at 1.59 ppm to traces of water in the solution. The other resonances are due to diethylsuccinate and are identified in the text..... 200

70. Plots of the results of a typical standard addition experiment conducted on a CDCl_3 solution of diethylsuccinate, the resonances for which are normalized to 1,4-dioxane. Lines A to C correspond to the triplet, quartet and singlet resonances of diethylsuccinate, respectively. The calculated X-Intercept is $-50 \mu\text{L}$ 201
71. A spin-echo NMR spectrum obtained with a τ_2 delay of 0.06 second on a sample of hemolyzed erythrocytes. Several resonances used to determine the concentrations of some of the compounds in the sample by a standard addition procedure are labelled in the spectrum..... 209
72. 360 MHz single-pulse spectrum of GSH (top) and GSSG (bottom)..... 233
73. 360 MHz spin-echo NMR spectrum ($\tau_2 = 0.04$ second) of hemolyzed red blood cells which had been washed with saline D_2O . Several compounds are identified in the spectrum. The resonances indicated at 2.88 and 2.91 ppm are due only to GSH..... 236
74. A series of spin-echo spectra ($\tau_2 = 0.04$ second) obtained as increments of a t-BHP

- solution were added to a sample of hemolyzed erythrocytes to titrate the GSH. The GSH resonances at 2.88 and 2.91 ppm are observed to decrease with the addition of t-BHP..... 238
75. The titration curve for the NMR titration shown in Figure 74. The sum of the intensities of the GSH resonances at 2.88 and 2.91 ppm, normalized against the ergothioneine resonance at 3.25 ppm, is plotted as a function of t-BHP added. Also shown are the normalized glycine and creatine resonances at 3.54 and 3.01 ppm, respectively..... 241
76. The titration curve for a sample of unwashed HRBC. The sum of the intensities of the GSH resonances at 2.88 and 2.91 ppm, normalized against the ergothioneine resonance at 3.25 ppm, is plotted as a function of t-BHP added. Initially, a short plateau was observed followed by a linearly decreasing titration curve..... 247
77. A series of spin-echo spectra ($\tau_2 = 0.04$ second) obtained as increments of t-BHP solution were added to a sample of intact erythrocytes..... 248

78. The titration curve for the NMR titration shown in Figure 77. The sum of the intensities of the GSH resonances at 2.88 and 2.91 ppm, normalized against the ergothioneine resonance at 3.25 ppm, is plotted as a function of t-BHP added. Initially, a plateau was observed followed by a linearly decreasing titration curve. Also shown are the normalized glycine and creatine resonances at 3.54 and 3.01 ppm, respectively..... 250
79. 360 MHz spin-echo NMR spectra ($\tau_2 = 0.04$ second) of a sample of hemolyzed erythrocytes which had been dialyzed to remove small molecules following the titration of the GSH with t-BHP. (A) is a portion of the spectrum showing a residual glycine resonance at 3.54 ppm. (B) is the same sample after the addition of DTE to release GSH (3.76 ppm) bound to hemoglobin as a disulfide..... 255

CHAPTER I

INTRODUCTION

Pulsed Fourier transform (FT) methods for measuring high resolution nuclear magnetic resonance (NMR) spectra have largely displaced conventional continuous wave methods. In the simplest FT NMR experiment, a single pulse of radio frequency (RF) radiation is applied to the sample for a short time in order to excite sample nuclei. Following the pulse, the excited nuclei induce an electromotive force (EMF) in the receiver coil, the amplitude of which decays with time as the nuclei relax back to equilibrium. The EMF is measured as a function of time giving the so-called free induction decay (FID) which, when Fourier transformed, yields an intensity versus frequency spectrum. Signal averaging is possible by precisely controlling the timing of the RF pulse and signal acquisition such that transients following successive pulses add coherently to increase the signal to noise (S/N) ratio as the square root of the number of scans. The use of FT NMR with signal averaging has greatly increased the range of practical applications of NMR. Typical examples include the routine measurement of

spectra for ^{13}C and other isotopically dilute nuclei at the natural abundance level and the measurement of high resolution spectra for individual compounds in samples as complex as whole red blood cells.

State-of-the-art spectrometers are not only capable of performing the single-pulse FT NMR experiment, but also have the capability for doing multiple-pulse experiments involving a series of carefully timed RF pulses prior to the acquisition of the FID. One such multiple-pulse experiment is the so-called spin-echo experiment [1]. Having been described in 1950 by Hahn, only four years after the first reports of the NMR phenomenon itself [2,3], it is among the oldest and simplest of the various multiple-pulse sequences which have been devised. Originally developed for measuring spin-spin relaxation times, it is now finding many other applications as a result of the development of minicomputers and the fast FT algorithm [4]. This thesis is concerned with analytical applications of the spin-echo pulse sequence, including the simplification and assignment of carbon-13 spectra and the analysis of complex solutions and intact biological systems.

A. Pulsed FT NMR

The classical picture of NMR considers the nucleus as a spinning, charged particle which generates a magnetic moment, μ . When placed in a static magnetic field, B_0 , which is oriented along the z axis, μ precesses about the direction of the field with an angular frequency:

$$\omega_0 = -\gamma B_0 \quad (1)$$

as shown in Figure 1A. γ is the magnetogyric ratio for the particular nuclear species involved. The angular frequency, ω_0 , denoted the Larmor frequency, corresponds to the resonance frequency of the nucleus. For a spin $1/2$ nucleus, there are two possible orientations of the magnetic moment in the magnetic field corresponding to the $+1/2$ and $-1/2$ spin states. For a spin $+1/2$ nucleus, the magnetic moment has a component along the direction of B_0 (Figure 1A) while for a spin $-1/2$ nucleus, it has a component opposing B_0 . When discussing pulsed FT NMR, it is easier to deal with magnetic moments in a rotating frame of reference, as illustrated in Figure 1B, where the x' - y' plane rotates about the z' axis at the Larmor frequency. In this coordinate system, μ is no longer rotating but remains stationary. When considering a

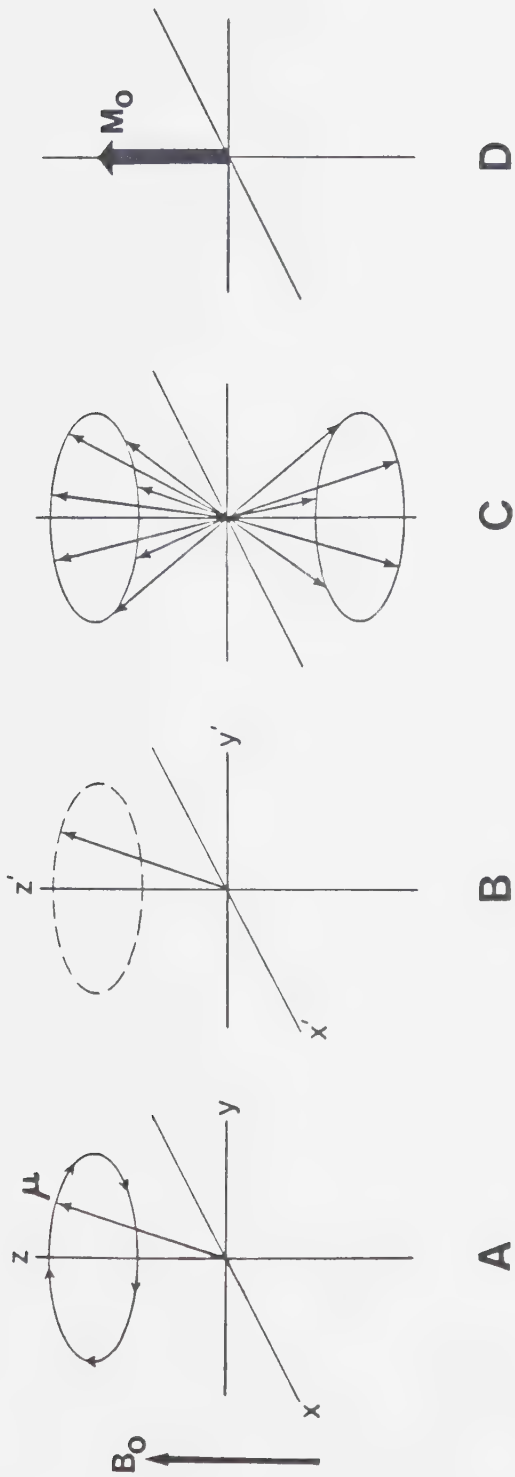


Figure 1. The behavior of spin 1/2 nuclei in a magnetic field, B_0 . (A) A single nuclear magnetic moment, μ , precessing about B_0 . (B) Conversion to the rotating frame in which μ is stationary in the x' - y' plane. (C) Many μ in sample; spin +1/2 nuclei above the x' - y' plane and spin -1/2 nuclei below. (D) Vector summation of the individual μ giving rise to a net macroscopic magnetization, M_0 .

sample, there are many precessing nuclei, some with a component aligned with B_0 and others with a component opposed to it as shown in Figure 1C. There is an energy difference between the two spin states leading to slightly more magnetic moments being aligned with the magnetic field (lower energy) than opposed to it (higher energy). In each of these two orientations, the individual nuclear magnetic moments are randomly distributed about B_0 . There will be a net magnetization resulting from the summation of all the individual magnetic moments, because there are more aligned with the magnetic field than opposed to it, directed along the positive z' axis. This net magnetization, M_0 , is shown in Figure 1D.

In order to detect any signal from the sample, the equilibrium magnetization, M_0 , must be tipped off the z' axis to give a component in the $x'-y'$ plane. Once there is a component of M_0 in the $x'-y'$ plane, $M_{x'y'}$, this component rotates coherently about B_0 at the Larmor frequency and induces an EMF in the receiver coil surrounding the sample [5]. The equilibrium magnetization, M_0 , is tipped off the z' axis by the application of an RF pulse, B_1 , conventionally applied along the x' axis. The magnetic portion of the RF pulse causes M_0 to rotate about the x' axis as illustrated in Figure 2. The strength of B_1 and its duration, t_p , will determine the angle, θ , through which M_0 is rotated.

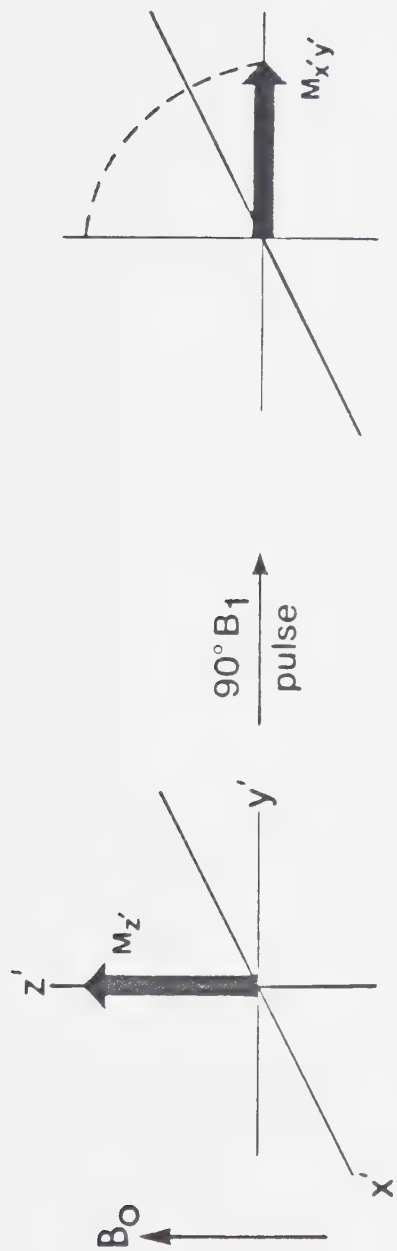


Figure 2. The rotation of the magnetization from along the z' axis into the $x'-y'$ plane by the application of an RF field, B_1 , directed along the x' axis.

$$\theta = \gamma B_1 t_p \quad (2)$$

Figure 2 illustrates the situation for $\theta = 90^\circ$, referred to as a $90^\circ B_1$ pulse. θ can be increased or decreased by increasing or decreasing t_p , for example a 180° pulse can be obtained by doubling t_p . Once the RF field is turned off, M_x, y , is detected by the EMF it induces in the receiver coil.

The induced EMF will be seen to decay with time as a result of relaxation of the nuclear spin system back to equilibrium. The two principle types of relaxation which occur are known as spin-lattice relaxation and spin-spin relaxation. These are both exponential processes characterized by time constants T_1 and T_2 , respectively. In spin-lattice relaxation, energy exchanges between the nuclear spin system and its surrounding molecular framework, the lattice, resulting in the exponential recovery of M_z , towards its equilibrium value, M_0 . The recovery of M_z , is described by the rate equation:

$$\frac{dM_z}{dt} = \frac{(M_0 - M_z)}{T_1} \quad (3)$$

where M_z , is the magnitude of the magnetization at time t . For a $90^\circ B_1$ pulse, the return of M_z , to M_0 is described by [6]:

$$M_{z'} = M_0(1 - e^{-t/T_1}) \quad (4)$$

T_1 relaxation times can be measured in pulsed FT NMR by following the rate of recovery of $M_{z'}$ to its equilibrium value. This can be done with the inversion-recovery experiment [7] in which the equilibrium magnetization is first inverted by a 180° RF pulse and then allowed to undergo spin-lattice relaxation for a period of time, τ_1 , after which $M_{z'}$ is sampled by a 90° pulse.

$$180^\circ - \tau_1 - 90^\circ - \text{Acquisition} \quad (\text{Sequence I})$$

The rate of spin-lattice relaxation determines the rate at which the experiment can be repeated to increase the S/N ratio. In order to avoid saturation effects arising from incomplete spin-lattice relaxation, a wait of about five T_1 values is necessary before pulsing the system again to allow $M_{z'}$ to return to equilibrium [7].

Whereas spin-lattice relaxation is an enthalpic process, spin-spin relaxation is an entropic process involving the dephasing of the magnetization in the $x'-y'$ plane. It is described by the rate equation:

$$\frac{-dM_{x'y'}}{dt} = \frac{M_{x'y'}}{T_2} \quad (5)$$

For a 90° pulse, the decay of $M_{x'y'}$ is given by [6]:

$$M_{x'y'} = M_0 e^{-t/T_2} \quad (6)$$

In pulsed FT NMR, spin-spin relaxation determines the rate of decay of the FID. It results in the exponential decay of the EMF collected by the receiver coil since the signal collected is proportional to $M_{x'y'}$. Ideally, T_2 values could be measured by following the decrease in amplitude of the detected signal as a function of time. In actual practice, this is not usually possible because of magnetic field inhomogeneities. As a result of magnetic field inhomogeneities, some nuclei experience slightly larger magnetic fields and others slightly smaller fields which results in some nuclei precessing more rapidly than the average and others more slowly. This leads to a dephasing of the magnetization in the $x'-y'$ plane and thus a decay in the detected signal which is generally more rapid than that caused by spin-spin relaxation alone. The spin-echo experiment was devised to overcome the effects of magnetic field inhomogeneities on spin-spin relaxation time measurements [1].

B. The Spin-Echo Experiment

The spin-echo pulse sequence consists of an initial 90° pulse, a delay period of length τ_2 , a 180° pulse and a second delay period of length τ_2 .

$90^\circ - \tau_2 - 180^\circ - \tau_2 - \text{Acquisition}$

(Sequence II)

The behavior of the magnetization during the sequence is illustrated in Figure 3A. Initially, the net magnetization is located along the positive z' axis. The 90° RF pulse, applied along the positive x' axis, rotates the net magnetization onto the positive y' axis. During the first delay period, τ_2 , $M_{y'}$ decreases in magnitude due to spin-spin relaxation and the fanning out of the individual magnetic moments about the y' axis due to magnetic field inhomogeneities. The application of the 180° pulse at time τ_2 rotates the magnetic moments about the x' axis such that $M_{x'y'}$ is now directed along the negative y' axis. Those nuclei which were precessing faster than the average due to magnetic field inhomogeneities now find themselves behind the average and those precessing slower find themselves ahead. Over the course of the second τ_2 delay period, the effects of magnetic field inhomogeneities on the dispersion of the individual magnetic moments in the $x'-y'$ plane are

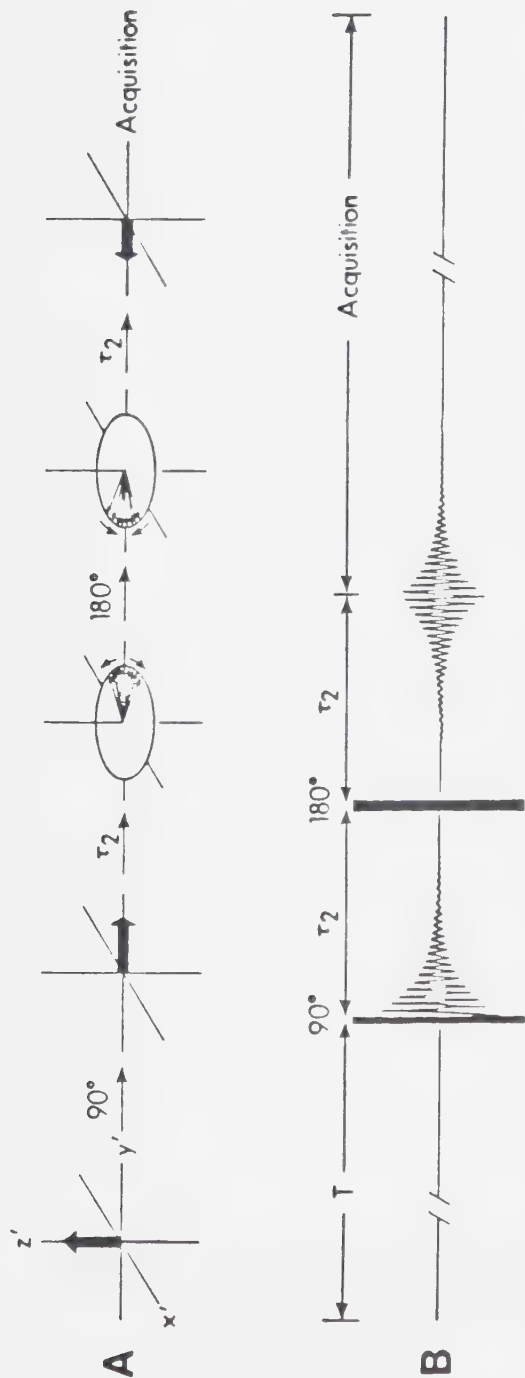


Figure 3. The spin-echo experiment. (A) The behavior of the magnetization during the experiment. (B) The spin-echo pulse sequence.

reversed, while spin-spin relaxation effects are not. This results in most of the magnetization in the $x'-y'$ plane being directed along the negative y' axis at time $2\tau_2$.

The refocussing of the nuclear magnetization at time $2\tau_2$ by the reversal of magnetic field inhomogeneity effects gives rise to the spontaneous evolution of an echo in the time domain as shown in Figure 3B. Spin-spin relaxation effects, not refocussed by the 180° pulse, are generally much smaller than those caused by magnetic field inhomogeneities. Therefore, the decay of the FID following the initial 90° pulse is due chiefly to magnetic field inhomogeneity effects. The reversal of these effects during the second τ_2 delay period leads to the growth of the echo which reaches its maximum at time $2\tau_2$ following the initial 90° pulse. The amplitude of the signal at this point is reduced due to spin-spin relaxation and can be described by:

$$M_{2\tau_2} = M_0 e^{-(2\tau_2/T_2)} \quad (7)$$

By measuring the echo amplitude at several different τ_2 delay times, a plot of the natural logarithm of the amplitude versus $2\tau_2$ can be constructed. This will yield a straight line, the slope of which is the negative reciprocal of the T_2 relaxation time.

This method yields reliable spin-spin relaxation times only when diffusion is negligible on the time scale of the pulse sequence. Diffusion effects will manifest themselves in the incomplete refocussing of the magnetization at time $2\tau_2$ and thus a reduced signal [8]. If molecules diffuse from one region to another region where B_0 is different, the magnetic field experienced by sample nuclei before the 180° pulse will be different from that experienced after it. This leads to an incomplete refocussing of the nuclear magnetic moments at time $2\tau_2$. For the case where diffusion effects are significant, the magnetization in the $x'-y'$ plane is given by:

$$M_{2\tau_2} = M_0 \exp[-(2\tau_2/T_2) - (\frac{2}{3}\gamma^2 G^2 D \tau_2^3)] \quad (8)$$

where G and D are the magnitude of the magnetic field gradient and the diffusion coefficient, respectively [9]. In instances where diffusion effects are negligible and can be safely ignored, Equation 8 reduces to that shown in Equation 7.

The initial development of the spin-echo sequence was to enable the measurement of T_2 relaxation times and self-diffusion coefficients by following the decrease in amplitude of the spin-echo as the delay periods, τ_2 , were increased [1]. As the delay periods become longer, the

decrease in amplitude of the spin-echo due to diffusion becomes more important. In order to correct for any errors introduced into T_2 determinations by such diffusion effects, Carr and Purcell [10] modified the simple spin-echo experiment by using a series of 180° pulses spaced at intervals of $2\tau_2'$.

$$90^\circ - (\tau_2' - 180^\circ - \tau_2')_n - \text{Acquisition} \quad (\text{Sequence III})$$

With this pulse sequence, τ_2 can be kept short enough that diffusion is negligible between 180° refocussing pulses. The amplitude of the spin-echo at time $2\tau_2'$ is free of distortion due to diffusion effects. However, there is a problem in that missetting of the 180° pulse has a cumulative effect as illustrated in Figure 4. In Figure 4, the 180° pulse is misset by α such that the magnetization, initially in the $x'-y'$ plane (Figure 4A), will be below the $x'-y'$ plane after one 180° pulse (Figure 4B). A second 180° pulse, misset by the same amount, will move the magnetization further out of the $x'-y'$ plane (Figure 4C). The measured component of the magnetization in the $x'-y'$ plane will thus decrease with each successive 180° pulse causing errors in T_2 determinations. Meiboom and Gill [11] modified the Carr-Purcell method to eliminate these errors caused by inaccurate 180° pulses.

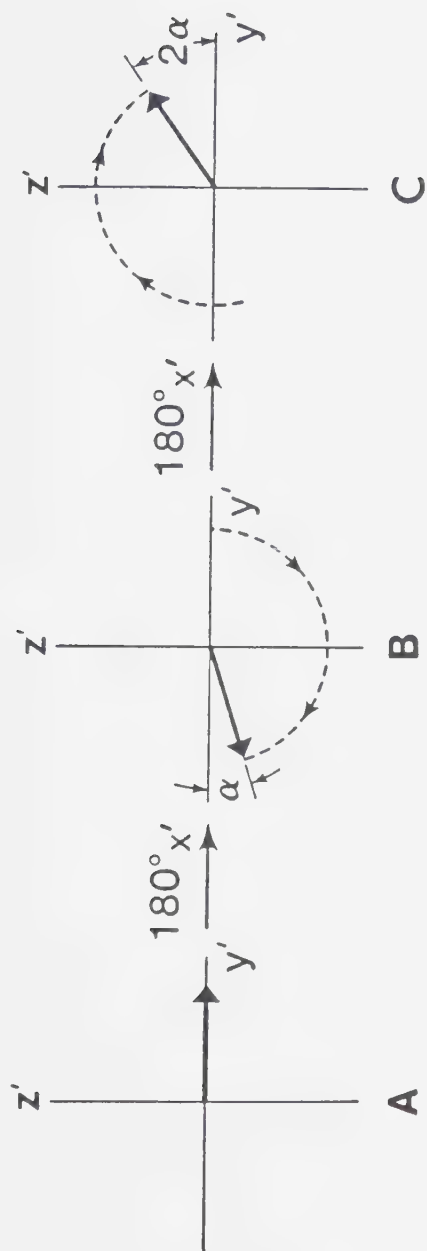


Figure 4. The Carr-Purcell modification of the spin-echo experiment showing the cumulative effect of missetting the 180° pulse by α .

In the so-called Carr-Purcell-Meiboom-Gill method, the initial 90° pulse is applied along the x' axis and successive 180° pulses are applied along the y' axis as indicated by the subscripts in Sequence IV.

$$90^\circ_{x'} - (\tau_2' - 180^\circ_{y'} - \tau_2')_n - \text{Acquisition} \quad (\text{Sequence IV})$$

This has the effect of eliminating errors due to missetting of the 180° pulse following even numbered pulses as shown in Figure 5. If the Larmor frequency and frequency of the rotating frame are different, for example if the nuclear magnetization is precessing slightly faster, then over the length of the first τ_2' delay the magnetization will move slightly ahead of the y' axis as shown in Figure 5A. By applying the 180° refocussing pulse along the y' axis, the magnetization is flipped about this axis. If the flip angle for the 180° pulse is actually less than 180° , the magnetization following the pulse will be above the $x'-y'$ plane as shown in Figure 5B. Over the next two τ_2 delay periods, the magnetization will first catch up to the y' axis and then move ahead (Figure 5C). The next 180° pulse will find the projection of $M_{x'y'}$ in the $x'-y'$ plane exactly where it was before the initial 180° pulse. The 180° pulse applied at this point, which is misset the same amount as the initial 180°

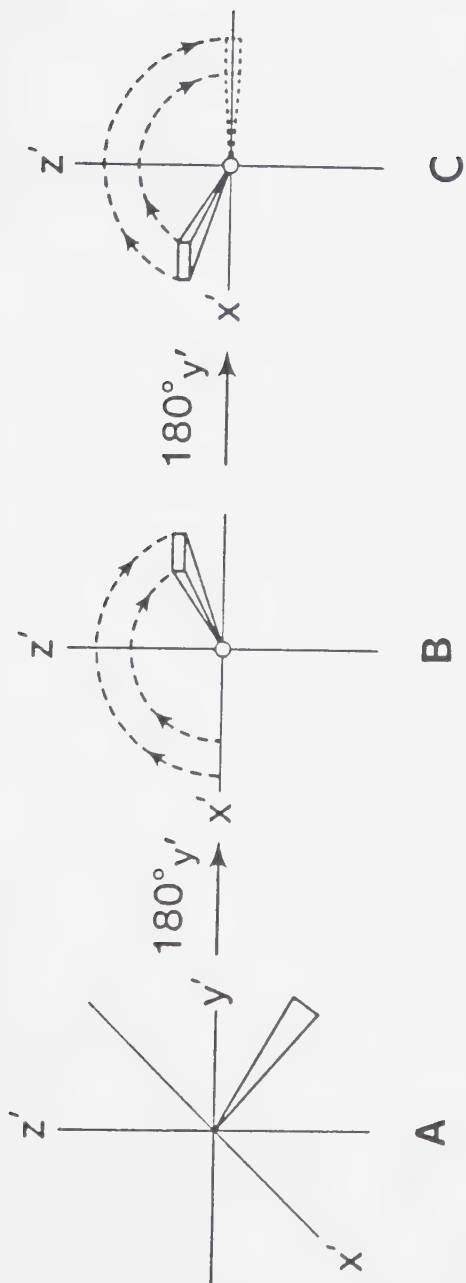


Figure 5. The Carr-Purcell-Meiboom-Gill modification of the spin-echo experiment showing how misset 180° pulses are compensated on even numbered echoes.

pulse, will flip the magnetization about the y' axis to end up exactly in the $x'-y'$ plane as shown in Figure 5C.

The above techniques for determining T_2 relaxation times were for many years restricted to single-line spectra. For multi-line spectra, the fact that the exciting RF radiation was applied as a nonselective "broadband" pulse results in all the nuclei of a certain species being excited. The amplitude of the resulting signal is a composite of all the resonances in the sample and any attempted measurement of T_2 relaxation times could provide only a composite T_2 value.

$$M_{2\tau_2} = M_{0(1)} e^{-(2\tau_2/T_2(1))} + M_{0(2)} e^{-(2\tau_2/T_2(2))} + \dots$$

$$+ M_{0(n)} e^{-(2\tau_2/T_2(n))} \quad (9)$$

This restriction no longer applies to state-of-the-art NMR spectrometers. With the development in the mid 1960's of the fast Fourier transformation algorithm by Cooley and Tukey [4], the spin-echo sequence and its modifications could be extended to the measurement of T_2 relaxation times for multi-line spectra. The development of the fast FT algorithm is in fact responsible for many of the new applications of the spin-echo experiment. In this procedure, the second half of the spin-echo is collected

in digital form as a FID (Figure 3B) and Fourier transformed to produce the corresponding frequency domain spectrum [12]. The measurement of T_2 relaxation times for resonances in multi-line spectra by pulsed FT methods has been discussed in detail by Freeman and Hill [13].

C. Features of the Spin-Echo Experiment

The sense of resonances in a spin-echo spectrum, that is whether peaks are positive or negative in intensity, can be different from those in a conventional single-pulse spectrum. Magnetization located along the positive y' axis is conventionally taken to correspond to a positive resonance. The 180° pulse of the spin-echo experiment flips the magnetization from the positive y' axis to the negative y' axis. Figure 6 shows the signals which result for a single magnetization vector located along each of the axes in the $x'-y'$ plane. Magnetization located along the positive y' axis is conventionally phased to give positive peaks (Figure 6A) while that located along the negative y' axis gives negative peaks (Figure 6C). Magnetization found along either x' axis gives out of phase signals in the Fourier transformed spectrum as shown in parts B and D of Figure 6. In practice, the convention of phasing peaks in spin-echo spectra opposite to that of single-pulse spectra is often dispensed with and spin-echo

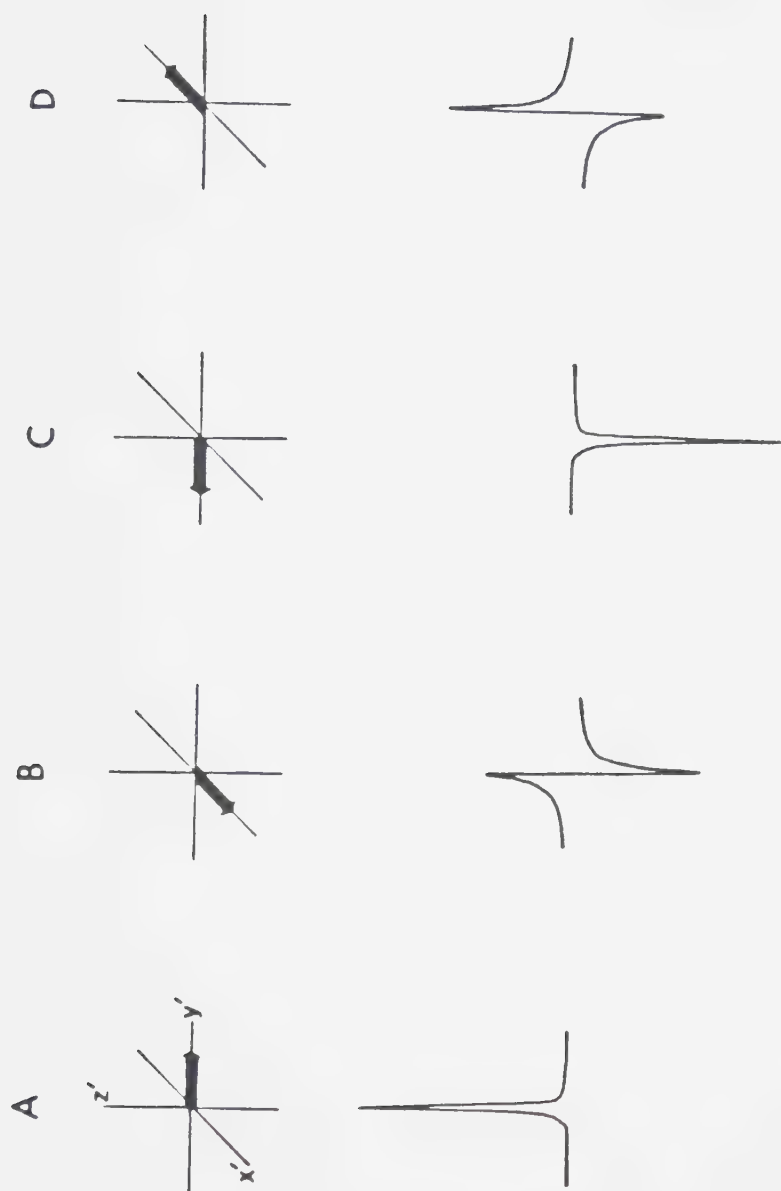


Figure 6. Signals resulting from Fourier transformation of magnetization located along the positive and negative x' and y' axes at acquisition.

spectra are phased to give positive resonances even though the magnetization lies along the negative y' axis.

Another feature which appears in spectra measured using the spin-echo sequence involves the effects caused by differential spin-spin relaxation. Different nuclei will generally have different T_2 relaxation times and thus their magnetization in the $x'-y'$ plane will decay at differing rates. This is illustrated in Figure 7 where lines A to E represent the magnetization measured at time $2\tau_2$ for resonances with T_2 relaxation times of 2.0, 1.0, 0.5, 0.2 and 0.1 seconds, respectively. This differential spin-spin relaxation has been utilized to provide increased spectral simplification and resolution enhancement [14] but leads to problems in trying to obtain quantitative information from the intensities of resonances in spin-echo spectra.

Differential spin-spin relaxation can be utilized to provide increased spectral simplification by eliminating resonances from the nuclei with shorter T_2 relaxation times. The spin-spin relaxation time is related to molecular mobility which in turn is related to molecular size. In general, the larger the molecule the shorter the T_2 values for its magnetically active nuclei. Thus, resonances from large molecules decrease in intensity and disappear from spin-echo spectra as τ_2 is increased more

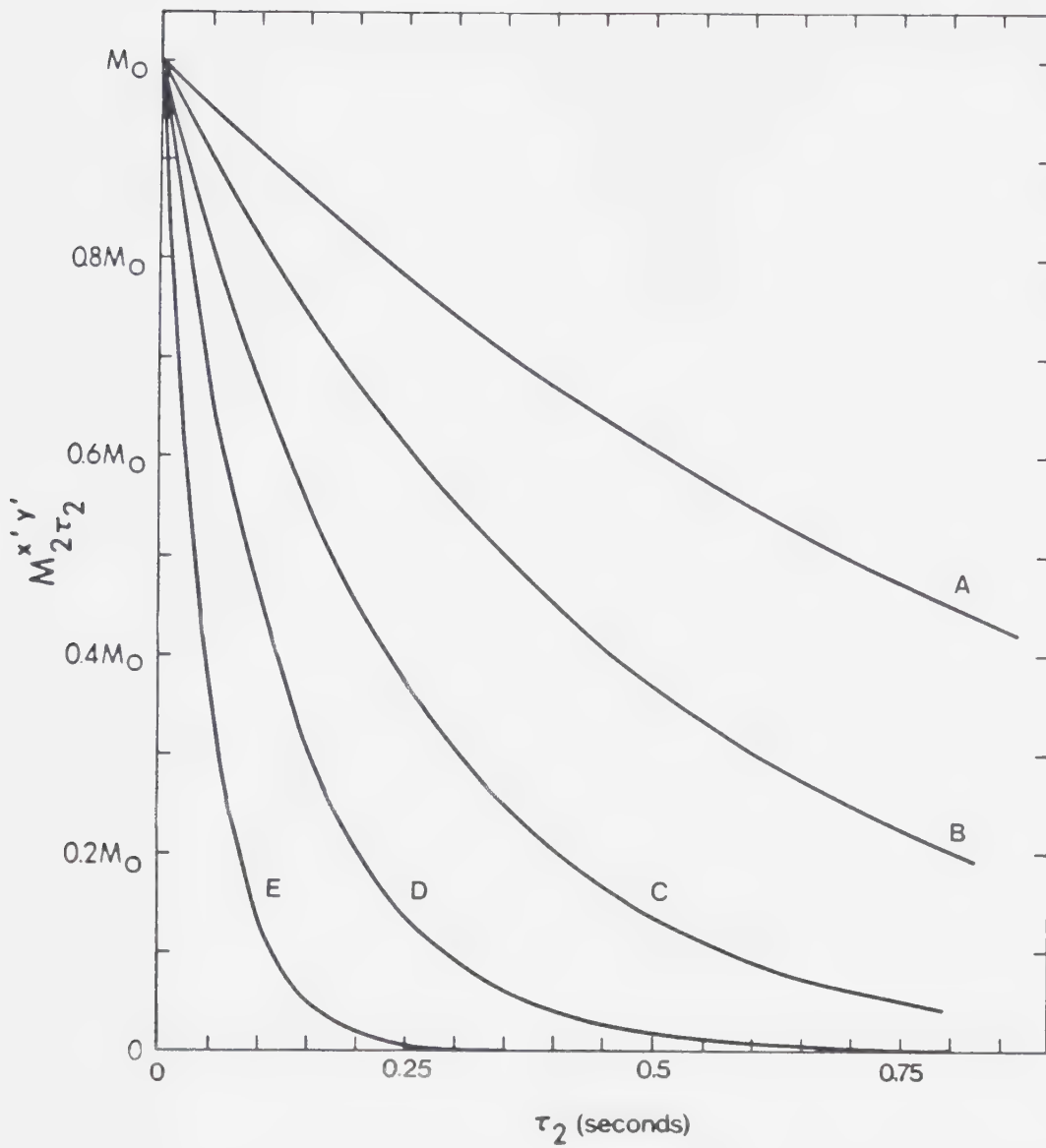


Figure 7. Decay of the magnetization in the x' - y' plane with time as a function of the spin-spin (T_2) relaxation time. Lines A to E correspond to T_2 values of 2, 1, 0.5, 0.2 and 0.1 seconds, respectively.

rapidly than those from smaller molecules. This is illustrated by the spectra obtained on a sample of red blood cells (Figure 8) [15]. Figure 8A shows the spectrum obtained using the conventional single-pulse experiment. Note the broad rather featureless envelope from which very little information can be gleaned. The spectrum obtained with the spin-echo sequence using a τ_2 delay of 60 milliseconds is presented in Figure 8B. In this spectrum, numerous sharp resonances are noted which have been assigned to some of the smaller molecules present in the erythrocyte [16,17].

Although differential T_2 relaxation provides a valuable means of spectral simplification, it complicates the determination of quantitative data in spin-echo spectra. In single-pulse FT NMR spectroscopy, the relative concentrations of compounds in a sample are determined from the relative areas of resonances. The determination of relative concentrations from spin-echo spectra cannot be carried out using this procedure because differential spin-spin relaxation causes the various resonances in the spin-echo NMR spectrum to be decreased in intensity by different amounts. Thus, the intensity of resonances for equal numbers of nuclei having different T_2 values will be different. In order to determine relative concentrations in spin-echo spectra, more elaborate methods than direct area comparisons need to be developed.

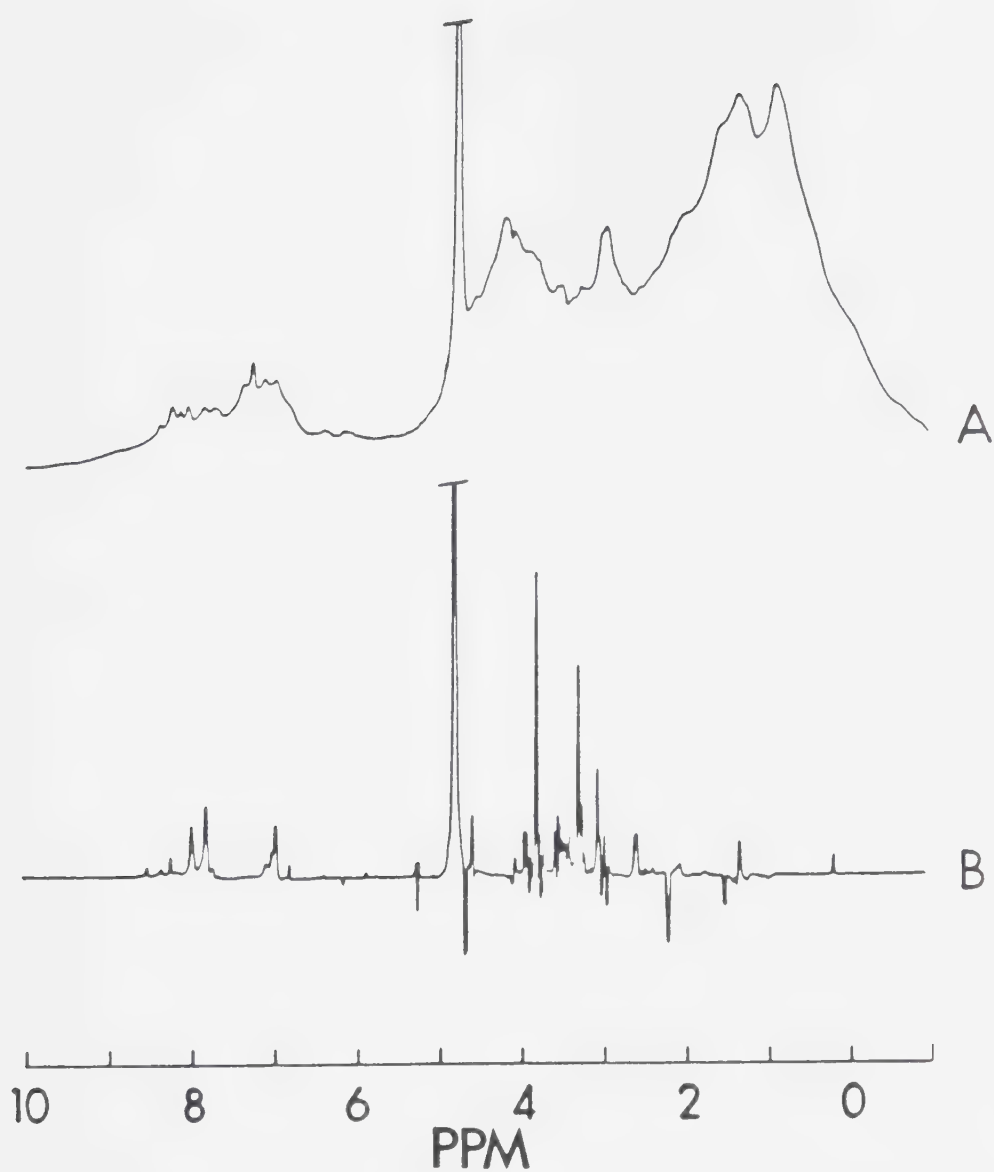


Figure 8. 400 MHz NMR spectra of red blood cells which had been washed with saline D_2O . (A) Single-pulse spectrum. (B) Spin-echo spectrum with $\tau_2 = 0.06$ second. Reproduced with permission from reference 15.

A third feature which complicates spin-echo spectra is the phenomenon of phase modulation of the components of multiplets [13,15]. Phase modulation results from spin-spin coupling and can be explained in terms of the behavior of the magnetization during the spin-echo sequence. If a homonuclear coupled, first-order doublet is considered, one half of the sample nuclei are coupled to other nuclei whose spin orientation gives rise to a slower precessional frequency while the other half are coupled to nuclei resulting in a faster precessional frequency. The difference between these two frequencies is the spin-spin coupling constant, J . The energy level diagram for a system of this type is shown in Figure 9. The nuclei being observed and those causing the coupling labelled A and X, respectively, are denoted as α and β corresponding to the $+1/2$ and $-1/2$ spin states. The transitions A_S and A_F correspond to the slower precessing and the faster precessing components of the doublet resulting from the A portion of the AX spin system. The 180° pulse flips both the A nuclei and the X nuclei. This results in an inversion of all the spin states of the nuclei such that following the 180° pulse those nuclei in level 1 are now in level 4 and vice versa. Likewise, an exchange of nuclei between levels 2 and 3 has occurred. Transitions of the nuclei which previously gave rise to A_S

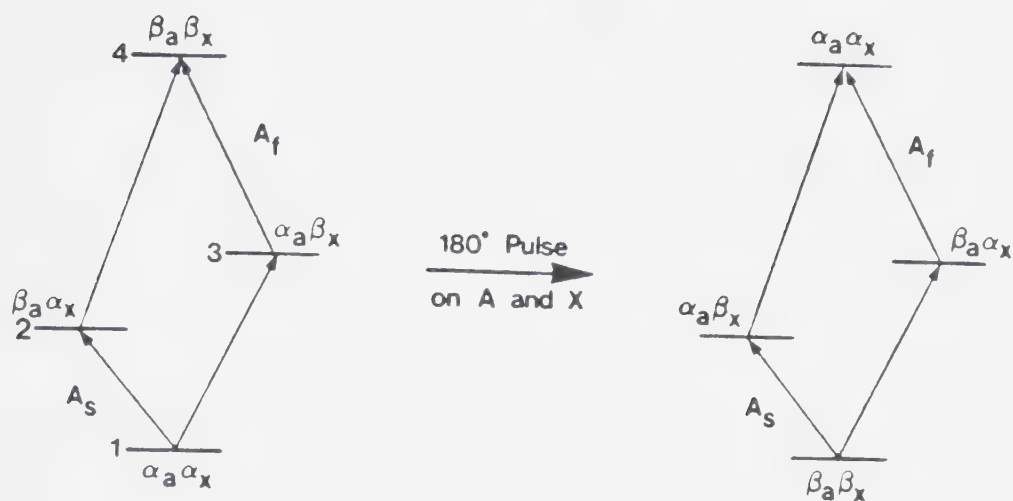


Figure 9. The energy level diagram for the case of two homonuclear spin-spin coupled nuclei before and after the application of a nonselective 180° pulse.

now give rise to A_f and transitions which gave rise to A_f now account for the A_s transitions. This results in the previously slower moving doublet component, A_s , precessing faster after the 180° pulse and the previously faster component precessing slower. Figure 10 illustrates this situation for the magnetization arising from a doublet during the spin-echo experiment. If the frequency of the rotating frame is taken to be halfway between the two components of the doublet, then following the initial 90° pulse, one component will fall behind the positive y' axis and one will move ahead. After the 180° pulse, the two components will continue to diverge whereas magnetic field inhomogeneity effects will be reversed.

The result of this phase modulation is that following acquisition and Fourier transformation of the FID the resulting spectrum, after applying phase corrections, will contain out of phase resonances for the doublet components when they are not located along the y' axis at the time of acquisition. This is illustrated in Figure 11 where the position of the two components of the magnetization of a doublet at the start of acquisition are shown as a function of the delay time, expressed in units of $1/J$, along with the spectrum that results in each case. Figures 12 and 13 show the same phase modulation behavior for a triplet and a quartet, respectively. The phase

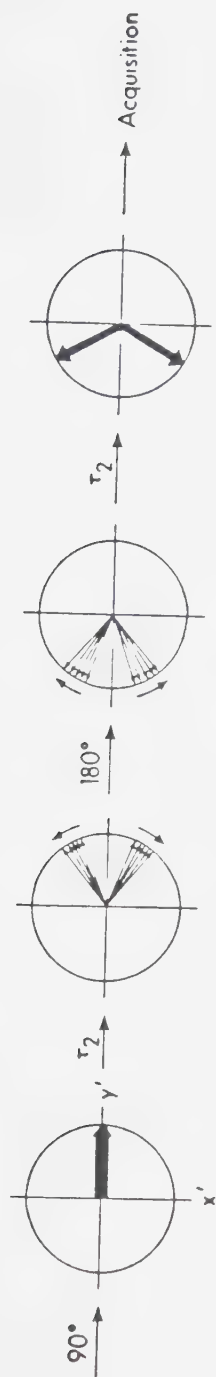


Figure 10. The behavior of the two components of the magnetization for a homonuclear coupled doublet during the spin-echo experiment.

Delay Time, τ_2

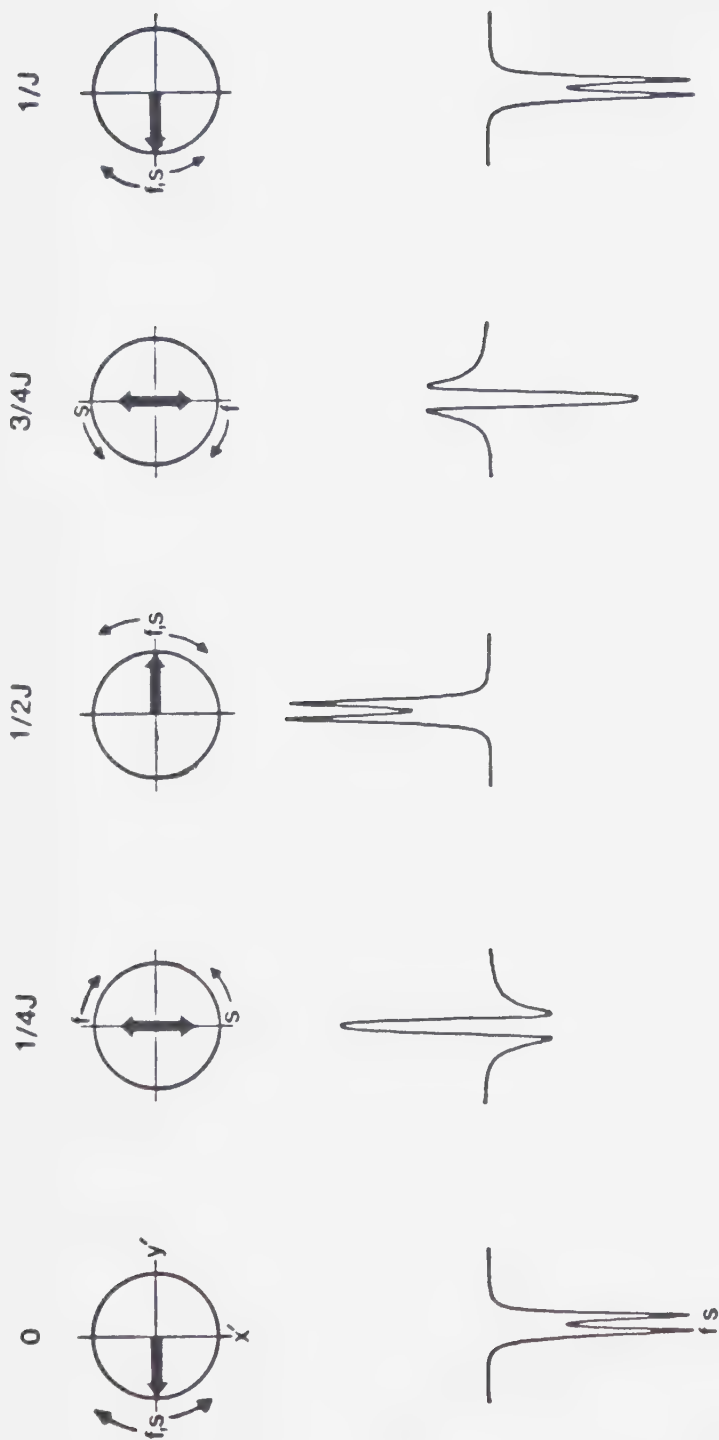


Figure 11. The phase modulation behavior of the components of a doublet as τ_2 varies. The top portion of the figure shows the orientation of the components of the magnetization at acquisition while the bottom portion shows the signal resulting upon Fourier transformation.

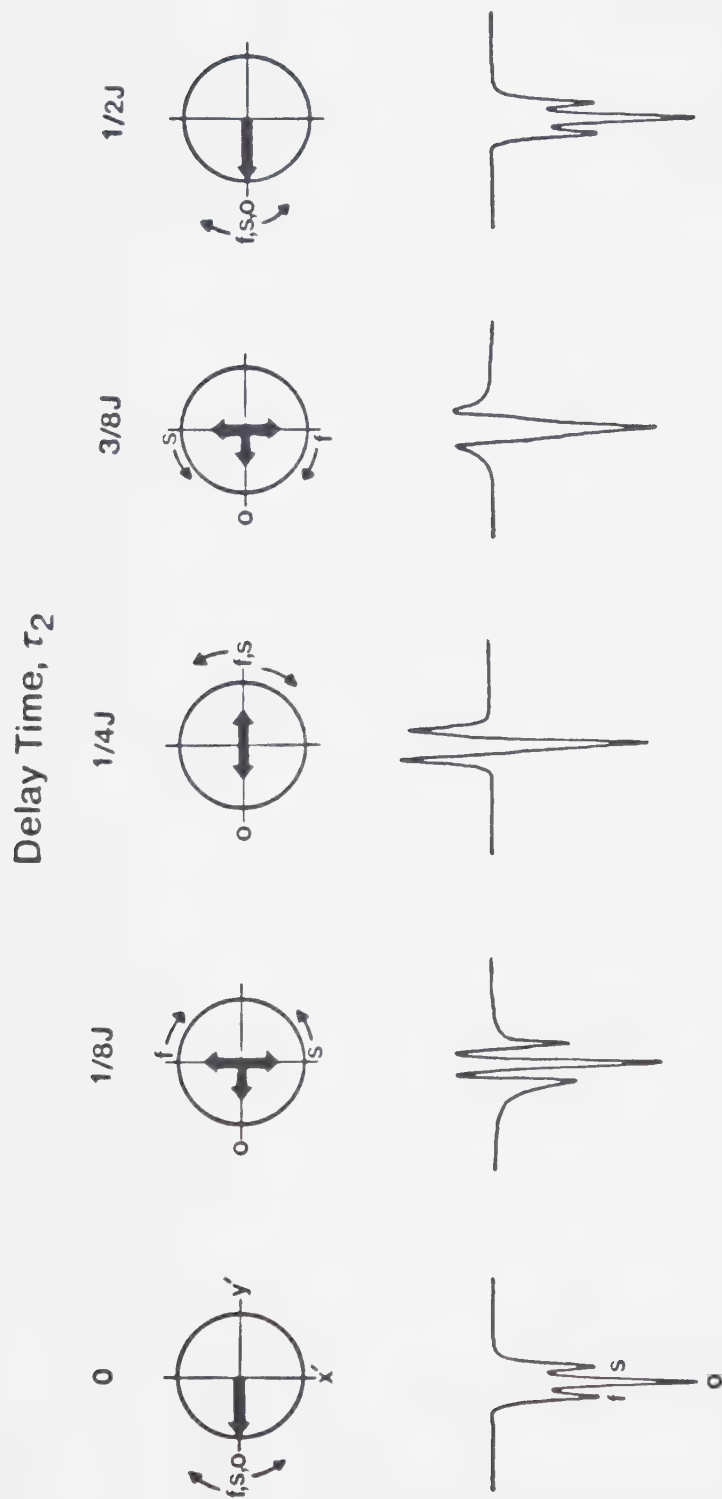


Figure 12. The phase modulation behavior of the components of a triplet as τ_2 varies. The top portion of the figure shows the orientation of the components of the magnetization at acquisition while the bottom portion shows the signal resulting upon Fourier transformation.

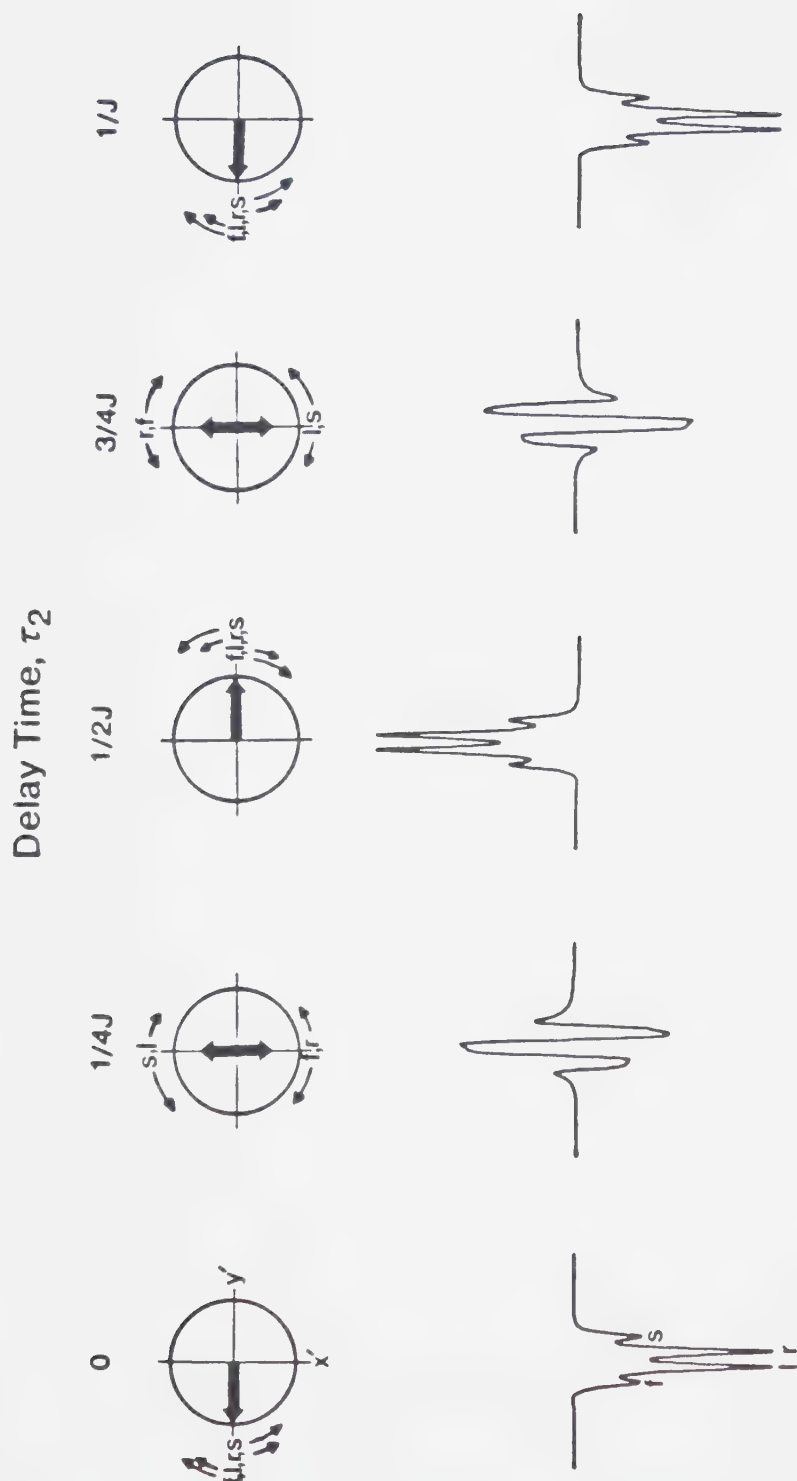


Figure 13. The phase modulation behavior of the components of a quartet as τ_2 varies. The top portion of the figure shows the orientation of the components of the magnetization at acquisition while the bottom portion shows the signal resulting upon Fourier transformation.

modulation behavior of multiplet signals will depend, in general, on the length of the delay periods, τ_2 , the magnitude of the spin-spin coupling constant, J , and the particular type of multiplet pattern involved. For first-order coupling, the relationship between the observed phase modulation behavior and J is relatively simple. However, when the coupling is not first-order, the phase modulation behavior becomes a more complicated function of J and cannot be easily predicted [13]. Not only do different multiplet patterns have different phase modulation behavior, but the various components of each multiplet will be modulated at different frequencies [15] as shown in Figures 12 and 13. For the purpose of measuring T_2 relaxation times, it is possible to obtain in-phase signals for a multiplet in the spin-echo experiment by adjusting the length of the delay periods such that the magnetization in the x' - y' plane falls entirely along one direction of the y' axis at the time of acquisition. Alternatively, the generation of a power spectrum (PS) may be used in some instances. This is derived by summing the squares of both the absorption mode, v , and the dispersion mode, u , signals over the entire frequency range and taking the square root of the resulting function.

$$PS = \sqrt{v^2 + u^2} \quad (10)$$

The power spectrum contains none of the phase modulation found in the conventional absorption mode spectrum but does contain broadened peaks with significant tailing on both sides, which often limits its applicability [13].

NMR spectra collected on nuclei other than ^1H , notably ^{13}C NMR spectra, exhibit heteronuclear coupling to ^1H nuclei. In this situation, the observed spin-spin coupling is due to interactions between the ^{13}C nuclei and their attached heteronuclei, ^1H atoms. In cases involving such heteronuclear spin-spin coupling, phase modulation effects are generally not observed. This is because the 180° pulse in the spin-echo sequence flips only the nuclear species under observation, ^{13}C nuclei, and not the species to which coupling occurs, ^1H nuclei. Figure 14 shows the energy level diagram for a heteronuclear AX spin system (^1H - ^{13}C for example) illustrating the behavior of the nuclear magnetization before and after the 180° pulse. Only the X spins are flipped by the 180° pulse so that the divergence of multiplet components due to spin-spin coupling is reversed in much the same way that magnetic field inhomogeneity effects are reversed. The application of suitable decoupling fields or 180° pulses to the nuclei responsible for the coupling can cause phase

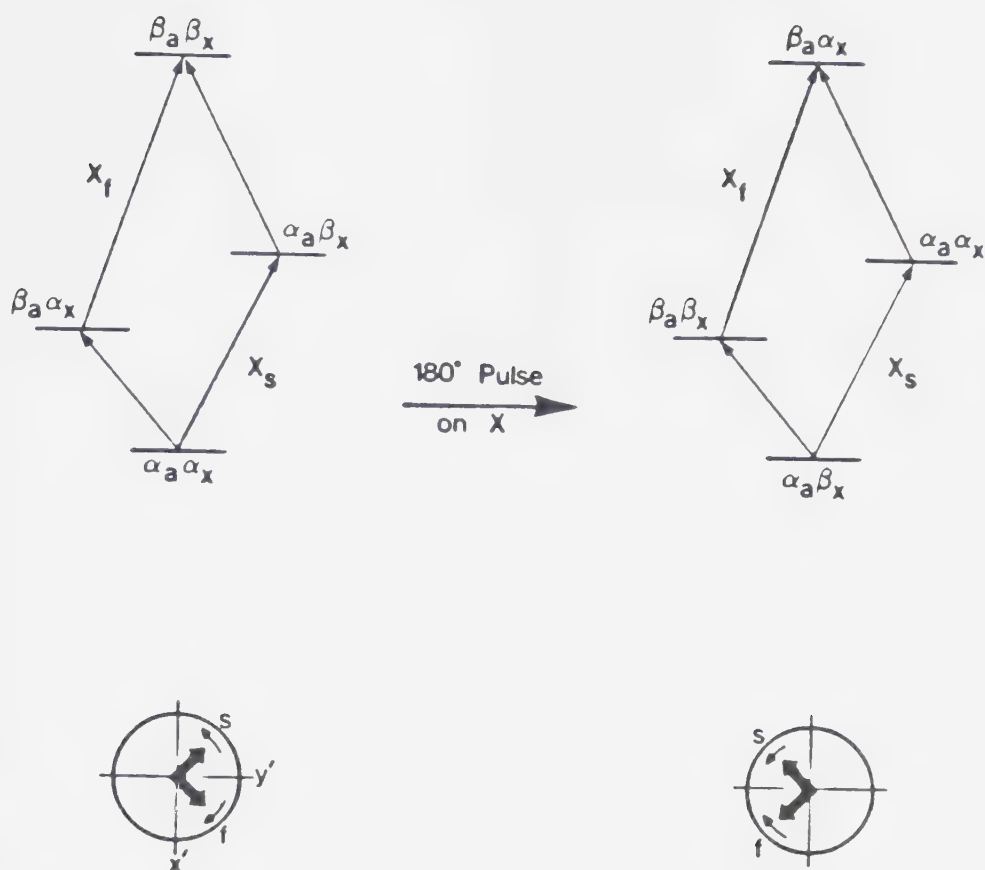


Figure 14. The energy level diagram for the case of two heteronuclear spin-spin coupled nuclei before and after the application of a 180° pulse to the X nuclear species. The bottom portion of the figure is a representation of the magnetization of the X nuclear species in the $x'-y'$ plane before and after the 180° pulse. The component of the magnetization which was precessing slower before the pulse is still precessing slower after the pulse and that precessing faster before the pulse is still precessing faster after the pulse.

modulation in cases involving heteronuclear coupling (Figure 15A and B). Decoupler scheme A in Figure 15 causes phase modulation effects in ^{13}C NMR spectra due to coupling to ^1H nuclei to be observed by applying broadband proton decoupling during one of the two delay periods [18,19]. This gated decoupling technique effectively destroys the ^{13}C - ^1H interactions [20] during this delay period such that the phase modulation which occurs during the second delay period does not converge at the time of acquisition. This is shown schematically for a ^{13}C doublet in Figure 16A. The x'-y' plane is represented in this sequence showing the behavior of the ^{13}C nuclear magnetization throughout the spin-echo sequence shown in Figure 15 with decoupler scheme A when the delay time is $1/4J$. An alternative approach for observing the phase modulation of ^{13}C multiplets in the spin-echo experiment involves the use of a 180° decoupler pulse applied simultaneously with the ^{13}C 180° pulse [21] as shown in Figure 15B. In this experiment, termed the spin-flip method, both the A and X spins are flipped such that the energy level diagram is described by Figure 9. Phase modulation occurs during both τ_2 delay periods and results in a continued divergence of the multiplet components as shown in Figure 16B. Since phase modulation occurs for twice the time as in the gated decoupling experiment

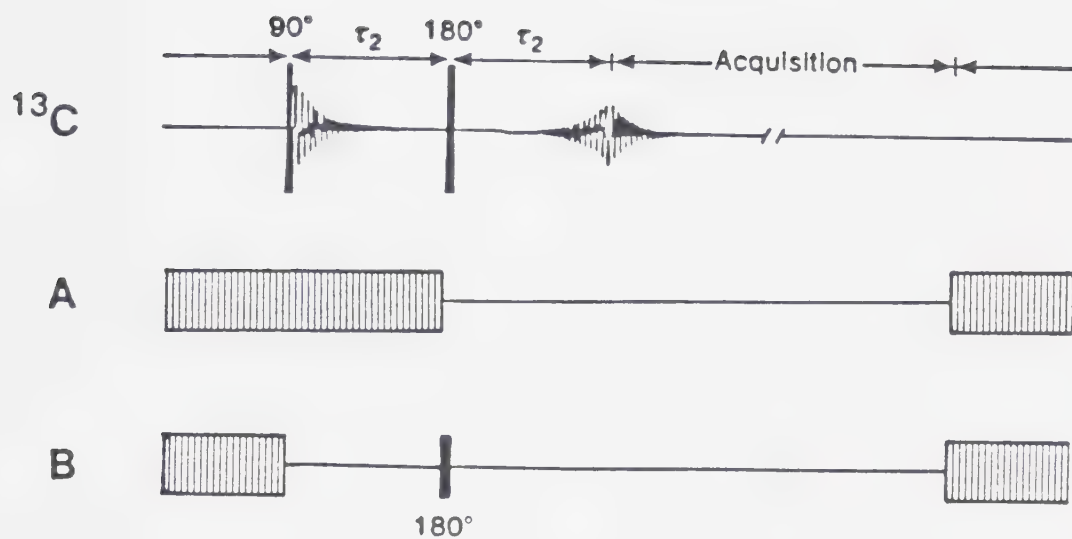


Figure 15. The ^{13}C spin-echo sequence with (A) the gated decoupling technique and (B) the spin-flip decoupler sequence.

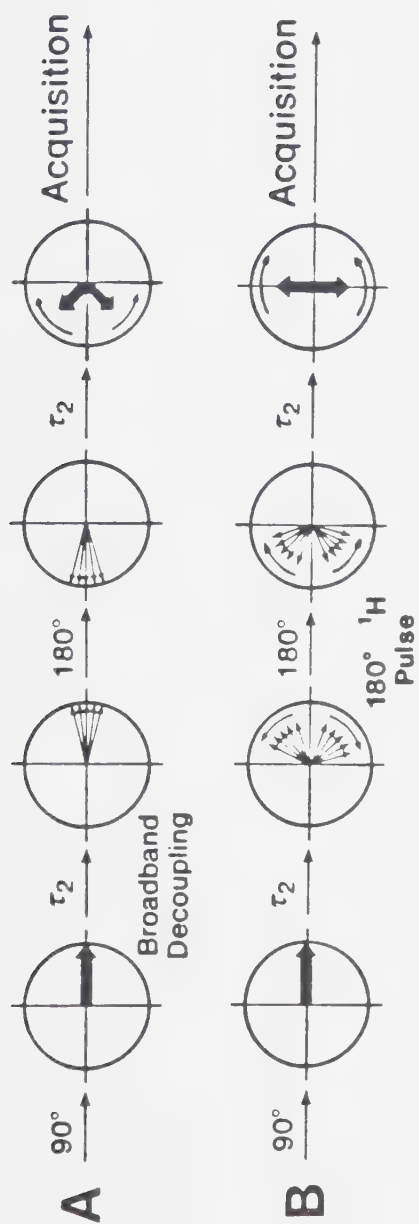


Figure 16. The behavior of the magnetization for a ^{13}C doublet due to coupling to a methine proton during the ^{13}C spin-echo experiment using (A) the gated decoupling sequence and (B) the spin-flip method.

(Figure 16A), the components have diverged twice as far for the same τ_2 delay time.

The technique of J-resolved two-dimensional NMR spectroscopy is based on the phase modulation phenomenon which occurs during the spin-echo experiment [6,18]. In this technique, a series of spin-echo spectra are collected at closely spaced τ_2 values. Two Fourier transformations are then carried out on the accumulated FIDs. The first is the usual Fourier transformation resulting in a series of phase modulated intensity versus chemical shift spectra. Before carrying out the second transformation, the data are rearranged by taking one point from each spectrum, at the same chemical shift, to construct each function for the second Fourier transformation. These functions are modulated due to the differing degree to which phase modulation has occurred in each of the original spectra. This modulation frequency is related to J and manifests itself in a second frequency dimension following Fourier transformation as peaks separated by J. The end result of the two Fourier transformations is a two-dimensional spectrum with chemical shift on one frequency axis and coupling constant on the second. In order to generate such a two-dimensional spectrum, the phase modulation must not be converged in the collected FIDs. For homonuclear (^1H - ^1H

for example) J-resolved spectra, no decoupling is necessary as discussed previously while for heteronuclear (^{13}C - ^1H for example) J-resolved spectra, decoupler irradiation must be applied [18] using either the gated decoupling or spin-flip methods shown in Figure 15A and B, respectively, in order to observe the J dimension.

D. Overview

This thesis is concerned with analytical applications of the spin-echo sequence to complex organic and biological samples. The results presented are either difficult or impossible to obtain by more conventional methods. The applications to be discussed are based on two of the features of the spin-echo experiment described above, namely differential spin-spin relaxation and the phase modulation of multiplets.

It is shown in Chapter III that the phase modulation effects can be used to assign carbon types (methyl, methylene, methine and quaternary) to resonances in ^{13}C spectra on the basis of the phase modulation behavior of the various types of multiplets [22]. This constitutes the first step in the assignment of a ^{13}C spectrum and is often a difficult step in the elucidation of the structure of complex organic compounds. It also is shown that phase modulation effects can be used to determine spin-spin

coupling constants in complex spectra where such information is difficult or impossible to obtain by other methods [22].

In Chapter IV, some qualitative aspects of differential spin-spin relaxation based on differences in molecular size are presented. Initially, a study relating measured T_2 relaxation times to molecular size as approximately determined by molecular weight is carried out. Then, a method of monitoring protein solutions to determine their purity with respect to small molecules based on T_2 discrimination is described. The remaining chapters deal with quantitative studies involving the spin-echo experiment in which observations are made on small molecules present in complex samples such as intact human erythrocytes. These chapters describe methods for the measurement of the concentrations of smaller molecules found in the human erythrocyte by several means. In Chapter V, generalized quantitation methods such as a standard addition approach and mathematical extrapolation procedures involving the use of proportionality constants are applied to relate the measured peak intensities in spin-echo spectra to concentrations. These methods should be applicable to virtually any compound in a wide range of samples. The final chapter describes the use of spin-echo NMR spectroscopy along with a very specific chemical

reaction occurring inside red blood cells to determine the concentration of an intracellular compound. In particular, a titrimetric method of measuring glutathione in red blood cells based on the enzyme catalysed reaction of t-butylhydroperoxide with glutathione is presented. The titration reaction is followed by using the spin-echo method in a noninvasive and nondestructive manner whereas conventional methods of measuring glutathione concentrations require the destruction of the cellular system.

CHAPTER II

EXPERIMENTAL

A. Chemicals

Bovine serum albumin, lysozyme, trypsin inhibitor, angiotensin I, angiotensin II, glycylglycine, glycylglycylglycylglycylglycine, glycylglycylglycylglycylglycylglycine, ergothioneine, creatine, 5,5'-dithiobis(2-nitrobenzoic acid), iodoacetamide (Sigma Chemical Co.), alanine, valine, diethylsuccinate (Eastman Kodak Co.), glycine, 1,4-dioxane (BDH Chemicals Ltd.), glycylglycylglycine, glycylglycylglycylglycine (Nutritional Biochemicals Corp.), t-butanol, 2-propanol, 3-pentanol (Fisher Scientific Co.) and tetramethylsilane (Merck, Sharp and Dohme Canada Ltd.) were all used as received.

Oxidized and reduced glutathione (Sigma Chemical Co.) were used as purchased. Standardization of reduced glutathione solutions was accomplished using the method given below.

t-Butylhydroperoxide (Aldrich Chemical Co.) was obtained as a 90% solution (balance: 5% t-butanol, 5% H₂O). Solutions were standardized using an iodine liberation procedure described below.

A sample of pure cholesterol was obtained from Dr. J.C. Vederas of the University of Alberta.

99.8 atom % D chloroform (Merck, Sharp and Dohme Canada Ltd.) and 99.7 atom % D deuterium oxide (Stohler Isotope Chemicals Canada Ltd. and Merck, Sharp and Dohme Canada Ltd.) were used as solvents without further purification. H_2O solutions were prepared in doubly distilled, deionized water.

pH adjustments in D_2O solutions were carried out using 35% w/w, 99 atom % D deuterium chloride and 40% w/w, 98 atom % D potassium hydroxide (Merck, Sharp and Dohme Canada Ltd.) or D_2O dilutions thereof.

All other chemicals were reagent grade and were used without further purification.

B. Solution Preparation

1. Standardization of Glutathione Solutions

A solution of approximately 20 mM reduced glutathione (GSH) was prepared in H_2O under argon and stored at 4°C when not in use. The 20 mM stock solution was standardized using the method of Benesch and Benesch [23] as modified by Reid [24]. In this procedure, the sulfhydryl group of GSH is treated with an excess of iodoacetamide according to the reaction:



The amount of thiol is obtained by titration of the protons liberated in this reaction with a strong base.

In order for the procedure to be applicable, two criteria must be met. Firstly, the initial and final pH for the titration must be identical and low enough to ensure that there is initially quantitative sulfhydryl protonation, yet high enough so that carboxylate buffering does not occur, which would result in poor precision. As the sulfhydryl pK_a for GSH is 9.2 [25,26] and the carboxylate pK_a 's are 2.12 and 3.53 [27], an initial and final pH of 5 was used. The second criterion to be met is for the reaction to occur in a reasonably short period of time to minimize oxidation of the thiol group. This necessitated raising the pH to approximately 9 after addition of the iodoacetamide to increase the reaction rate.

The base used to titrate the released protons was a 0.06963 M solution of NaOH prepared under carbonate-free conditions and standardized against primary standard potassium hydrogen phthalate, which had been dried at 120°C for two hours, using phenolphthalein as the end point indicator. A 0.04106 M HNO_3 solution was used as a back titrant to pH 5 and was standardized against the NaOH solution using phenolphthalein to signal the end point.

In the titration of the protons released from GSH in the reaction with iodoacetamide, two standards were used for color matching end points. The first contained approximately 70 mL of pH 5 buffer, six drops of phenolphthalein and four drops of methyl red. The second contained 120 mL of pH 5 buffer, six drops of phenolphthalein and eight drops of methyl red. These solutions were pink.

The standardization procedure consisted of adding six drops of phenolphthalein and four drops of methyl red to 20 mL of H₂O in an erlenmeyer flask. This solution was purged with argon for several minutes and a 15-mL aliquot of GSH solution added. The pH of the solution was adjusted to 5 and color matched with the first standard. At the same time, the volume of the solution was brought to near 70 mL. The initial readings for the acid and base containing burets were recorded at this point. About 0.2 g of iodoacetamide was dissolved in 5 mL of H₂O and added to the flask. Base was immediately added to raise the pH to around 9, signalled by the purple color of the phenolphthalein indicator. As the alkylation reaction with GSH progressed, the protons released tended to lower the pH. The pH was maintained at 9 by the addition of small increments of base. After several minutes, when the reaction appeared to be complete, the flask was set aside

under argon for a further two minutes. Four more drops of methyl red were added and the solution titrated to pH 5 and color matched with the second standard. The final buret readings of both acid and base were recorded. Blanks containing distilled water were run to account for any acidic or basic impurities in the iodoacetamide. The excess equivalents of base added over that of acid added in the titration is equal to the equivalents of thiol involved in the standardization. The GSH solution used as a standard in Chapter VI was a freshly prepared 10-fold dilution of this standardized solution.

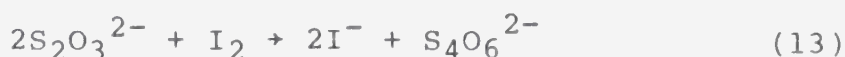
2. Standardization of t-Butylhydroperoxide Solutions

The t-butylhydroperoxide (t-BHP) solution used as the titrant for the GSH determinations in human erythrocytes, described in Chapter VI, was prepared by diluting a commercially obtained, concentrated t-BHP solution with D₂O. A solution was prepared to be approximately 0.14 M in t-BHP and was standardized using the iodine liberation method for organic hydroperoxides of Mair and Graupner [28] based on the work of Wagner and coworkers [29].

In the procedure used, a 1-mL aliquot of the t-BHP solution was refluxed with 10 mL of 20% w/v sodium iodide in 2-propanol and 25 mL of 10% v/v acetic acid in 2-propanol for about 10 minutes. Iodine was formed according to the reaction:



The presence of excess sodium iodide reduces the volatility of the liberated iodine by formation of the nonvolatile I_3^- anion. This prevented the loss of iodine during the refluxing. It was important that the t-BHP not come into contact with neutral sodium iodide solution as hydroperoxide decomposition other than by that generating iodine would occur. The liberated iodine was titrated with standardized thiosulfate according to the reaction:



A standard thiosulfate solution (0.08 M) was prepared and standardized according to the procedure outlined by Harris and Kratochvil [30].

In the t-BHP standardization procedure, blanks were necessary to account for the small amount of iodine generated by air oxidation during the refluxing. The concentration of t-BHP was determined as one half the equivalents of thiosulfate used in the titration of the liberated iodine. The actual titrant used in the NMR titration of erythrocyte samples was a 10-fold dilution of the stock solution standardized above. The stock solution was stored at 4°C when not in use.

3. Other Solutions

Solutions of ethanol, alanine, 2-propanol and 3-pentanol were prepared for the ^1H phase modulation studies of Chapter III by dissolving small amounts in D_2O to give an acceptable S/N ratio after several minutes of signal averaging. A CDCl_3 solution of cholesterol containing approximately 5% TMS was prepared in a similar manner for the ^{13}C phase modulation experiments.

For the spin-spin relaxation time studies of Chapter IV, approximately 2 mM solutions of glycine, diglycine, triglycine, tetraglycine, pentaglycine, hexaglycine, angiotensin II, angiotensin I, trypsin inhibitor, lysozyme and bovine serum albumin (BSA) were prepared in D_2O containing 0.16 M NaCl (saline D_2O). The pH^* of these solutions was adjusted to approximately 7. In the protein purity monitoring experiments, an approximately 3 mM solution of an older batch of BSA was prepared in saline D_2O .

The CDCl_3 solutions used in the quantitative studies in Chapter V were prepared by diluting stock solutions. One stock solution contained a known concentration of diethylsuccinate (approximately 0.4 M) and the other contained about 0.2 M 1,4-dioxane. Two solutions were prepared from the stock solutions. One contained 4 mM diethylsuccinate plus 2 mM 1,4-dioxane and the second

contained 40 mM diethylsuccinate. No standardizations were carried out on these solutions as the experiments performed with them depended only on the relative differences between the successive dilutions prepared.

Two other solutions were prepared in saline D₂O for the quantitative studies on human erythrocytes in Chapter V. The first contained approximately 50 mM t-butanol for use as an internal standard. The second contained known amounts, as determined by direct weighing, of several compounds. The concentrations of these compounds were in the range of 40 mM for GSH, 5 mM for ergothioneine, creatine, alanine and glycine and 3 mM for valine. The precision and accuracy of the results of the experiments utilizing this solution made elaborate standardization procedures unnecessary. The solution was stored at 4°C when not in use to prevent the oxidation of the sulfhydryl groups of several of the compounds.

C. Instrumentation

1. pH Measurements

All pH measurements were made using a digital pH meter (Orion Model 701) equipped with a microcombination electrode (Fisher Scientific Co.) consisting of a glass electrode and a porous ceramic junction, silver/silver chloride reference electrode. The pH meter was calibrated

using Fisher certified buffer solutions of pH 4.00, 7.00 and 10.00 (± 0.02) calibrated against freshly prepared NBS standard buffers. All pH measurements were made at $25 \pm 1^\circ\text{C}$.

Many of the pH measurements were made on D_2O solutions. Since the meter was standardized using H_2O buffers, pD could be calculated from the pH meter reading, pH^* , using the equation [31]:

$$\text{pD} = \text{pH}^* + 0.40 \quad (14)$$

For pH measurements in this work, this conversion was neglected since the pH^* readings obtained were sufficient to allow comparisons of relative pH.

2. Optical Measurements

All spectrophotometric measurements made when determining GSH in human erythrocytes by the DTNB method [32] in Chapter VI were conducted on a Cary 118 spectrophotometer using a tungsten-halogen visible lamp and a matched set of glass sample cuvetts of 1-cm path length. The observation wavelength was 412 nm.

3. NMR Measurements

^{13}C NMR spectra were obtained at a frequency of 100.6 MHz on a Bruker WH-400 spectrometer equipped with an

ASPECT 2000 data system. The deuterium resonance from the CDCl_3 solvent provided the lock for field/frequency stabilization. Chemical shifts were measured relative to the carbon signal from TMS added to the sample for this purpose. A spectral width of 7000 Hz was used and the FIDs were collected in 16K of data points giving a digital resolution of 0.854 Hz/point in the 8K real portions of the Fourier transformed spectra. 48 scans were acquired to produce all of the spectra recorded with broadband proton decoupling during acquisition while 480 scans were collected for the fully coupled spectrum and a total of 240 scans acquired to arrive at the fully coupled subspectra. The pulse lengths used for a 90° and a 180° ^{13}C pulse were 20.0 and 40.0 μsec , respectively. Quadrature detection was used with no phase alternation. Two watts of decoupling power were used for broadband ^1H decoupling. To eliminate phase anomalies in the spin-echo spectra the ^{13}C receiver coil was tuned for the cholesterol sample. The spin-echo difference experiments were done either by collecting sequentially the FIDs to be added or subtracted or by collecting alternately, in separate regions of memory, a single scan of one FID and then a single scan of the other. The second method is recommended to average out the effects of spectrometer instability and drift.

^1H NMR spectra were usually collected at a frequency of 360 MHz on a Bruker WM-360 spectrometer equipped with an ASPECT 2000 data system. The standard addition results on red blood cells were collected at 400 MHz on a Bruker WH-400 spectrometer with the same data system. The deuterium resonance from either D_2O or CDCl_3 provided the lock for field/frequency stabilization. In several instances spectra were obtained on aqueous samples containing no deuterium by running the spectrometer in the unlocked mode. Chemical shifts were measured relative to the methyl proton signal from TMS in the case of CDCl_3 solutions or relative to the methyl resonance of sodium 2,2-dimethyl-2-silapentane-5-sulfonate in the case of aqueous solutions. In CDCl_3 solutions, either TMS itself or 1,4-dioxane (3.750 ppm) was added as a chemical shift reference. In aqueous solutions, the resonances were referenced to the methyl resonance of added t-butanol (1.236 ppm) or the methylene signal of glycine (3.540 ppm). A spectral width of 4000 Hz was generally employed and the FIDs were collected in 16K of data points giving a digital resolution of 0.488 Hz/point. For spin-echo spectra obtained on red blood cells, 100 to 400 scans were acquired for each spectrum while for single-pulse red blood cell spectra only 20 scans were recorded. Solution studies involving spin-spin relaxation time measurements

in Chapter IV were carried out by collecting 100 to 200 scans per spectrum. Standard addition experiments on CDCl_3 solutions in Chapter V employed 8 scans for each spectrum. The pulse lengths used for 90° and 180° pulses were usually about 7.4 and 15.4 μsec for the WM-360 spectrometer and 10.7 and 21.4 μsec for the WH-400 spectrometer. Quadrature detection was used throughout the ^1H NMR experiments with no phase alternation during spin-echo experiments.

D. Dialysis Measurements

The dialysis experiments performed as part of the protein purity monitoring studies of Chapter IV were carried out using 14.6 mm diameter, Spectrapor 1, cylindrical, membrane tubing with a molecular weight cutoff of 6,000 to 8,000 daltons (Spectrum Medical Industries). The tubing, which was received in a 23 mm width flattened strip, was softened by soaking for several minutes in saline D_2O . This also served to wash away the small amount of glycerin associated with the commercially procured membrane. The ends of the tubing were closed by knotting them or by using plastic closures (Spectrum Medical Industries).

The dialysis tubing was filled with a saline D_2O solution of the protein to be dialysed and then suspended

in a cylinder containing several times the volume of saline D₂O as contained in the dialysis sac. Dialysis was allowed to occur with constant stirring of the external medium at 4°C for a period of several hours to one day.

E. Erythrocyte Pretreatment

Samples of human erythrocytes utilized in many experiments were obtained from healthy donors. Venous blood was collected in EDTA containing Vacutainers (Becton, Dickinson and Company Canada Ltd.) of approximately 7 mL volume by qualified medical personnel. The hematocrit, which is the percent of the blood volume consisting of red cells, was measured for each sample and was generally found to be between 40 and 50 percent.

The preparation of the erythrocytes for NMR experiments was initiated by separating the blood cells from the plasma by spinning down the cells at 2500 rpm for 5 to 10 minutes in the Vacutainers. The plasma and buffy coat (white cells) were drawn off by Pasteur pipet and the red cells transferred from one or more Vacutainers to a larger polyethylene centrifuge tube. The cells were washed by suspending them in twice their volume of saline D₂O. The tube was sealed with Parafilm (American Can Co.) and shaken vigorously to mix the contents thoroughly.

After allowing the sample to stand for several minutes at room temperature, during which time H_2O in the cells was replaced by D_2O and glucose and lactate were dialysed out of the cells, the centrifuge tube was spun at 6000 rpm and $4^{\circ}C$ for 5 to 10 minutes. The supernatant was drawn off by Pasteur pipet and discarded. The red cells were generally washed twice more in the centrifuge tube, maintaining a 2:1 ratio of saline D_2O :red cells, using the same procedure outlined above. For those experiments which used hemolyzed red cells, the packed cells were lysed following the last wash by either a freeze-thaw technique or by sonication. In the freeze-thaw method, the red cells were alternately frozen in a dry ice-acetone bath and thawed to room temperature until all the cell membranes were ruptured. This was easily ascertained since the lysed cells yielded a clear, ruby red solution as compared to the opaque, packed whole cells. If sonication was used to hemolyze the red cells, a titanium probe was immersed in the packed cells and 20 kHz ultrasonic vibrations applied from a Sonicator (Heat Systems-Ultrasonics) to disrupt the cells. As a final step prior to drawing off samples for experiments, the red cells, whole or lysed, were oxygenated for approximately two minutes by bubbling with 95% O_2 -5% CO_2 (Union Carbide Canada Ltd.). This was necessary to ensure good

resolution in NMR spectra collected on the erythrocyte samples. If the erythrocyte samples were not well oxygenated, very broad, poorly resolved resonances resulted.

Samples for use in experiments were drawn off with 18-gauge, 1.5-inch, Yale needles (Becton, Dickinson and Company Canada Ltd.) mounted on 1-mL disposable syringes (McGaw Supply Ltd.). Those samples for NMR experiments, generally 0.5 ml, were placed in 5-mm O.D. NMR tubes (Wilmad Glass Co.).

F. DTNB Method for Glutathione Determination in Erythrocytes

A standard clinical method which is used for the determination of reduced GSH in erythrocytes is that of Beutler et al. [32]. It is based on the intensity of the yellow color developed by sulfhydryl containing solutions when they are treated with 5,5'-dithiobis(2-nitrobenzoic acid) (DTNB). The reaction involves the reduction of the DTNB by the sulfhydryl groups, which are oxidized to form a disulfide, yielding a highly colored yellow anion, the optical density of which is measured at 412 nm using a spectrophotometer. The reaction occurs at room temperature and is insensitive to even large temperature changes. The quantity of DTNB present is of little

importance as long as it is in excess of the concentration of sulfhydryl group. The reaction is very fast and complete color development occurs in less than 30 seconds with no fading of color for over 5 minutes thereafter. The color development is entirely satisfactory for a pH range of 5.7 to 8.3.

The procedure used to determine the concentration of GSH in red cells involved lysing 0.1 or 0.2 mL of packed cells by osmotic shock by making them up to 2 mL with H_2O . The osmotic pressure caused the rupture of the cell membranes. At this point, the GSH present in the solution was quite susceptible to air oxidation so 3 mL of precipitating solution containing 1.67 g glacial metaphosphoric acid, 0.1 g EDTA and 30 g NaCl per 100 mL was added. In the acidic solution, the GSH was relatively stable for several hours [33]. About 5 minutes after the addition of the precipitating solution, the mixture was centrifuged and filtered to remove precipitated protein. Either 1 or 2 mL of the filtrate, containing the GSH, was made up to 8 mL with phosphate buffer (0.3 M Na_2HPO_4). A 1-mL portion of a solution of DTNB (40 mg/100 mL of 1% sodium citrate) was added and the solution mixed well. Then, the absorbance at 412 nm was measured approximately 5 minutes after adding the DTNB solution. The concentration of GSH in the erythrocytes was determined

from the reading obtained utilizing the molar extinction coefficient for the DTNB anion of 13,600 at 412 nm [32]. Standards containing between 0.1 and 0.5 mL of a standardized 2 mM GSH solution were also analyzed to verify the procedure.

G. Calculations

Peak heights for resonances in NMR spectra were either measured by hand or determined by the Bruker software used with the ASPECT 2000 computer system of the NMR spectrometers. All area measurements were made by the computer software.

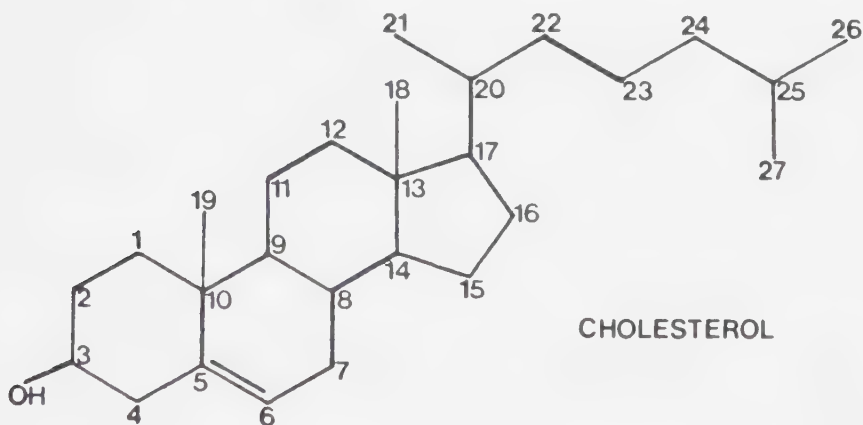
Linear regression analysis was performed using the linear regression software supplied with Texas Instruments calculators. Standard deviations of the slopes and abscissa intercepts were determined using a CASIO FX-702P programmable calculator. Non-linear curve fitting calculations were performed using an adapted form of the general curve fitting program KINET [34] utilizing the matrix regression procedure described by Wentworth [35]. This program was run on the University of Alberta AMDAHL 470 V/8 computer system.

CHAPTER III

SIMPLIFICATION OF ^{13}C SPECTRA AND MEASUREMENT OF ^{13}C - ^1H COUPLING CONSTANTS BY SPIN-ECHO TECHNIQUES

A. Introduction

^{13}C NMR spectra are normally measured with broadband ^1H decoupling which has the effect of collapsing ^{13}C multiplets caused by coupling to ^1H nuclei to singlets [20,36]. The spectral simplification and increased sensitivity which results has significantly advanced the routine use of ^{13}C NMR. This is illustrated by the spectra for cholesterol in Figure 17.



The ^{13}C spectrum of cholesterol has been assigned previously [37]; the assignments are given in Table 1.

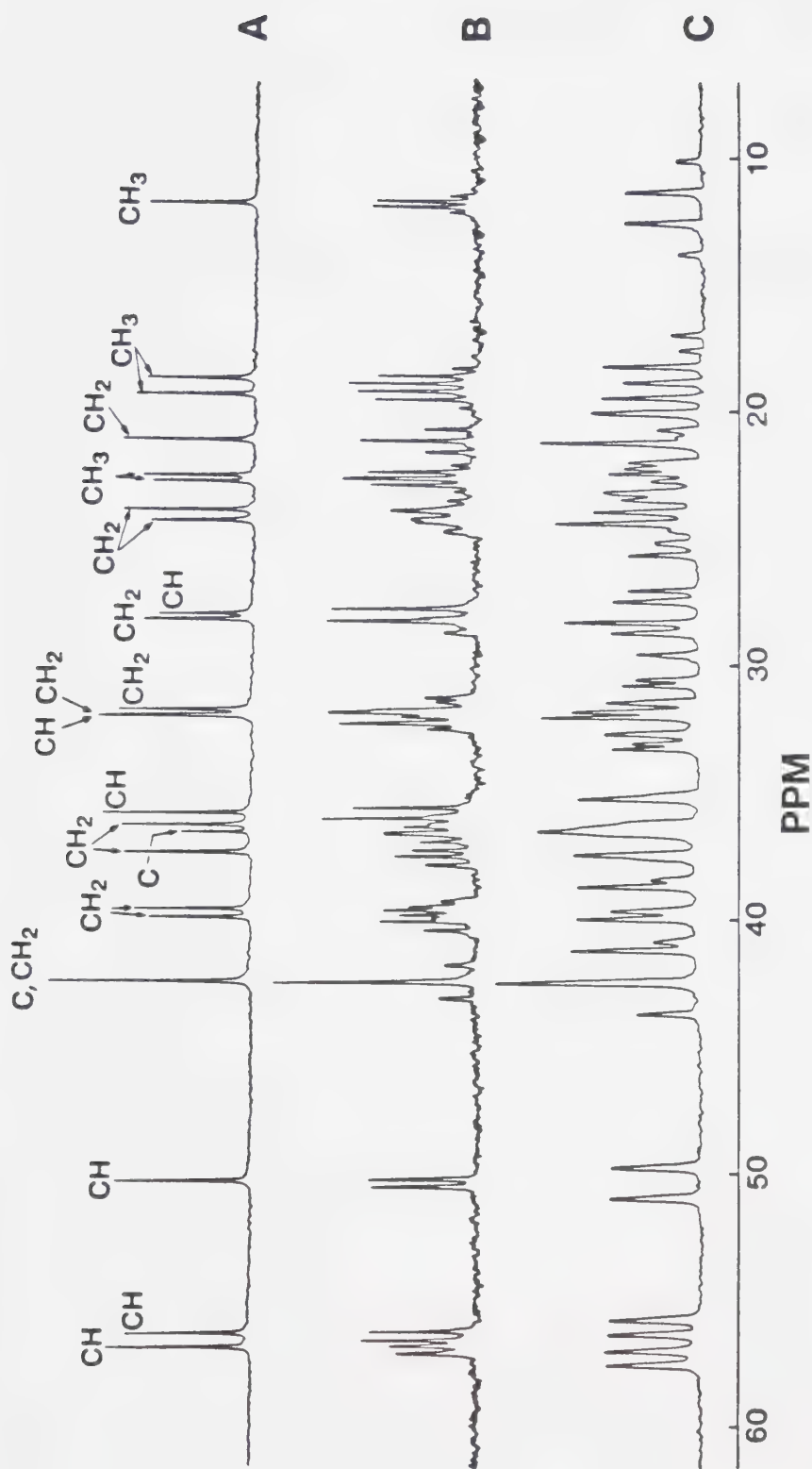


Figure 17. The high field portion of the (A) broadband ^1H decoupled, (B) single frequency off-resonance decoupled and (C) fully coupled 100.6 MHz ^{13}C spectra of cholesterol.

Table 1
Carbon Types and ^{13}C Chemical Shifts for Cholesterol

<u>Carbon^(a) Position</u>	<u>Carbon Type</u>	<u>Chemical^(b) Shift</u>
1	CH ₂	37.40
2	CH ₂	31.80
4	CH ₂	42.45
7	CH ₂	31.99
8	CH	32.06
9	CH	50.33
10	C	36.60
11	CH ₂	21.19
12	CH ₂	39.95
13	C	42.45
14	CH	56.91
15	CH ₂	24.34
16	CH ₂	28.25
17	CH	56.38
18	CH ₃	11.90
19	CH ₃	19.42
20	CH	35.85
21	CH ₃	18.78
22	CH ₂	36.31
23	CH ₂	23.93
24	CH ₂	39.61
25	CH	28.03
26	CH ₃	22.57
27	CH ₃	22.79

(a) Resonances from carbons 3, 5 and 6 fall outside the spectral window used.

(b) In ppm vs TMS. Obtained from Spectrum A in Figure 25.

The chemical shifts obtained from this study agree to within ± 0.3 ppm with those reported earlier [37]; the differences are most probably caused by concentration effects [38]. Spectrum C in Figure 17 is the ^{13}C spectrum of cholesterol measured with full proton coupling.

Resonances for methine, methylene and methyl carbons (CH , CH_2 and CH_3) give rise to doublets, triplets and quartets, respectively, due to coupling to the directly bonded ^1H nuclei. Longer range coupling is not resolved in Spectrum C. Because of the large number of resonances over the small spectral range there is extensive overlap of resonances making spectral interpretation difficult. In contrast, Spectrum A measured with complete proton decoupling consists of single resonances for each of the different carbons. In addition to the spectral simplification, sensitivity is increased since the intensity is concentrated in a single resonance rather than being distributed among the components of a multiplet. A further increase in sensitivity, up to a factor of approximately three, results when proton decoupling is used due to the nuclear Overhauser effect [39].

The use of this technique, however, results in the loss of assignment and structural information which is contained in the scalar couplings between the ^{13}C and ^1H

nuclei. Part of the coupling information can be retrieved for purposes of assigning resonances to methyl, methylene, methine and quaternary carbon sites with the single frequency off-resonance proton decoupling experiment (SFORD) [40,41]. In this technique, decoupler irradiation is applied at a frequency somewhat removed from the ^1H resonance frequency resulting in a reduction of the observed ^{13}C - ^1H couplings. As a result, the ^{13}C resonances are still split into multiplets due to coupling to directly bonded ^1H nuclei but the magnitude of the splitting is reduced. Thus, the resonance for a methyl carbon will be a quartet in the SFORD spectrum but the separation between the lines in the quartet is reduced. The SFORD spectrum for cholesterol is shown in Figure 17B. Some resonances in this spectrum can be assigned to CH , CH_2 and CH_3 carbons by the characteristic doublet, triplet and quartet patterns, for example the resonances at 50.33, 21.19 and 11.90 ppm, respectively. Although most of the multiplicities in Figure 17B are identifiable, ambiguities arise in the regions around 32 and 24 ppm. In the first case, overlapping resonances make the off-resonance spectrum virtually useless. In the second case, broadening of the signals is observed, probably due to second-order effects [42,43] resulting from the tightly coupled proton spectrum. Both situations will become more

severe at lower magnetic field strengths. Shifts of up to 0.08 ppm for carbons 9 and 17 (50.33 and 56.38 ppm) were detected between the center of the multiplet in the off-resonance spectrum and the shifts obtained in the noise-decoupled spectrum. These shifts are undoubtedly attributable to temperature sensitive shielding changes [44] induced by the lower proton decoupler power levels used in the off-resonance experiment. Comparisons made between the two experiments could lead to erroneous assignments especially in regions of high spectral congestion.

In this chapter, alternate methods for assigning ^{13}C resonances to carbon types (C, CH, CH_2 and CH_3) are devised based on the phenomenon of phase modulation of multiplet patterns in NMR spectra measured by the spin-echo method [22]. The assignment scheme is based on the differing phase modulation behavior of methyl, methylene, methine and quaternary carbon types. In addition, experiments are described with which subspectra containing resonances from only quaternary carbons, resonances from methylene and quaternary carbons or resonances from methyl and methine carbons can be obtained. Methods are also described for determining the magnitude of ^{13}C - ^1H spin-spin coupling constants based on the dependence of the phase modulation effects on $^1J_{^{13}\text{C}-^1\text{H}}$. The above

experiments are presented using cholesterol as an example to demonstrate their utility in characterizing ^{13}C NMR spectra.

The chapter begins with an application of the phase modulation phenomenon to determine the ^1H - ^1H spin-spin coupling constants in ^1H spectra. This is presented in order to introduce the important aspects of the phase modulation behavior of multiplets in spin-echo NMR spectra using a simpler spin system. Following the discussion of phase modulation in ^1H spin-echo spectra, the phenomenon is investigated in ^{13}C spin-echo NMR spectra.

B. Intensity Modulation of Singlets in Spin-Decoupled Spin-Echo Spectra

In FT NMR, the RF excitation pulses are generally nonselective so that all nuclei of a given type, for example ^1H or ^{13}C , are simultaneously affected. Consequently, as discussed in the introduction, the individual lines in ^1H - ^1H multiplet patterns are phase modulated in ^1H spin-echo FT NMR spectra. This is because the nonselective 180° pulse inverts the spin states of all ^1H nuclei so that the nuclei giving rise to the individual components of a multiplet pattern precess at different frequencies before and after the 180° pulse. The frequency of the phase modulation is a function of the ^1H - ^1H

spin-spin coupling constant as well as the type of multiplet. In fact, the different components of a multiplet will undergo phase modulation at different rates [15] as shown in Figures 11 to 13 and Table 2.

The nature of the phase modulation of multiplet patterns can be altered by spin decoupling. If phase modulation is allowed to occur during the two delay periods of the proton spin-echo experiment and then selective decoupling is applied during acquisition of the FID at the chemical shift of those protons causing the splitting of the multiplet, a collapsed singlet will be observed which is intensity modulated as a function of the delay time τ_2 . The observation and decoupling pulse sequences are shown in Figure 18. Figure 19 presents the case of an ^1H doublet caused by coupling to a methine proton. This doublet will be used to illustrate the intensity modulation resulting as τ_2 , expressed as a function of $1/J$, is varied. The upper portion of the figure shows the two components of the magnetization at the time of acquisition in the $x'-y'$ plane of a coordinate system rotating at a frequency midway between the precessional frequencies of the two components. The two components are represented by the vectors labeled f and s corresponding to the components precessing faster and slower than the $x'-y'$ plane. Initially, with $\tau_2 = 0$ the

Table 2
Phase Modulation Frequencies for Components of
Various Multiplet Types

<u>Multiplet Type</u>	<u>Component</u>	<u>Modulation Frequency</u>
Singlet	1	0
Doublet	1,2	J
Triplet	2	0
	1,3	2J
Quartet	2,3	J
	1,4	3J
Pentet	3	0
	2,4	2J
	1,5	4J
Sextet	3,4	J
	2,5	3J
	1,6	5J
Heptet	4	0
	3,5	2J
	2,6	4J
	1,7	6J

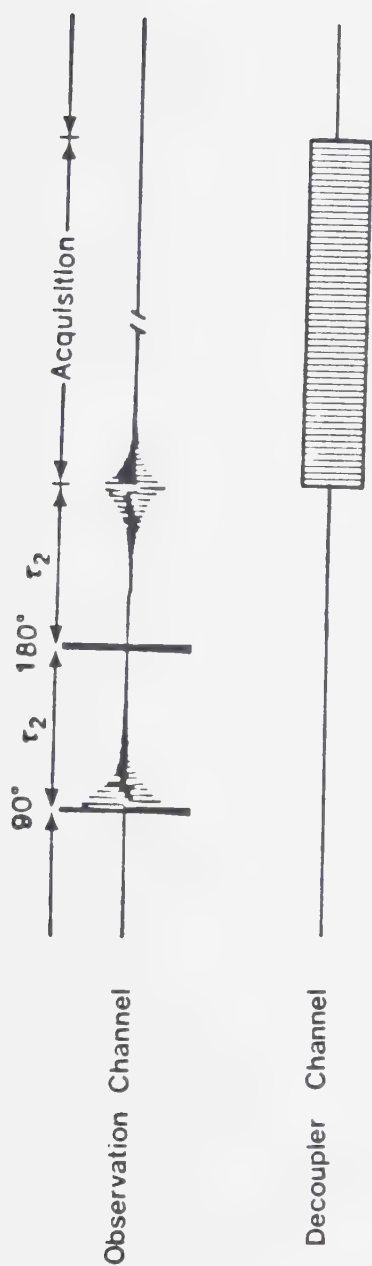


Figure 18. The observation and decoupling pulse sequences for the generation of intensity modulated, decoupled singlets in ^1H spectra. The 90° and 180° pulses of the observation channel are broadband while the decoupler irradiation is applied over a narrow frequency range centered at the resonance frequency of the ^1H nuclei coupled to the nuclei under observation.

Delay Time, τ_2

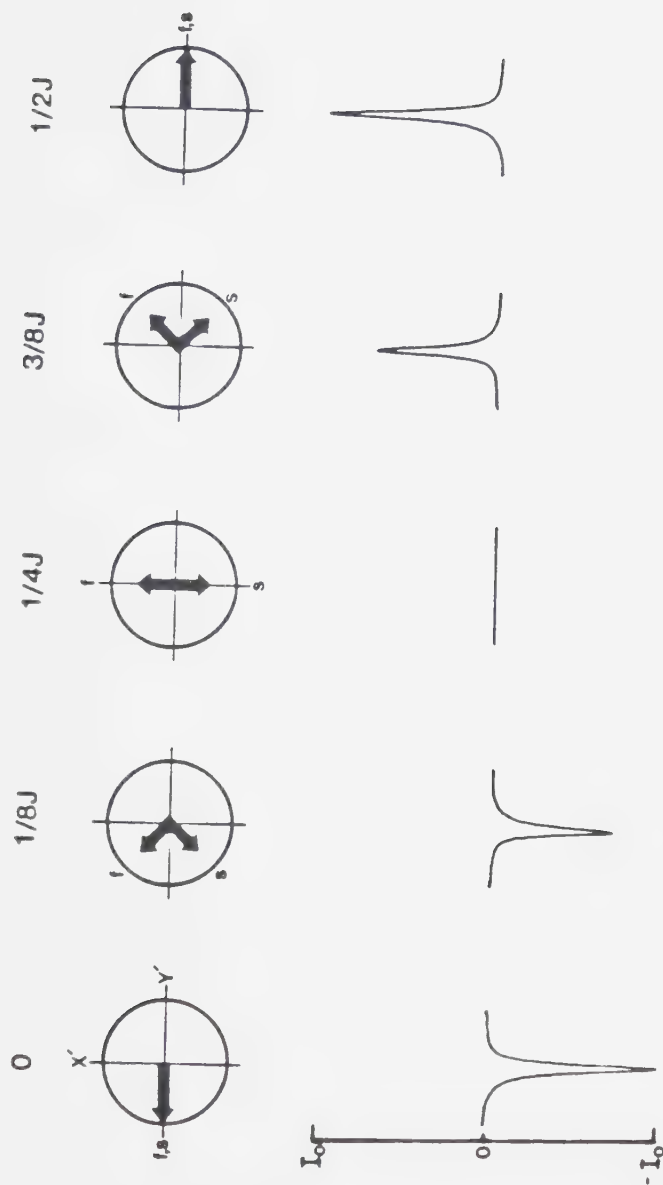


Figure 19. The intensity modulation behavior of the decoupled, ^1H singlet resulting from coupling to a methine proton at various τ_2 delay times. The top portion of the figure shows the orientation of the two components of the magnetization at acquisition while the bottom portion shows the decoupled singlet which results upon Fourier transformation.

two components are oriented together along the negative y' axis at the time of acquisition. If decoupling is applied during acquisition to the methine proton which splits the resonance into a doublet, a singlet of intensity $-I_0$ is obtained as shown in the lower part of Figure 19. As τ_2 is increased the different precessional frequencies of the doublet components cause them to diverge giving rise at acquisition to a decoupled singlet whose intensity corresponds to the vector sum of the two components on the y' axis. The successive frames of Figure 19 show the orientation of the doublet components at acquisition and the intensity of the resulting decoupled singlet as τ_2 is increased. This intensity modulation is a direct result of the phase modulation which the components of the multiplet are undergoing during the two delay periods and can be described by the relationships given in Table 3 for various multiplet types. These expressions also take into account the effects of spin-spin relaxation which occurs over the time interval $2\tau_2$.

The equations presented in Table 3 are derived from the phase modulation behavior of the individual components of a multiplet. For example, the two components of a doublet precess at frequencies of $J/2$ faster and $J/2$ slower than the y' axis rotating at a frequency midway between the precessional frequencies of the two

Table 3

Equations Describing the Intensity Modulation of
Decoupled Singlets for Various Multiplet Types

$$I = I_0 \exp(-2\tau_2/T_2^*) \chi^{(a,b)}$$

Multiplet Type	χ
Singlet	1
Doublet	$\cos(2\pi J\tau_2)$
Triplet	$\frac{1}{2} + \frac{1}{2} \cos(4\pi J\tau_2)$
Quartet	$\frac{3}{4} \cos(2\pi J\tau_2) + \frac{1}{4} \cos(6\pi J\tau_2)$
Pentet	$\frac{3}{8} + \frac{1}{2} \cos(4\pi J\tau_2) + \frac{1}{8} \cos(8\pi J\tau_2)$
Sextet	$\frac{5}{8} \cos(2\pi J\tau_2) + \frac{5}{16} \cos(6\pi J\tau_2) + \frac{1}{16} \cos(10\pi J\tau_2)$
Heptet	$\frac{5}{16} + \frac{15}{32} \cos(4\pi J\tau_2) + \frac{3}{16} \cos(8\pi J\tau_2) + \frac{1}{32} \cos(12\pi J\tau_2)$

(a) For homonuclear spin-spin coupling (e.g. ^1H - ^1H) or heteronuclear coupling (e.g. ^{13}C - ^1H) when measured by the spin-flip method.

(b) $\exp(-2\tau_2/T_2^*)$ takes account of spin-spin relaxation which occurs. T_2^* is the effective spin-spin relaxation time.

components. The phase difference of the doublet components, with respect to the y' axis, at time $2\tau_2$ following the initial 90° pulse of the spin-echo experiment is $\pm \cos(2\pi J\tau_2)$. The projection of the two magnetization vectors on the y' axis contributes to the resonance intensity in the spin-echo spectrum. Taking into account the effects of T_2 relaxation yields an intensity of:

$$I = I_0 e^{-(2\tau_2/T_2^*)} \cos(2\pi J\tau_2) \quad (15)$$

where T_2^* is the effective spin-spin relaxation time which includes contributions from diffusion and other effects on the measured T_2 relaxation time. Equations for the other multiplet types are derived in a similar manner.

C. Determination of ^1H - ^1H Coupling Constants from Intensity Modulated Spin-Echo Spectra

The intensity modulation behavior of decoupled singlets predicted by the equations in Table 3 is used in this section as the basis of a method for measuring ^1H - ^1H spin-spin coupling constants. The procedure involves measuring the intensity of the decoupled singlet for a series of τ_2 values. The intensity versus τ_2 data are

then fit by a non-linear least-squares procedure to the appropriate equation in Table 3 to obtain a value for ${}^3J_{1H-1H}$.

To illustrate the procedure for a variety of multiplet types, spin-spin coupling constants are determined for the compounds ethanol, alanine, 2-propanol and 3-pentanol. Ethanol provides an example of a triplet and a quartet, alanine a doublet and a quartet, 2-propanol a doublet and a heptet and 3-pentanol a pentet. To determine the coupling constant for each multiplet, 37 spin-echo spectra were recorded at τ_2 delay times ranging from 0.1 second to 0.37 second at intervals of 0.1 second. The data for the decoupled singlets resulting from the triplet (CH_3 protons) and quartet (CH_2 protons) of ethanol as well as the curves predicted by the parameters obtained from the non-linear least-squares fits are shown in Figure 20. The results for all the compounds are listed in Table 4 along with values for the ${}^1H-{}^1H$ coupling constants measured directly from single-pulse spectra for comparison. In all cases, the ${}^3J_{1H-1H}$ values obtained from the intensity modulation behavior agree with those measured directly within the uncertainty limits of the experimental techniques.

Although the ${}^1H-{}^1H$ spin-spin coupling constants for the examples given here can be measured directly from the

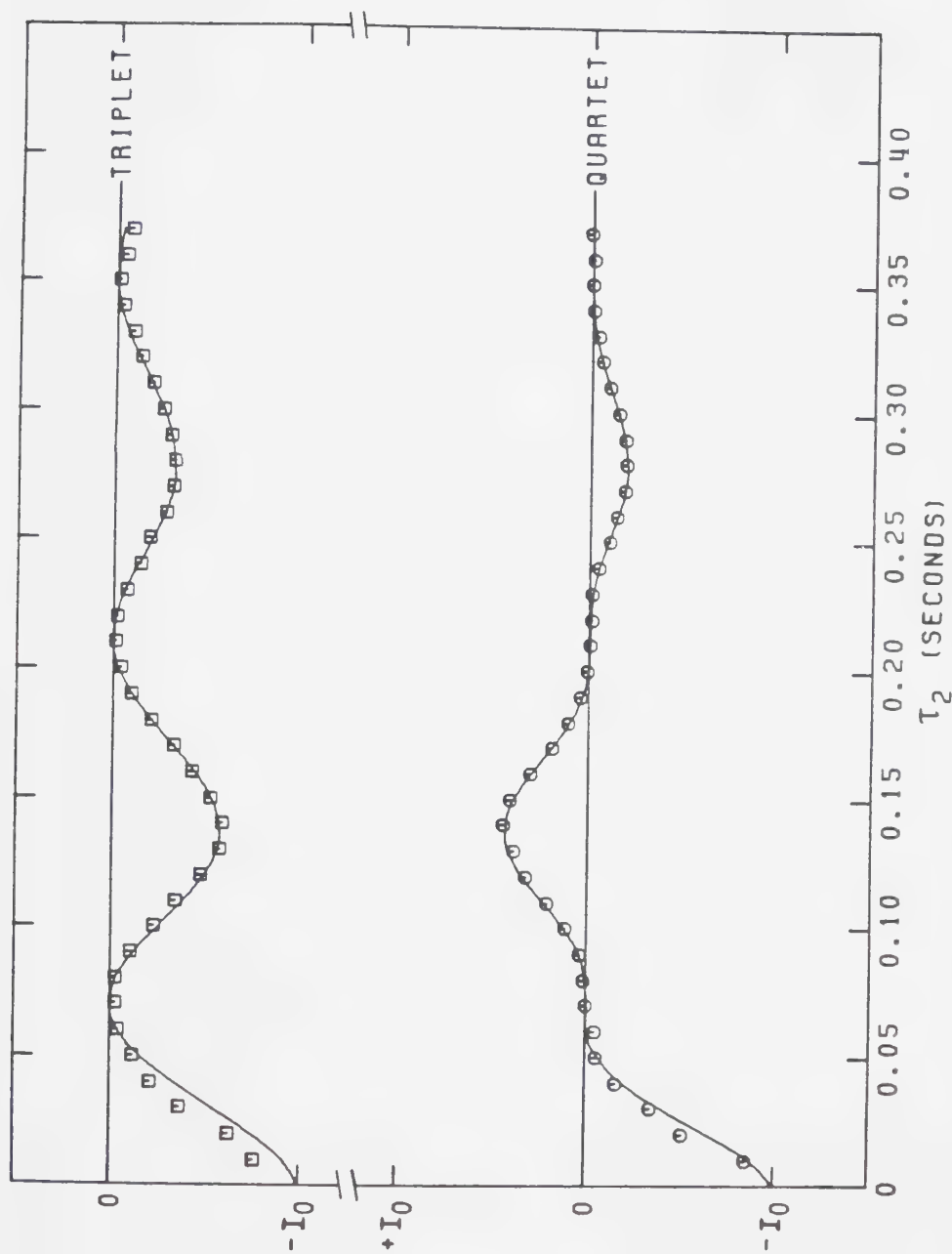


Figure 20. Fits of intensity versus τ_2 data sets for the intensity modulated, decoupled singlets resulting from the CH_3 (triplet) and CH_2 (quartet) protons of ethanol. The solid lines are the non-linear least-squares results derived by using the equations in Table 3 to fit the experimental data.

Table 4

Three-Bond ^1H - ^1H Coupling Constants for Various Compounds

Compound	Multiplet Type	$^3J_{^1\text{H}-^1\text{H}}$ (a)	$^3J_{^1\text{H}-^1\text{H}}$ (b)
Ethanol	Triplet	7.10	7.08 ± 0.07
	Quartet	7.10	7.04 ± 0.03
Alanine	Doublet	7.20	7.31 ± 0.04
	Quartet	7.20	7.36 ± 0.40
2-Propanol	Doublet	6.21	6.22 ± 0.04
	Heptet	6.21	6.16 ± 0.60
3-Pentanol	Pentet	6.10	6.26 ± 0.28

(a) In Hz. Measured directly from single-pulse spectra. Uncertainty of 0.24 Hz due to digital resolution.

(b) Determined indirectly by fitting intensity modulated, decoupled ^1H singlets to the equations given in Table 3. The uncertainty estimates given are the standard error estimates calculated by the non-linear least-squares program.

single-pulse spectrum, that is not always the case. For example, resolution may not be sufficient if the coupling constants are small or if the resonances are naturally broad, as is often the case in the ^1H spectra of proteins. In such cases, the method described above is useful. It should be mentioned that less precise estimates of the coupling constants can be obtained directly from the intensity modulation behavior by using the delay time at which the intensity of the singlet is at a null. For example, for a triplet the first null occurs at $\tau_2 = 1/4J$.

D. Phase and Intensity Modulation in ^{13}C Spectra

In this section, phase and intensity modulation of resonances in ^{13}C spectra measured by the spin-echo method will be discussed. The pulse sequence and various decoupler timing schemes for these experiments are shown in Figure 21. Nonselective pulses are applied to the carbon spins while the ^1H decoupler will be considered to be broadband. In all the sequences shown in Figure 21, the decoupler is on between repetitions of the pulse/acquisition sequence to achieve nuclear Overhauser enhancement [39].

As discussed in Chapter I, ^{13}C spectra measured by the spin-echo pulse sequence with broadband ^1H decoupling

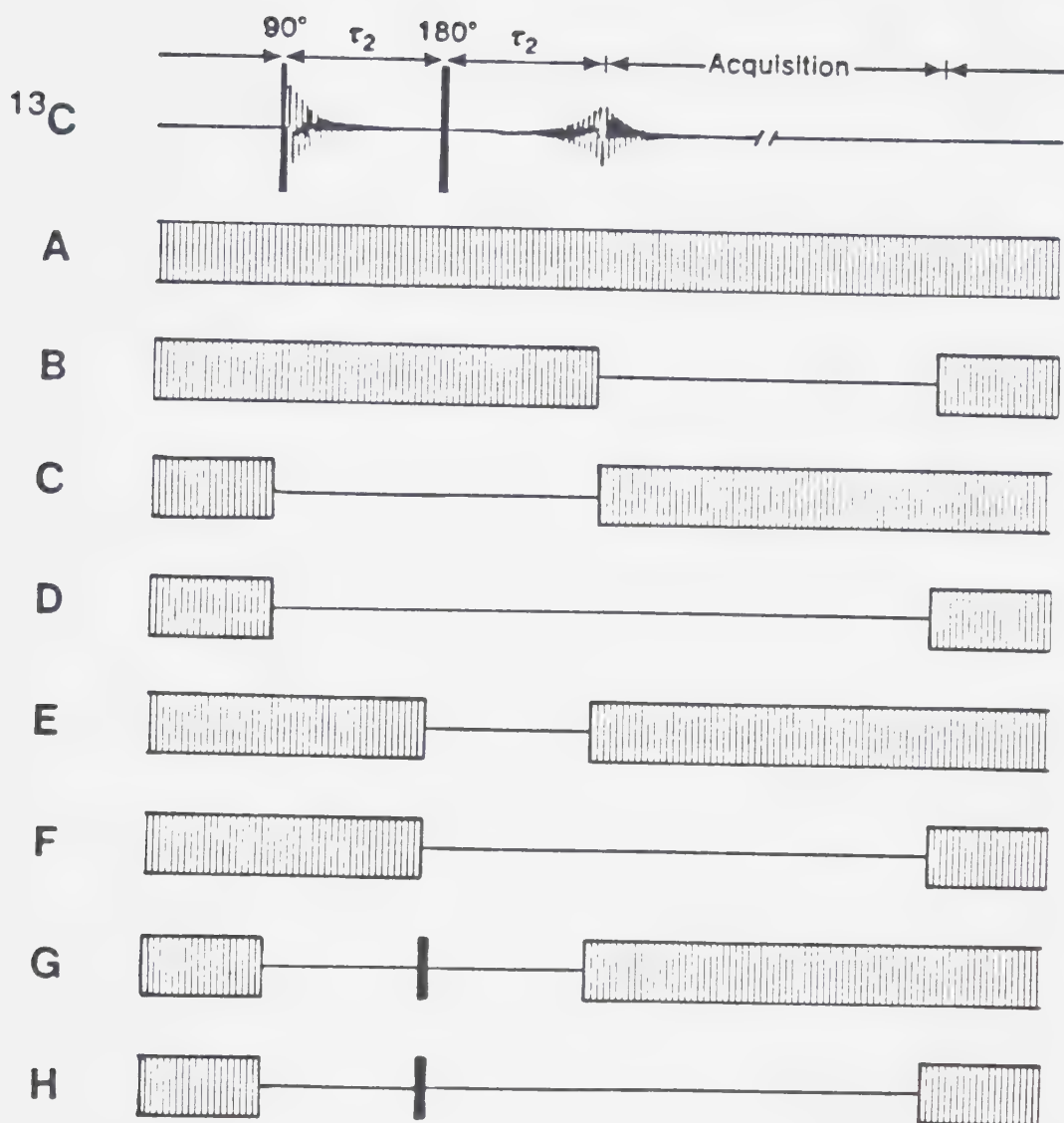


Figure 21. The ^{13}C spin-echo pulse sequence (top) with various ^1H decoupler schemes, A to H.

throughout the pulse sequence and acquisition (decoupler scheme A) consist of singlets all in phase with each other. In order to observe phase modulation effects in ^{13}C spin-echo spectra, it is necessary to modify the decoupling so that the precessional frequency of the different components of a ^{13}C multiplet are different during the two delay periods. This can be accomplished in two ways: i) by applying a 180° ^1H pulse simultaneously with the 180° ^{13}C pulse with the broadband ^1H decoupler off during the delay periods, the spin-flip method [45] (decoupler schemes G and H) or ii) by gating the broadband ^1H decoupler off during one of the two delay periods, the gated decoupling method [15,18] (decoupler schemes E and F).

If broadband ^1H decoupling is applied during both delay periods (decoupler scheme A or B in Figure 21), no phase modulation occurs since the average precessional frequency for a particular ^{13}C nucleus is the same during both delay periods. This is illustrated schematically for a ^{13}C doublet (CH) in Figure 22A. The resulting signal obtained at acquisition will appear as an inverted singlet (decoupler scheme A) or as an inverted, in-phase multiplet (decoupler scheme B). If ^{13}C spectra are measured with the ^1H decoupler off during the spin-echo pulse sequence and gated on during acquisition (decoupler scheme C) or

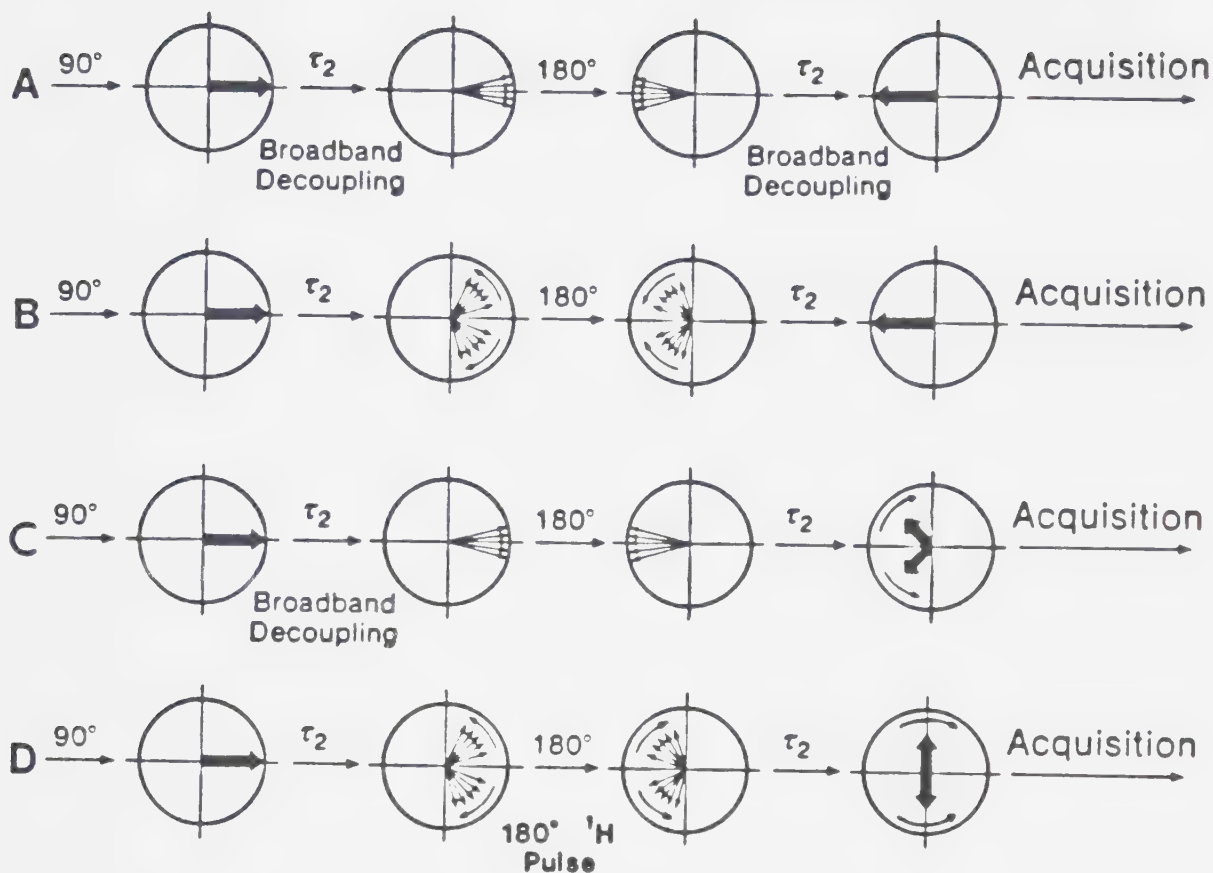


Figure 22. Vector representations of the magnetization from a methine carbon during the spin-echo pulse sequence with (A) broadband decoupling during both evolution periods, (B) no decoupling, (C) broadband decoupling during the first evolution period and (D) a 180° ^1H pulse applied simultaneously with the 180° ^{13}C pulse. The magnetization is in the $x'-y'$ plane of a coordinate system rotating at a frequency midway between the two precessional frequencies of a coupled methine carbon.

with the decoupler off during both the pulse sequence and acquisition (decoupler scheme D), the dephasing of the ^1H coupled ^{13}C nuclei during the first half of the experiment will be refocussed in the second half as illustrated in Figure 22B. The two components of the doublet schematically represented here have coalesced at time $2\tau_2$ because the same component of the doublet is precessing more rapidly both before and after the 180° pulse. If, however, the broadband ^1H decoupler is on during only one of the two evolution periods, for example the evolution period following the 90° pulse as represented by decoupler schemes E and F of Figure 21, the individual components of a multiplet can be out of phase with respect to each other at time $2\tau_2$ in which case phase modulation will be observed in the resulting spectrum. The behavior of the magnetization from the two components of a ^{13}C doublet in such an experiment with $\tau_2 = 1/4J$ is shown schematically in Figure 22C. During the evolution period following the 90° pulse, the two components precess as a singlet because of ^1H decoupling and the magnetization is defocussed because of magnetic field inhomogeneity. Following the 180° pulse, the decoupler is gated off and the two components precess at different frequencies. With $\tau_2 = 1/4J$, they are $\pm 45^\circ$ out of phase with the negative y' axis at the start of acquisition. If the decoupler is gated on

at the start of acquisition (decoupler scheme E), a negative singlet of reduced intensity will result. If the decoupler is left off during acquisition (decoupler scheme F), a doublet with both components out of phase is obtained.

With the spin-flip method [45] (decoupler schemes G and H), the decoupler is off during the delay periods. Phase modulation is caused by applying a broadband 180° ^1H pulse simultaneously with the 180° ^{13}C pulse. As a result, the ^{13}C nuclei which precessed faster before the 180° pulses precess slower after the pulses and vice versa. This is shown by sequence D in Figure 22. This happens because the ^{13}C nuclei are coupled to ^1H nuclei in opposite spin states before and after the 180° pulses. It should be noted from the figure that the phase modulation frequency in spectra measured by the spin-flip method is twice that of spectra measured by the gated decoupling method since the components of the multiplet are dephasing during both of the delay periods.

With decoupler schemes E to H of Figure 21, the relative phase of the components of a multiplet at time $2\tau_2$ after the 90° pulse depends on the length of τ_2 relative to $1/J$. Figure 23 shows these phase relationships for the components of the various types of ^{13}C multiplets as a function of the delay time τ_2 for the

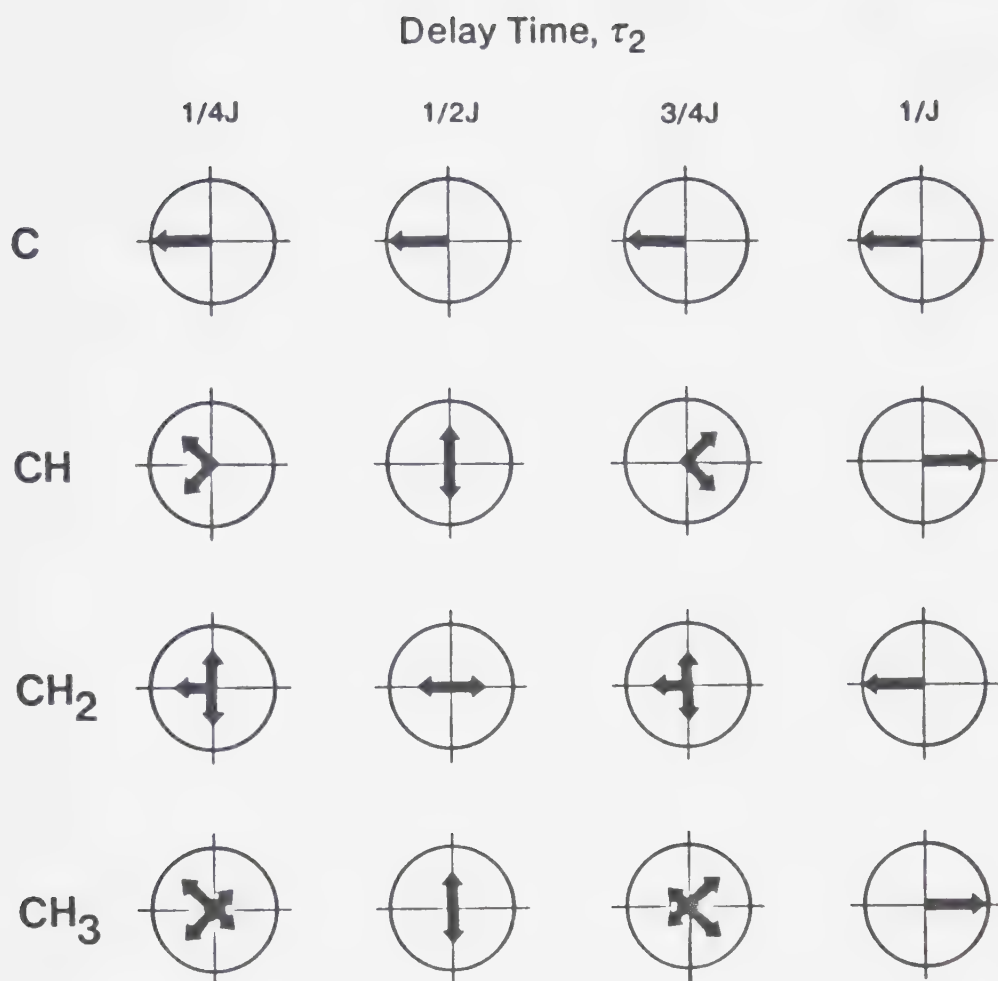


Figure 23. Vector representations of the magnetization from quaternary, methine, methylene and methyl carbons following the ^{13}C spin-echo pulse sequence in Figure 21 with decoupler scheme E or F. The diagrams show the magnetization at the start of acquisition as a function of the length of the delay time.

gated decoupling experiment (decoupler schemes E and F of Figure 21). If the spin-flip technique is used, the corresponding τ_2 delay times will be halved. It should be noted that quaternary carbons do not undergo phase modulation since they have no directly bonded protons to cause ^{13}C - ^1H spin-spin coupling. From these diagrams, it can be seen that the singlet obtained for a methine carbon measured with decoupler scheme E is inverted at a τ_2 of $1/4J$. The singlet will be of reduced intensity since the intensity is the vector sum of the components along the y' axis. At a τ_2 delay of $1/2J$, the resonances will have zero intensity since the two components lie along the positive x' and negative x' axis and thus cancel when ^1H decoupling is applied. At a τ_2 of $3/4J$, the singlet is positive and of reduced intensity while at a τ_2 of $1/J$, it is positive and of full intensity, neglecting T_2 relaxation. With decoupler scheme F, multiplet patterns are observed, however, the individual lines are phase modulated because the individual components of the nuclear magnetization are out of phase at the start of acquisition as illustrated in Figure 23.

The diagrams of Figure 23 also show the relative positions in the x' - y' plane of the nuclear magnetization giving the individual components of CH_2 and CH_3 multiplet patterns at the time of acquisition. It can be seen that

the singlet obtained from a methylene carbon with broadband ^1H decoupling during acquisition will be inverted, go to zero at $\tau_2 = 1/2J$ and then grow as an inverted signal as τ_2 is increased up to $1/J$. The ^1H decoupled singlet for a methyl carbon will also be inverted, go to zero at $\tau_2 = 1/2J$ but then grow as a positive singlet as τ_2 is increased up to $1/J$. Equations describing the intensity modulation behavior for the gated broadband decoupling experiment are presented in Table 5. Included in these expressions is a term accounting for spin-spin relaxation effects. These equations are derived in the same manner as those presented in the previous section and listed in Table 3. The intensity modulation as a function of τ_2 predicted by these equations, neglecting T_2 relaxation, is shown in Figure 24 for the various types of carbon multiplets caused by coupling to directly bonded protons. The intensity or phase modulation caused by these directly bonded coupling interactions is the largest of all the ^{13}C - ^1H couplings and dominates the modulation behavior in ^{13}C spin-echo spectra measured with decoupler schemes E to H of Figure 21.

Table 5

Equations Describing the Intensity Modulation of

 ^1H Decoupled, ^{13}C Singlets

$$I = I_0 \exp(-2\tau_2/T_2^*) \chi^{(a)}$$

Carbon Type	χ
Quaternary (C)	1
Methine (CH)	$\cos(\pi\tau_2J)$
Methylene (CH_2)	$\frac{1}{2} + \frac{1}{2} \cos(2\pi\tau_2J)$
Methyl (CH_3)	$\frac{3}{4} \cos(\pi\tau_2J) + \frac{1}{4} \cos(3\pi\tau_2J)$

(a) Measured by the gated decoupling method.

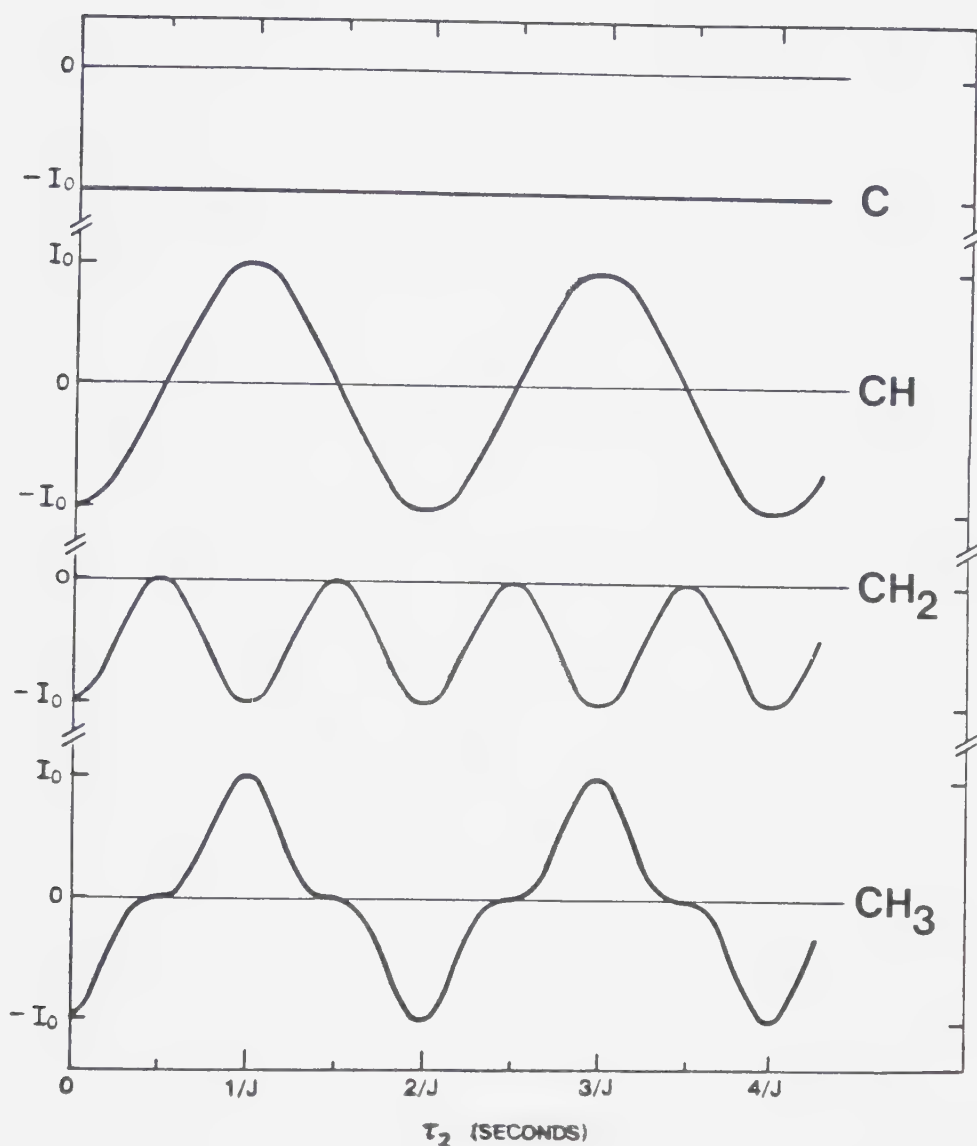


Figure 24. Calculated intensities, neglecting T_2^* relaxation, of quaternary, methine, methylene and methyl carbon resonances in spin-echo spectra measured with decoupler scheme E in Figure 21 as a function of the length of the delay time.

E. Assignment of Carbon Types

In this section, a method is developed for assigning ^{13}C resonances to methyl, methylene, methine and quaternary carbon types [22]. The method is based on the intensity modulation of ^1H decoupled ^{13}C singlets in spin-echo spectra. The modulation could be generated using either the spin-flip or the gated decoupling methods. The gated decoupling technique was used in this work because of several factors. First, with the spin-flip method, the ^1H power level for a 180° ^1H pulse must be somewhat higher than the ^1H power level required for broadband decoupling. Thus, this experiment is more difficult as it requires changing the ^1H power levels during the pulse sequence. Second, the spin-flip method requires that the power of the ^1H pulse be uniform over the entire ^1H spectral region, which is extremely difficult to achieve.

The strategy of the method developed can be seen by comparison of the different curves in Figure 24. Specifically, the intensity and the sense of the singlets depend on the carbon type. With three experiments, this dependence can be used to assign carbon resonances according to carbon type. In the first experiment, quaternary and methylene carbons are distinguished from methine and methyl carbons by measuring the spin-echo spectrum with $\tau_2 = 1/J$. As can be seen from Figure 24,

resonances from quaternary and methylene carbons are negative in intensity while those from methine and methyl carbons are of positive intensity. In the next experiment, resonances for quaternary carbons are distinguished from those for methylene carbons by measuring the spin-echo spectrum using a τ_2 of $1/2J$. Examination of Figure 24 shows that at this delay time the ^1H decoupled singlets for CH , CH_2 and CH_3 carbons are nulled, whereas the resonances for quaternary carbons are still negative. In the third experiment, resonances for methyl carbons are distinguished from those for methine carbons. Examination of the curves for CH and CH_3 carbons in Figure 24 shows that there is no delay time at which their intensities are radically different in order to easily distinguish CH from CH_3 carbons. The major differences occur around the null points; that is, the intensity changes rapidly with delay time in the region of the null point for the CH carbons, whereas the change is more gradual for the CH_3 carbons. CH carbons can be distinguished from CH_3 carbons using this difference in behavior. The simplest way is to measure a spin-echo spectrum using the largest τ_2 delay at which the intensity of the CH_3 resonance is still near zero, for example, approximately $3/5J$. At this delay time, the intensity of a singlet for a CH carbon is $0.309 I_0$ whereas that for a

CH₃ carbon is 0.030 I₀. The disadvantage of this experiment, however, is that the spectrum will contain resonances from quaternary and methylene carbons which might interfere with the assignment if they appear close to the CH and CH₃ resonances. A better procedure is to eliminate resonances for the C and CH₂ carbons by doing a difference experiment. The difference experiment is based on the fact that the intensity of C and CH₂ resonances is the same at delay times equally spaced on either side of the null point, whereas those for CH and CH₃ carbons are of opposite sign. Thus, if a spectrum measured with a delay of $\tau_2 = 1/2J - a$, where $1/2J$ is the delay time at the null point, is subtracted from a spectrum measured with a τ_2 of $1/2J + a$ the C and CH₂ resonances are cancelled whereas the CH and CH₃ resonances are additive. Calculations show that $2/5J$ and $3/5J$ are appropriate for the two delay times. With these delay times, the intensity of the CH resonance will be 0.618 I₀ and that of the CH₃ resonance will be 0.059 I₀ in the difference spectrum.

Application of these experiments will be described later using cholesterol as an example. First, however, it is necessary to consider the magnitude of ¹³C-¹H coupling constants since they determine the delay times used in these experiments. Extensive tables of ¹³C-¹H coupling

constants are given by Stothers [46]. Representative examples are listed in Table 6. Examination of the table indicates that the magnitude of $^1J_{^{13}\text{C}-^1\text{H}}$ depends upon the hybridization of the carbon as well as the nature of any heteroatoms bonded to the carbon. Coupling constants for the sp^3 hybridized carbons in Table 6 are around 125 hertz suggesting that this can be taken as a typical value for sp^3 hybridized carbons. The effect of small differences from this value on assignments made by this method are discussed later. The coupling constants for sp^2 hybridized carbons are generally larger and vary over a much wider range, however, the assignment of these carbons is usually more straightforward than for sp^3 hybridized carbons and other techniques can be used.

The three experiments described above will be illustrated by assigning the ^{13}C resonances of cholesterol to carbon types. The spectra are presented in Figure 25. In the experiments, an average $^1J_{^{13}\text{C}-^1\text{H}}$ of 125 hertz was used. Figure 25A presents the ^{13}C spin-echo spectrum obtained with decoupler scheme E of Figure 21 using a τ_2 delay of 0.008 second, corresponding to $1/J$. The methyl and methine carbon resonances are positive and the methylene and quaternary resonances are negative. Figure 25B shows the spin-echo spectrum at a τ_2 delay of 0.004 second, corresponding to $1/2J$. At this τ_2 delay, the

Table 6
Representative One-Bond ^{13}C - ^1H Coupling Constants for
Various Carbon Hybridization States

Hybridization State	Compound	$J_{^{13}\text{C}-^1\text{H}}$ (a)
sp^3	CH_4	125
	CH_3CH_3	125
	$\text{C}(\text{CH}_3)_4$	124
	$(\text{CH}_3)_2\text{C}=\text{C}(\text{CH}_3)_2$	124
	$\text{CH}_3\text{C}\equiv\text{CCH}_3$	131
	HOCH_3	142
	HCOCH_3	127
	CH_3COCH_3	127
	ØCOCH_3	126
	HOCOCH_3	129
	CNCH_3	145
	$\text{N}(\text{CH}_3)_3$	132
	1,4-Dioxane	142
sp^2	$\text{CH}_2=\text{CH}_2$	157
	HCHO	172
	3,3-Dimethylcyclopropene	221 (C-1)
	Cyclohexene	157 (C-1)
	Benzene	159
	Imidazole	208 (C-2) 190 (C-4, 5)
	Pyridine	180 (C-2, 6) 157 (C-3, 5) 160 (C-4)
sp	$\text{CH}\equiv\text{CH}$	249

(a) In Hz. Data taken from Stothers [46].

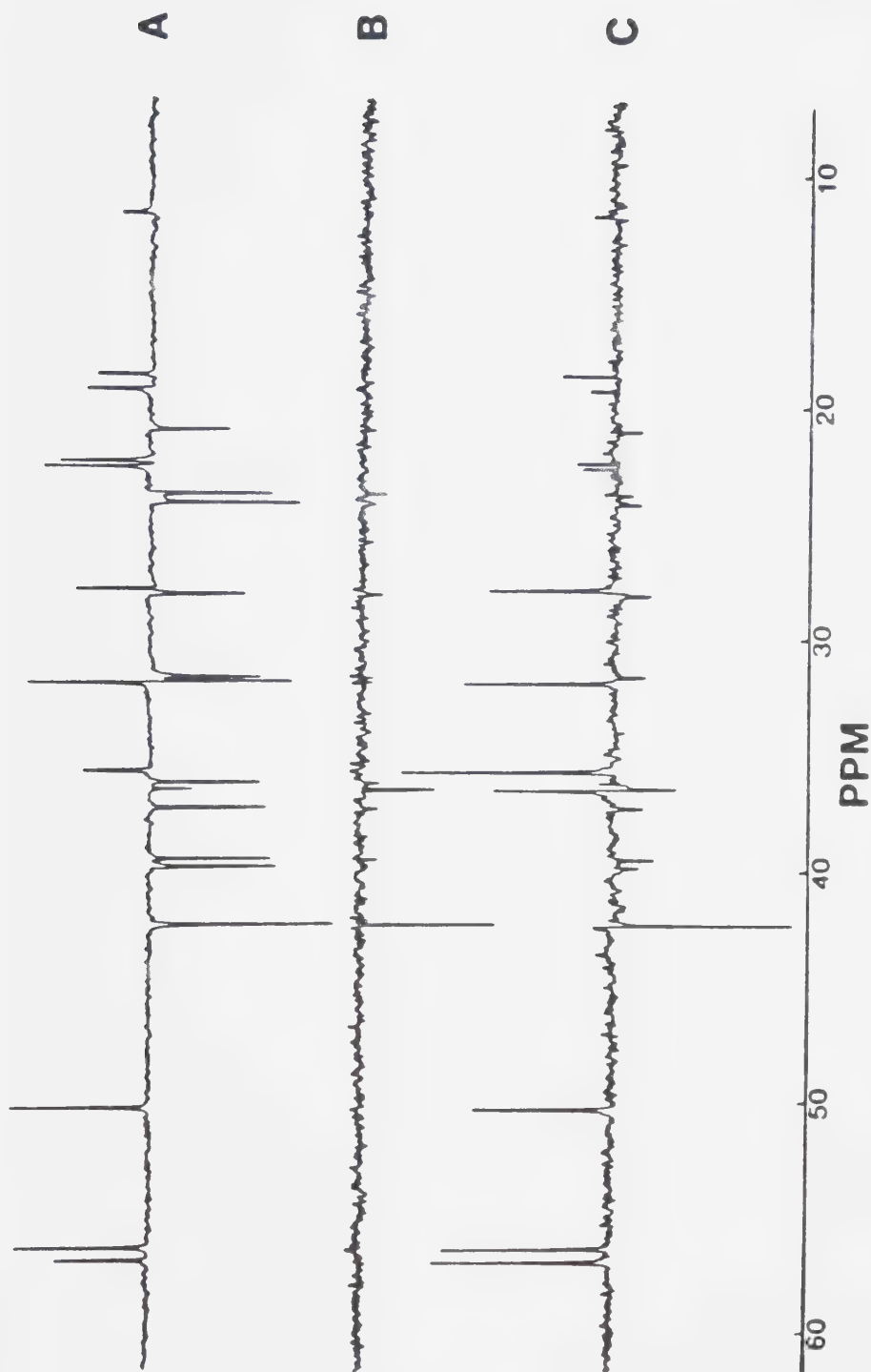


Figure 25. The high field portion of the ^{13}C spin-echo spectra of cholesterol measured with decoupler scheme E in Figure 21. (A) was measured with $\tau_2 = 0.008$ second, (B) is the difference spectrum obtained by subtracting the FID collected with $\tau_2 = 0.0032$ second from that collected with $\tau_2 = 0.0048$ second and (C) was measured with $\tau_2 = 0.004$ second.

spectrum contains only resonances from quaternary carbons allowing the assignment of the other negative resonances in Spectrum A to methylene carbons. The assignment of resonances to carbon types is completed with Figure 25C which shows the spin-echo difference spectrum obtained by subtracting the $\tau_2 = 0.0032$ second (2/5J) FID from the $\tau_2 = 0.0048$ second (3/5J) FID. Spectrum C was obtained by Fourier transformation of the difference FID. As described above, this experiment distinguishes between resonances from methine and methyl carbons. Thus, from the spectrum in Figure 25C, we can clearly determine that of the positive resonances in Figure 25A those at 56.91, 56.38, 50.33, 35.85, 32.06 and 28.03 ppm are attributable to methine carbons.

Since the delay times used in the three experiments described above were chosen for $^1J_{^{13}\text{C}-^1\text{H}}$ of 125 hertz, it is necessary to consider if erroneous assignments would be made if the coupling constants were different from this value. To answer this question, the intensities that would be obtained for C, CH, CH₂ and CH₃ carbons in each of these experiments were calculated as a function of the coupling constant when delays are chosen for a coupling constant of 125 hertz. The results of the calculations for the first experiment in which methine and methyl carbons are distinguished from quaternary and methylene

carbons are presented in Figure 26. It is clear from these results that the maximum intensities, both positive and negative, are obtained when the coupling constant is 125 hertz. However, these results also indicate that erroneous assignment of resonances to the C, CH₂ and the CH, CH₃ classes is unlikely since the resonances for C and CH₂ carbons are negative as J varies from 80 to 170 hertz and those for CH and CH₃ carbons are positive over this range. The results of the calculations for the second experiment in which quaternary carbons are distinguished from methylene carbons are shown in Figure 27. Again, these results show that an erroneous assignment is unlikely unless the coupling constant is very different from 125 hertz. At the extremes of the range of coupling constants shown, resonances for the methylene carbons never become greater than 29% of their full intensity. The results of the calculations for the third experiment are shown in Figure 28. In this experiment, an erroneous assignment of a resonance to a CH₃ carbon rather than a CH carbon or vice versa could occur if the intensity of a CH₃ resonance is similar to that of a CH resonance. The curves in Figure 28 indicate this is the case at the extremes of the coupling constant range shown. However, these curves show that for the coupling constant range typical of sp³ carbons (see Table 6) the CH resonance is

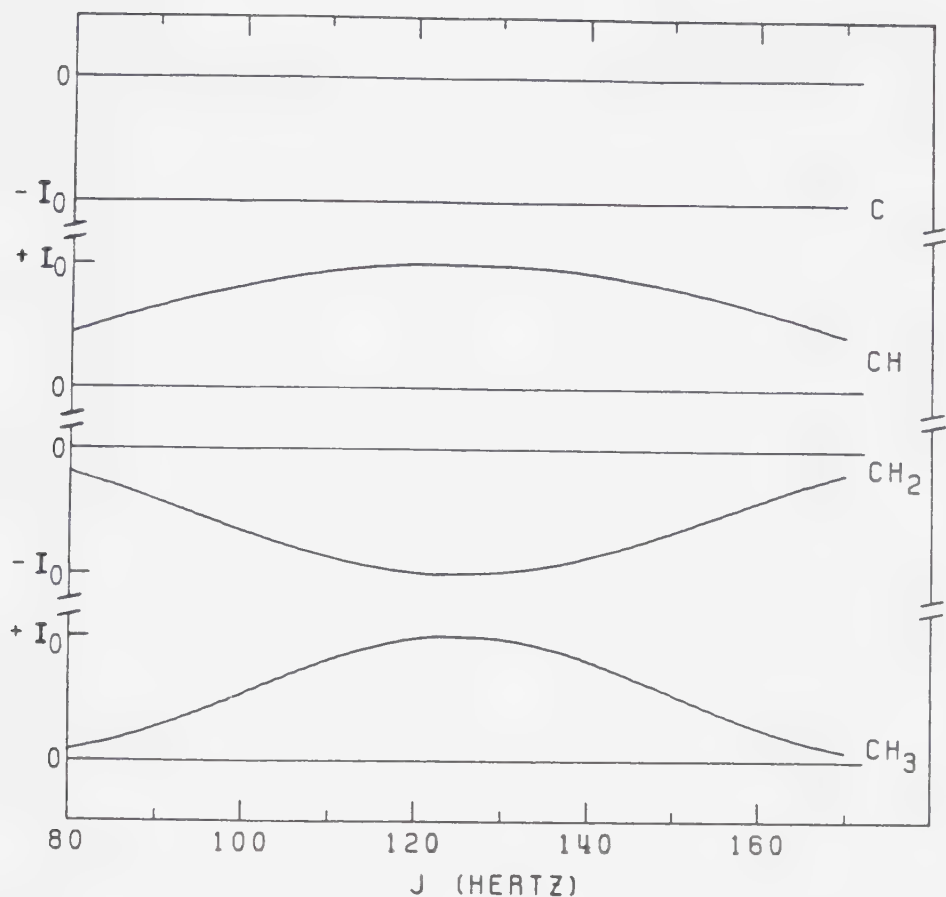


Figure 26. The intensity of ^1H decoupled, ^{13}C singlets resulting from a spin-echo experiment with $\tau_2 = 0.008$ second and decoupler scheme E of Figure 21 as a function of $^1J_{^{13}\text{C}-^1\text{H}}$ for the various carbon types.

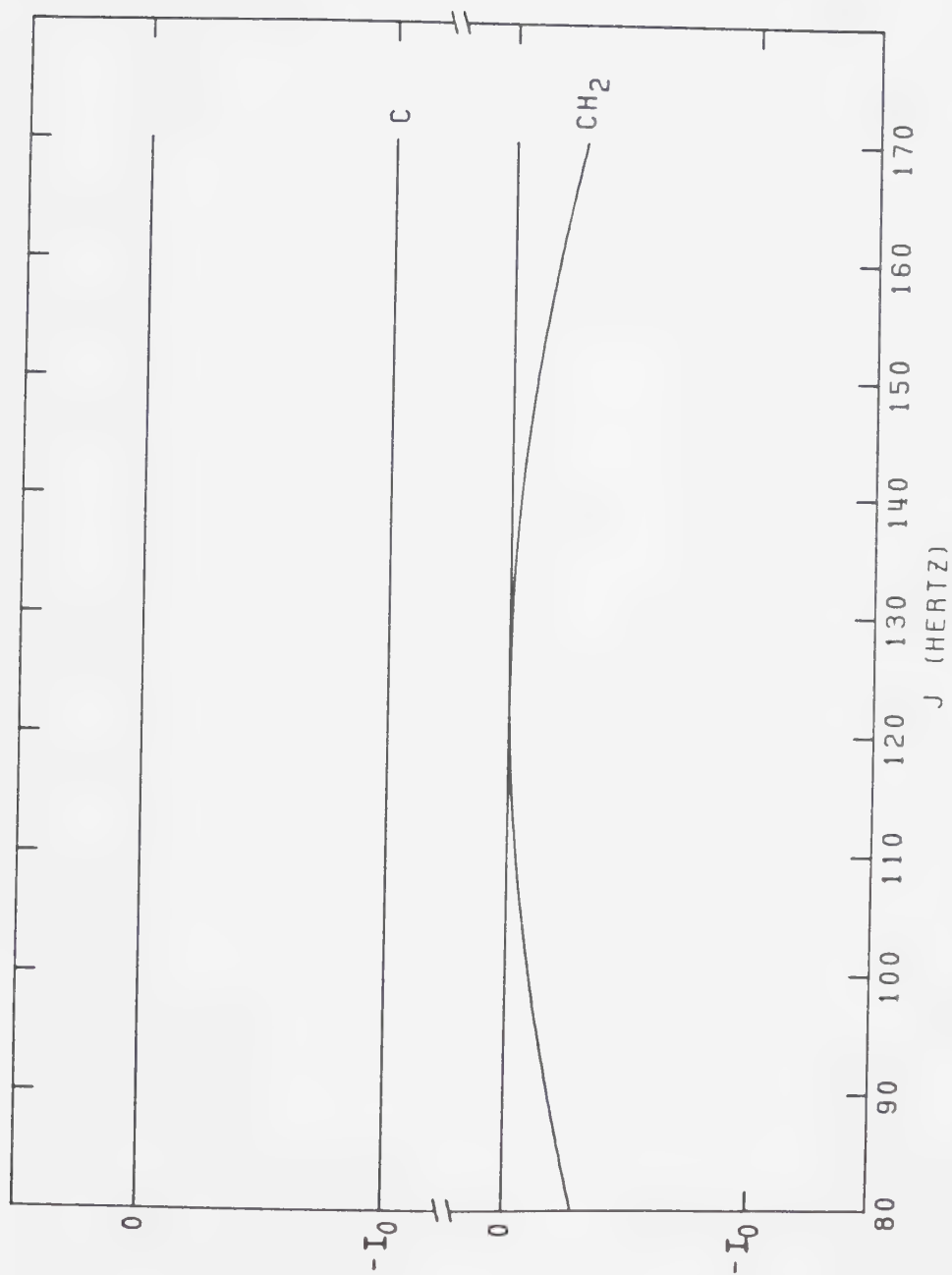


Figure 27. The intensity of ^1H decoupled, ^{13}C singlets for quaternary (C) and methylene (CH_2) carbons measured by a spin-echo experiment with $\tau_2 = 0.004$ second and decoupler scheme E of Figure 21 as a function of $^1J_{^{13}\text{C}-^1\text{H}}$.

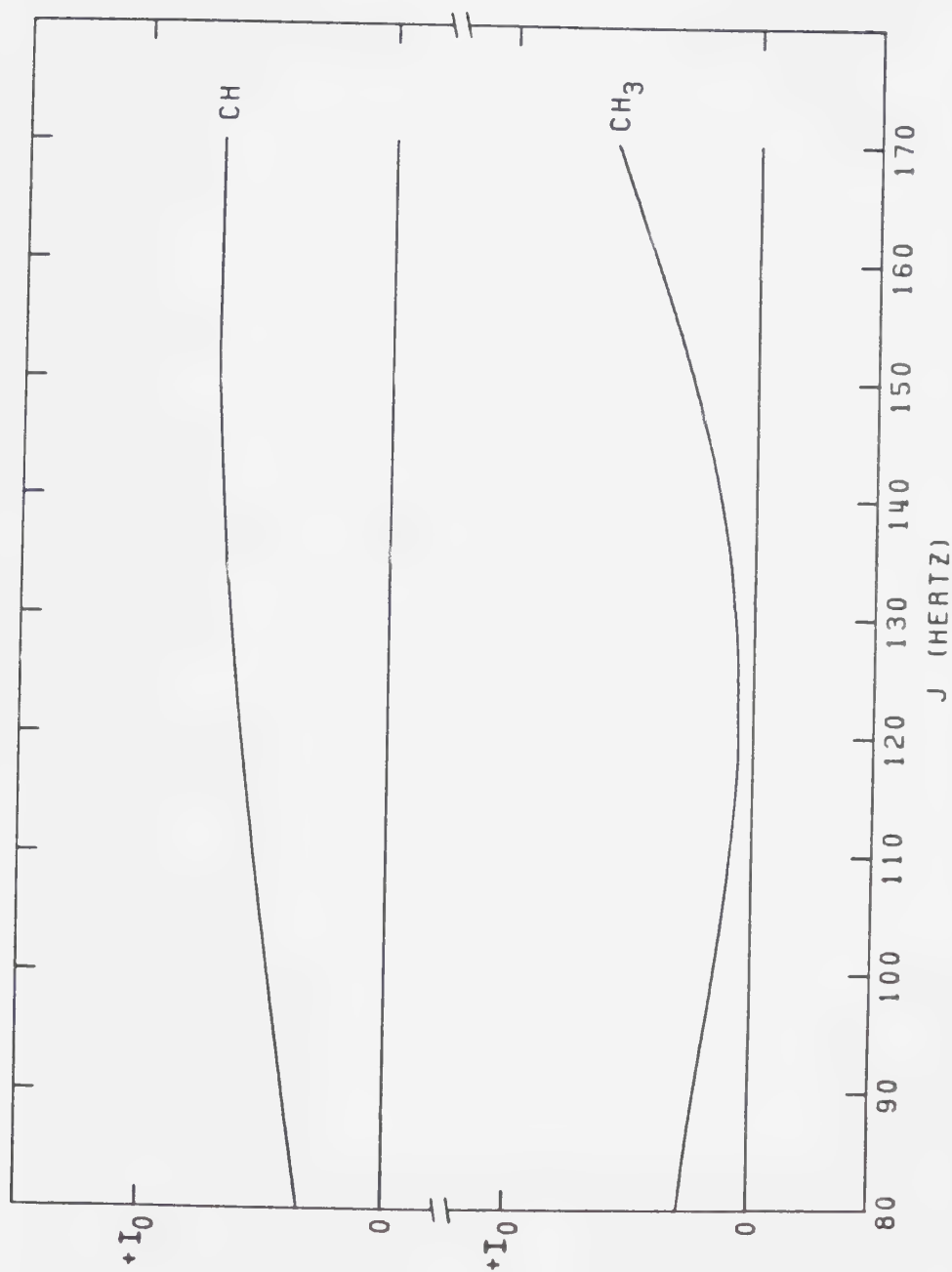


Figure 28. The intensity of 1H decoupled, ^{13}C singlets for methine (CH) and methyl (CH_3) carbons measured by a spin-echo difference experiment, conducted by subtracting the FID measured at $\tau_2 = 0.0032$ second from the FID measured at $\tau_2 = 0.0048$ second using decoupler scheme E of Figure 21, as a function of $^1J_{^{13}C-^1H}$.

considerably more intense and thus an erroneous assignment is unlikely. For example, the intensity of a CH resonance having a $^1J_{^{13}\text{C}-^1\text{H}}$ of 105 hertz is $0.505 I_0$, whereas that for a CH_3 resonance is $0.120 I_0$, while for a coupling constant of 145 hertz the intensity of a CH resonance is $0.690 I_0$ and that of a CH_3 is $0.194 I_0$.

F. Generation of Subspectra

As described above, a subspectrum containing only resonances from quaternary carbons can be obtained with the spin-echo experiment using a τ_2 delay of $1/2J$ and decoupler scheme E or F of Figure 21. This provides considerable spectral simplification if one is only interested in quaternary resonances. In this section, additional methods are described for spectral simplification through the measurement of subspectra containing resonances from either methylene and quaternary carbons or methyl and methine carbons [22]. The basis of the method is the phase modulation of resonances in spin-echo spectra.

The subspectrum containing resonances for methylene and quaternary carbons can be obtained by adding the spin-echo spectrum obtained with decoupler scheme E to that obtained with decoupler scheme A at a delay time of

$\tau_2 = 1/J$. At this delay time, the resonances in the first spectrum are negative for quaternary and methylene carbons and positive for methine and methyl carbons, whereas in the second spectrum the resonances are all negative. Thus, in the spectrum obtained by addition, the intensities of the quaternary and methylene carbons are additive giving an intensity of $-2I_0$, whereas those for the methine and methyl carbons cancel. Subtraction of the same two spectra will result in a subspectrum for the other carbon resonances.

Figure 29 shows the subspectra measured for cholesterol by the subtraction of the two spin-echo spectra described above (Figure 29A) and by the addition of the two spin-echo spectra (Figure 29B). The two spin-echo spectra were measured using a τ_2 delay of 0.008 second, corresponding to an optimal $^1J_{^{13}\text{C}-^1\text{H}}$ of 125 hertz. The top subspectrum in Figure 29 contains the methyl and methine carbon resonances while the bottom one contains the methylene and quaternary carbon resonances. The procedure used to obtain these subspectra involved performing the two different spin-echo experiments in alternate scans. The FIDs for the two experiments were collected in different regions of memory. Spectrum A was obtained by subtracting the FID measured with decoupler scheme A from that measured with decoupler scheme E and

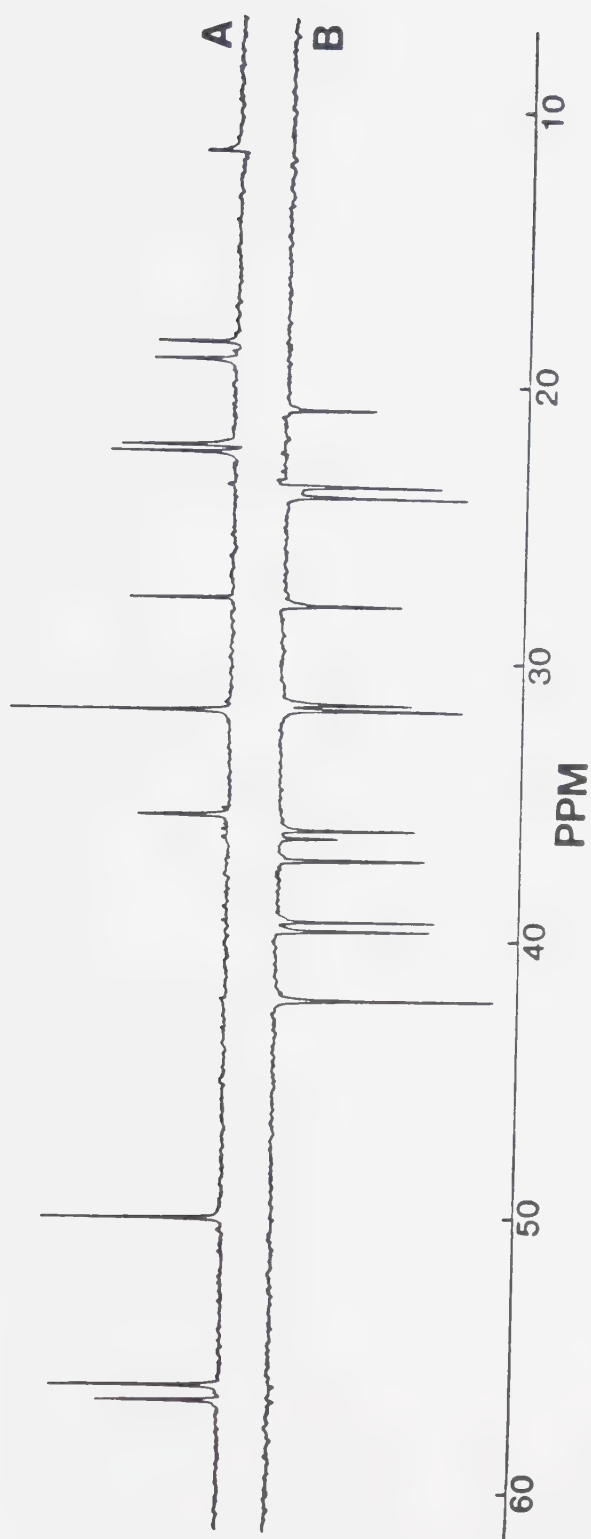


Figure 29. Subspectra containing (A) resonances from methine and methyl carbons and (B) quaternary and methylene carbons. (B) was obtained by addition of two spin-echo FIDs measured with $\tau_2 = 0.008$ second and decoupler schemes A and E of Figure 21. (A) was obtained by subtracting the FID measured with decoupler scheme A from that measured with scheme E.

Fourier transforming the difference FID. Spectrum B was obtained by addition of the same two FIDs and Fourier transformation of the resulting FID. The above procedure was used to collect the FIDs since small drifts in magnetic field and other instrumental factors will affect both FIDs more or less equally. Alternatively, the two FIDs could be collected one at a time in the conventional manner and then added and subtracted to produce subspectra. However, any instrumental variations will not affect the two FIDs collected equally. This can lead to the imperfect cancellation or addition of resonances in the subspectra obtained. The generation of subspectra can also be carried out using the Fourier transformed spectra rather than the two FIDs, however, slightly better phasing and nulling of resonances is obtained when the addition or subtraction is carried out on the FIDs themselves.

As shown in Figure 30, the same two subspectra can be obtained with full proton coupling if the above experiments are carried out with the decoupler gated off during acquisition. This corresponds to the use of decoupler schemes B and F in Figure 21 in place of schemes A and E, respectively. Alternatively, the decoupler can be turned off for the whole spin-echo sequence as well as at acquisition (decoupler scheme D) instead of using decoupler scheme B since the result as discussed for

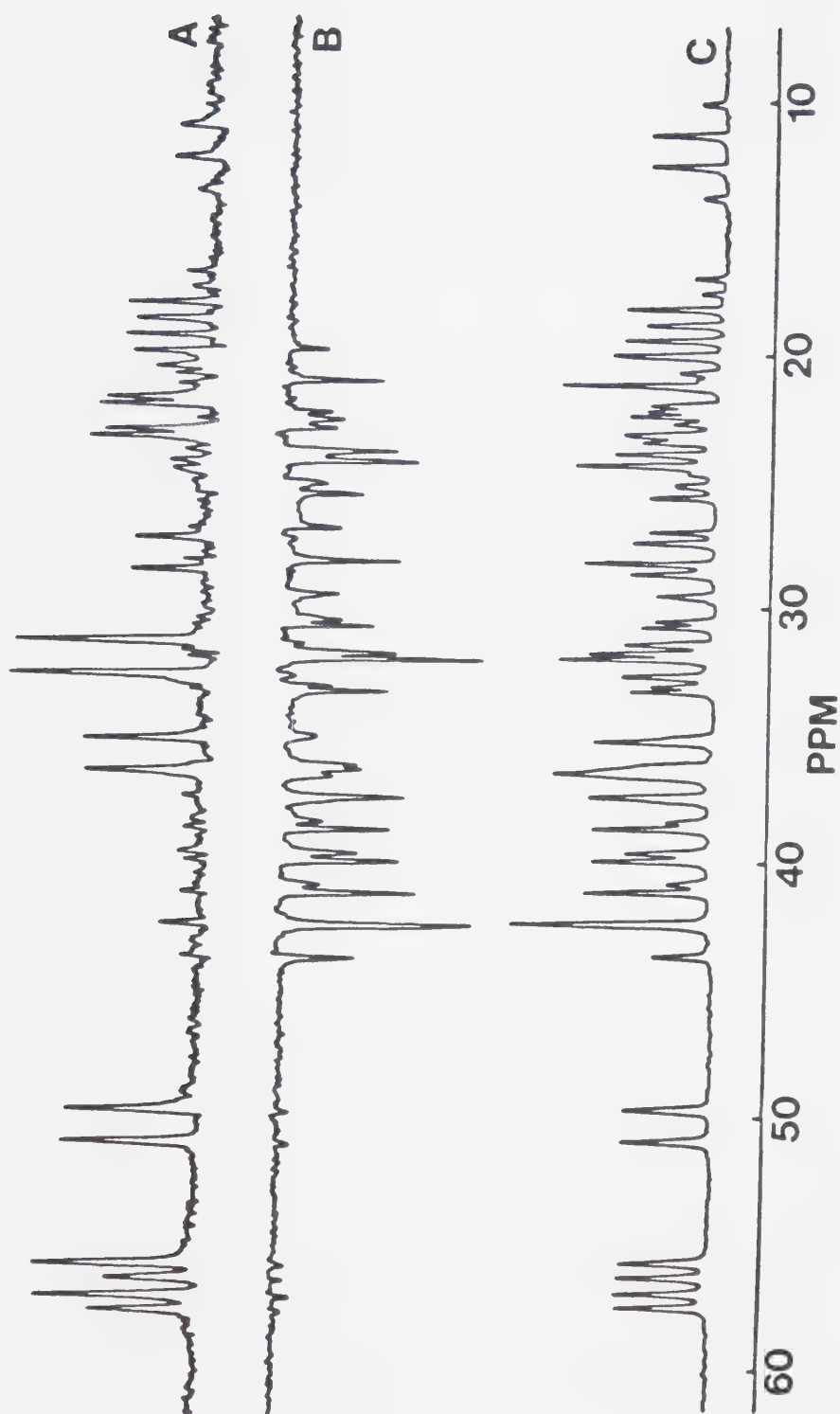


Figure 30. The high field portion of (A) the fully coupled subspectrum for the methine and methyl carbons, (B) the fully coupled subspectrum for the quaternary and methylene carbons and (C) the fully coupled spectrum of cholesterol.

Figure 22A and B is identical. Figure 30A and B show the coupled subspectra for the methine and methyl and the quaternary and methylene carbons, respectively, of cholesterol. The fully coupled spectrum measured by the single-pulse experiment is presented in Figure 30C for comparison.

This method for generating subspectra assumes that in the spin-echo spectra obtained with decoupler schemes E or F the resonances are at full intensity, positive or negative depending on the carbon type, so that there is complete cancellation of methine and methyl resonances or quaternary and methylene resonances when the FIDs are added or subtracted, respectively. From Figure 24, it is clear that this will be the case only when $\tau_2 = 1/J$. When this condition is not perfectly satisfied, there will be small peaks in the subspectra due to imperfect cancellation. To determine the dependence of the intensity of these small peaks on the coupling constants, their intensity was calculated as a function of $^1J_{^{13}\text{C}-^1\text{H}}$. The results of the calculations for the quaternary-methylene carbon and the methine-methyl carbon subspectra are shown in Figures 31 and 32, respectively. These calculations were done for the condition that $\tau_2 = 0.008$ second, that is $\tau_2 = 1/J$ for $J = 125$ hertz.

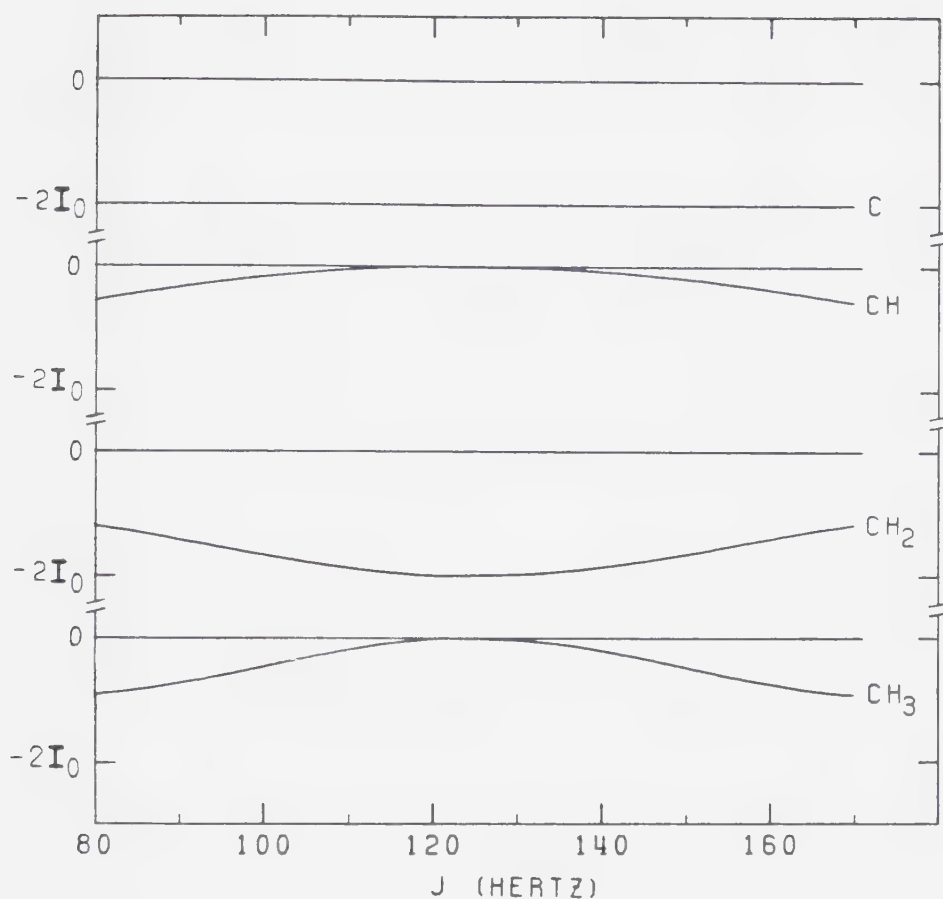


Figure 31. The intensities of resonances in subspectra measured by addition of two spin-echo FIDs with $\tau_2 = 0.008$ second and decoupler schemes A and E of Figure 21 as a function of $^1J_{^{13}\text{C}-^1\text{H}}$ for the various carbon types.

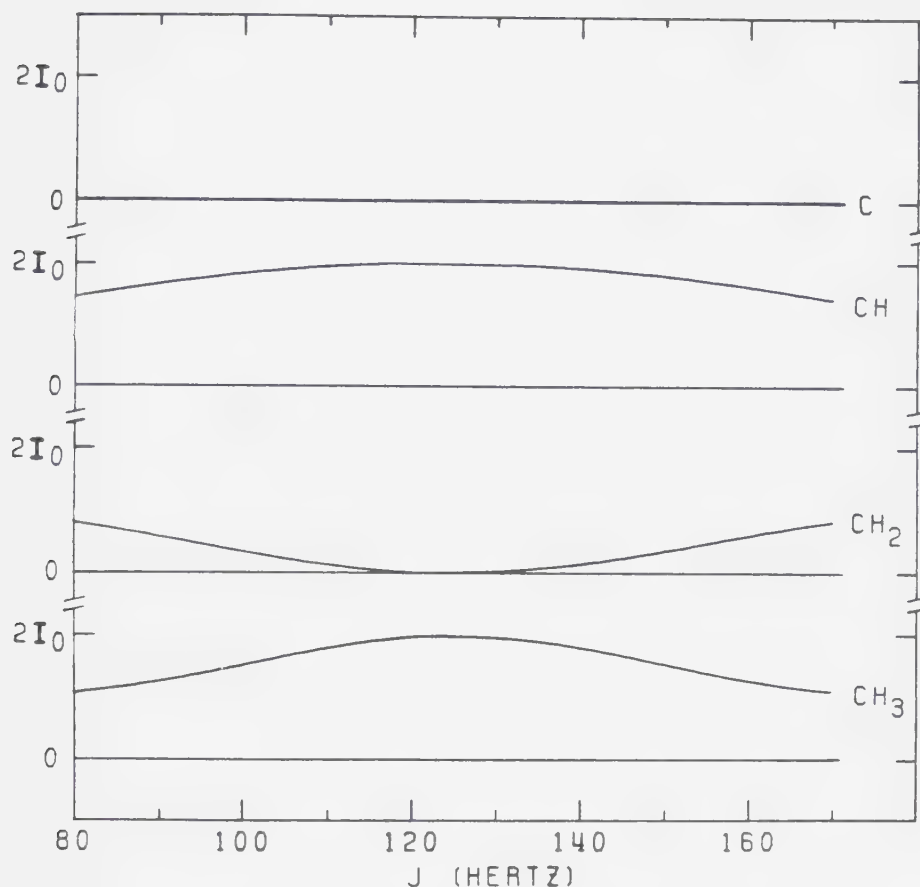


Figure 32. The intensities of resonances in subspectra generated by the subtraction of an FID obtained with $\tau_2 = 0.008$ second and decoupler scheme A of Figure 21 from an FID obtained with $\tau_2 = 0.008$ second and decoupler scheme E as a function of $^1J_{^{13}\text{C}-^1\text{H}}$ for the various carbon types.

The curves for the CH and CH₃ carbons in Figure 31 indicate that larger residual peaks are to be expected for methyl resonances. However, the curves also show that these peaks will be of relatively small intensity as compared to those from the C and CH₂ carbons. For example, at $J = 135$ hertz, the intensity of the resonances for the four carbon types are $-2I_0$ for quaternaries, $-0.031 I_0$ for methines, $-1.938 I_0$ for methylenes and $-0.091 I_0$ for methyls. The curve for CH₂ carbons in Figure 31 indicates that as $^1J_{13C-1H}$ deviates from the optimal value, the intensity of a CH₂ resonance decreases. In contrast, the intensity of the quaternary carbon resonance is independent of J since it is not phase modulated. Similar conclusions are reached from Figure 32. As $^1J_{13C-1H}$ deviates from the condition $\tau_2 = 1/J$, there is imperfect cancellation of the CH₂ resonance, however, there is perfect cancellation of the quaternary carbon resonances since these resonances are not phase modulated.

G. Measurement of $^{13}C-^1H$ Coupling Constants

Carbon-proton coupling constants can be measured directly from 1H coupled ^{13}C spectra in many cases. For example, in Figure 30C coupling constants can be measured directly from the quartet and doublet patterns at 11.90

and 50.33 ppm. However, this is sometimes difficult or impossible due to the overlap of multiplet patterns, for example in the 15 to 45 ppm region of Figure 30C. In this section, two methods based on the spin-echo technique are described for measuring $^1J_{^{13}\text{C}-^1\text{H}}$ [22].

In the first method, the problem of overlap is reduced to some extent by using the fully coupled subspectra measured by the spin-echo difference technique described in the previous section. The results in Figure 30 show that for cholesterol subspectra containing only quaternary and methylene or methine and methyl resonances are far less congested than the fully coupled spectrum containing resonances from all the carbons. Coupling constants which cannot be obtained from the complete spectrum due to spectral overlap can be obtained directly from the two subspectra. The coupling constants obtained from the subspectra are listed in Column 4 of Table 7. For comparison, those coupling constants which can be measured directly from the fully coupled spectrum (Spectrum C in Figure 30) are listed in Column 3. Not all the coupling constants can be determined unambiguously from this spectrum. However, there is sufficient spectral simplification in the subspectra to allow the direct measurement of all the directly bonded $^{13}\text{C}-^1\text{H}$ coupling constants. The values obtained from these two measurement

Table 7

One-Bond $^{13}\text{C}-^1\text{H}$ Coupling Constants of Cholesterol

Carbon ^(a) Position	Carbon Type	$J_{^{13}\text{C}-^1\text{H}}$ ^(b)	$J_{^{13}\text{C}-^1\text{H}}$ ^(c)	$J_{^{13}\text{C}-^1\text{H}}$ ^(d)
1	CH ₂	126.8	127.2	127.1
2	CH ₂	127.2	129.4	127.7
4	CH ₂	126.8	127.7	129.2
7	CH ₂	125.5	127.2	125.2
8	CH	125.5	126.4	126.8
9	CH	122.1	124.6	122.9
10	C	-	-	-
11	CH ₂	(e)	125.9	124.5
12	CH ₂	125.5	125.9	125.8
13	C	-	-	-
14	CH	122.1	125.5	123.1
15	CH ₂	(e)	128.1	128.2
16	CH ₂	125.1	125.5	127.7
17	CH	122.5	124.6	123.9
18	CH ₃	124.2	124.6	124.2
19	CH ₃	125.5	127.7	124.5
20	CH	(e)	125.5	124.5
21	CH ₃	124.6	124.6	124.4
22	CH ₂	(e)	126.4	123.4
23	CH ₂	(e)	124.6	124.3
24	CH ₂	122.9	125.5	123.5
25	CH	125.5	127.2	125.3
26	CH ₃	(e)	123.8	124.5
27	CH ₃	(e)	124.6	123.2

(a) Resonances from carbons 3, 5 and 6 fall outside the spectral window used.

(b) In Hz. Measured directly from Spectrum C in Figure 17. Uncertainty of ± 1.8 Hz due to digital resolution.

(c) Measured directly from the fully-coupled subspectra in Figure 30. Uncertainty of ± 1.8 Hz.

(d) Determined indirectly by fitting intensity modulated singlets in spin-echo spectra measured with decoupling scheme E in Figure 21 to the equations in Table 5. The average standard deviation of the estimates as calculated by the non-linear least-squares program is ± 0.6 Hz.

(e) Could not be measured due to overlap.

procedures agree within the precision of the measurements which is limited by the digital resolution of the spectra.

In the second method, the coupling constants are determined indirectly from the intensity modulation of the ^1H decoupled ^{13}C singlets in a series of spin-echo spectra measured as a function of the delay time. Similar to the method described previously for determining proton-proton coupling constants, this method involves fitting the intensity data for a series of intensity modulated ^{13}C resonances measured with decoupler scheme E of Figure 21 at various τ_2 delay times to the equations presented in Table 5. The intensity modulation of the proton decoupled singlets for carbons 17, 1 and 21 of cholesterol which are methine, methylene and methyl carbons, respectively, are shown in Figure 33. The directly bonded carbon-proton coupling constants obtained by non-linear least-squares fitting of data of this type to the appropriate equation in Table 5 are presented in Column 5 of Table 7. I_0 , T_2^* and J were treated as unknowns in the non-linear least-squares calculations. The solid curves in Figure 33 are the theoretical curves predicted by the parameters obtained from the non-linear least-squares calculations. In the case of carbons 4 and 13, a methylene carbon and a quaternary carbon, respectively, the resonances overlap in the decoupled spectrum. The coupling constant for the

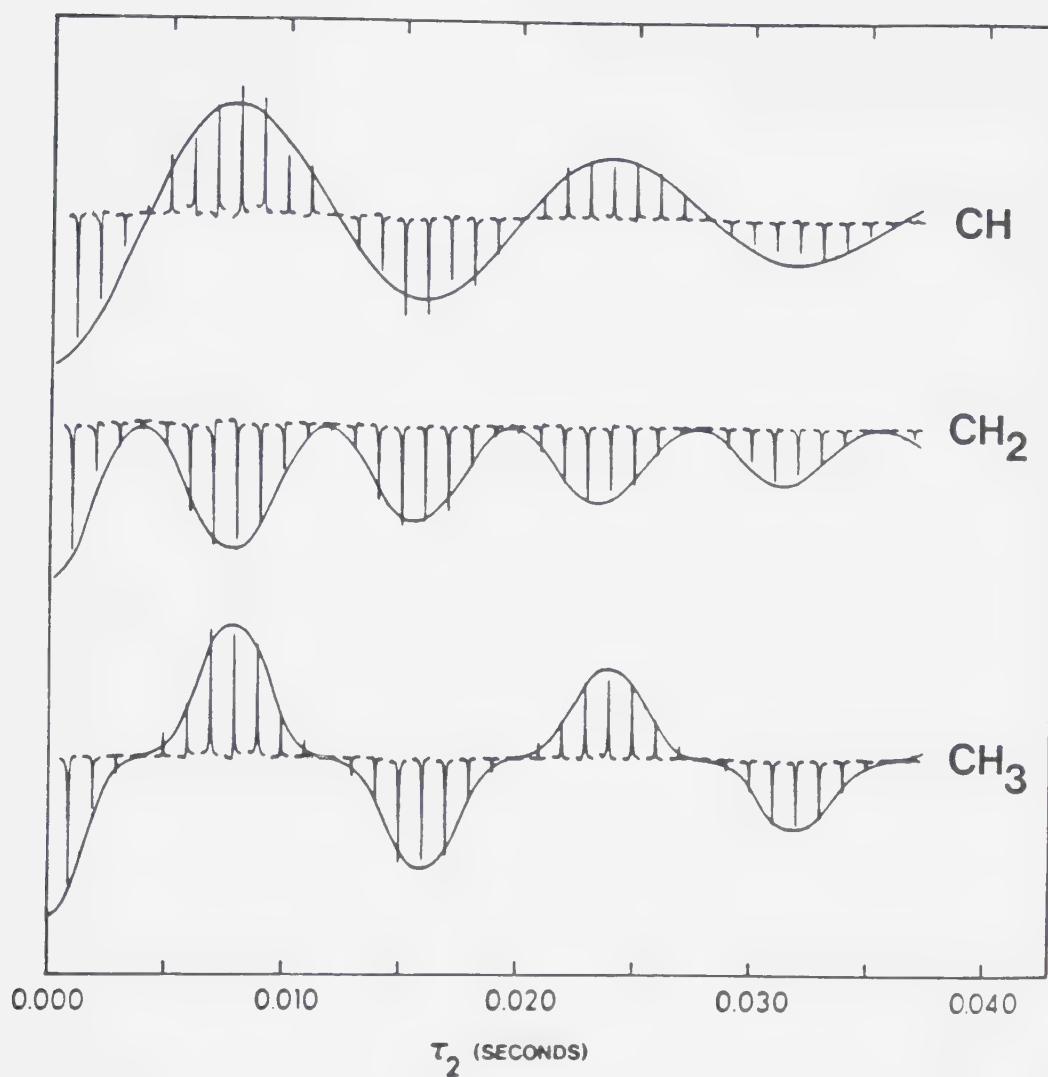


Figure 33. The singlets obtained with decoupling scheme E in Figure 21 for the methine carbon at 56.38 ppm (top), the methylene carbon at 37.40 ppm (middle) and the methyl carbon at 18.78 ppm (bottom) as a function of the length of the delay interval. The smooth curves are predicted with the parameters obtained from the non-linear least-squares fits of the data to the Equations in Table 5.

methylene carbon was obtained by fitting the intensity data to a composite equation containing expressions for both carbons.

$$I = I_0(4) e^{-(2\tau_2/T_2(4))} [1/2 + 1/2 \cos(2\pi J(4)\tau_2)] \\ + I_0(5) e^{-(2\tau_2/T_2(5))} \quad (16)$$

The carbon-proton coupling constants quoted in Column 5 of Table 7 were obtained from non-linear least-squares fits on data sets containing 37 intensity versus τ_2 data points. To determine if the number of data points can be reduced with no significant loss in the precision of the $^1J_{^{13}\text{C}-^1\text{H}}$ values, the non-linear least-squares calculations were done on several smaller data sets derived from the complete data sets. It was found that better results were obtained with the smaller data sets if a relatively large range of τ_2 delay times were used rather than a small τ_2 range by comparing non-linear least-squares calculations conducted on data sets containing every second, third or fourth data point to non-linear least-squares calculations on truncated data sets. For example, if only the first 15 points were used, the uncertainty in the estimated coupling constant increased approximately threefold, whereas if every third spectrum was used (13 points), the

uncertainty approximately doubled. Data sets containing ten points with a wide τ_2 range were considered adequate to yield fairly precise coupling constants in most instances.

Several trials were conducted in which the wrong equation was used to fit the data in the non-linear least-squares procedure. Extremely poor results were obtained for all improper combinations of equations and intensity modulation data other than for fits of methine data using the methyl equation and vice versa. In these instances, where the modulation behavior of the two carbon types involved differs significantly only in the region about $\tau_2 = 1/2J$ (see Figure 24), the use of the incorrect equation always resulted in a somewhat larger standard error value for the coupling constant although the magnitude of $^1J_{^{13}\text{C}-^1\text{H}}$ itself was very close to that obtained using the correct equation.

H. Discussion

The spectra in Figure 25 demonstrate that ^{13}C resonances can be unambiguously assigned to methyl, methylene, methine and quaternary carbons by the spin-echo technique with gated proton decoupling. Spectrum A separates the resonances into two groups, as indicated by the sense of the resonance, with resonances from methyl

and methine carbons being positive in intensity and those from methylene and quaternary carbons being negative in intensity. Spectra B and C complete the assignment, with Spectrum B identifying the quaternary resonances and Spectrum C differentiating between the methyl and methine resonances. The carbon type assignments afforded by the three spectra of Figure 25 are totally unambiguous compared to the single frequency off-resonance decoupling technique (Figure 17B) where severe assignment difficulties are found in the congested regions of the spectrum around 32 and 24 ppm. As well, assignment errors due to temperature induced chemical shift changes present in the off-resonance experiment [44] are avoided with the spin-echo gated decoupling scheme. The spectra in Figure 25 when compared to those in Figure 17 A and B clearly provide a more reliable technique for the assignment of resonances to carbon types, particularly in the ^{13}C spectra of large molecules.

Spectrum A in Figure 25 provides all the information of the standard broadband, proton decoupled experiment (Spectrum A in Figure 17) and, in addition, distinguishes methyl and methine carbons from methylene and quaternary carbons. The chemical shift information in both spectra is identical owing to the fact that the same duty cycle and power levels are used so that the sample experiences

no temperature changes. In fact, more chemical shift information may be obtained if overlapping peaks are separated on the basis of carbon type as is the case for cholesterol carbons 7 and 8 which overlap to give the resonance at 32.02 ppm in Figure 17A whereas they are clearly distinguished at 31.99 and 32.06 ppm, respectively, in Figure 25A. Of course, in the case of precisely overlapped resonances such as carbons 4 and 13 of cholesterol found at 42.45 ppm, separation will not be noted although a cancellation effect is possible if the two resonances have different senses. The S/N ratio is the same in both spectra, neglecting T_2^* effects in the spin-echo experiment which should be small at the short τ_2 delay times used, since the full nuclear Overhauser effect developed in the single-pulse experiment with broadband decoupling is retained in the spin-echo experiment with decoupling scheme E in Figure 21. Thus, for many compounds the spectrum with broadband decoupling is not necessary. In those cases where some of the ^{13}C resonances are quite broad or where quaternary or methylene carbons overlap precisely with methine or methyl carbons, the single-pulse spectrum may be required. If the spectrum contains very broad resonances, they may be considerably reduced in intensity due to spin-spin relaxation during the delay periods.

The phase modulation behavior of carbon multiplets is independent of spectrometer frequency since it depends only on the magnitude of the directly bonded ^{13}C - ^1H coupling constants. The choice of 125 hertz as a typical value for $^1J_{^{13}\text{C}-^1\text{H}}$ for an sp^3 hybridized carbon and, therefore, the use of τ_2 delay times of 0.008 second for $1/J$, 0.0048 second for $3/5J$, 0.004 second for $1/2J$ and 0.0032 second for $2/5J$ was appropriate in the case of cholesterol. As shown by the results in Figures 26 to 28, these delay times should be appropriate for virtually all sp^3 hybridized carbon atoms since erroneous assignments are unlikely for the normal range of coupling constants for these carbons (Table 6). For compounds containing carbon resonances with larger carbon-proton coupling constants, for example vinylic carbons or carbons in saturated or unsaturated heterocycles (Table 6), a more appropriate value for $^1J_{^{13}\text{C}-^1\text{H}}$ can be chosen from the extensive tables for one-bond coupling constants of representative compounds given by Stothers [46]. These carbons, however, do not generally present assignment problems. As indicated in Figures 26 to 28, moderate variations in the ^{13}C - ^1H coupling constants from that of the optimal value for which τ_2 is chosen can be safely tolerated with no assignment errors over a range of about ± 20 hertz around the coupling constant used to determine the τ_2 values.

Recently, several investigators have proposed the use of very similar and in some cases nearly identical [47] techniques to those presented in this work for the assignment of resonances to carbon types in ^{13}C spectra. The use of the spin-flip method involving the application of a 180° pulse to the proton spins at the midpoint of the ^{13}C spin-echo sequence instead of broadband decoupling for one of the evolution periods yields the same results [45]. As mentioned earlier in this chapter, two disadvantages of this method are that the 180° ^1H pulse has to have a uniform power distribution over the entire ^1H frequency range and it is necessary to use different ^1H power levels for the 180° ^1H pulse and broadband ^1H decoupling during acquisition. The so-called attached proton test for ^{13}C spectra utilizes a double spin-echo sequence with the broadband ^1H decoupler off for one of the evolution periods of the first spin-echo to assign carbon sites [48]. As well, an assignment technique based on a double spin-echo sequence employing the spin-flip method for the first spin-echo and broadband decoupling for one of the evolution periods in the second has been proposed [49].

Other techniques which rely on the modulation of the ^{13}C spectrum by proton coupling have been proposed for assignment purposes including the delayed INEPT

(insensitive nuclei enhanced by polarization transfer) [50] and the refocussed INEPT [51,52] experiments. The pulse sequence for the INEPT experiment without refocussing is:

$$90^{\circ}_{1H}(x) - \tau - 180^{\circ}_{1H}(x), 180^{\circ}_{13C} - \tau - 90^{\circ}_{1H}(y), 90^{\circ}_{13C} - \text{Acquisition}$$

(Sequence V)

As indicated by this pulse sequence, it is necessary to apply 180° and 90° pulses to the 1H and ^{13}C nuclei simultaneously and to shift the phase of the 180° and 90° 1H pulses [53]. The INEPT experiments are thus much more demanding of the spectrometer than the spin-echo experiments described in this work. Also, in the delayed INEPT experiment, a large phase variation is introduced across the spectrum [50]. In the spin-echo experiment, the only decoupler requirements involve the ability to gate the decoupler on and off over the course of the experiment.

Several techniques relying on modification of the ^{13}C spectrum have also been proposed for assignment purposes. Multiplication of the second half of the echoes from a series of spin-echo sequences of differing lengths of the evolution period by suitable masking functions is one such method [54,55]. Another involves the scaling of

the carbon-proton couplings throughout the entire ^{13}C spectrum as an alternative to off-resonance decoupling [56,57]. These so-called J-scaling methods rely on the ability to perform ^1H spin flips between carbon-13 acquisition sampling points which is available in only a few laboratories. As with the usual off-resonance method, J-scaling suffers from reduced sensitivity due to the splitting of intensity into several lines and uncertainties in assignment in crowded regions of the spectrum. Subspectra containing only resonances from non-protonated carbons can be obtained from spin-echo spectra measured with inefficient proton decoupling [58], however, this method would seem to offer no advantages over the spin-echo experiment with gated decoupling using a τ_2 of $1/2J$. As well, assignment methods based on J-resolved [18,59] and correlation [60,61] two-dimensional NMR techniques are available but are time consuming to carry out.

The spectra in Figure 30 and the results listed in Table 7 indicate the utility of using fully coupled subspectra for the measurement of directly bonded ^{13}C - ^1H coupling constants. Good estimates of these coupling constants are also obtained by analysis of the intensity of ^1H decoupled, ^{13}C singlets measured as a function of τ_2 . This approach should be applicable to quite large

molecules since measurements are made on fully decoupled spectra. It should be noted that even in cases involving superimposed resonances this technique can be utilized as long as the non-linear least-squares fits are performed using a composite equation describing the behavior of both components of the superimposed line. The use of intensity modulation analysis is to be preferred over the use of subspectra in cases involving a large range of carbon-proton coupling constants where subspectra may be difficult to generate by using an average value for $^1J_{^{13}\text{C}-^1\text{H}}$. However, in cases where subspectra can be successfully generated using a compromise $^1J_{^{13}\text{C}-^1\text{H}}$ value the measured coupling constants at the limits of the $^1J_{^{13}\text{C}-^1\text{H}}$ range will not be in error since it is the positions of the resonances in the subspectra that are important not their intensities.

Longer range couplings such as geminal ($^{13}\text{C}-\text{C}-^1\text{H}$) or vicinal ($^{13}\text{C}-\text{C}-\text{C}-^1\text{H}$) couplings will produce contributions to the intensity modulation of ^{13}C resonances which are included in the T_2^* term of the non-linear least-squares procedure since such couplings are much smaller than the directly bonded carbon-proton couplings and will, thus, modulate at much lower frequencies. Typical values for aliphatic geminal and vicinal coupling constants, $^2J_{^{13}\text{C}-^1\text{H}}$ and $^3J_{^{13}\text{C}-^1\text{H}}$, are around one to six hertz [46]. In the

measurement of proton-proton coupling constants, longer range couplings were observed to produce minor secondary modulations in the intensity versus τ_2 behavior of decoupled singlets. This is because the magnitude of the longer range coupling constants were not as different from the $^3J_{^{13}\text{C}-^1\text{H}}$ values as they were in the case of the carbon-proton coupling constants.

The results of using smaller data sets with a wide τ_2 range rather than a restricted τ_2 range in measuring the carbon-proton coupling constants conforms to what is intuitively expected. The wide τ_2 range will allow better definition of the intensity modulation behavior and any random fluctuations in peak intensity will have less effect than in cases involving a restricted range of τ_2 delay times.

Several other methods have been described for measuring $^{13}\text{C}-^1\text{H}$ coupling constants in spectra where overlap of multiplet patterns prevents direct measurement including methods based on selective excitation with gated decoupling [62-64]. These methods require a number of experiments equal to the number of multiplets to be observed and also require more signal averaging per experiment since the intensity is distributed over the multiplet patterns. Overlapping multiplets can also be separated to allow the measurement of $^1J_{^{13}\text{C}-^1\text{H}}$ by two-

dimensional spectroscopy [18,59,60] but this approach as noted previously is time consuming.

CHAPTER IV

DIFFERENTIAL SPIN-SPIN RELAXATION OF ^1H NUCLEI ON COMPOUNDS OF VARYING MOLECULAR WEIGHT

A. Introduction

Generally, spin-spin relaxation times for the various nuclei present in a sample are quite different. The range of T_2 relaxation times for the ^1H nuclei of the various compounds of a sample can be used to provide a means of spectral simplification and resolution enhancement in ^1H NMR spectra [6,15]. Such resolution enhancement is based on discrimination against the larger compounds which have the shorter T_2 relaxation times. The resonances from these compounds are eliminated from the spin-echo NMR spectrum while those from the smaller compounds are still present and thereby significantly more resolved.

The processes which govern the rate of spin-spin relaxation comprise those which generate either static or fluctuating magnetic fields in the sample. These include magnetic dipole-dipole interactions, chemical shift anisotropy, spin rotation, scalar coupling, paramagnetic center effects, spin-spin exchange and orientation effects

of one sample nucleus in relation to other nuclei [65]. The T_2 relaxation rate is often dominated by dipole-dipole interactions. When this is the case, the expression which describes the T_2 relaxation time for two nuclei separated by a distance r is [66]:

$$\frac{1}{T_2} = \frac{3}{20} \frac{\gamma^4 \hbar^2}{r^6} f(\tau_c) \quad (17)$$

where:

$$f(\tau_c) = 3\tau_c + \frac{5\tau_c}{1 + \omega_0^2 \tau_c^2} + \frac{2\tau_c}{1 + 4\omega_0^2 \tau_c^2} \quad (18)$$

ω_0 is the resonance frequency of the nuclei involved and τ_c is the correlation time. The correlation time is a measure of the mobility of the molecule. It is a parameter describing the characteristic time scale of molecular motions in solution. Typical values for τ_c range from 3×10^{-12} second for H_2O to about 10^{-8} second for a protein of molecular weight 20,000 [67]. In general, the larger the compound the more restricted is its mobility in solution and the longer the correlation time becomes. 1H nuclei of larger molecules with longer correlation times tend to have shorter T_2 relaxation times while those of smaller molecules with shorter correlation times have longer T_2 values. T_2 is thus proportional to

$f(\tau_c)^{-1}$. The relationship between τ_c and $f(\tau_c)^{-1}$ is shown graphically in Figure 34 for ^1H nuclei at a resonance frequency of 360 MHz. The plot is non-linear in the region where $\omega_0\tau_c$ approaches unity, which includes the τ_c range for most molecules of moderate size.

In this chapter, a study of the T_2 relaxation behavior for a variety of compounds was carried out in order to evaluate the rate at which spin-spin relaxation occurs for compounds of differing molecular size during the spin-echo experiment. Although the use of the spin-echo method for resolution enhancement on the basis of different T_2 relaxation times has been presented earlier [6,15], the detailed dependence on molecular size has never been studied. This provides the basis for an empirical choice of τ_2 delay time to eliminate resonances for compounds above a certain molecular size. It also allows the delineation of the relationship between the molecular size of a compound, as measured by its molecular weight, and the T_2 relaxation times for the protons of the compound.

The application of T_2 discrimination occurring during the spin-echo experiment to the measurement of the NMR spectrum of small molecules in the presence of obscuring macromolecules is well known [6,14,16,68]. It is shown in this chapter that a useful application of such T_2

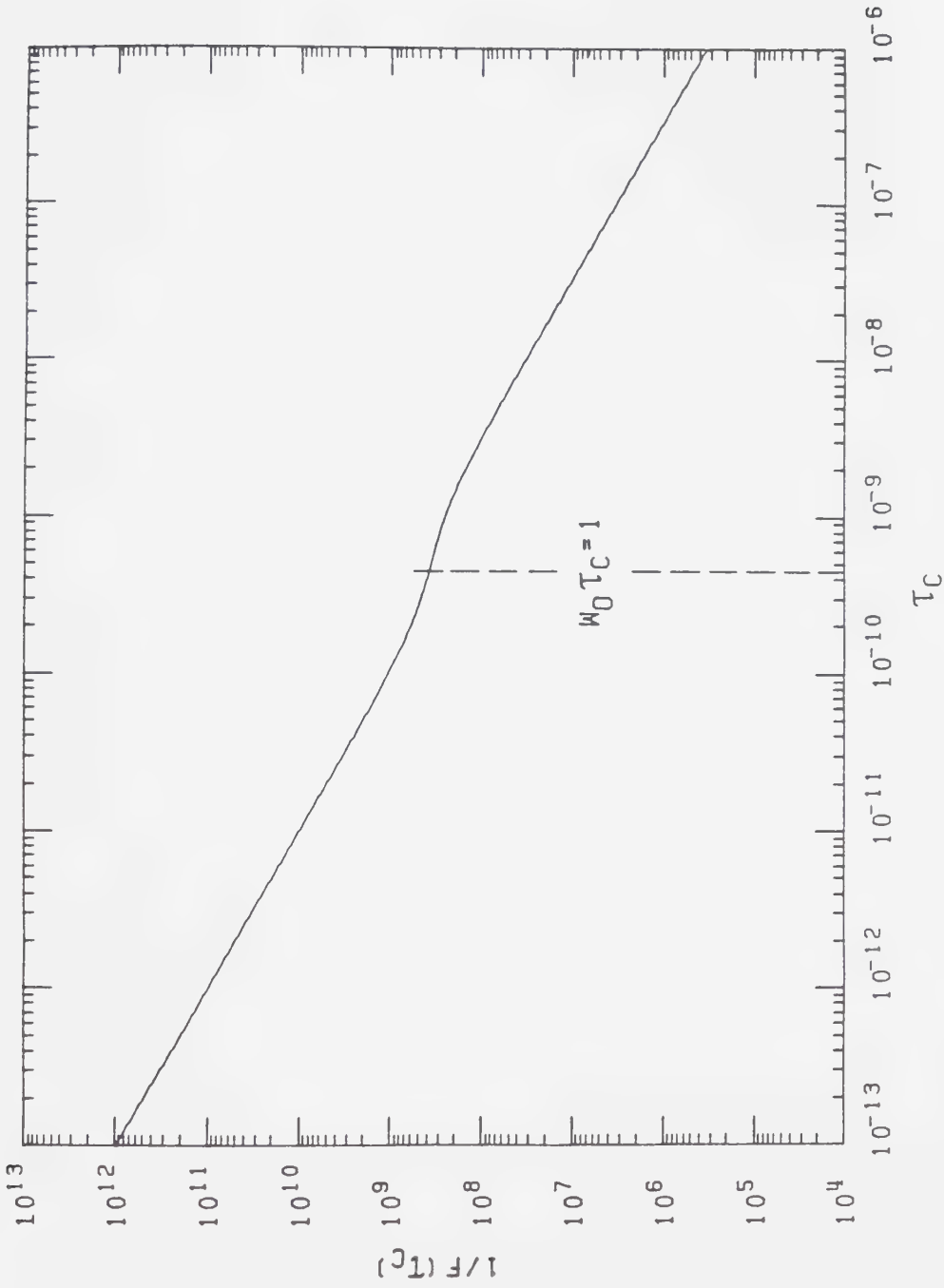


Figure 34. The relationship between τ_C and $f(\tau_C)^{-1}$ (see text) for protons at a resonance frequency of 360 MHz. At $\omega_0 \tau_C = 1$, $\tau_C = 2.78 \times 10^{-9}$ second.

discrimination experiments is the qualitative determination of the presence of small molecule contaminants in protein solutions. The procedure involves measuring a spin-echo spectrum with a sufficiently long τ_2 delay time such that the resonances from the protein are eliminated in the NMR spectrum while those from smaller contaminant molecules will still be observed. This is used to monitor the effectiveness of cleanup procedures applied to the protein solution by monitoring the intensity of the contaminant resonances. This procedure was used to follow the cleanup of a solution of commercially obtained bovine serum albumin (BSA) and in the preparation of a hemoglobin solution from a sample of hemolyzed human erythrocytes utilizing dialysis [69] as the purification procedure.

B. T_2 Studies on a Series of Compounds of Increasing Molecular Weight

The measurement of spin-spin relaxation times in solution is generally accomplished using either the simple spin-echo experiment [1] or one of its more elaborate modifications which eliminate diffusion effects [10,11]. The determination of T_2 values for the various protons of a compound is achieved by plotting the natural logarithm of the intensity of each resonance against the total

length of the evolution period over which spin-spin relaxation is occurring. In the spin-echo experiment the evolution period is $2\tau_2$ while in the Carr-Purcell and Carr-Purcell-Meiboom-Gill (CPMG) modifications it is $(2\tau_2')_n$. The slope of the resulting linear relationship is the negative reciprocal of the T_2 relaxation time. For the simple spin-echo experiment:

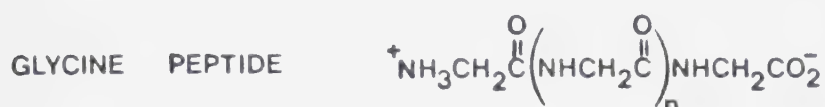
$$\ln I_{2\tau_2} = \ln I_0 - \frac{2\tau_2}{T_2} \quad (19)$$

where I_0 is the initial intensity of the resonance under study and $I_{2\tau_2}$ is its intensity at time $2\tau_2$.

For resonances belonging to multiplets, which are phase modulated as τ_2 is varied, τ_2 delay times corresponding to points where the multiplet is in-phase or 180° out-of-phase (inverted) must be chosen unless the CPMG pulse sequence is used with very short τ_2 delays such that the 180° pulse repetition rate is fast compared with the range of resonance frequencies. This will inhibit phase modulation from occurring over the delay periods [13]. An alternative means of dealing with phase modulation is to display the spectrum in the absolute value mode as a power spectrum [13].

Spin-spin relaxation times were measured with the spin-echo technique for the proton resonances of compounds

having a wide range of molecular weights, from 75 g/mole to 68,000 g/mole. At the low molecular weight end a series of glycine peptides were used:



where n ranged from 0 to 4. The values for the measured T_2 relaxation times are listed in Table 8 for glycine, diglycine ($n = 0$), triglycine ($n = 1$), tetraglycine ($n = 2$), pentaglycine ($n = 3$) and hexaglycine ($n = 4$). The two equivalent protons of each amino acid residue are labelled A, B, C, D, E or F beginning at the end of the molecule containing the terminal amino group. Figure 35 is an example of a series of spin-echo spectra, measured at increasing τ_2 delay times, for diglycine from which the T_2 relaxation times were evaluated. Similar series of spectra were measured for the other glycine peptides. Plots of intensity of the various resonances versus τ_2 delay time, normalized to one at a τ_2 delay of zero, are presented for each of the glycine peptides in Figures 36 to 41.

The assignment of resonances to the protons for each glycine peptide was carried out by collecting single-pulse spectra for each peptide as a function of pH* and

Table 8

T_2 Relaxation Times^(a) Measured for the Methylene Protons of a Series of Glycine Peptides

Compound	Molecular Weight	pH [*] (b)	A (c)	B	C	D	E	F	Average
Glycine	75.07	7.77	2.40 ±0.04						2.40
Diglycine	132.1	7.48	0.30 ±0.01	0.35 ±0.02					0.32
Triglycine	189.2	7.32	0.30 ±0.01	0.23 ±0.01	0.30 ±0.01				0.28
Tetraglycine	246.2	7.35	0.39 ±0.01	0.31 ±0.01	0.26 ±0.01	0.37 ±0.01			0.33
Pentaglycine	303.3	7.33	0.40 ±0.01	0.31 ±0.01	0.28 ±0.01	0.25 ±0.01	0.37 ±0.01		0.32
Hexaglycine	360.3	7.14	0.32 ±0.01	0.29 ±0.01	0.27 ±0.01	0.27 ±0.01	0.24 ±0.01	0.36 ±0.01	0.29

(a) Measured in seconds.

(b) Uncorrected for isotope effects due to D₂O.

(c) A through F refer to the two equivalent protons of each glycine residue beginning at the end bearing the terminal amino group.

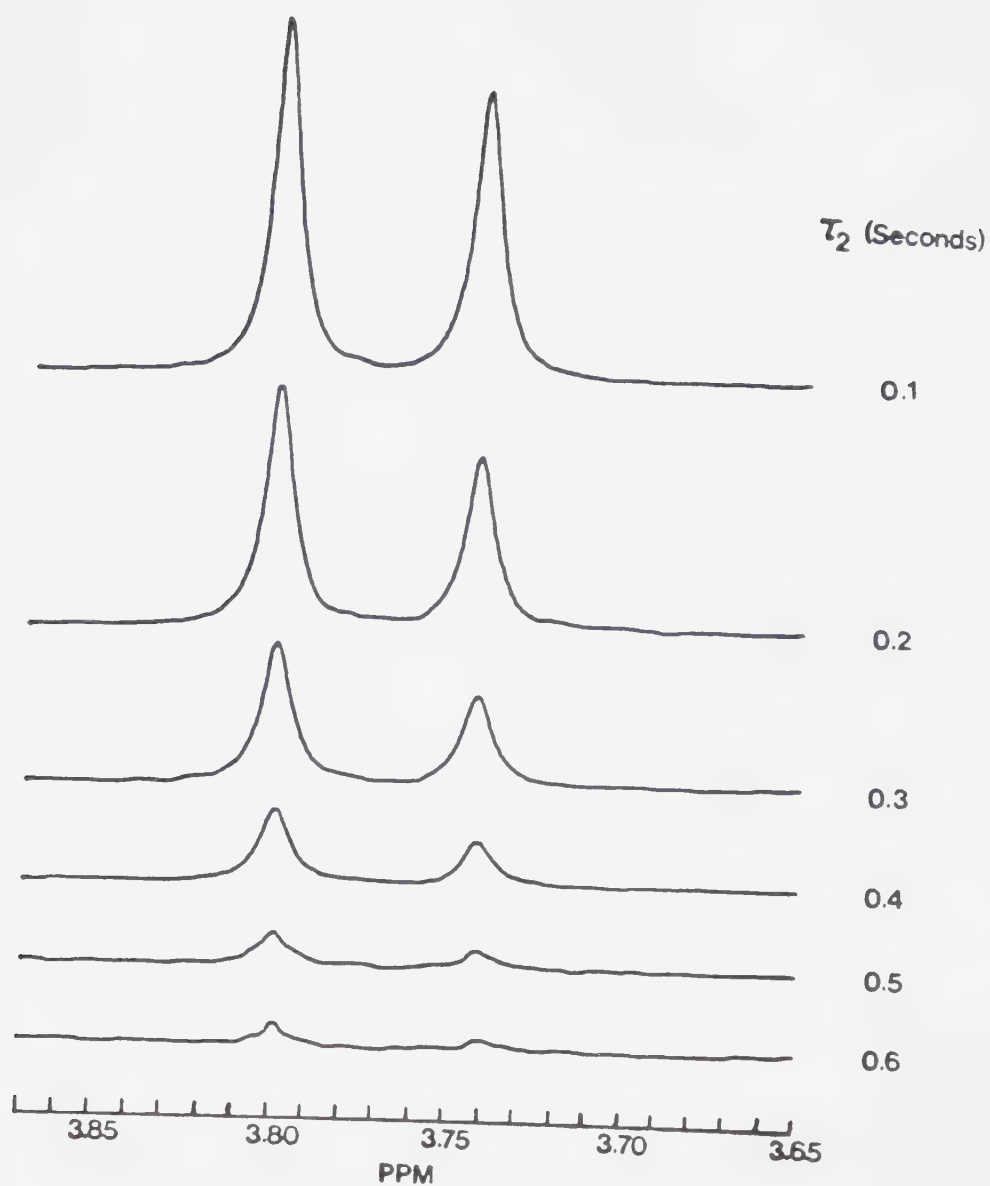


Figure 35. A series of spin-echo spectra at various τ_2 delay times for diglycine from which T_2 relaxation times can be evaluated.

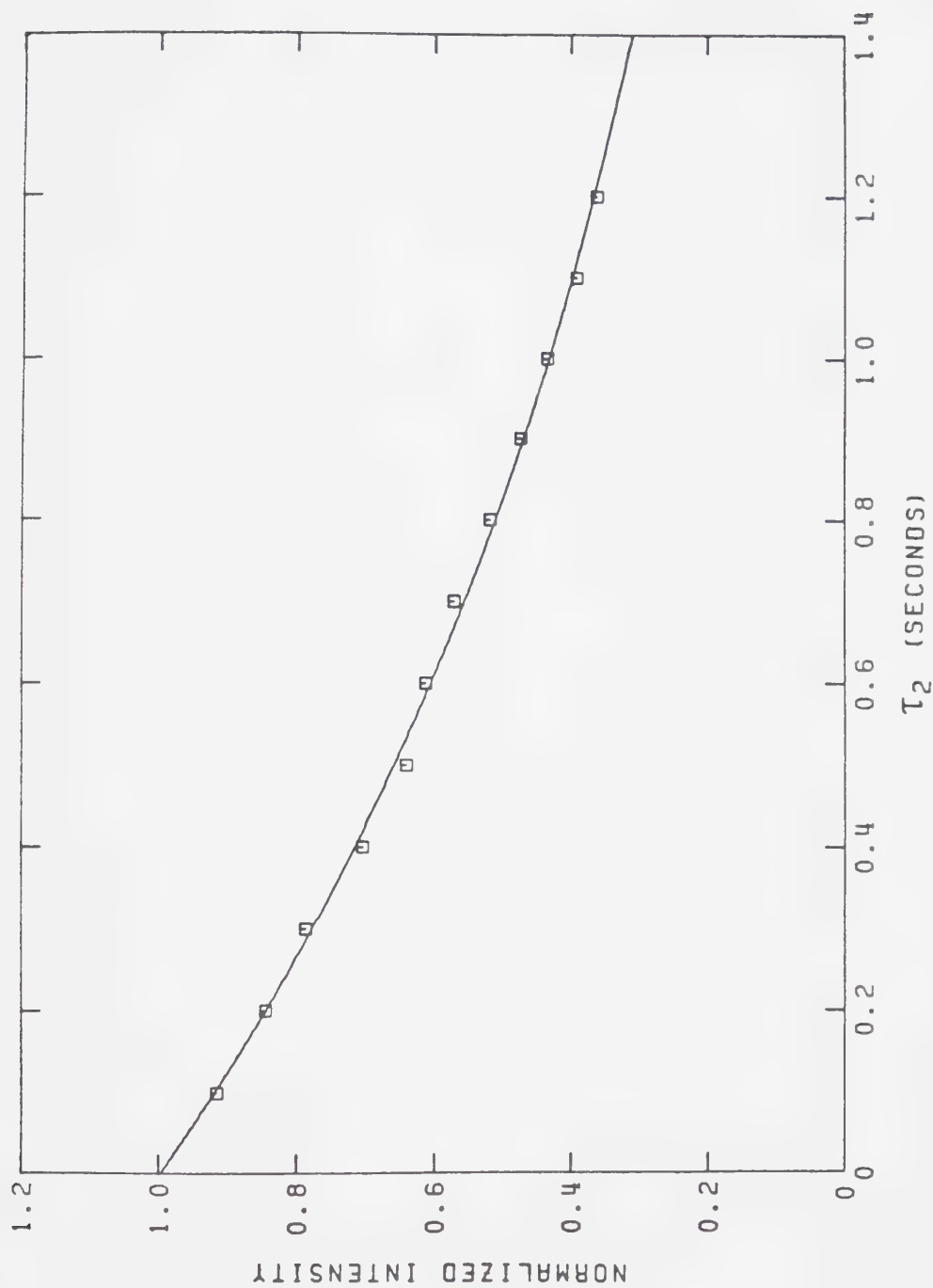


Figure 36. A plot of intensity versus τ_2 delay time, normalized to one at a τ_2 delay of zero for the methylene protons of glycine. The solid curve was calculated using the T_2 value in Table 8.

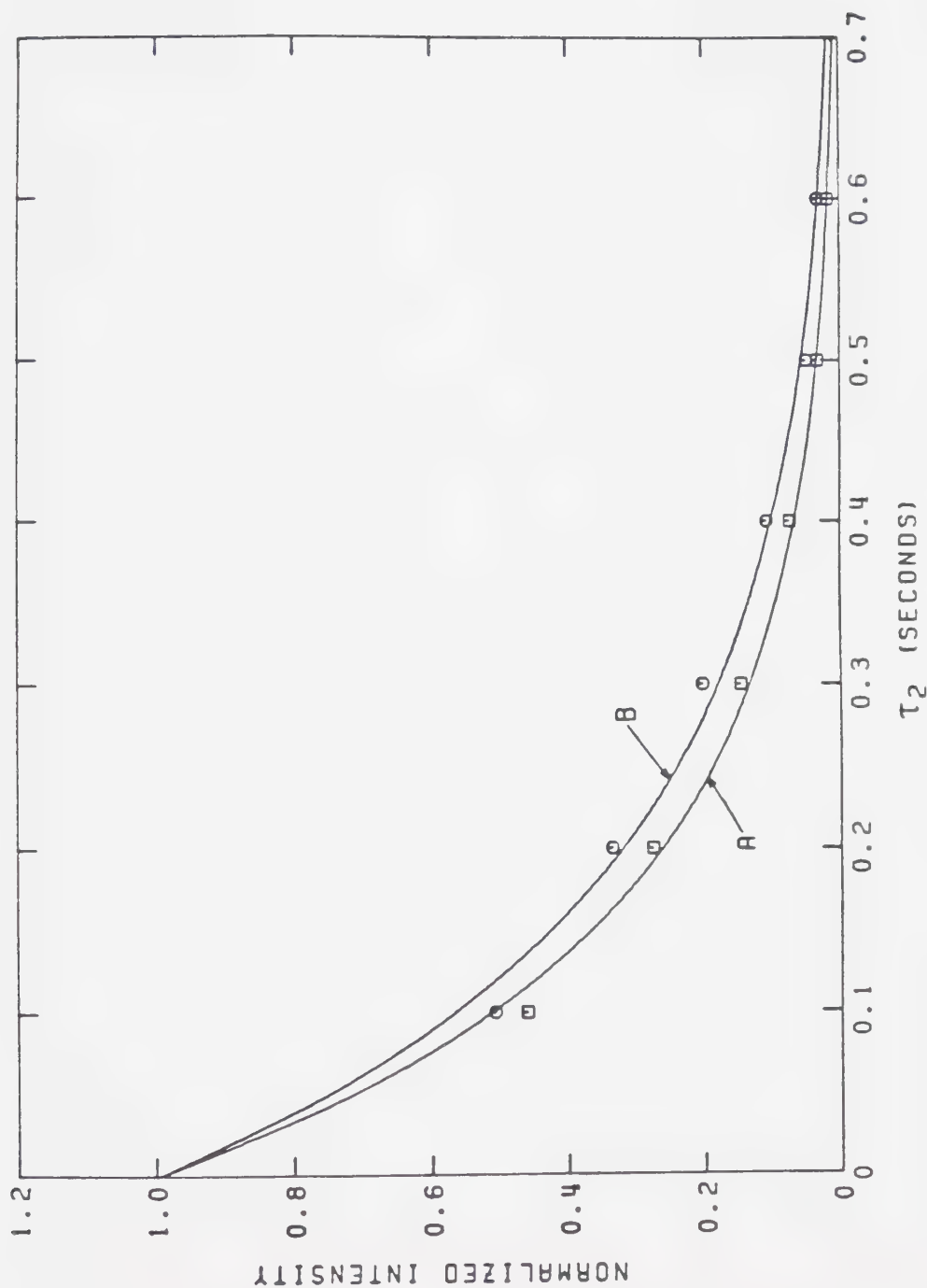


Figure 37. Plots of intensity versus τ_2 delay time, normalized to one at a τ_2 delay of zero for the methylene protons of diglycine. The solid curves were calculated using the T_2 values in Table 8. (A) \square is for the methylene protons nearest the terminal amino end of the molecule. (B) \circ is for the methylene protons nearest the terminal carboxylate end.

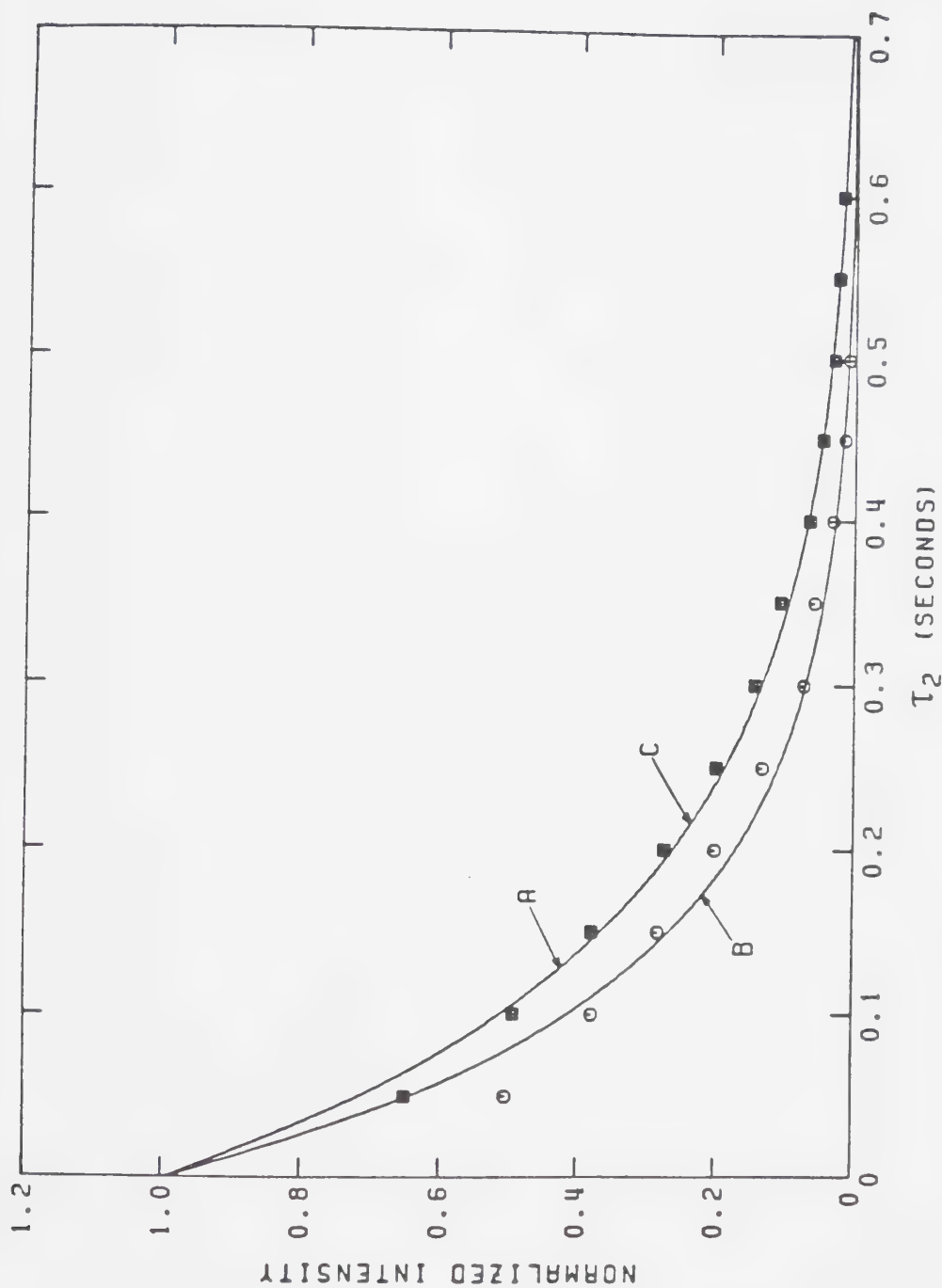


Figure 38. Plots of intensity versus τ_2 delay time, normalized to one at a τ_2 delay of zero, for the methylene protons of triglycine. The solid curves were calculated using the T_2 values in Table 8. (A) \square , (B) \circ and (C) \triangle represent the two equivalent methylene protons of each glycine residue from the N-terminal to the C-terminal end of the molecule. The resonances giving rise to (A) and (C) were coincident in the NMR spectra.

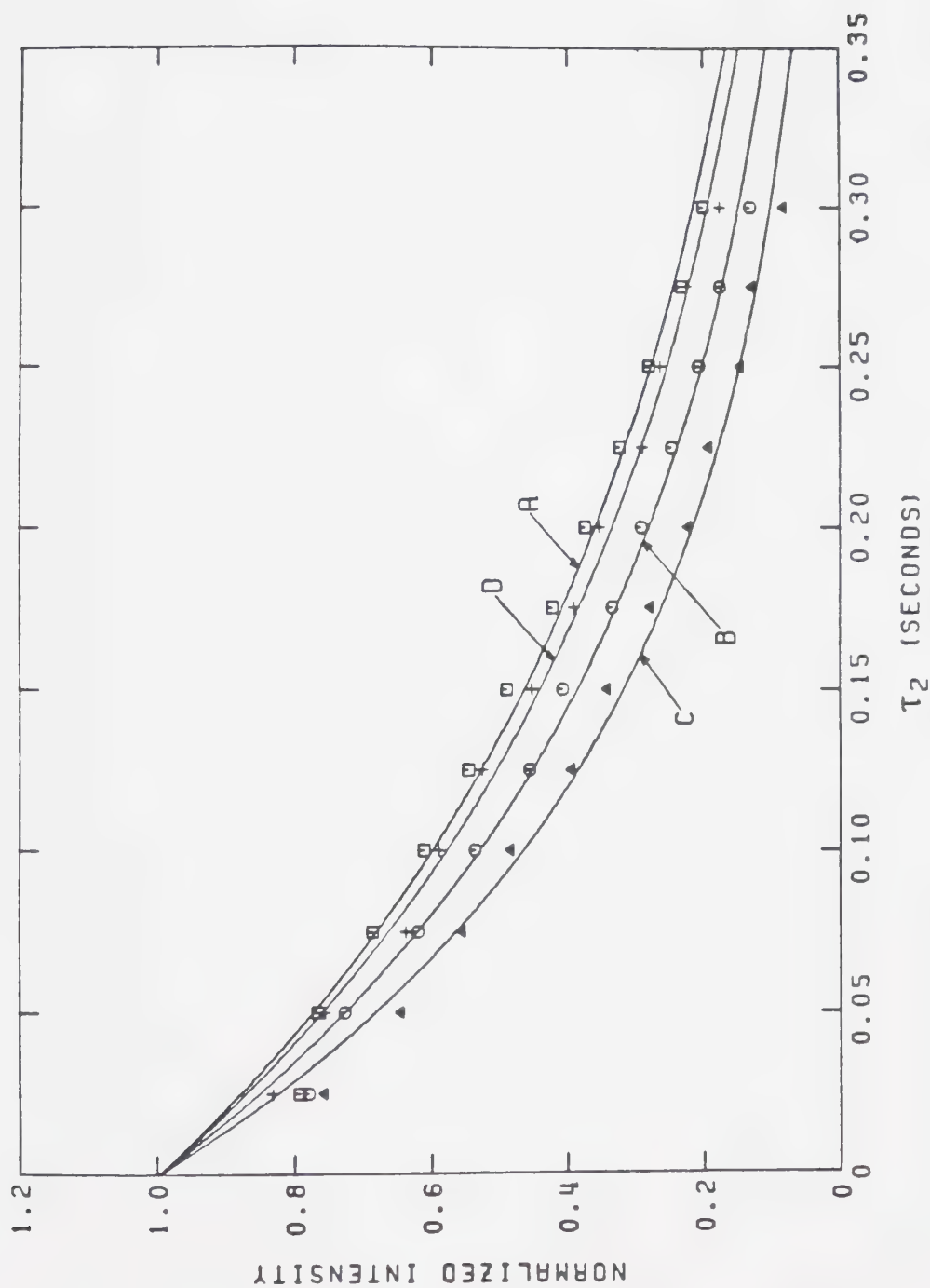


Figure 39. Plots of intensity versus τ_2 delay time, normalized to one at a τ_2 delay of zero for the methylene protons of tetraglycine. The solid curves were calculated using the T_2 values in Table 8. (A) \square , (B) \triangle , (C) \triangle and (D) \circ represent the two equivalent methylene protons of each glycine residue from the N-terminal to the C-terminal end of the molecule.

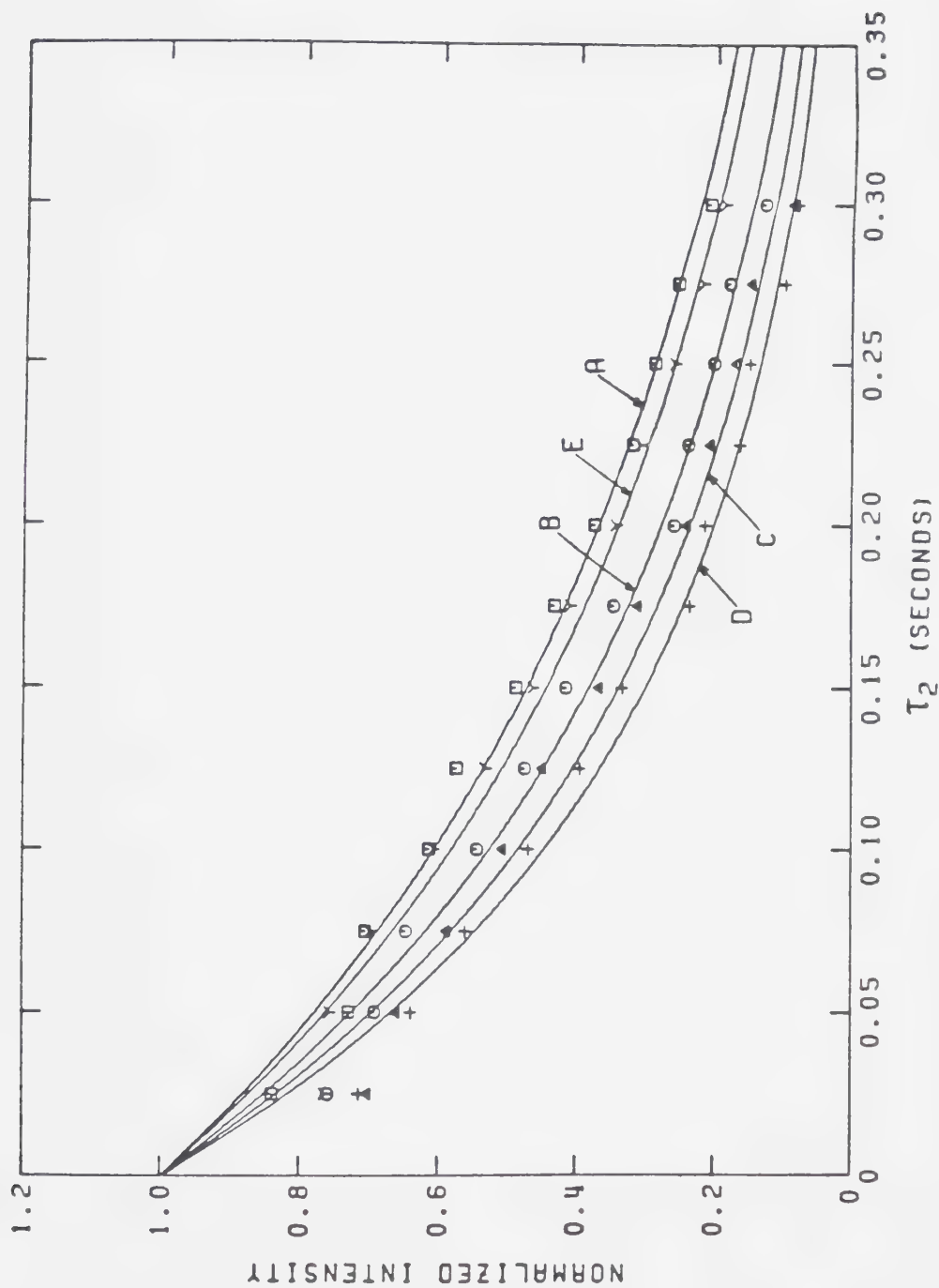


Figure 40. Plots of intensity versus τ_2 delay time, normalized to one at a τ_2 delay of zero, for the methylene protons of pentaglycine. The solid curves were calculated using the T_2 values in Table 8. (A) \square , (B) \circ , (C) Δ , (D) $+$ and (E) γ represent the two equivalent methylene protons of each glycine residue from the N-terminal to the C-terminal end of the molecule.

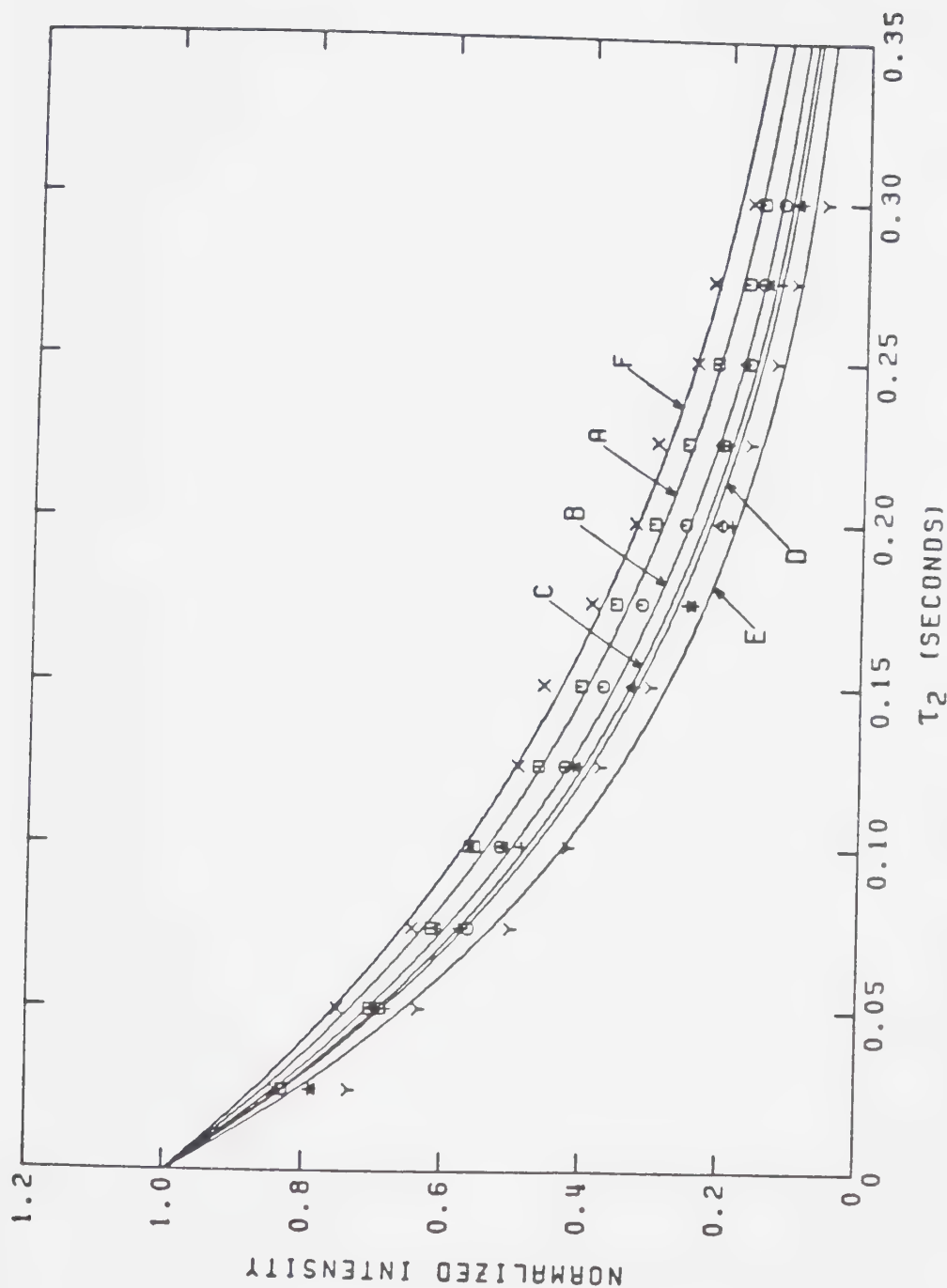


Figure 41. Plots of intensity versus T_2 delay time, normalized to one at a T_2 delay of zero for the methylene protons of hexaglycine. The solid curves were calculated using the T_2 values in Table 8. (A) \square , (B) \circ , (C) Δ , (D) $+$, (E) Y and (F) X represent the two equivalent methylene protons of each glycine residue from the N-terminal to the C-terminal end of the molecule.

monitoring the chemical shifts of the various resonances. The results of these experiments are diagrammed in Figures 42 to 46. The rationale behind the assignments is that the effects of protonation or deprotonation of the terminal amino and carboxylate groups on the chemical shifts of the methylene protons of the glycine residues decreases the further removed the protons are from the functional group [70]. Since the systems are in fast exchange [71], the observed chemical shift is a weighted average for each resonance at a certain pH* which depends on the protonation states of the two functional groups. Protonation of either the amino or carboxylate group always gives rise to a downfield change in the chemical shift of the neighbouring glycine protons [72]. The carboxylate group deprotonates at a lower pH* than the ammonium group. Typically, the carboxylate pK_a is around 3 to 3.5 while the ammonium pK_a is generally about 8 to 8.5 [73].

In fact, the pK_a's of both the terminal amino and carboxylate groups for each glycine peptide can be determined by fitting the chemical shift versus pH* data for the resonances of the nearest protons to these functional groups to an equation of the form [74]

$$\delta_o = \frac{\delta_{NC}^+ [H^+]^2 + \delta_{NC}^+ [H^+] K_a (COOH) + \delta_{NC}^- K_a (COOH) K_a (NH_3^+)}{[H^+]^2 + K_a (COOH) [H^+] + K_a (COOH) K_a (NH_3^+)} \quad (20)$$

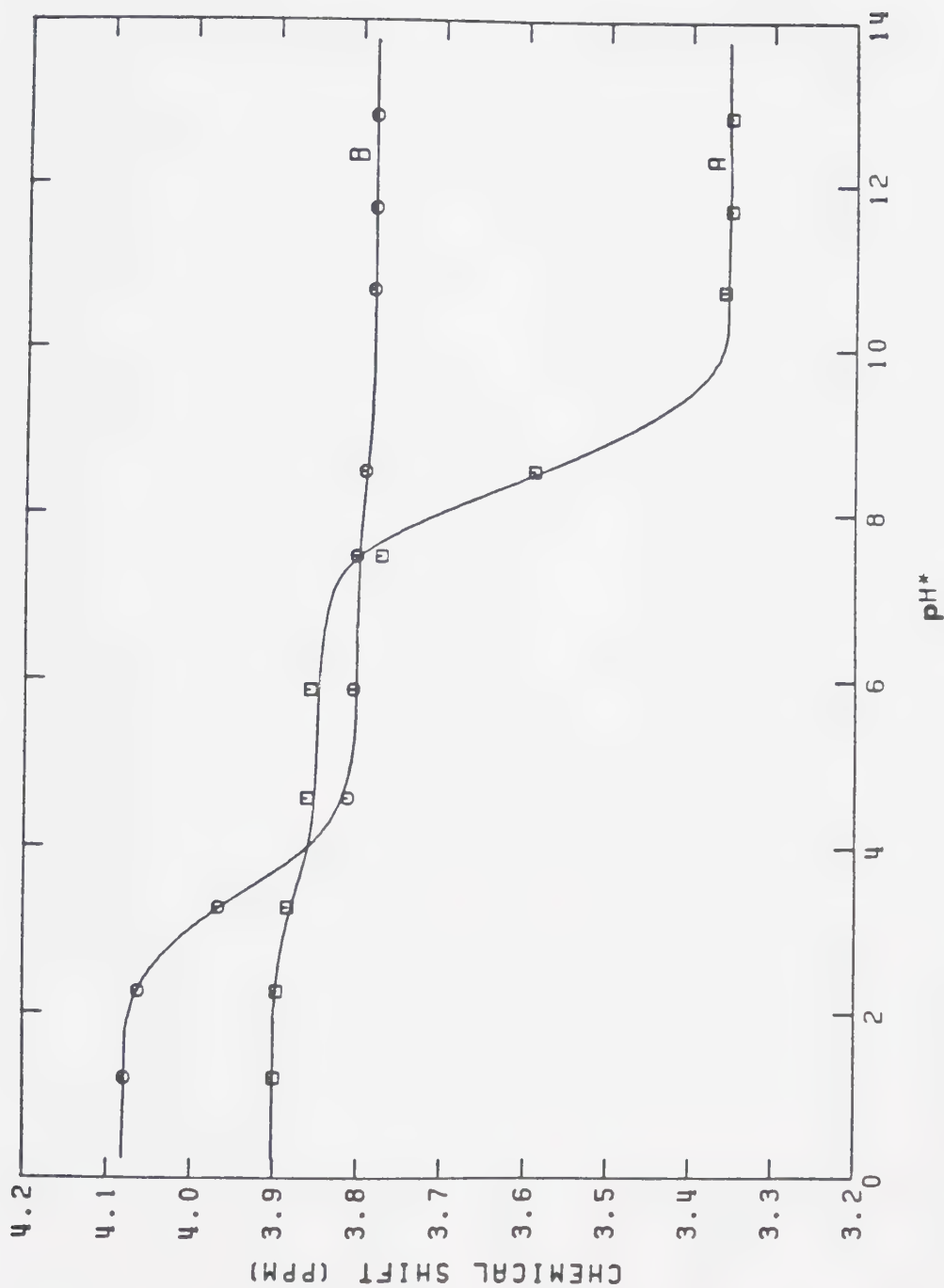


Figure 42. Plots of chemical shift versus pH* for the methylene protons of diglycine. (A) is for the methylene protons nearest the terminal amino end of the molecule. (B) is for the methylene protons nearest the terminal carboxylate end.

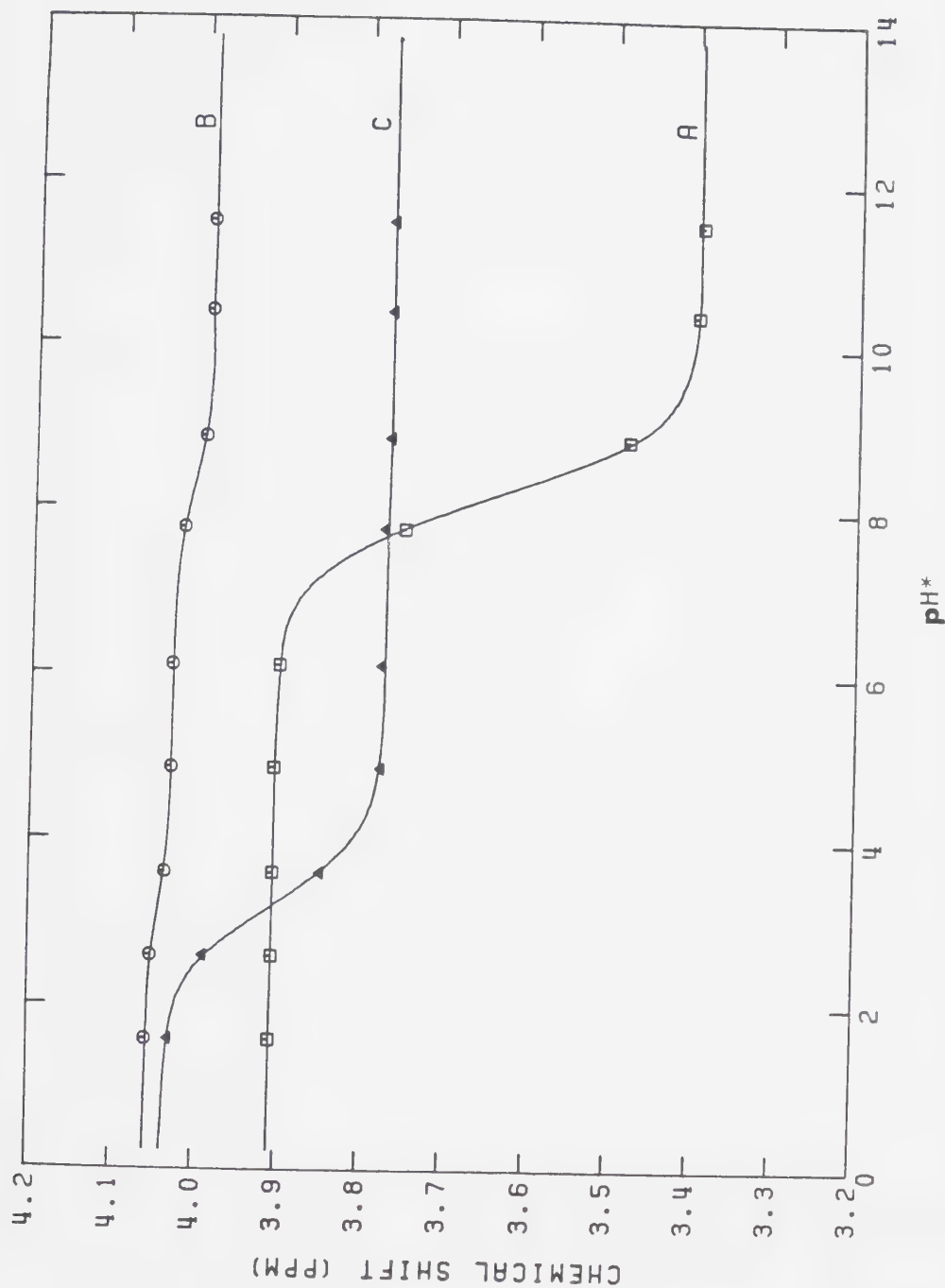


Figure 43. Plots of chemical shift versus pH* for the methylene protons of triglycine. (A) to (C) represent the two equivalent methylene protons of each glycine residue from the N-terminal to the C-terminal end of the molecule.

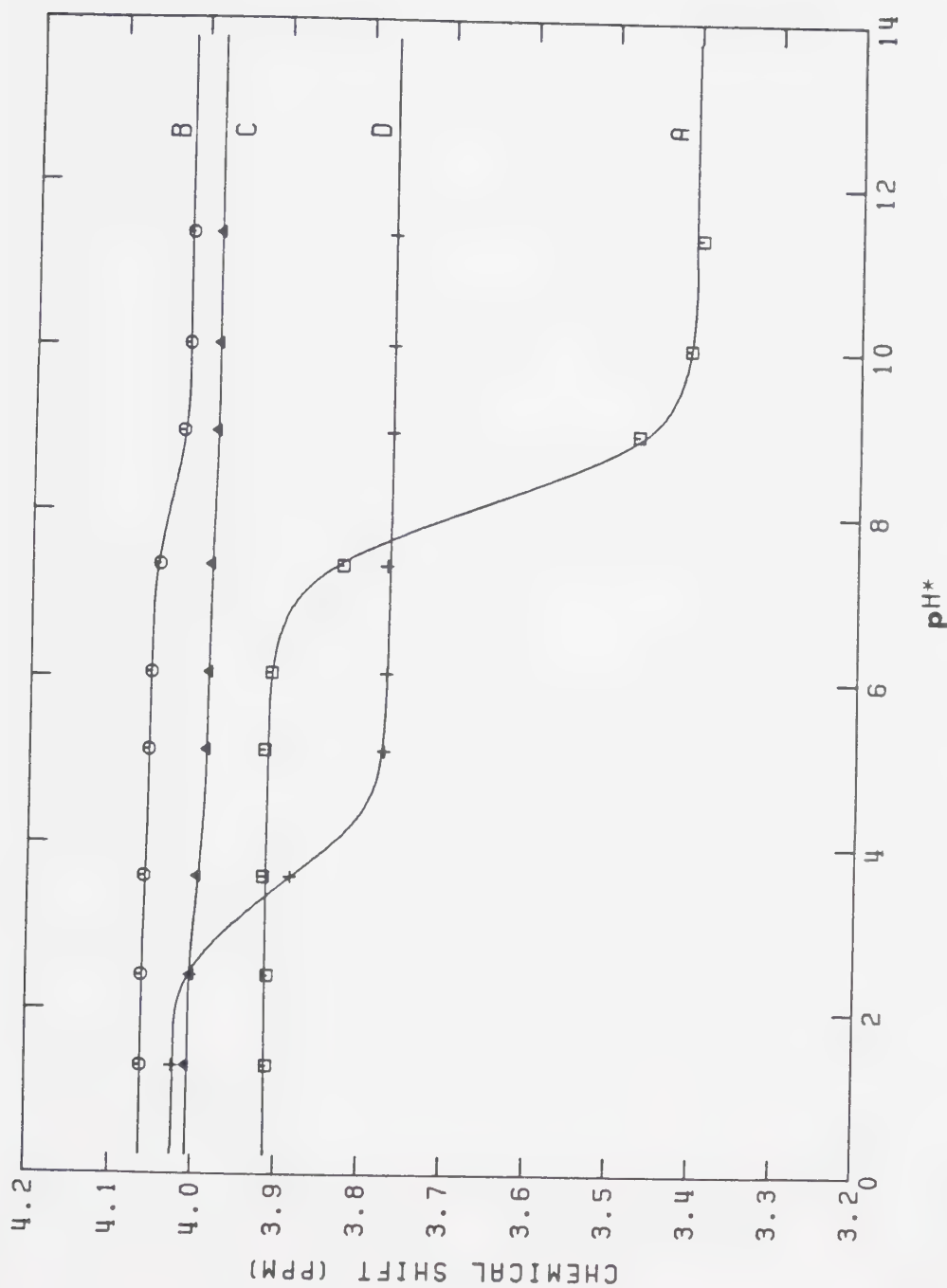


Figure 44. Plots of chemical shift versus pH* for the methylene protons of tetraglycine. (A) to (D) represent the two equivalent methylene protons of each glycine residue from the N-terminal to the C-terminal end of the molecule.

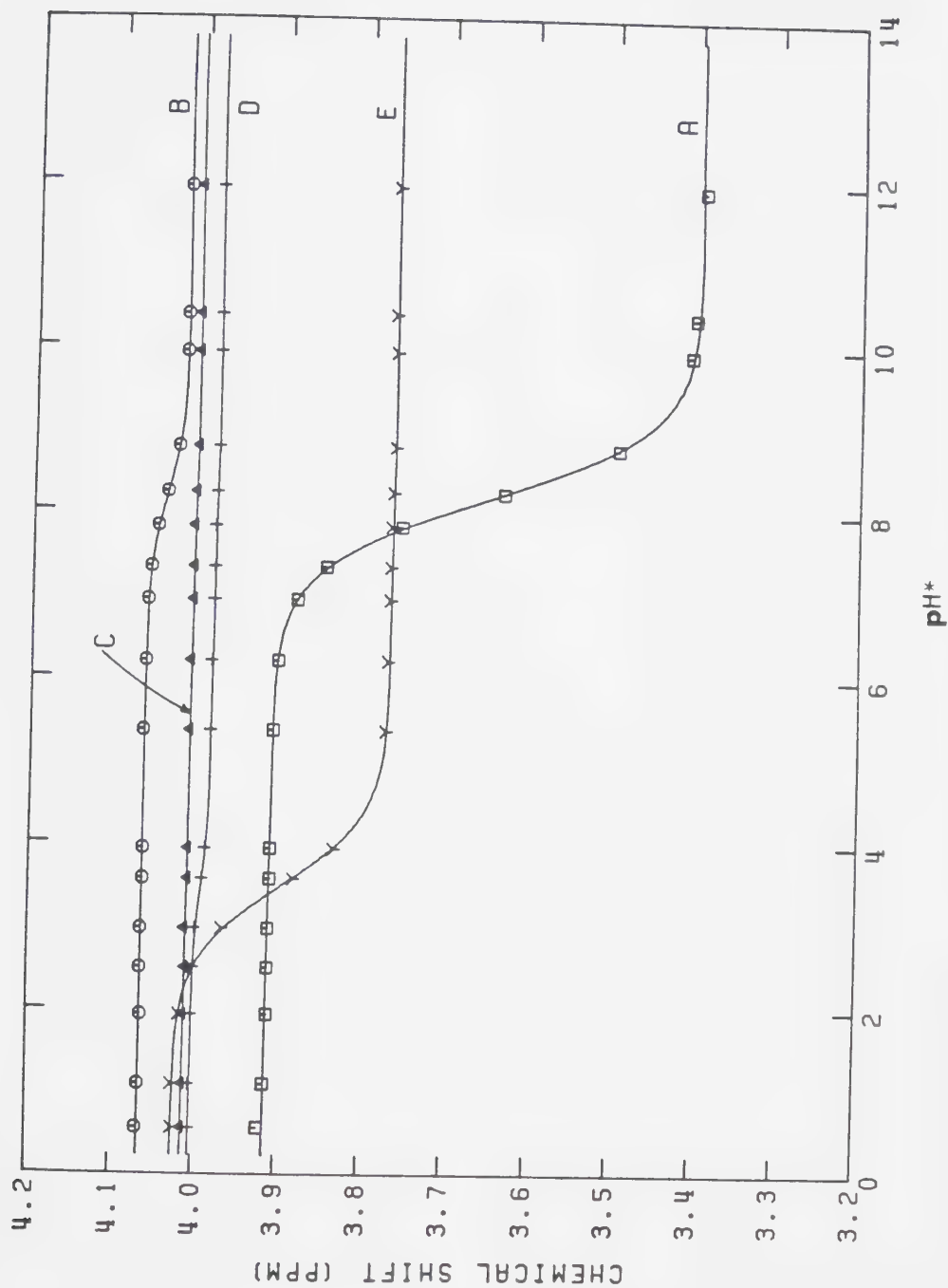


Figure 45. Plots of chemical shift versus pH* for the methylene protons of penta-glycine. (A) to (E) represent the two equivalent methylene protons of each glycine residue from the N-terminal to the C-terminal end of the molecule.

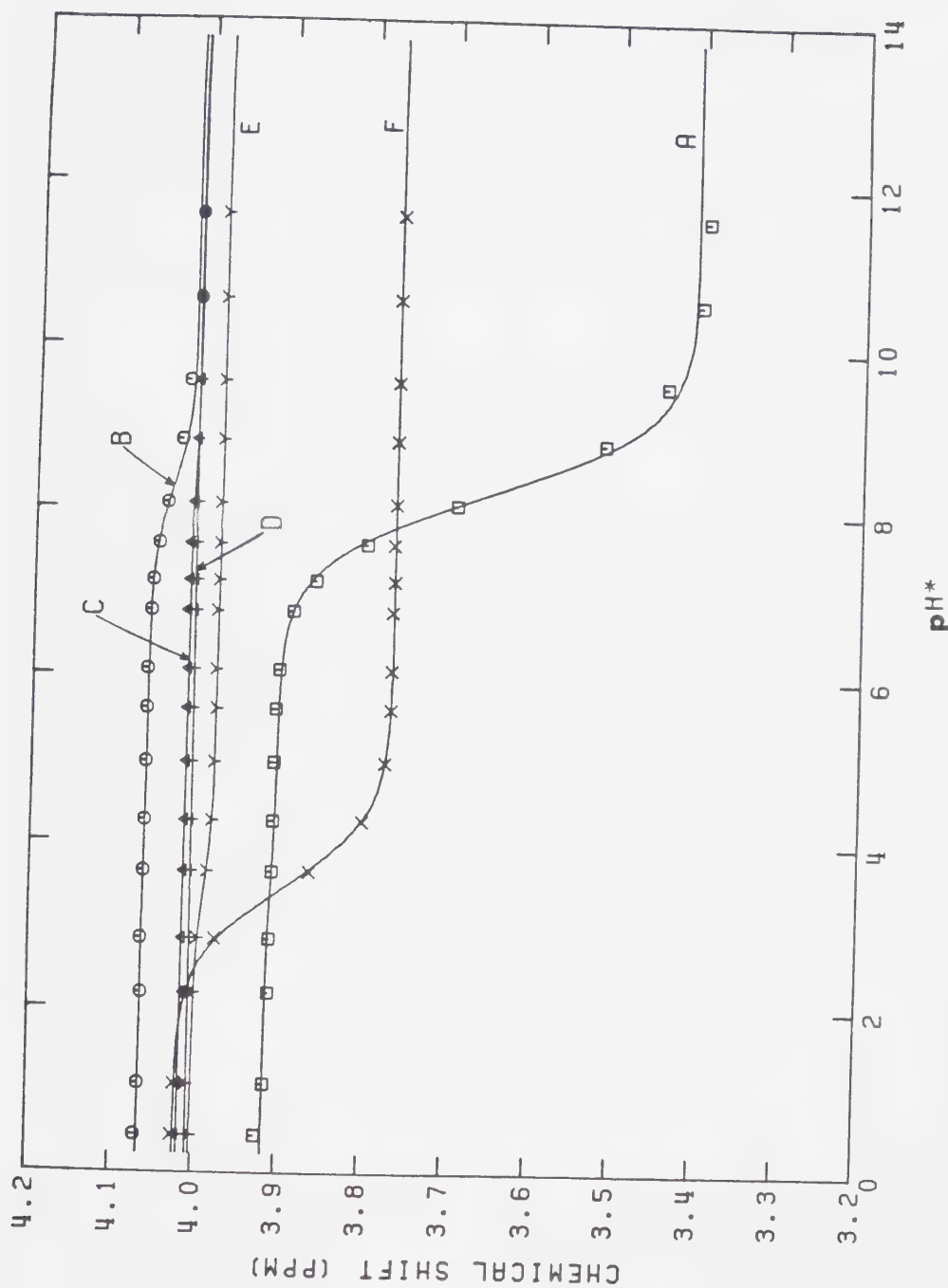


Figure 46. Plots of chemical shift versus pH* for the methylene protons of hexaglycine. (A) to (F) represent the two equivalent methylene protons of each glycine residue from the N-terminal to the C-terminal end of the molecule.

where δ_o is the observed chemical shift and δ_{NC}^+ , δ_{NC}^{+-} and δ_{NC}^- refer to the chemical shifts of the fully protonated species, the protonated amino and deprotonated carboxylate species and the fully deprotonated species, respectively. In practice, it is usually better to fit the experimental data to the equation:

$$\delta_o = \frac{10^{(pH - pK_a)} \delta_A + \delta_{HA}}{10^{(pH - pK_a)} + 1} \quad (21)$$

when the resonance involved is affected by only one of the two functional groups on the peptide. The other functional group is separated by the intervening glycine residues and has a negligible effect on the chemical shift of the resonance under consideration. In this case, δ_{HA} and δ_A refer to δ_{NC}^{+-} and δ_{NC}^- in determining an ammonium pK_a and δ_{NC}^+ and δ_{NC}^{+-} for a carboxylate pK_a . Table 9 presents the experimentally determined pK_a values for the amino and carboxylate groups of the glycine peptides from diglycine to hexaglycine as determined in D_2O by fitting the chemical shift versus pH^* data in Figures 42 to 46 to Equation 21 with KINET. The measured values for the carboxylate pK_a 's are very similar in magnitude with an average value of 3.41. The ammonium pK_a 's are also close to each other with an average of 8.20 for the five pK_a

Table 9

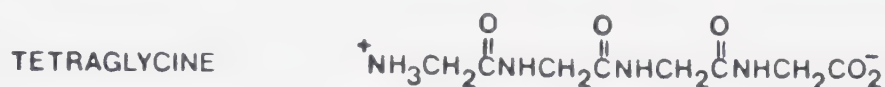
pK_a Values Measured for a Series of Glycine Peptides

Compound	Carboxylate pK _a		Amino pK _a	
	<u>Experimental (a)</u>	<u>Literature (b)</u>	<u>Experimental (a)</u>	<u>Literature (b)</u>
Diglycine	3.40 ± 0.03	3.20	8.42 ± 0.06	8.22
Triglycine	3.22 ± 0.03	3.24	8.13 ± 0.01	8.20
Tetraglycine	3.51 ± 0.02	3.24	8.08 ± 0.05	7.89
Pentaglycine	3.47 ± 0.01	-	8.16 ± 0.01	-
Hexaglycine	3.45 ± 0.01	-	8.21 ± 0.03	-

(a) Determined in D₂O. pH* of solutions uncorrected for deuterium isotope effects.(b) Determined in H₂O. Values from Sillén and Martell [75].

values determined. For comparison, literature values for H₂O solutions are also listed [75].

As an example of the assignment scheme for the peptide protons, the case of tetraglycine (Figure 44) will be considered in detail. As the pH* is lowered from above



pH* 11 the amino group will become protonated first. The A protons being closest to the amino group will experience the greatest shielding changes and thus the greatest change in chemical shift and can be assigned as indicated in Figure 44. The B protons are the next nearest to the protonation site and have the next greatest change in chemical shift as shown in Figure 44. The effect of protonation of the amino group on the C and D protons is very slight due to their greater distances from the protonation site. As the pH* continues to drop the carboxylate group eventually protonates. Here the A and B protons are little affected while the D protons being closest to the protonation site experience the largest chemical shift change as shown in Figure 44. The C protons also experience some shielding changes as recorded in Figure 44 and can either be assigned on this basis or by the process of elimination since the other protons have

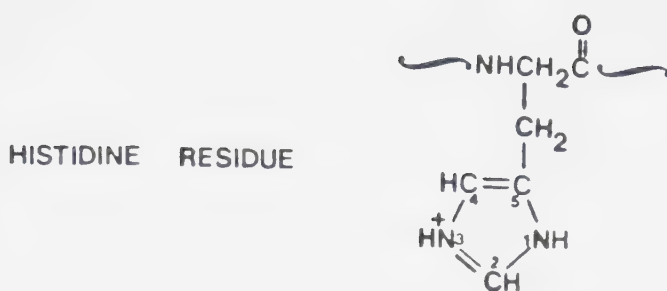
already been assigned. Thus, at the pH^* at which the T_2 measurements shown in Table 8 and diagrammed in Figure 39 were made, pH^* 7.35, the resonances at 3.77, 3.80, 3.98 and 4.04 ppm correspond to the D, A, C and B protons, respectively.

Similar methods for the assignment of protons to resonances were employed for the other glycine peptides studied (Figures 42, 43, 45 and 46). The chemical shifts for the resonances of the two terminal glycine residues are always further upfield, except for the protons of the terminal residue containing the carboxylate group at very low pH^* , which implies shielding by the two functional groups, particularly in their deprotonated forms. The shielding changes on protonation are greater for the amino group than for the carboxylate group as indicated by the magnitude of the chemical shift change for the adjacent protons in each case.

There is an initial drop in the T_2 values (Table 8) in going from glycine to diglycine but very little change thereafter in the average T_2 relaxation times among the various glycine peptides. This implies a reduction in the molecular mobility of the peptides over that of glycine, which may be due to the restrictions imposed on rotation by the loss of spherical shape in the peptides. The lack of additional decreases in T_2 relaxation times with

increasing chain length tends to support this view. In all the glycine peptides studied, the T_2 relaxation times of the two terminal glycine residues tend to be longer than those of the protons of the internal glycine residues which reflects the increased mobility of the terminal residues of the molecules. As well, the protons of the internal glycine residues show a trend towards decreasing T_2 relaxation times as one moves from the terminal amino group towards the terminal carboxylate group. The pH^* at which the T_2 measurements were made appears to alter the observed relaxation times somewhat, as experiments performed at two different pH values for triglycine demonstrate. At a pH^* of 7.32 T_2 values for the A, B and C protons of triglycine were measured as 0.300, 0.228 and 0.300 seconds, respectively, while at a pH^* of 5.92 the measured relaxation times were found to be 0.604, 0.275 and 0.348 seconds. The T_2 relaxation times at the two pH^* values are not orders of magnitude different although the observed differences are significant. The effect of pH^* on the measured T_2 values was minimized in the T_2 determinations by adjusting the pH^* of the glycine peptide solutions to be approximately the same.

A number of higher molecular weight compounds were also studied in order to determine typical T_2 relaxation times for their protons. A T_2 value for the imidazole proton on carbon 2 of the histidine residue in position 6



of angiotensin II (1031.2 g/mole) was obtained as were T_2

ANGIOTENSIN II Asp-Arg-Val-Tyr-Ile-His-Pro-Phe

values for the imidazole protons of carbon 2 of the histidine residues in positions 6 and 9 of angiotensin I

ANGIOTENSIN I Asp-Arg-Val-Tyr-Ile-His-Pro-Phe-His-Leu

(1416.6 g/mole). The imidazole protons on carbon 2 of histidine residues were used to evaluate T_2 relaxation times for angiotensin I and II because the other resonances were either phase modulated in the spin-echo spectra or buried beneath resonances which were phase modulated. Representative T_2 relaxation times at several chemical shifts corresponding to broad peaks in the spectra were obtained for trypsin inhibitor [76] (~6,000 g/mole), lysozyme [77] (~14,400 g/mole), bovine serum albumin (~65,000 g/mole) and hemoglobin (~68,000

g/mole). In the case of hemoglobin, a solution of hemolyzed red blood cells was used since the majority of the signal at short τ_2 delay times was due to hemoglobin resonances and little was due to the other, generally smaller molecules, in the erythrocytes. The term "representative T_2 " describes the composite nature of the relaxation times measured at a particular chemical shift for the high molecular weight proteins due to overlapping of the numerous broad resonances at each chemical shift. To illustrate the overlapping nature of the resonances in such spectra, the single-pulse spectrum for lysozyme is presented in Figure 47. The sharp resonances at 1.91 and 1.24 ppm belong to acetate present as an impurity and t-butanol added as a chemical shift reference, respectively. Plots of normalized intensity versus τ_2 delay time for the various resonances evaluated for the compounds discussed above are shown in Figures 48 to 53. The measured T_2 relaxation times for these compounds are presented in Table 10. The relatively large amount of scatter in many of the curves in Figures 50 to 53 for the representative T_2 values is due to the composite nature of the intensity measured at each chemical shift. Most of the resonances are undergoing phase modulation which leads to non-exponential changes in intensity with varying τ_2 delay times.

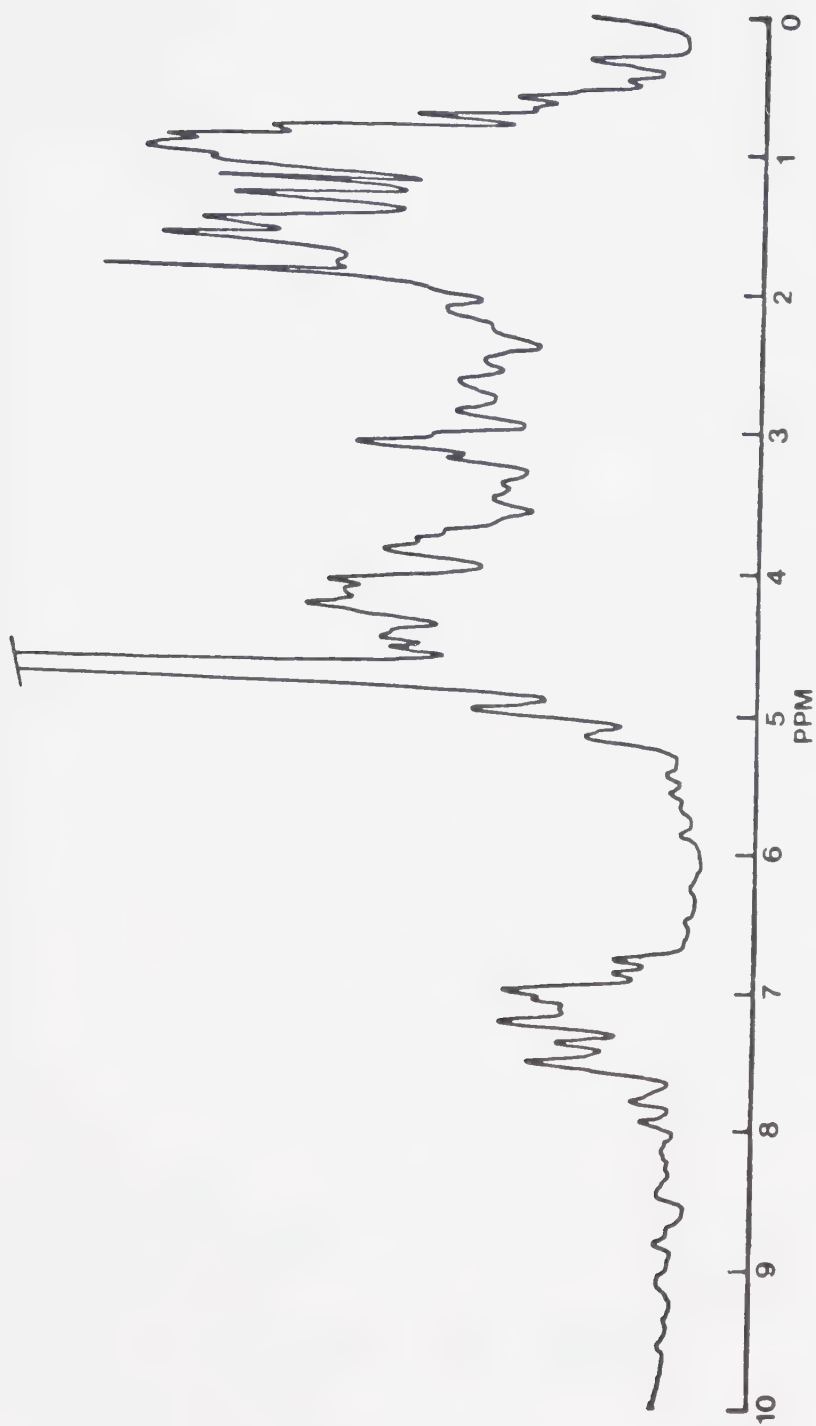


Figure 47. 360 MHz single-pulse NMR spectrum of a 2 mM solution of lysozyme. The

sharp resonance at 1.91 ppm is due to acetate present as an impurity while the resonance at 1.24 ppm is due to t-butanol added as a chemical shift reference.

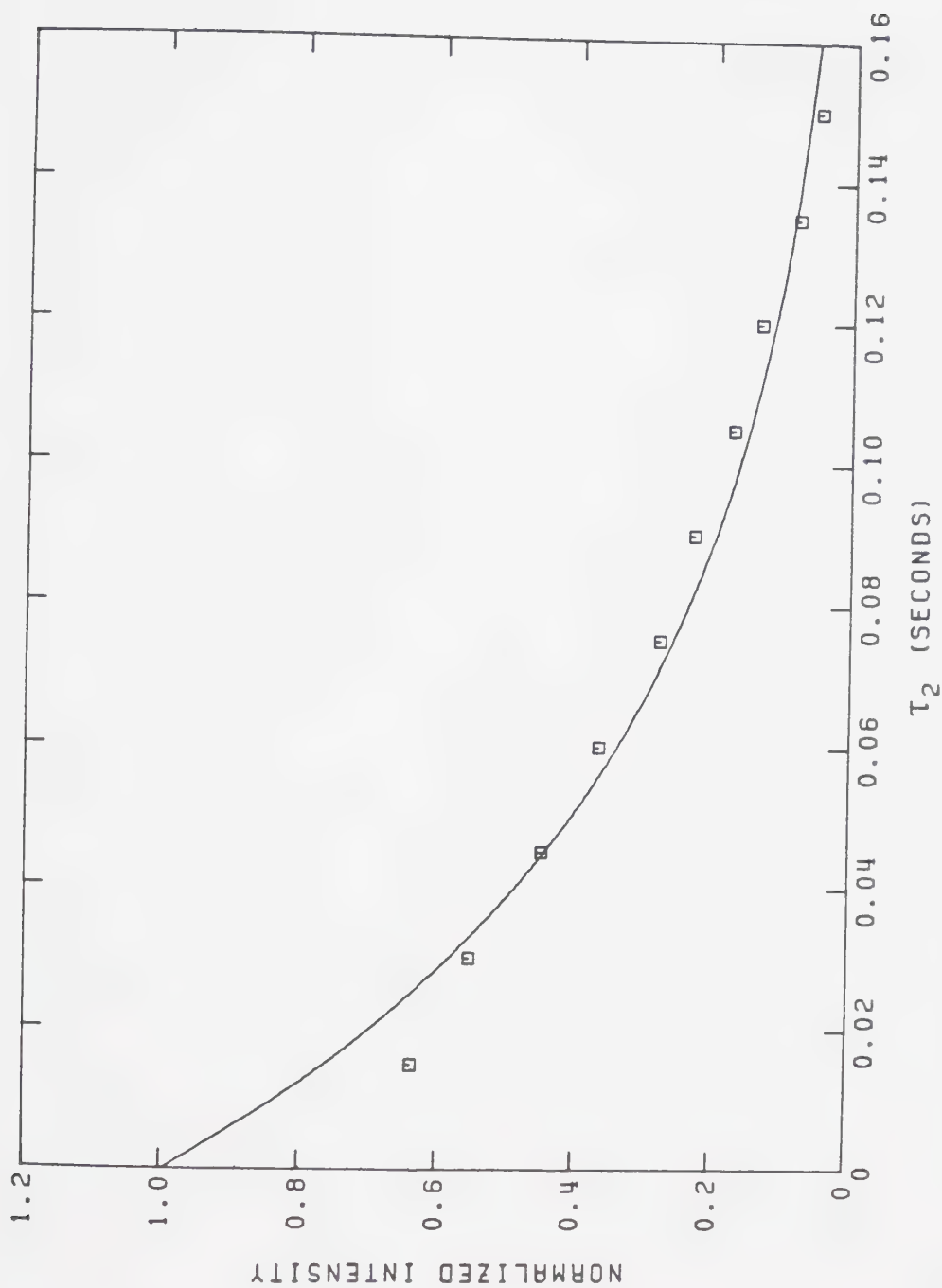


Figure 48. A plot of intensity versus τ_2 delay time, normalized to one at a τ_2 delay of zero, for the imidazole proton on carbon 2 of the histidine residue in position 6 of angiotensin II. The solid curve was calculated using the T_2 value in Table 10.

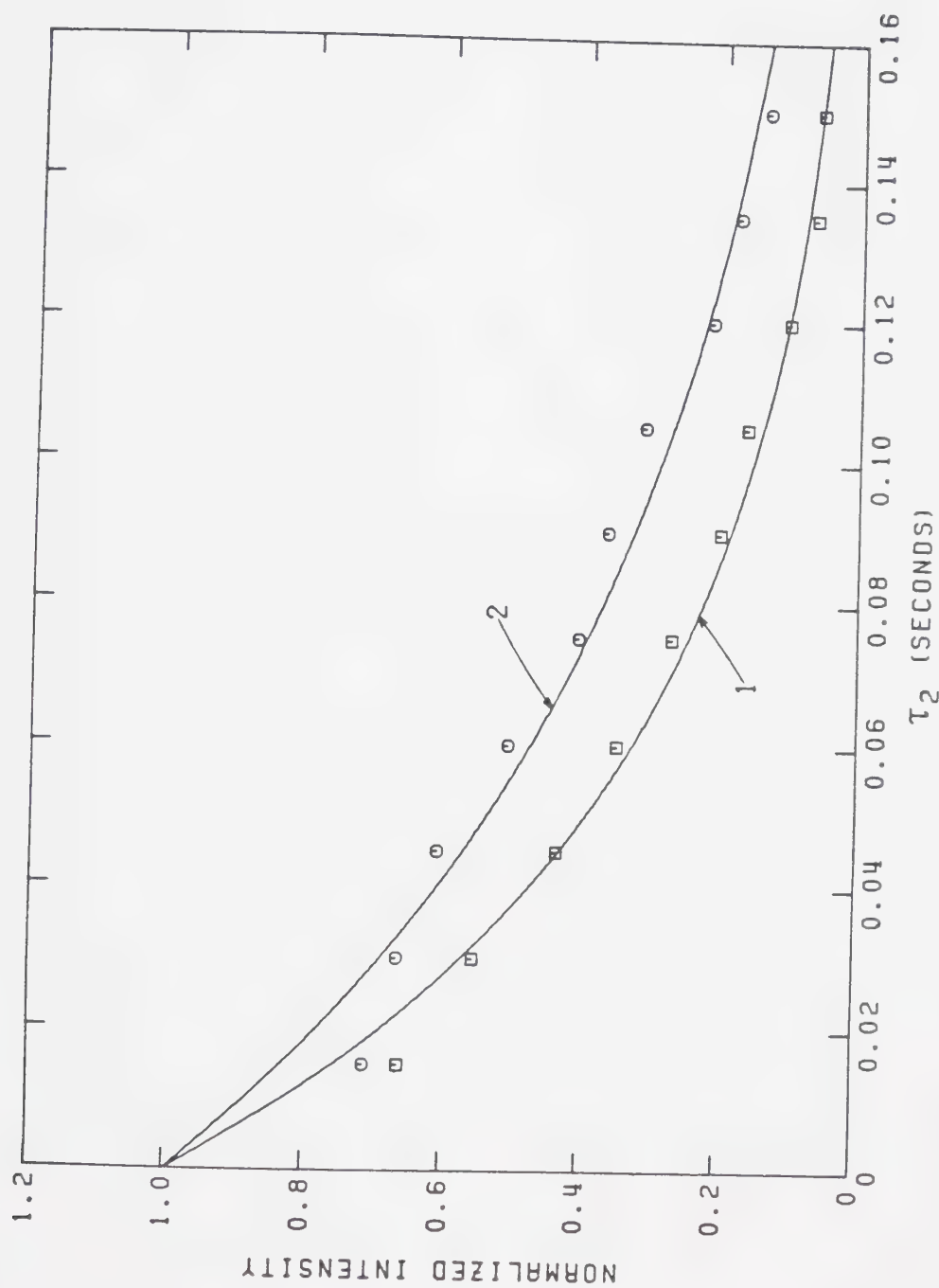


Figure 49. Plots of intensity versus τ_2 delay time, normalized to one at a τ_2 delay of zero, for the imidazole protons on carbon 2 of the histidine residues in positions 6 and 9 of angiotensin I. The solid curves were calculated using the T_2 values in Table 10. Curve 1 is for the histidine in position 6 and curve 2 for that in position 9.

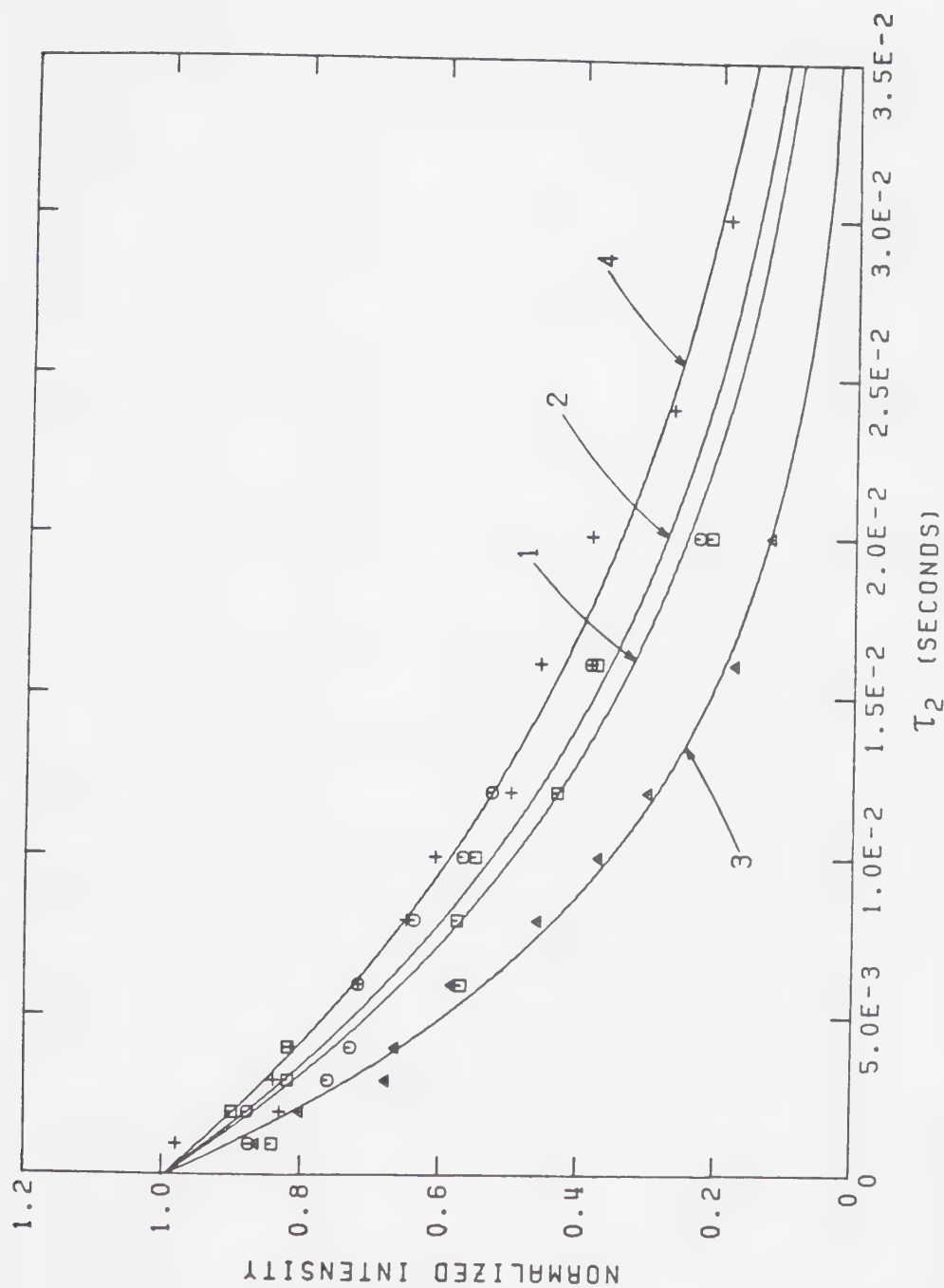


Figure 50. Plots of intensity versus τ_2 delay time, normalized to one at a τ_2 delay of zero, for several chemical shifts in the spectrum of trypsin inhibitor. The solid curves were calculated from the T_2 values in Table 10. Curves 1, 2, 3, and 4 are for 7.88, 7.58, 3.81 and 1.64 ppm, respectively.

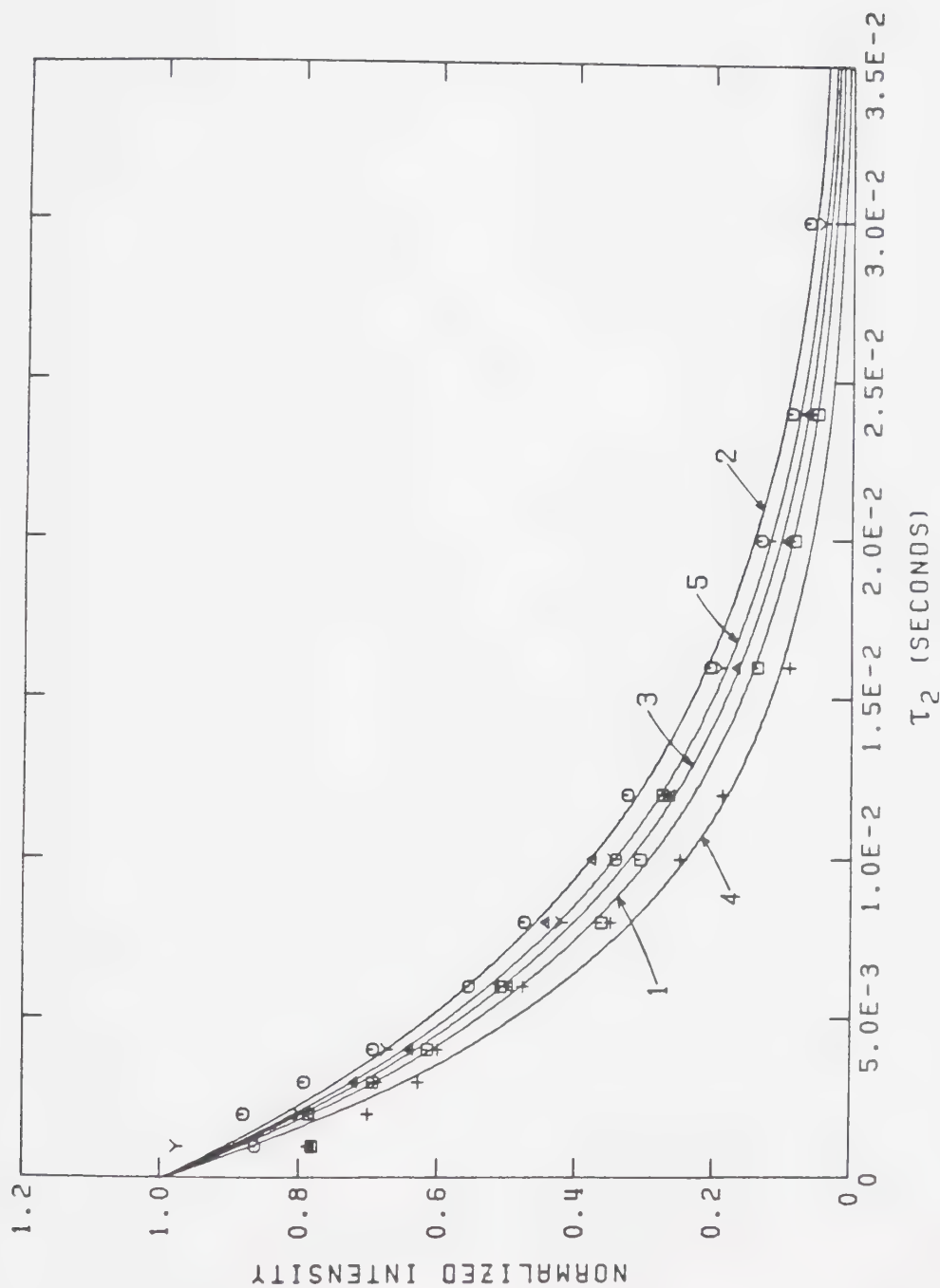


Figure 51. Plots of intensity versus T_2 delay time, normalized to one at a T_2 delay of zero for several chemical shifts in the spectrum of lysozyme. The solid curves were calculated using the T_2 values in Table 10. Curves 1□, 2○, 3△, 4+ and 5▽ are for 7.21, 6.98, 4.28, 3.12 and 1.04 ppm, respectively.

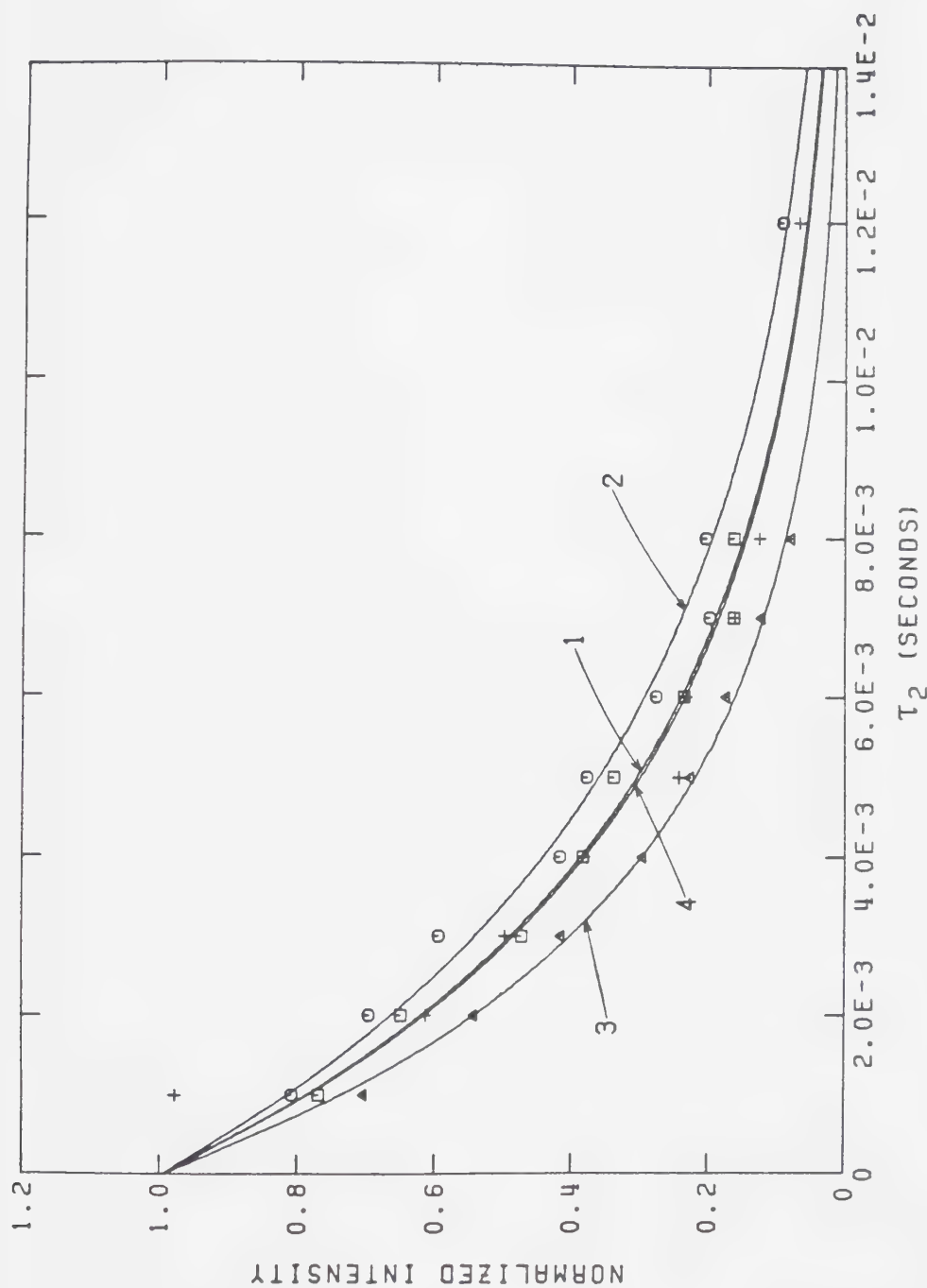


Figure 52. Plots of intensity versus T_2 delay time, normalized to one at a T_2 delay of zero for several chemical shifts in the spectrum of bovine serum albumin. The solid curves were calculated using the T_2 values in Table 10. Curves 1 \square , 2 \circ , 3 \triangle and 4 $+$ are for 6.79, 4.03, 1.69 and 0.93 ppm, respectively.

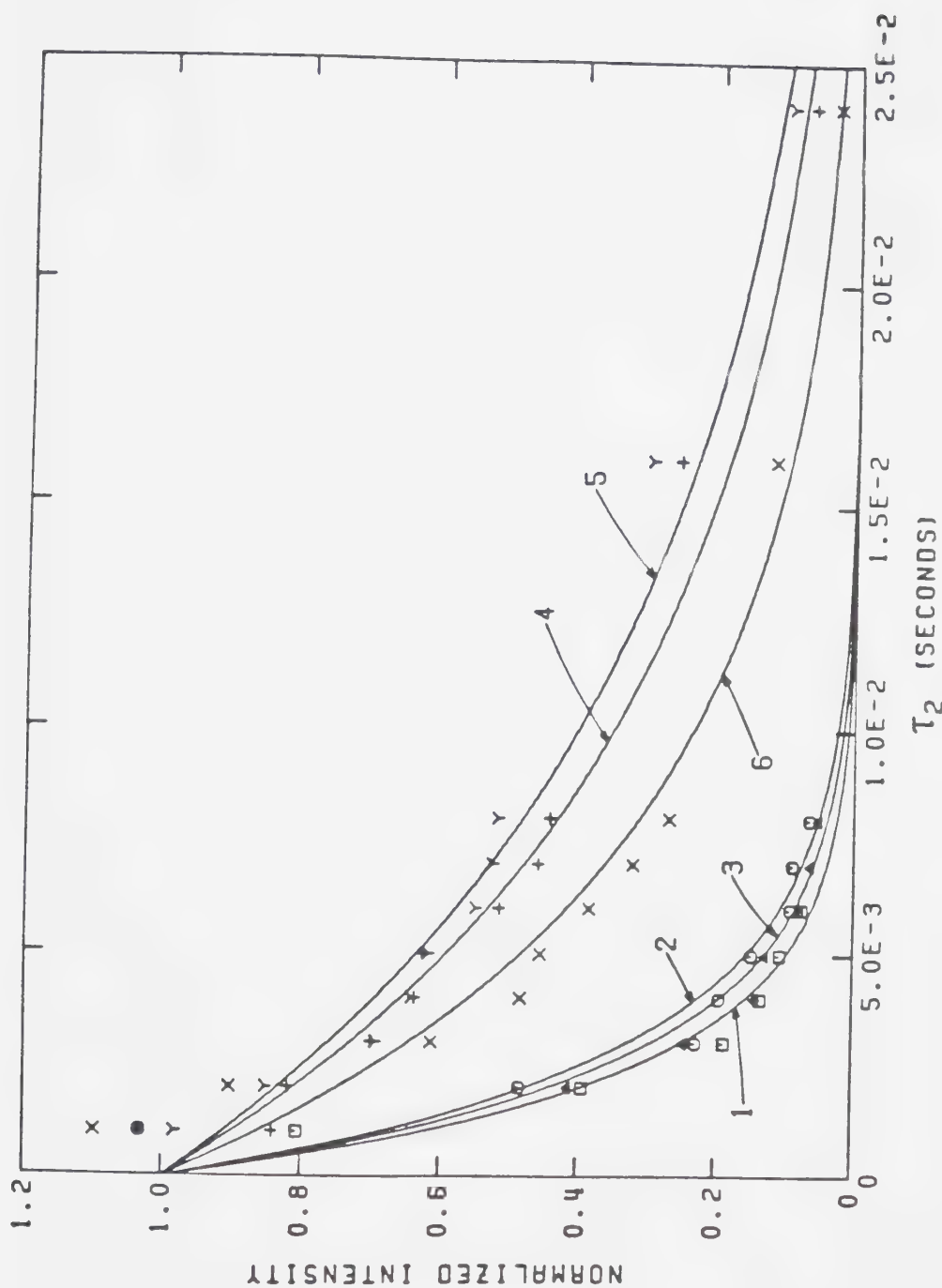


Figure 53. Plots of intensity versus τ_2 delay time, normalized to one at a τ_2 delay of zero, for several chemical shifts in the spectrum of hemoglobin. The solid curves were calculated using the T_2 values in Table 10. Curves 10, 20 and 3A are for the non-histidine region at 4.10, 1.16 and 0.76 ppm, respectively. Curves 4+, 5Y and 6X are for the histidine region at 8.01, 7.78 and 6.90 ppm.

Table 10

T₂ Relaxation Times Measured for Higher Molecular Weight Compounds

Compound	Molecular Weight	pH*(a)	Chemical Shift(b)	T ₂ (c)	Average
Angiotensin II	1031.2	7.78	7.76 (C-2 of His 6)	0.111±0.007	0.111
Angiotensin I	1416.6	7.41	7.86 (C-2 of His 6) 7.70 (C-2 of His 9)	0.108±0.005 0.162±0.010	0.135
Trypsin Inhibitor	6,000	7.00	7.88 7.58 3.81 1.64	0.028±0.002 0.031±0.003 0.019±0.001 0.037±0.001	0.029
Lysozyme	14,400	6.70	7.21 6.98 4.28 3.12 1.04	0.0164±0.0004 0.0206±0.0006 0.0177±0.0005 0.0141±0.0006 0.0188±0.0002	0.0175
BSA	65,000	7	6.79 4.03 1.69 0.93	0.0084±0.0005 0.0098±0.0005 0.0066±0.0002 0.0083±0.0006	0.0083

Table 10 (Cont'd.)

Compound	Molecular Weight	pH*(a)	Chemical Shift(b)	T ₂ (c)	Average
Hemoglobin	68,000	7	8.01 (histidine)	0.0191±0.0012	0.0183
				0.0220±0.0013	
				0.0138±0.0007	
			4.10 (non-histidine)	0.0044±0.0005	0.0049
				0.0054±0.0006	
				0.0049±0.0005	

(a) Uncorrected for isotope effects due to D₂O.

(b) Measured relative to DSS.

(c) Measured in seconds.

For hemoglobin, T_2 values were measured for both histidine and non-histidine portions of the spectrum. The results indicate that for histidine protons the T_2 relaxation times were appreciably longer than the non-histidine proton relaxation times, reflecting the somewhat greater mobility of the imidazole protons of the amino acid histidine [14]. Generally, the measured T_2 relaxation times were observed to follow a trend to shorter values as the molecular weight of the compounds increased. This is illustrated graphically in Figure 54 where an average T_2 value for each compound, based on the magnitude of those evaluated, is plotted against molecular weight for all the compounds studied. A linear least-squares fit was conducted, excepting glycine from the calculation and using an average T_2 for hemoglobin incorporating both the histidine and non-histidine T_2 values, to establish the position of the line in Figure 54. The correlation coefficient of close to -0.99 indicates a reasonable degree of linearity for the inverse relationship between molecular weight and T_2 relaxation time.

Figure 55 shows the intensity versus τ_2 delay time behavior for several of the compounds studied plotted on the same coordinate system. From this plot, it is obvious that resonances from the larger protein molecules can be

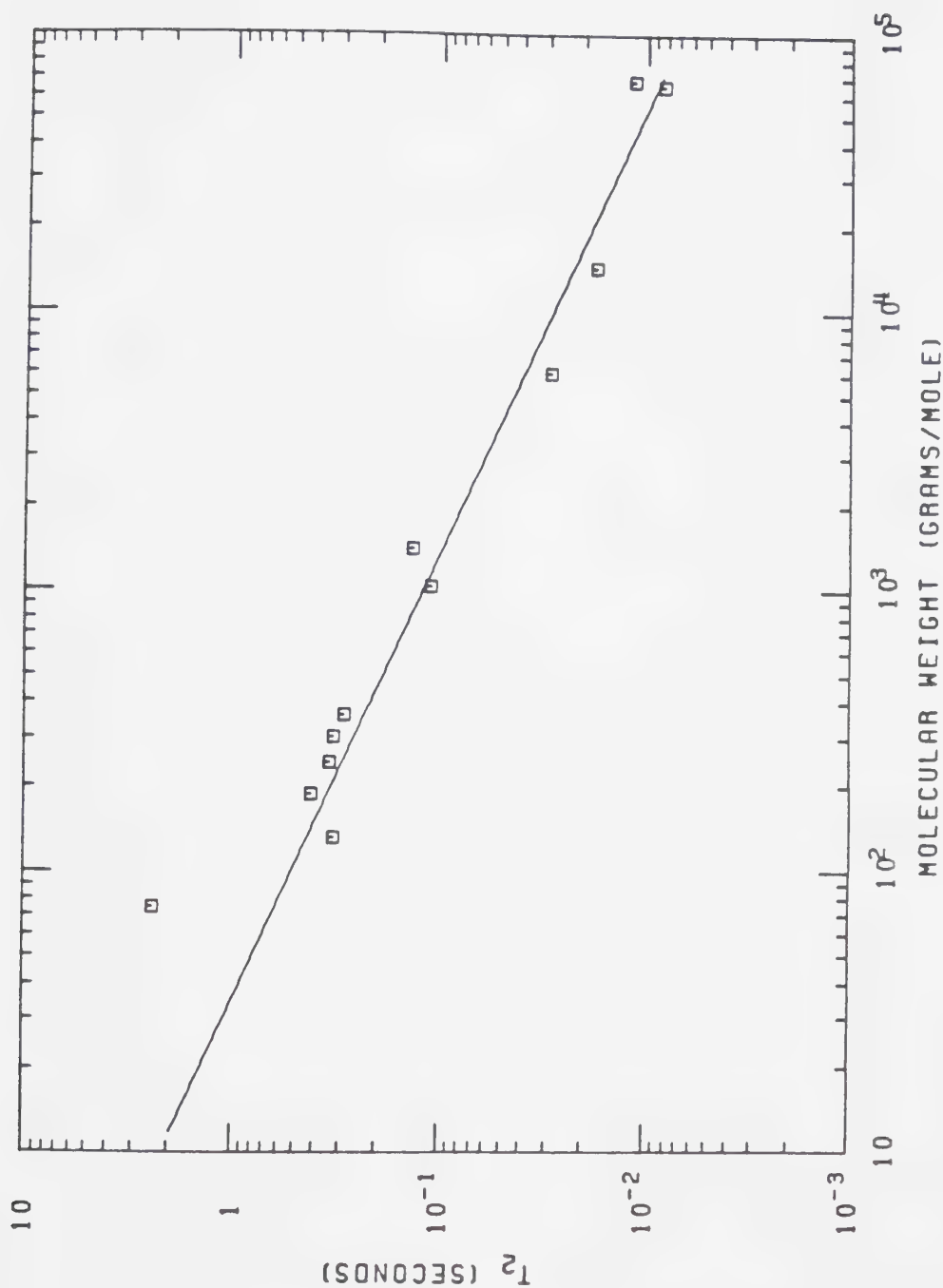


Figure 54. A plot of the average T_2 relaxation times for each of the compounds discussed in Figures 36 to 41 and Figures 48 to 53 versus their molecular weights. The straight line results from a linear least-squares fit to the points, excluding glycine (upper left), and has a correlation coefficient of -0.9853 .

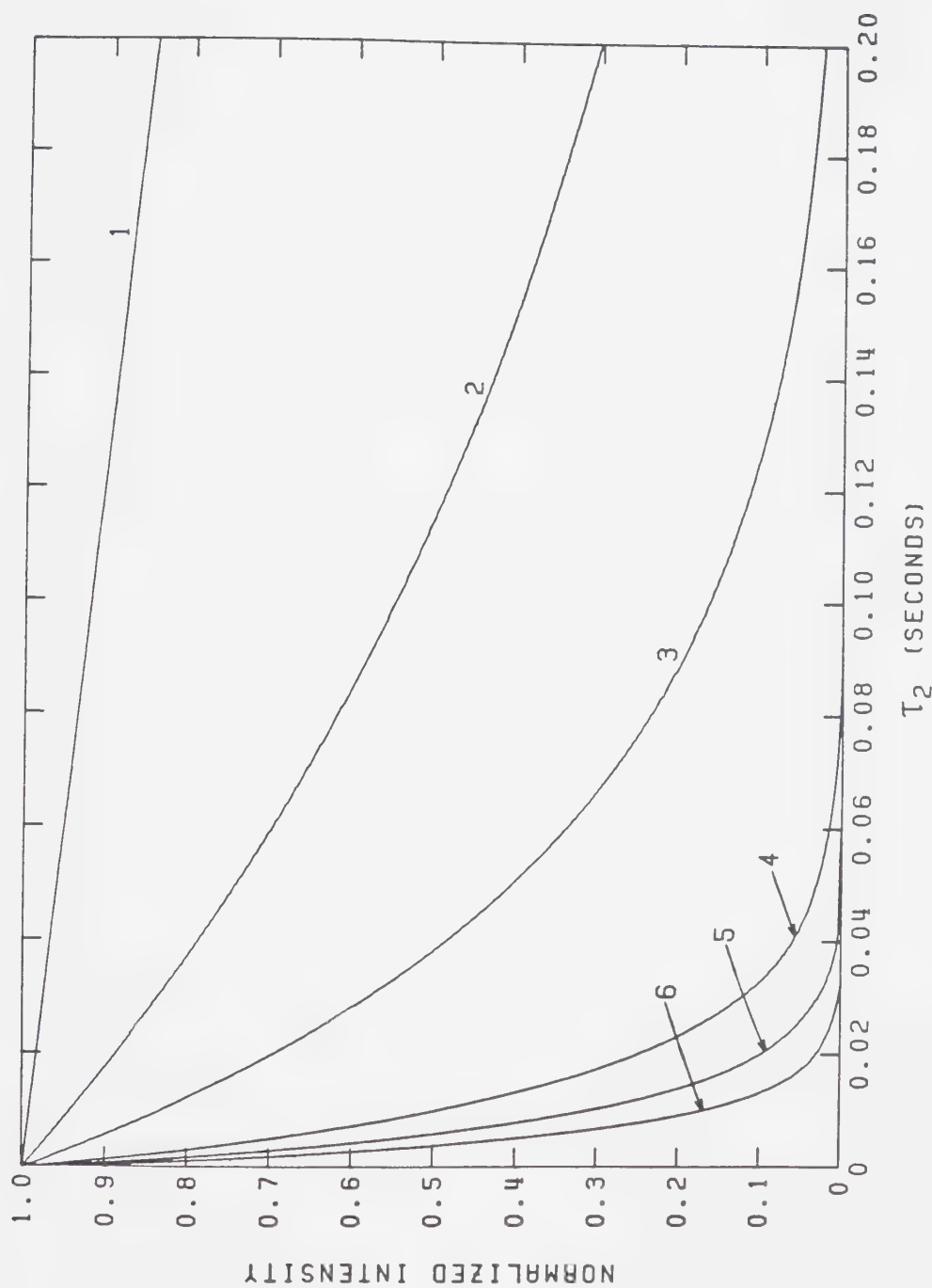


Figure 55. The calculated intensity versus τ_2 behavior during the spin-echo experiment for several compounds using the average T_2 values for each compound plotted in Figure 54. Curves 1 to 6 correspond to glycine, tetraglycine, angiotensin II, trypsin inhibitor, lysozyme and hemoglobin, respectively.

eliminated while those of the smaller compounds are retained to a significant degree by using a τ_2 delay of around 60 milliseconds [15]. At this delay time, the signals from tetraglycine (curve 2) are still present at approximately 70% of their initial intensity while only about 1.5% of the lysozyme signals (curve 5) remain in the spectrum. An even more dramatic example of using the spin-echo method to enhance the resonances of one compound over another is provided by glycine (curve 1) and hemoglobin (curve 6). In this case, around 95% of the glycine signal remains while the hemoglobin resonances have been virtually eliminated at a τ_2 delay of 60 milliseconds. In the spin-echo spectra of red blood cells, this is confirmed as glycine is observed at 3.54 ppm when the hemoglobin resonances are eliminated [17]. Figure 56 presents the single-pulse spectrum and spin-echo spectra measured at 20, 60 and 100 milliseconds for a solution containing 2 mM of both tetraglycine and lysozyme. As the delay time is increased the lysozyme signals disappear much faster than those of tetraglycine.

The spin-spin relaxation times measured in these experiments may not reflect the true T_2 values, particularly for the glycine peptides which have relatively long T_2 relaxation times, due to diffusion effects lowering the measured T_2 values. These effects

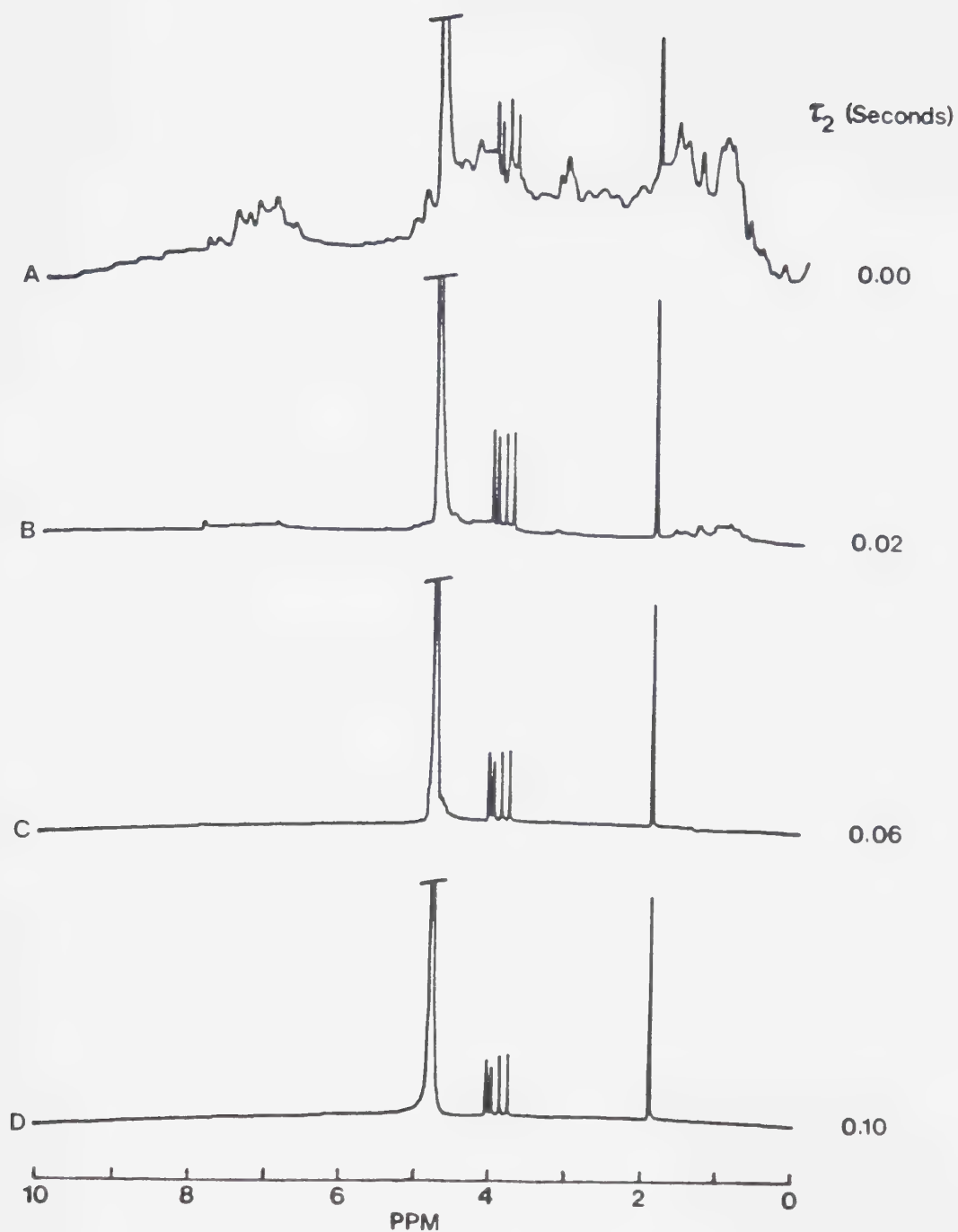


Figure 56. The single-pulse spectrum (A) and spin-echo spectra measured at various τ_2 delay times (B to D) for a 2 mM solution of both tetraglycine and lysozyme.

could have been avoided by using the CPMG pulse sequence [13]. However, this was not done since the purpose of the experiments was to obtain values appropriate to the spin-echo technique, since this technique is generally used to obtain resolution enhancement on the basis of T_2 differences. The measured T_2 relaxation times, although not strictly accurate, are practical values the differences between which can be used to afford resolution enhancement.

C. Monitoring of Small Molecules in Protein Solutions

The existence of T_2 discrimination in the spin-echo experiment can be utilized to determine the presence of contaminant molecules in protein preparations. By using a τ_2 delay time of 60 milliseconds, resonances from the protein, which as shown in the previous section will have relatively short T_2 relaxation times, will have disappeared from the NMR spectrum. Any remaining resonances must therefore belong to smaller molecules which are contaminants in the solution. If it is desired to remove the small molecules, the progress of cleanup procedures can be followed by monitoring the decrease in intensity of the contaminant peaks in the spin-echo spectrum. The results of such an experiment are described in this section for two proteins, a commercially obtained

sample of bovine serum albumin (BSA) and hemoglobin prepared from hemolyzed human erythrocytes. In both cases, the small molecules were removed by dialysis. In this procedure, a membrane of an appropriate molecular weight cutoff is chosen so that the contaminant molecules diffuse out of the protein solution into the surrounding medium while the protein itself, being unable to pass through the membrane, is retained inside the dialysis sac [69].

The results of this cleanup procedure are shown in Figures 57 to 59 for the dialysis of the BSA. A 7.5-mL portion of a 0.003 M solution of BSA in saline D₂O was dialyzed using a membrane with a molecular weight cutoff of 6,000 to 8,000 daltons against 28 to 29 mL of saline D₂O for 12 hours at 4°C following which a sample was withdrawn. The dialysis sac was then placed in fresh saline D₂O for a further 12 hours for a second dialysis after which another sample was withdrawn. This procedure was repeated for all subsequent dialyses. Figure 57A presents the single-pulse spectrum measured before any dialysis and consists of a broad envelope of resonances arising from the protein itself plus several relatively sharp signals. Two intense resonances are immediately obvious in the spectrum. That at 4.80 ppm is due to HDO while that at 3.73 ppm has been tentatively assigned to

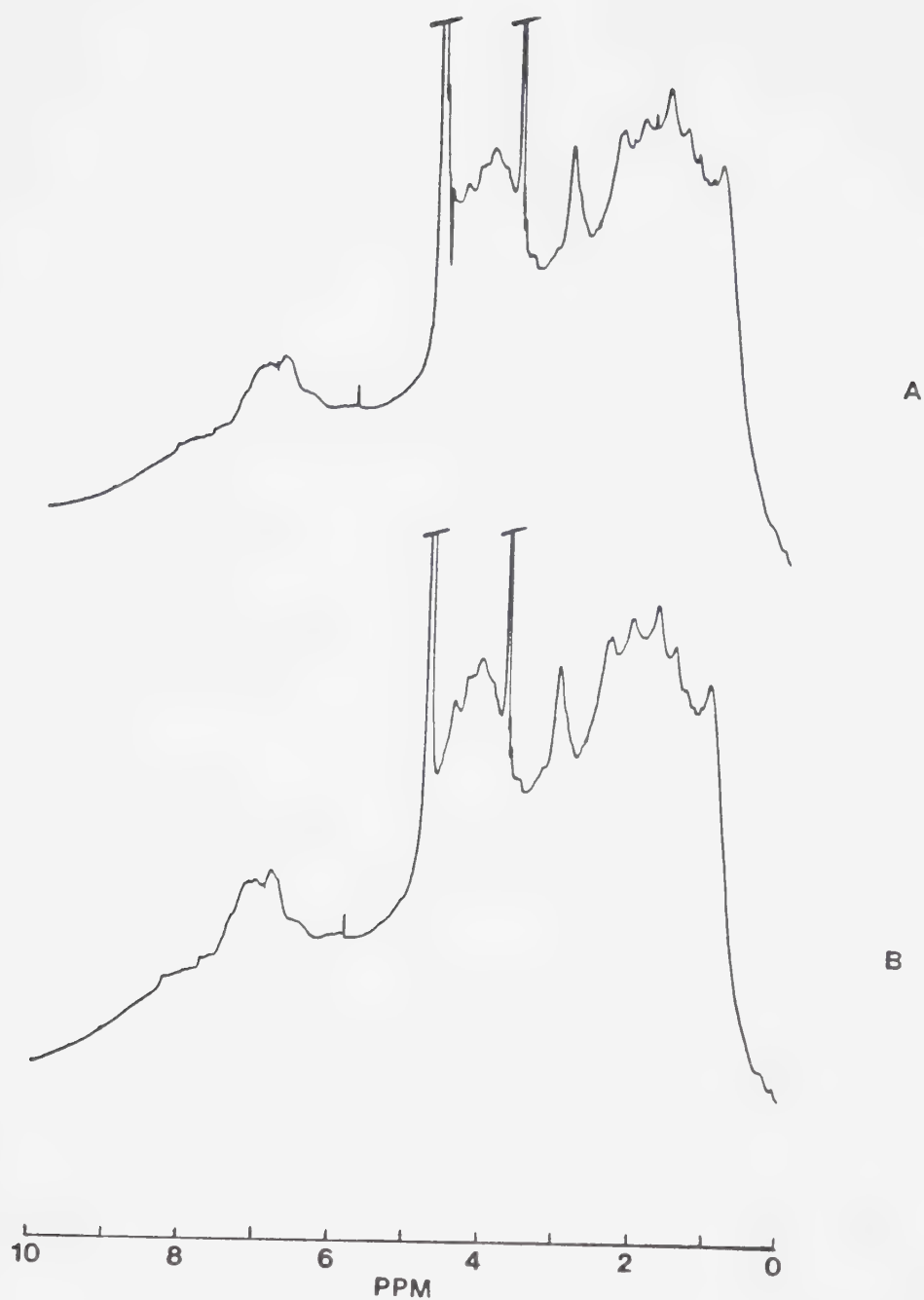


Figure 57. Single-pulse spectra of a solution of 0.003 M bovine serum albumin (A) before dialysis and (B) after 5 dialyses against saline D₂O.

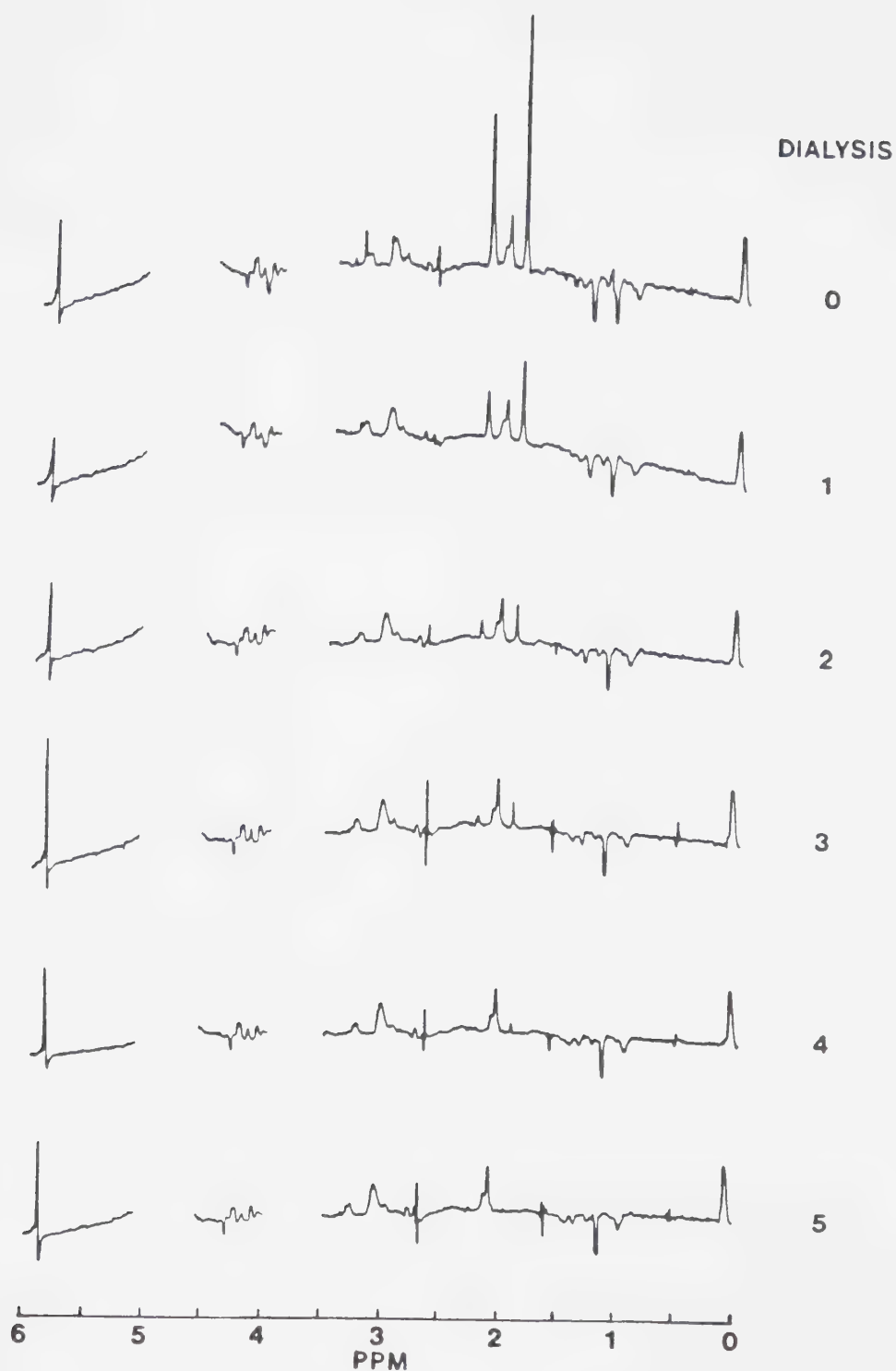


Figure 58. Spin-echo spectra ($\tau_2 = 0.06$ second) of a solution of 0.003 M bovine serum albumin after successive dialyses against saline D_2O .

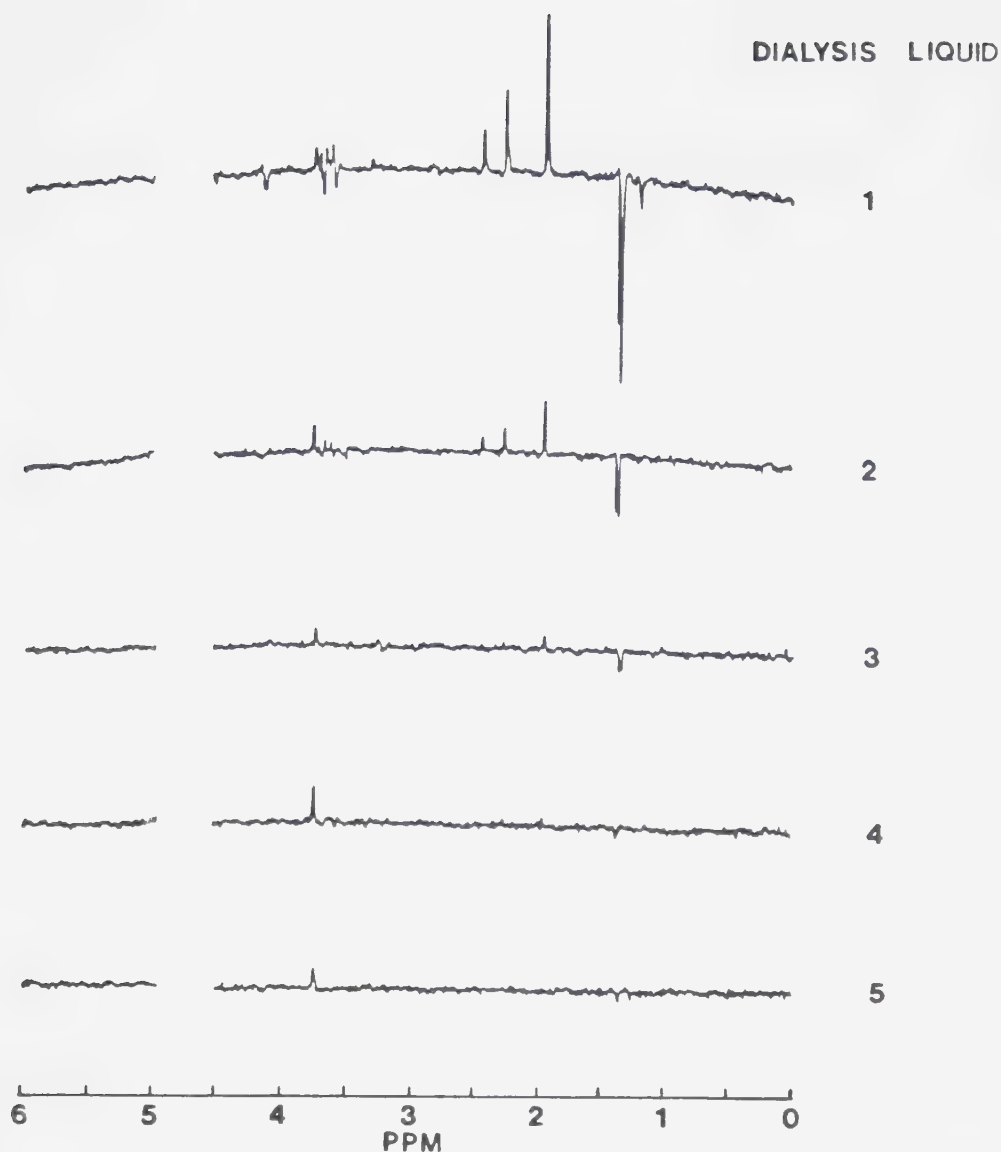


Figure 59. Spin-echo spectra ($\tau_2 = 0.06$ second) of successive dialysis media against which a 0.003 M solution of bovine serum albumin was dialyzed.

the presence of polyglycine contaminants in the protein owing to the chemical shift and singlet character of the resonance [78]. The smaller sharp peak at 5.88 ppm is an artifact in the spectrum caused by the reflection of the resonance at 3.73 ppm about the carrier, which was located at the HDO frequency. The presence of smaller contaminant molecules cannot be adequately determined from this spectrum. Figure 75B shows the single-pulse spectrum after five dialyses. Differences between the two spectra are very slight and other than the disappearance of two small peaks at 2.22 and 1.93 ppm cannot be attributed to the removal of small molecule contaminants. The fact that the peak at 3.73 ppm does not decrease indicates that its molecular weight is greater than 6,000 to 8,000 g/mole since it does not dialyze away. This tends to support the assignment of the signal as being due to a long chain polyglycine contaminant. The spectra in Figure 58 are spin-echo spectra measured with a τ_2 delay of 60 milliseconds for the BSA solution before any dialysis and after one, two, three, four and five dialyses. Both the HDO peak at 4.80 ppm and the peak at 3.73 ppm assigned to high molecular weight polyglycine contaminants are blanked out due to their overwhelming intensity in the spectra. Resonances occurring at 5.88, 2.66, 1.58 and 0.51 ppm which are out-of-phase in the spectra are artifacts

introduced by interactions between the polyglycine resonance at 3.73 ppm and the carrier frequency at 4.80 ppm. As well, the peak at 0.07 ppm is an artifact introduced by the spectrometer. Several of the peaks in the spectra, specifically those at 3.29, 2.22, 1.93 and 1.34 ppm, are observed to decrease and eventually disappear from the spectra with successive dialyses. Some peaks in the spectra do not decrease in intensity during the dialyses, notably those at 3.03, 2.06 and 1.15 ppm. These could be due either to the more mobile portions of the BSA having relatively long T_2 relaxation times or to larger contaminant molecules not removed by the dialyses. Figure 59 presents spin-echo spectra of the external dialysis medium after each dialysis. Resonances are observed at 4.12, 3.73 to 3.52, 2.44, 2.24, 1.93, 1.34 and 1.20 ppm. Some of these, those at 3.73, 2.24, 1.93 and 1.34 ppm, correspond to those observed in the BSA solution itself. All of the observed resonances disappear with successive dialyses except that at 3.73 ppm. This peak is due to seepage of BSA solution into the external medium through the ends of the dialysis sac and corresponds to a tiny amount of polyglycine in the external dialysis liquid. The results of this cleanup procedure on the commercially obtained BSA indicate the removal of several small molecule contaminants as shown in

the spectra of the BSA solution or those of the dialysis liquid. The monitoring of the dialysis liquid would seem to indicate that all dialyzable molecules are removed after four or five dialyses.

The second demonstration of the monitoring of small molecules in a protein solution is afforded by the preparation of a hemoglobin solution from a sample of hemolyzed human erythrocytes. The hemolyzed cells were spun at 15,000 rpm for 45 minutes to remove all the cell debris from the hemolysate. The resulting solution contains almost 99% hemoglobin and only 1% other proteins and smaller molecules [79]. The small molecules were removed by a dialysis procedure similar to that employed for the BSA cleanup. The only differences were that 10 mL of hemolysate were dialyzed against 25 mL of saline D₂O. Figure 60A and B show the single-pulse spectra measured before any dialysis and after five dialyses. Disregarding minor differences in resolution any changes in the spectrum after five dialyses can hardly be attributed to the removal of the small molecules present in the red blood cells. Figure 61 shows a series of spin-echo spectra measured with a τ_2 delay of 60 milliseconds for successive dialyses of the hemolysate. The decrease in virtually all resonances with the exception of that at 3.00 ppm with each dialysis indicates the removal of the

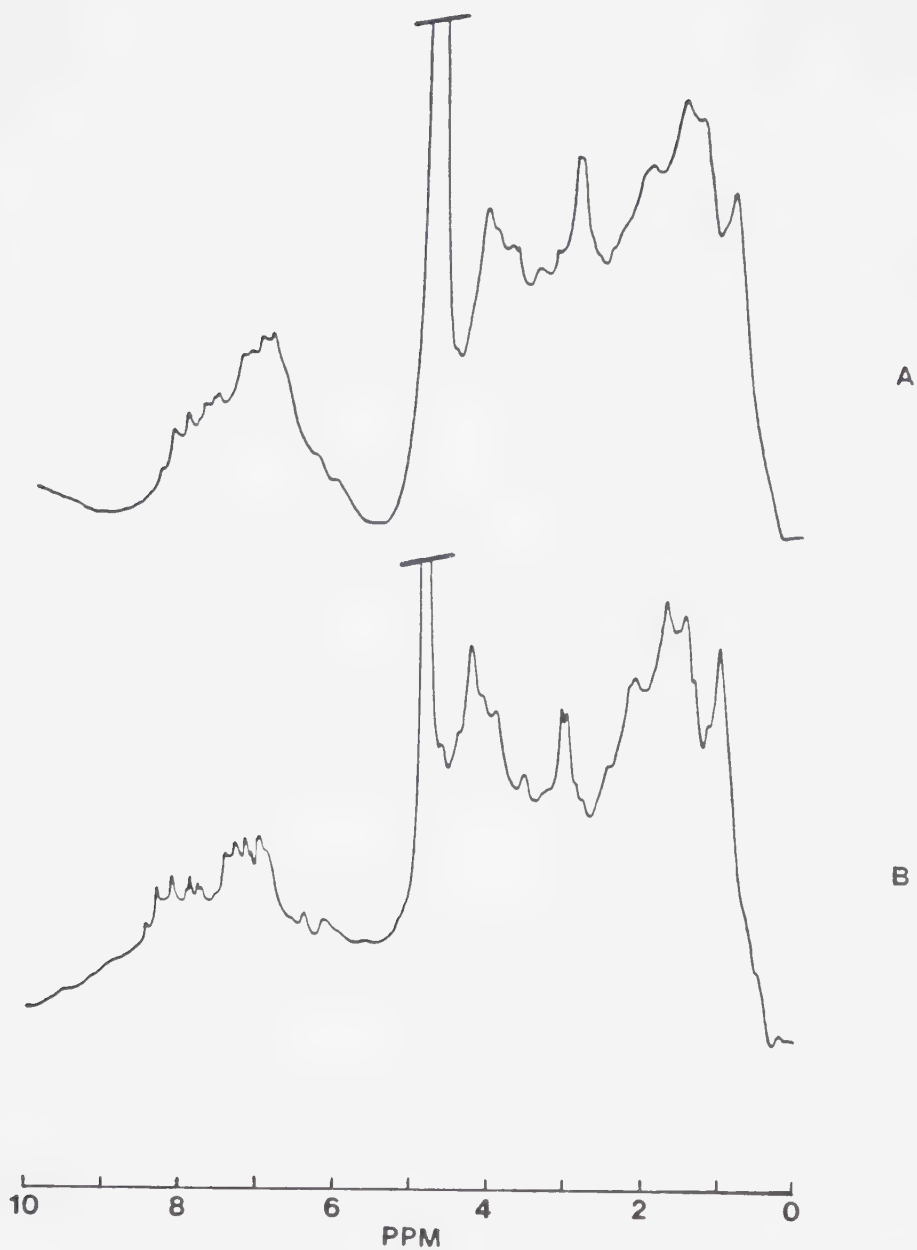


Figure 60. Single-pulse spectra ($\tau_2 = 0.06$ second) of a solution of hemolyzed red blood cells (A) before dialysis and (B) after 5 dialyses against saline D_2O .

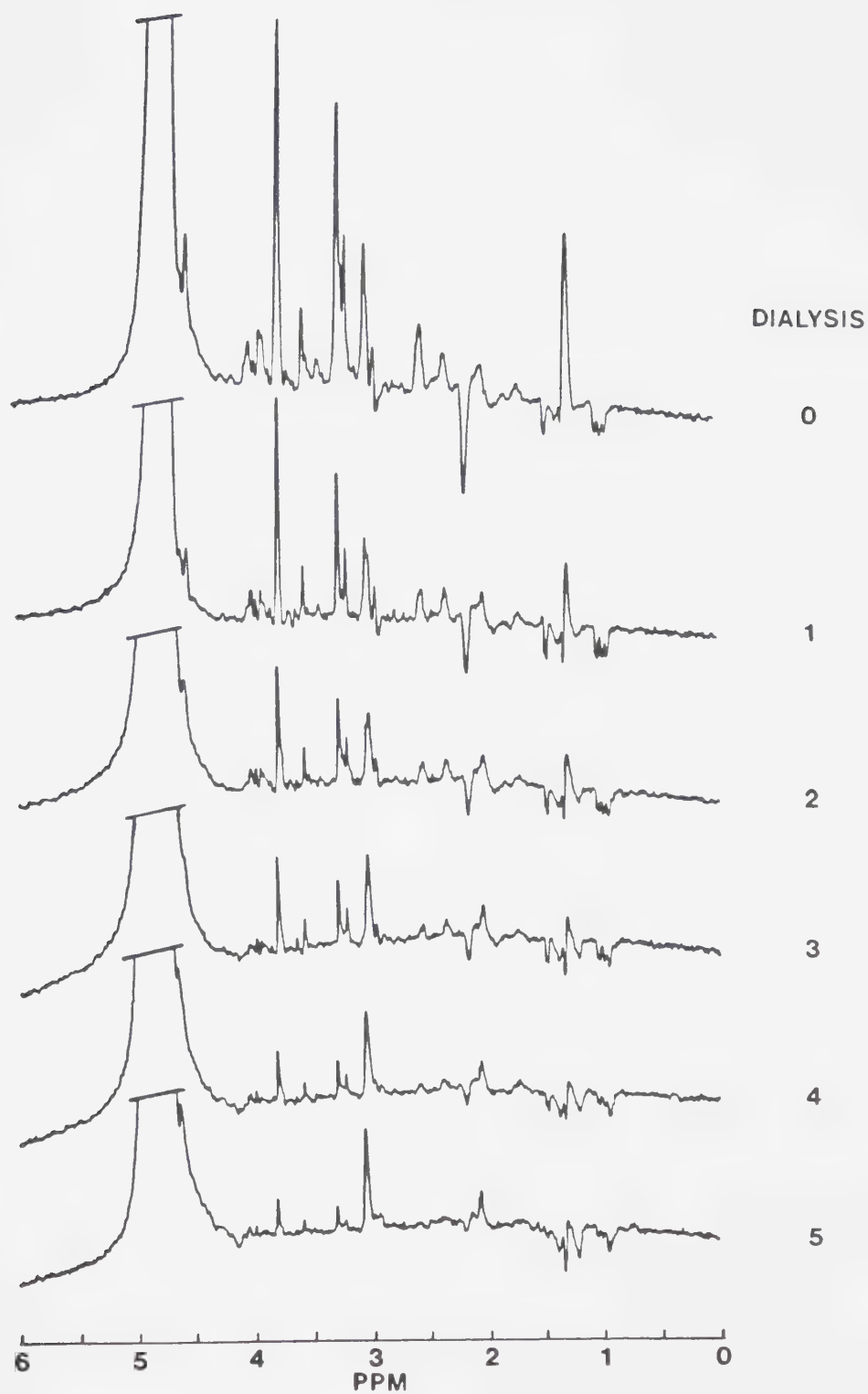


Figure 61. Spin-echo spectra ($\tau_2 = 0.06$ second) of a solution of hemolyzed red blood cells after successive dialyses against saline D_2O .

small molecules from the hemolysate. Figure 62 showing the spin-echo spectra measured on the dialysis liquids of each dialysis also indicates the removal of the small molecules. The dialysis liquid from the fifth dialysis shows very little of anything present and represents the end of useful dialysis. Any further dialyses will serve no purpose as no more small molecules are being removed. The dialyzed hemolysate after the fifth dialysis can be considered a solution of hemoglobin with a small amount of other protein impurities.

The question of how much of a certain small molecule needs to be present before a detectable signal is noted in the spin-echo NMR spectrum has to be considered when evaluating the usefulness of this method of monitoring small molecule contaminants in protein preparations. Figure 63A shows a portion of the spin-echo spectrum of dialyzed red blood cells after five dialyses measured with a τ_2 of 60 milliseconds. A small residual resonance for glycine is found at 3.54 ppm. Figure 63B was measured under the same conditions but the concentration of glycine was increased by 0.1 mM. The increase in the 3.54 ppm resonance indicates a detection limit for glycine, based on 2.5 times the peak to peak noise, of roughly 0.03 mM. The detection limits for other compounds will be of a similar magnitude so that in general levels of less than

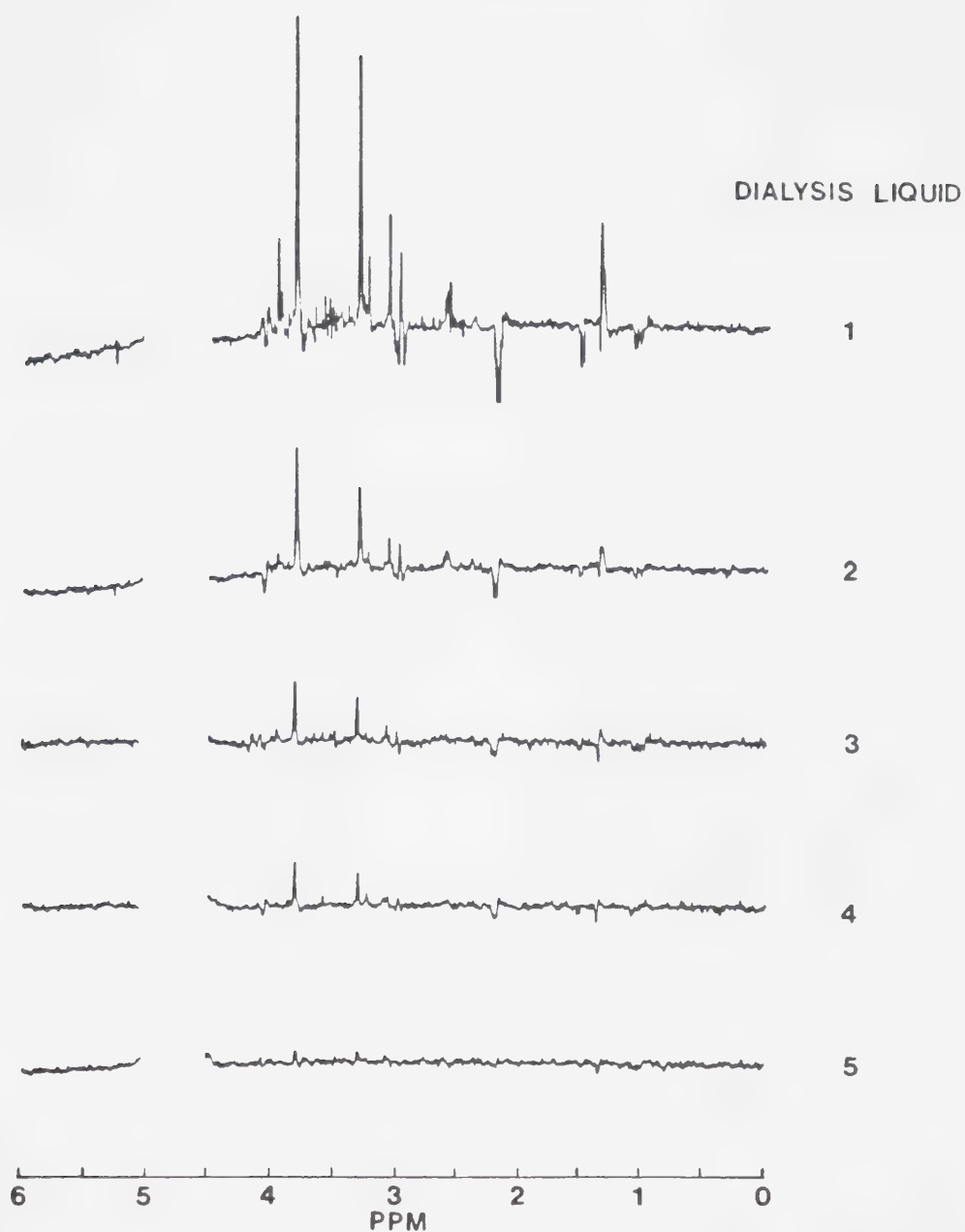


Figure 62. Spin-echo spectra ($\tau_2 = 0.06$ second) of successive dialysis media against which a solution of hemolyzed red blood cells was dialyzed.

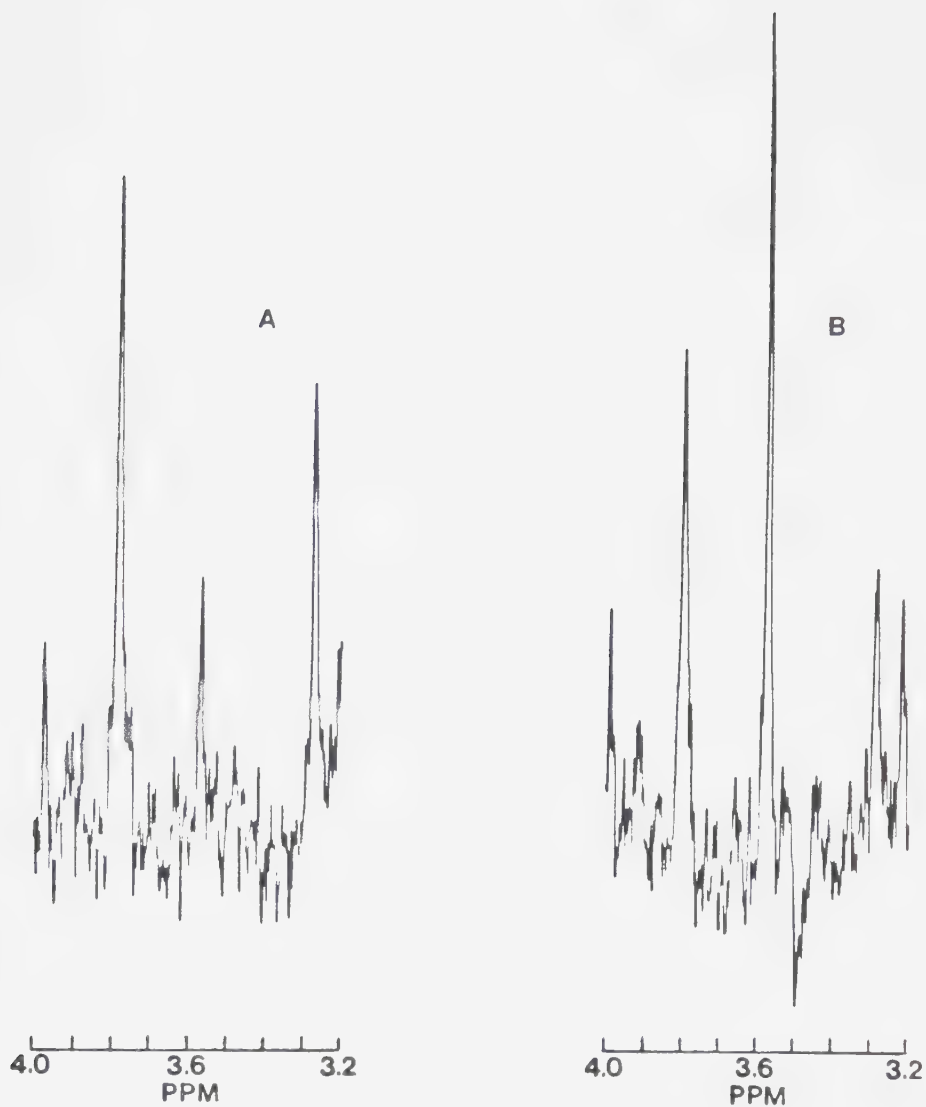
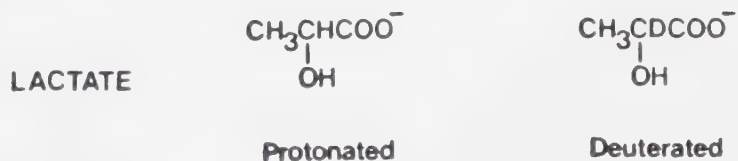


Figure 63. A portion of the spin-echo spectra ($\tau_2 = 0.06$ second) of hemolyzed red blood cells (A) after 5 dialyses against saline D_2O and (B) the same sample after the addition of glycine to raise the concentration by 0.1 mM . The glycine resonance is located at 3.54 ppm .

0.1 mM should be detected for most small compounds. These detection limits can be improved by increasing the number of scans collected in generating a spin-echo spectrum.

One further example of using the T_2 discrimination afforded by the spin-echo experiment to follow processes occurring in solutions containing obscuring macromolecules involves the preparation of erythrocyte samples for NMR experiments. The procedure employed generally involves washing whole red blood cells several times with saline D_2O to replace most of the H_2O in the cells with D_2O . Figure 64 shows spin-echo spectra measured with a τ_2 of 60 milliseconds before any washing and after one to four washes with saline D_2O . The removal of glucose and lactate is also accomplished by this procedure. The replacement of H_2O by D_2O can be followed by noting the decrease in intensity of the signal at 4.80 ppm. Inverted resonances for lactate at 4.09 and 1.26 ppm are noted in the spin-echo spectrum before any washing of the red blood cells. Upon washing with D_2O , this protonated lactate is washed out of the cells. In lactate which is subsequently produced by metabolism, carbon 2 is deuterated. This



causes the signal at 4.09 ppm to disappear and that at

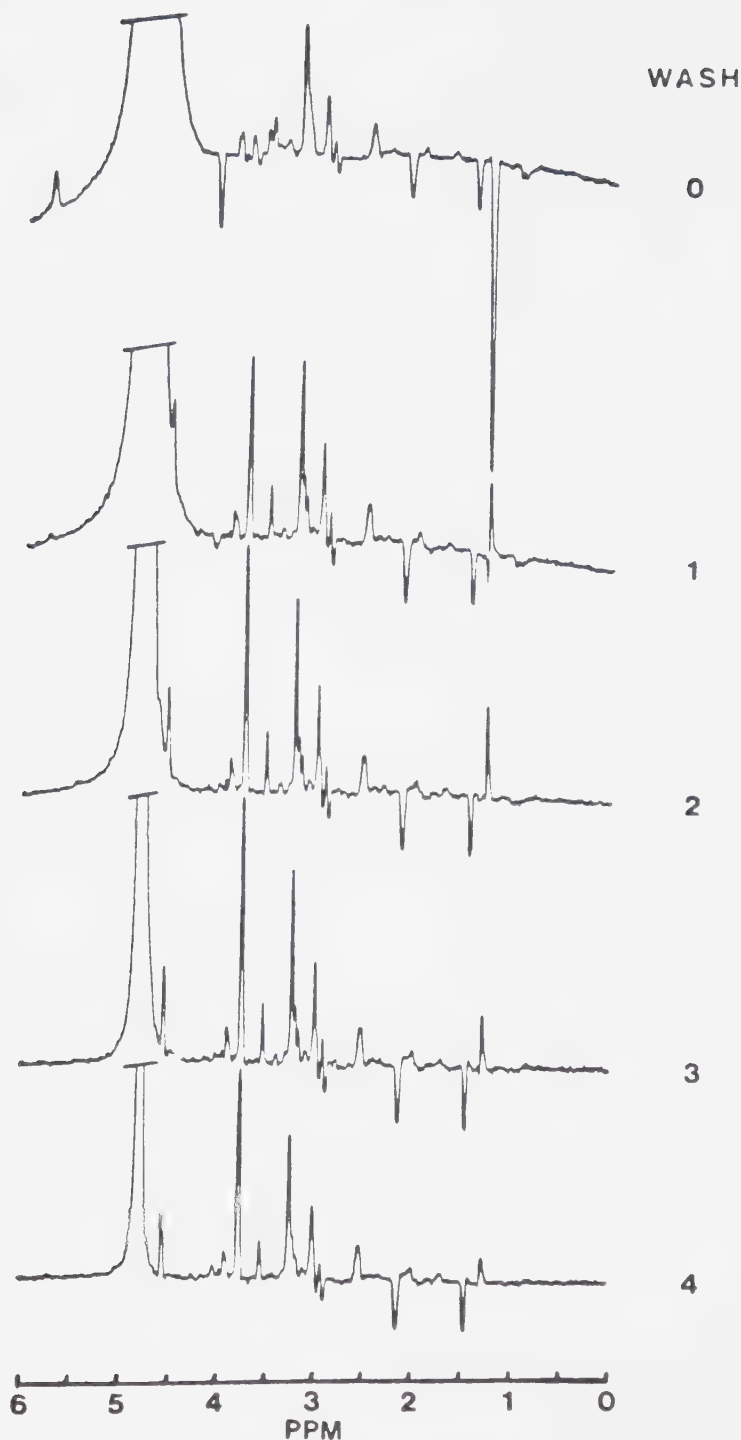
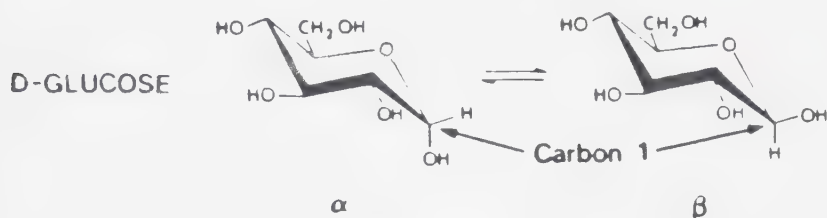


Figure 64. Spin-echo spectra ($\tau_2 = 0.06$ second) of intact erythrocytes after successive washings with twice the volume of saline D_2O .

1.26 ppm to become positive since there is no longer any coupling to a proton on carbon 2. Further washing removes more lactate as evidenced by the decrease in the 1.26 ppm signal. Intense resonances for glucose in the erythrocytes are difficult to see in the spectra of Figure 64 due to the large water peak in the initial spectra. This peak hides the resonance for the carbon 1 proton of both the α and β conformers of glucose located at 5.22 and 4.63 ppm, respectively. The other glucose resonances for



the carbon bonded protons are found in the region of 3.9 to 3.2 ppm. The carbon 1 proton resonances would be visible in the latter spectra of Figure 64 where the water peak is substantially reduced if the glucose had not been washed out of the red blood cells. In Figure 64, a peak increased in intensity at 3.76 ppm as the red cells were washed. This peak corresponds to the carbon bonded protons of the glycine residue of glutathione whose coupling to the adjacent NH was destroyed as the nitrogen became deuterated. The growth of this peak is thus a measure of the extent of deuteration of the glutathione.

Aside from slight resolution changes, most of the other peaks in the spin-echo spectrum are not observed to change in intensity with successive washes, indicating that the concentrations of many of the free amino acids, short peptides and other small molecules in the cells are not detectably altered by these washings. This is probably due to the selective nature of the red cell membrane transporting some molecules across easily while impeding the passage of other molecules [80]. It was determined that three or four washes were necessary to deplete the red cells of glucose and remove most of the H_2O and lactate.

CHAPTER V

METHODS FOR OBTAINING QUANTITATIVE INFORMATION FROM SPIN-ECHO NMR SPECTRA

A. Introduction

As shown in Chapter IV, it is possible to selectively observe resonances for small molecules in solutions containing macromolecules by taking advantage of their different rates of spin-spin (T_2) relaxation with the spin-echo technique. However, the occurrence of differential spin-spin relaxation during the spin-echo experiment complicates the measurement of concentrations from resonance intensities. In the conventional single-pulse experiment, the relative concentrations of sample components can be determined by simply comparing the intensities of the resonances for the various sample components, taking into account the number of protons giving rise to each resonance. By knowing the concentration of one sample component, absolute concentrations can be determined for all the others. In spin-echo spectra, unless two compounds have the same spin-spin relaxation time, which must be experimentally

determined, the absolute concentration of one compound cannot be determined by a direct comparison of intensities alone, even if the concentration of the other compound is known.

The obvious answer to this problem of quantitative measurement is to avoid the use of the spin-echo experiment. However, in many samples, particularly biological samples, this is not possible due to the obscuring of the resonances of interest by those of macromolecules present in the sample as described in Chapter IV. For instance, the single-pulse spectrum of intact human erythrocytes (Figure 8A) consists of a broad envelope due chiefly to the protons of hemoglobin while in the spin-echo spectrum of such a sample (Figure 8B) well resolved resonances for the smaller molecules in the cells are observed with very few hemoglobin resonances remaining. It should in principle be possible to obtain the intracellular free molecule concentrations of these compounds in intact erythrocytes by NMR. Unlike other methods of obtaining these concentrations, NMR is noninvasive and nondestructive which offers obvious advantages for in vivo studies.

Very little research has been reported on the measurement of absolute concentrations in complex biological systems using NMR. Early work by Shaw and

Elsken [81] based on low resolution, single-pulse spectra employed area comparisons to measure the water content of materials. In the past decade, several high resolution, single-pulse ^{31}P NMR studies, pioneered by Moon and Richards [82], have been carried out on biological systems including absolute concentration measurements of several phosphorous containing compounds in frog muscle [83]. No effort has yet been made in attempting to measure concentrations using ^1H spin-echo NMR spectroscopy on such complex samples.

In the next two chapters, the results of studies of various methods for obtaining quantitative information from resonances in spin-echo spectra are presented. Such measurement techniques for determining concentrations from spin-echo NMR spectra must be based on procedures other than direct intensity comparisons because of the complications of differential T_2 relaxation. One such method to be investigated in Chapter VI involves the development of a titration procedure for measuring concentrations. This type of method is specific for a certain compound or group of compounds. More general techniques for measuring compounds in complex samples are described in this chapter. Two approaches are studied; (i) a standard addition method utilizing an internal standard and (ii) the utilization of proportionality

constants to mathematically extrapolate the measured intensities to a τ_2 delay time of zero where the relative intensities are proportional to relative concentrations as in single-pulse spectra. Both of these approaches allow the simultaneous quantitative determination of several compounds.

B. Spectral Digitization and Accurate Intensity Data

Before discussing the methods for measuring signals in spin-echo NMR spectra some appreciation of the digital resolution of the spectrum as it affects the accuracy of peak intensity determinations, measured by either areas or heights, must be gained. Because the measurement of quantitative intensity data is sought, the signals must be adequately defined so that accurate peak shapes are obtained. This requires that the upper half of a resonance be defined by at least 4 or 5 memory addresses [84]. However, if the signals are overdefined a significant increase in the times required for both acquisition and Fourier transformation of the FID results.

Generally, with state-of-the-art NMR spectrometers, FIDs can be digitally collected in a variety of sizes ranging from 1K (1024) to 32K or more of data points. Usually FIDs are collected in 1, 2, 4, 8, 16 or 32K of data points which give digital resolutions in the real

portion of the Fourier transformed spectrum when using a spectral window of 4000 Hz of 7.812, 3.906, 1.953, 0.977, 0.488 and 0.244 Hz/point, respectively. Spectra obtained on human erythrocytes have resonances with widths at half height, $W_{1/2}$, generally in the range of 4 to 8 Hz. These spectra are collected without spinning of the sample and are multiplied by an exponential function which broadens the lines by about 1 Hz. Most of the resonances in a spectrum of red blood cells have approximately the same $W_{1/2}$ although some differences are apparent for several of the peaks. $W_{1/2}$ values vary somewhat from spectrum to spectrum due to slight differences in shimming from sample to sample. In order to accurately digitize resonances with $W_{1/2}$ values of around 4 Hz requires at least an 8K FID, although this may not be fully adequate in some cases. For accurate peak representations in simpler solutions, such as the CDCl_3 solutions discussed later in this chapter, where the $W_{1/2}$ values are generally around 2 to 3 Hz, an FID of at least 16K in size is required. A choice of 16K was made for all the FIDs collected for the quantitative studies of the next two chapters in order to satisfy the requirements for the accurate definition of resonances at all times. The use of 32K FIDs was judged to be excessive in terms of the required data acquisition and Fourier transformation times as well as in terms of

the disk storage space that would be required to save such FIDs.

To illustrate the effects of FID size on the accurate representation of peak shapes, a series of spectra were collected on a 0.5-mL sample of D_2O , which contained a resonance from traces of HDO, at a variety of FID sizes. The results of this study are presented in Figure 65. The resonance shown has a $W_{1/2}$ of about 5 Hz and was collected using a spectral window of 4000 Hz, as was employed in all subsequent quantitative work. The FIDs collected in 1 or 2K of data points give exceedingly poor definition of the signal. The 4K FID is not entirely free of inaccuracies either. The 8, 16 and 32K FIDs are virtually indistinguishable. Since the $W_{1/2}$ of the resonance is about 5 Hz an 8K or greater FID will give an accurate peak shape while a 4K or less FID will not.

C. NMR Intensity Data

As a preliminary step to establish the quality of intensity data to be obtained from NMR spectra a calibration curve was prepared using dilutions of a 5.428 mM GSH stock solution. Eight 25-mL volumetric flasks were prepared, each containing measured amounts of this GSH solution delivered by buret. A constant amount of a 1.19-mM dimethylamine hydrochloride ($DMA \cdot HCl$) solution was

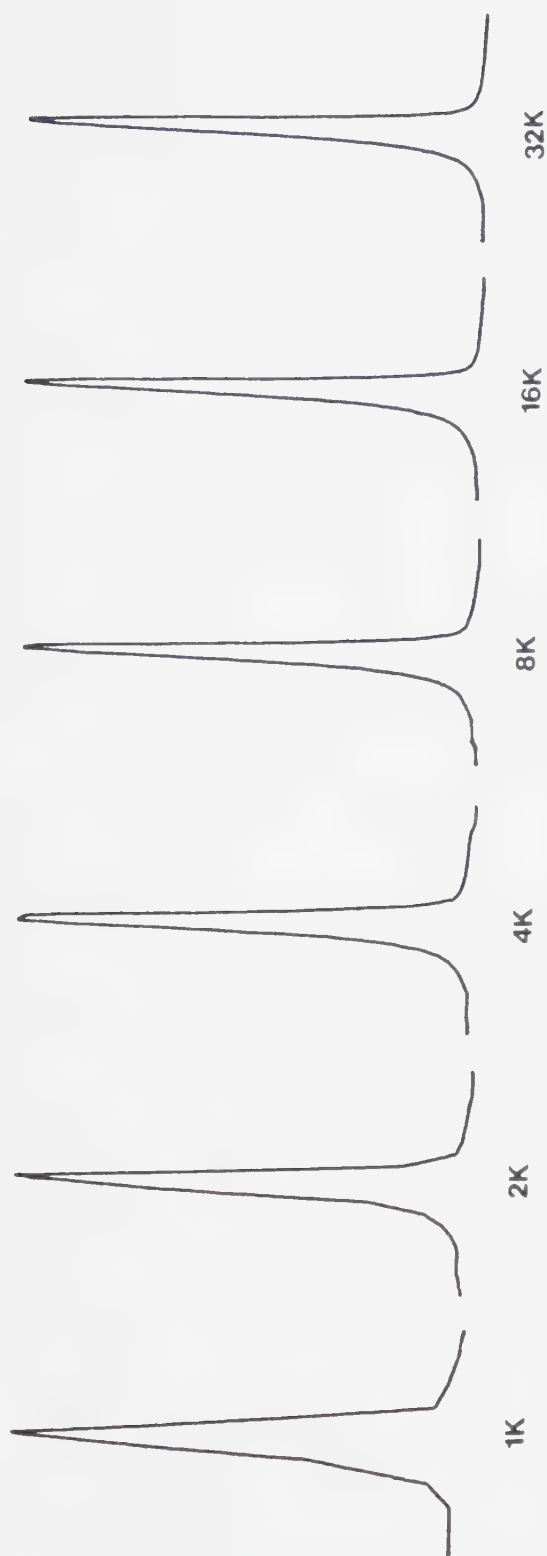
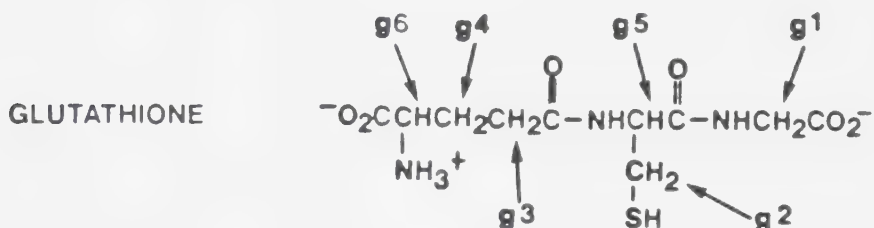


Figure 65. Single-pulse FT NMR spectra collected for a single resonance with a $w_{1/2}$ of 5 Hz using a spectral window of 4000 Hz at various length FIDs ranging from 1K to 32K of data points. Note the improvement in the definition of the peak shape in the longer FIDs.

added to the GSH dilutions as an internal standard prior to making the GSH solutions up to the mark. Table 11 presents details of the solutions prepared. Single-pulse FT NMR spectra were collected on each of these solutions. Figure 66 shows the spectrum obtained for the approximately 4 mM GSH solution with the DMA methyl resonance present at 2.66 ppm. The remainder of the resonances are due to GSH and are assigned to correspond to the diagram below.



The resonance for the g5 protons of GSH is further downfield near the HDO resonance around 4.8 ppm.

The intensities, either peak areas or heights, of the GSH resonances were normalized against the DMA methyl resonance in order to make relative comparisons between the spectra of the solutions. The normalization procedure consisted of dividing the intensities of the GSH resonances by that of the DMA internal standard. The purpose of the operation was to account for any variations between spectra which would affect both the GSH and DMA resonances to the same extent. The major factor which was

Table 11
Preparation of Solutions for Construction of an
NMR Calibration Curve

<u>Flask #</u>	<u>Volume of^(a) Stock Solution</u>	<u>[GSH]^(b)</u>	<u>[DMA]^(c)</u>
1	17.95	3.897	0.238
2	15.68	3.404	0.238
3	13.58	2.948	0.238
4	11.11	2.412	0.238
5	9.14	1.984	0.238
6	6.71	1.457	0.238
7	4.52	0.981	0.238
8	2.31	0.502	0.238

- (a) Milliliters of a 5.428 mM GSH stock solution delivered by buret to 25 mL volumetric flasks.
- (b) Final concentration after dilution in mM.
- (c) A 5.00 mL aliquot of a 1.19 mM dimethylamine hydrochloride solution delivered by pipet to each flask.

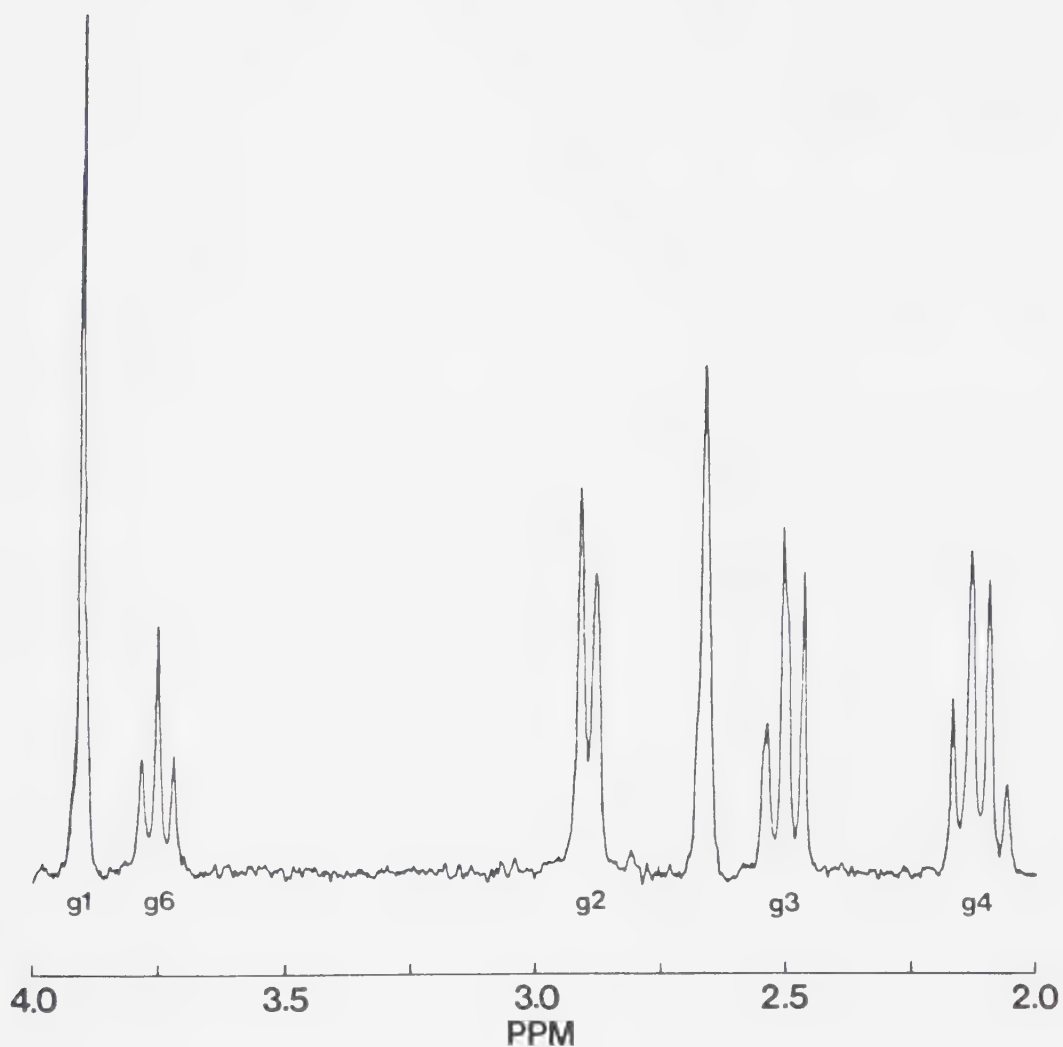


Figure 66. A single-pulse spectrum of a D_2O solution containing 4 mM GSH and 2 mM dimethylamine (DMA). The DMA resonance is located at 2.66 ppm. The other resonances, g1 to g4 and g6, belong to GSH. The g5 resonance of GSH is further downfield near the HDO peak.

compensated was the difference in resolution of the spectra due to slight shimming variations which caused changes in peak shapes. Such changes would affect peak heights much more than peak areas.

Plots of both normalized peak areas and normalized peak heights versus the concentration of GSH were constructed from the data for each of the GSH resonances. The plots for the gl resonance of GSH (the methylene protons of the GSH glycine residue) are shown in Figure 67 as typical of the results obtained. The solid lines are from linear least-squares fits of the experimental data. The precision and accuracy of the data can be evaluated by a consideration of the standard deviations of the slopes and $[\text{GSH}]$ intercepts from the least-squares fits. For the normalized peak height data in Figure 67, the slope of the regression line and its standard deviation is $0.306 \pm 0.005 \text{ mM}^{-1}$ and the $[\text{GSH}]$ intercept and its standard deviation is $-0.035 \pm 0.044 \text{ mM}$. The precision of the peak height measurements is fairly good based on the relative standard deviation of the slope of 1.8% while the accuracy of the measurements is acceptable since the calculated intercept on the $[\text{GSH}]$ axis of zero falls within the small absolute standard deviation of the $[\text{GSH}]$ intercept. The normalized peak area data shown in Figure 67 results in a slope for the

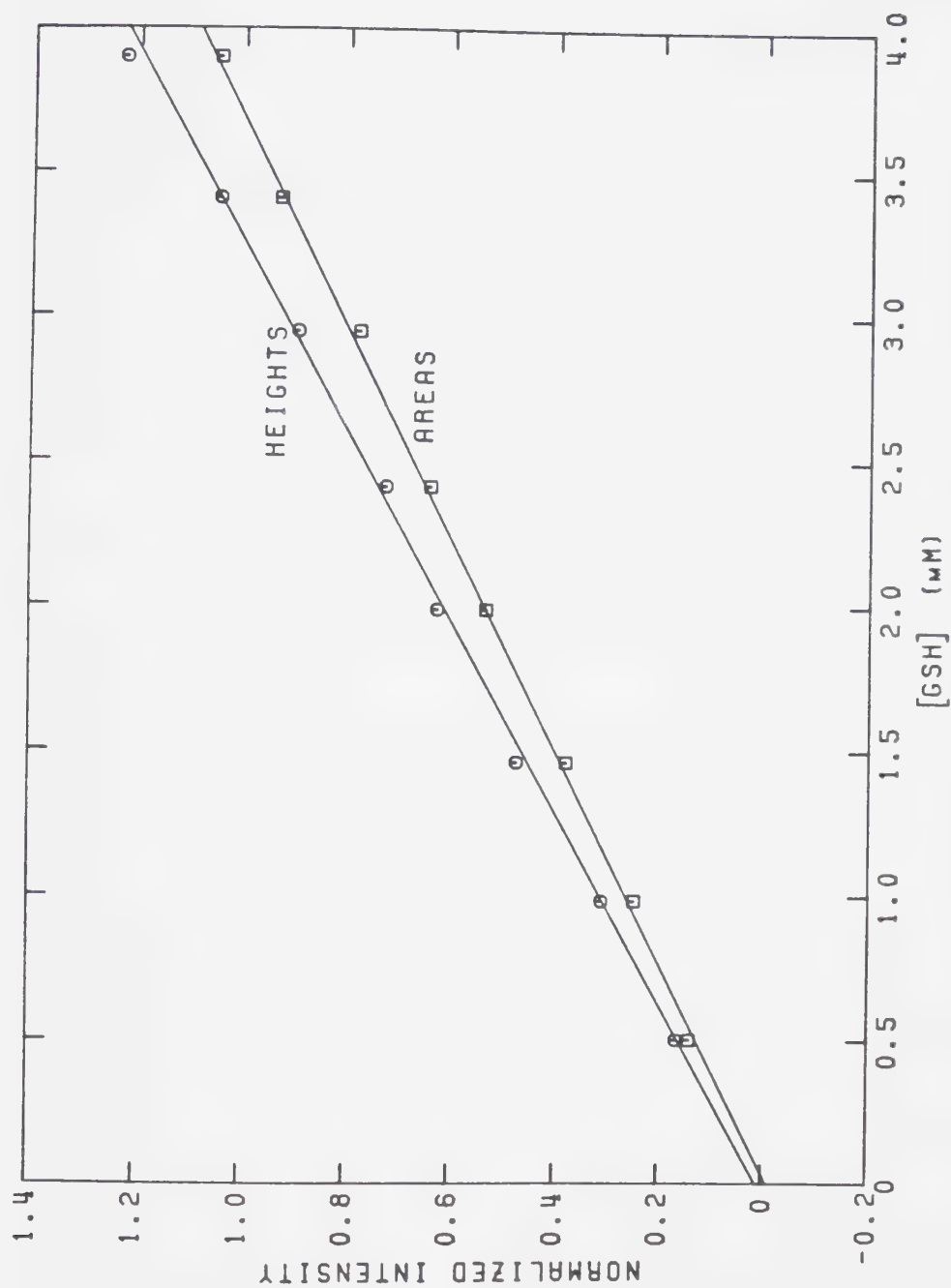


Figure 67. Plots of peak heights and peak areas for the gl resonance of GSH, normalized to the DMA resonance present as an internal standard, as a function of the GSH concentration. The solid lines represent linear least-squares fits of the experimental data.

regression line of $0.271 \pm 0.004 \text{ mM}^{-1}$ and a [GSH] intercept of $0.035 \pm 0.033 \text{ mM}$. Again the precision and accuracy of the data is good based on a relative standard deviation for the slope of 1.4% and the small absolute standard deviation range for the [GSH] intercept which is very close to zero. The two types of measurements (areas and heights) give essentially the same results. However, the difficulties that would be involved in measuring peak areas when the baseline is not flat make the measurement of peak heights preferable in such instances. As well, the measurement of peak heights is generally a much easier operation even when the spectrum baseline is flat.

D. The NMR Standard Addition Experiment

The use of a standard addition procedure, whereby small volumes of a concentrated solution containing the compound or compounds of interest are added to a portion of sample and measurements made on the sample solution between additions, constitutes one of the most general techniques for the measurement of virtually any compound. The major limitations on its use are that there must be some parameter which varies linearly with the amount of compound present and the response obtained must be due only to the compound of interest with no contributions from other sample components [85]. These

limitations can, however, be overcome using a complex calculation procedure developed by Saxberg and Kowalski [86]. The principle behind the standard addition method is that any sample or method interferences which influence the response of the compound of interest will affect the added portion of compound in the same manner [87]. In this way, any such matrix effects will be compensated for in the measurements allowing an accurate determination of the initial concentration of the compound in the sample. This is accomplished by performing a linear regression analysis on the response versus amount of compound added data. The negative intercept on the amount of compound added axis represents the amount of compound initially present in the sample.

In NMR spectroscopy, the intensity of a resonance is related to the amount of a compound present. For spin-echo NMR spectra, the presence of differential T_2 relaxation can be considered as a matrix effect which acts differently on various compounds. However, differential T_2 relaxation acts the same on the compound originally present and that added in a standard addition experiment. Thus the quantitative determination of compounds from resonance intensities in spin-echo spectra should be possible using the standard addition technique. As with any standard addition measurements,

the matrix effects must remain constant throughout the addition procedure [87]. In spin-echo NMR standard addition experiments, this means that the T_2 relaxation times for resonances studied must remain essentially constant for a sample over the course of the procedure.

The effects of a changing T_2 relaxation time for a resonance over the course of the standard addition experiment are shown in Figure 68. In this figure, calculated lines are presented for a spin-echo NMR standard addition experiment where incremental additions of a compound are made to triple the initial concentration at the end of the experiment. Each addition increases the intensity by 25% of the initial intensity. A long relaxation delay between successive scans is assumed in these calculations to avoid any saturation effects caused by an incomplete return to equilibrium. Line A represents the case for an invariant T_2 relaxation time over the course of the experiment. The linear least-squares line derived from the data has a perfect correlation coefficient of 1 and the intercept on the abscissa represents the true measure of the initial amount of compound present. Line B shows the results of a 20% decrease in T_2 from the beginning to the end of the experiment which occurs linearly over the course of the standard addition procedure. There is a fall off in the

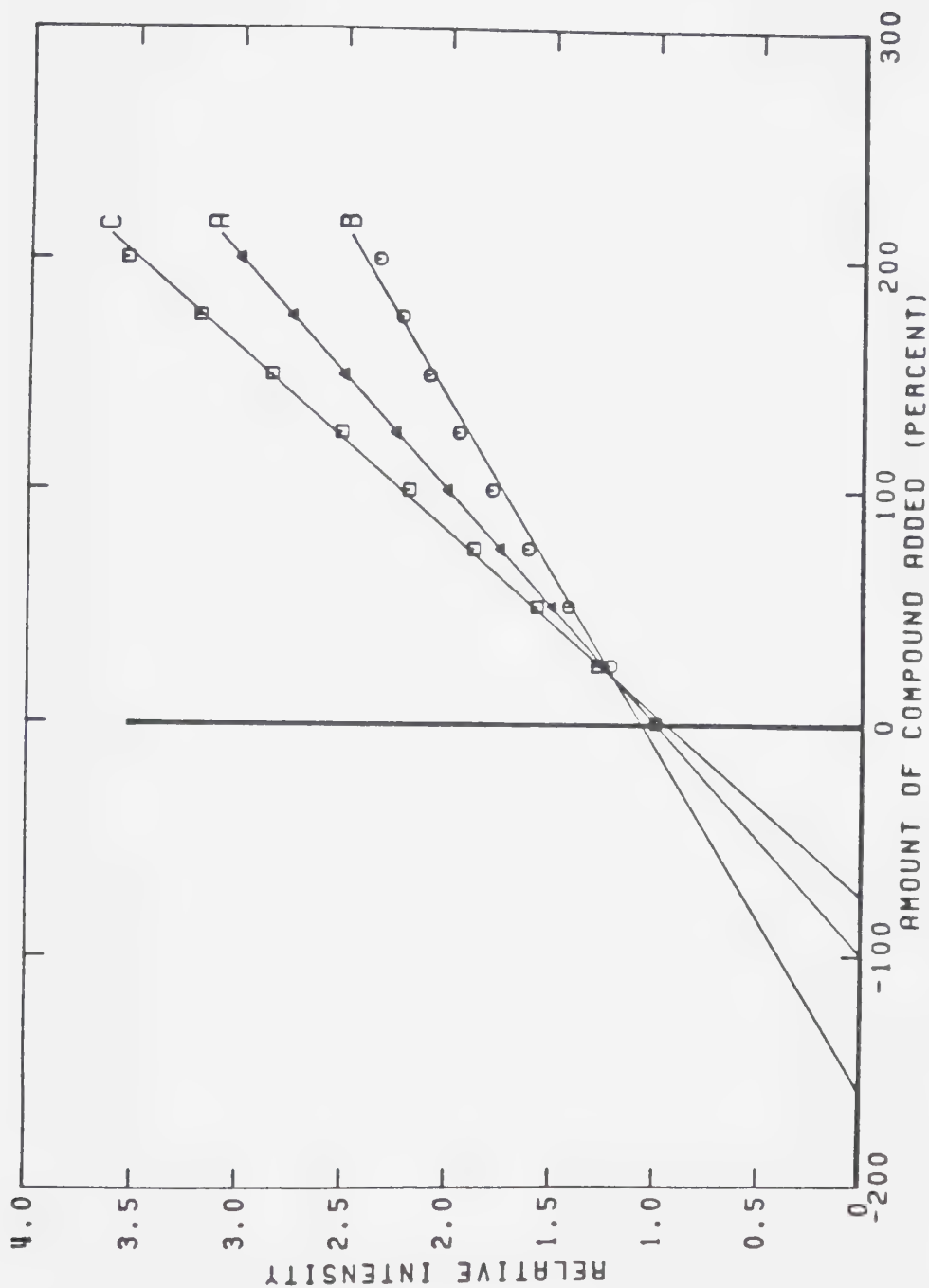


Figure 68.

Calculated standard addition plots for an experiment where compound is added to raise the concentration by 25% of the initial value with each increment until the initial concentration is tripled. Line A is the linear least-squares fit of the calculated points for the case of no change in the T_2 relaxation time over the course of the standard addition experiment. Lines B and C are linear least-squares fits of the points for a 20% linear decrease in T_2 and a 20% increase in T_2 , respectively, from the beginning to the end of the experiment.

experimental points due to the faster decay of the signal as T_2 decreases. The linear least-squares fit of the data is not as good as for Line A having a correlation coefficient of only 0.9947. The intercept on the abscissa is somewhat greater in magnitude than that of Line A resulting in an overestimation of the sample concentration by 59.7%. Line C shows the same type of behavior as Line B for the case where T_2 increases by 20% over the course of the standard addition experiment. The linear least-squares fit of the calculated points gives a correlation coefficient of 0.9993 and an abscissa intercept which yields a 25.3% discrepancy in the amount of compound initially present.

The use of an internal standard with the spin-echo NMR standard addition technique is needed to account for differences in resolution between the various spectra collected caused by shimming variations as discussed in the previous section. As well, an internal standard will account for other instrumental variations such as the receiver gain, the number of scans collected and the vertical scaling factors of the plotted spectra. More importantly, it will also account for dilution effects caused by adding portions of a solution to the sample to increase concentrations.

Initially, NMR standard addition experiments were performed on a simple system to evaluate the performance of the method. A CDCl_3 solution of diethylsuccinate was used for this purpose. The choice of this compound was



made for the reason that it gives rise to well resolved singlet, triplet and quartet proton resonances to be utilized to study the behavior of different multiplet types in the standard addition procedure. As well, the compound is readily soluble in chloroform, allowing ease of sample preparation.

Standard addition experiments were carried out on 0.5-mL samples of an approximately 4-mM solution of diethylsuccinate in CDCl_3 with approximately 2 mM of 1,4-dioxane added as an internal standard. The addition solution was exactly ten times more concentrated than the sample solution, since the sample was prepared as a one to ten dilution of this solution, and contained no internal standard. This preparation procedure eliminated the need for careful standardization of solutions. The intercept on the volume added axis should be -50 μL for a 0.5 mL sample. The standard addition experiments were performed by making 10- μL additions to the sample in an NMR tube

following which the tube was shaken for approximately one minute and an NMR spectrum measured. Spectra were recorded for 0 to 70 μL of addition solution using both the single-pulse experiment and the spin-echo experiment in order to compare the two techniques. As well, the results were evaluated using both peak areas and peak heights for both pulse sequences.

Figure 69 shows a single-pulse NMR spectrum of diethylsuccinate in CDCl_3 with the resonance for 1,4-dioxane present at 3.75 ppm. Singlet, triplet and quartet resonances for diethylsuccinate protons are noted at 2.66, 1.31 and 4.20 ppm, respectively. Also present in the figure is a single peak at 1.59 ppm due to traces of water in the solution. A singlet resonance at 7.30 ppm was also observed due to residual CHCl_3 in the solvent.

In the standard addition experiments performed on samples of the diethylsuccinate solution, a wait of at least $5T_1$ relaxation times (30 seconds) was used between successive scans to eliminate any saturation effects in the resulting spectra [7]. A standard addition plot for a typical experiment is shown in Figure 70. The results of all the standard addition experiments on diethylsuccinate are presented in Tables 12 to 14 for the singlet, triplet and quartet resonances of diethylsuccinate, respectively. The volume-added intercepts and standard

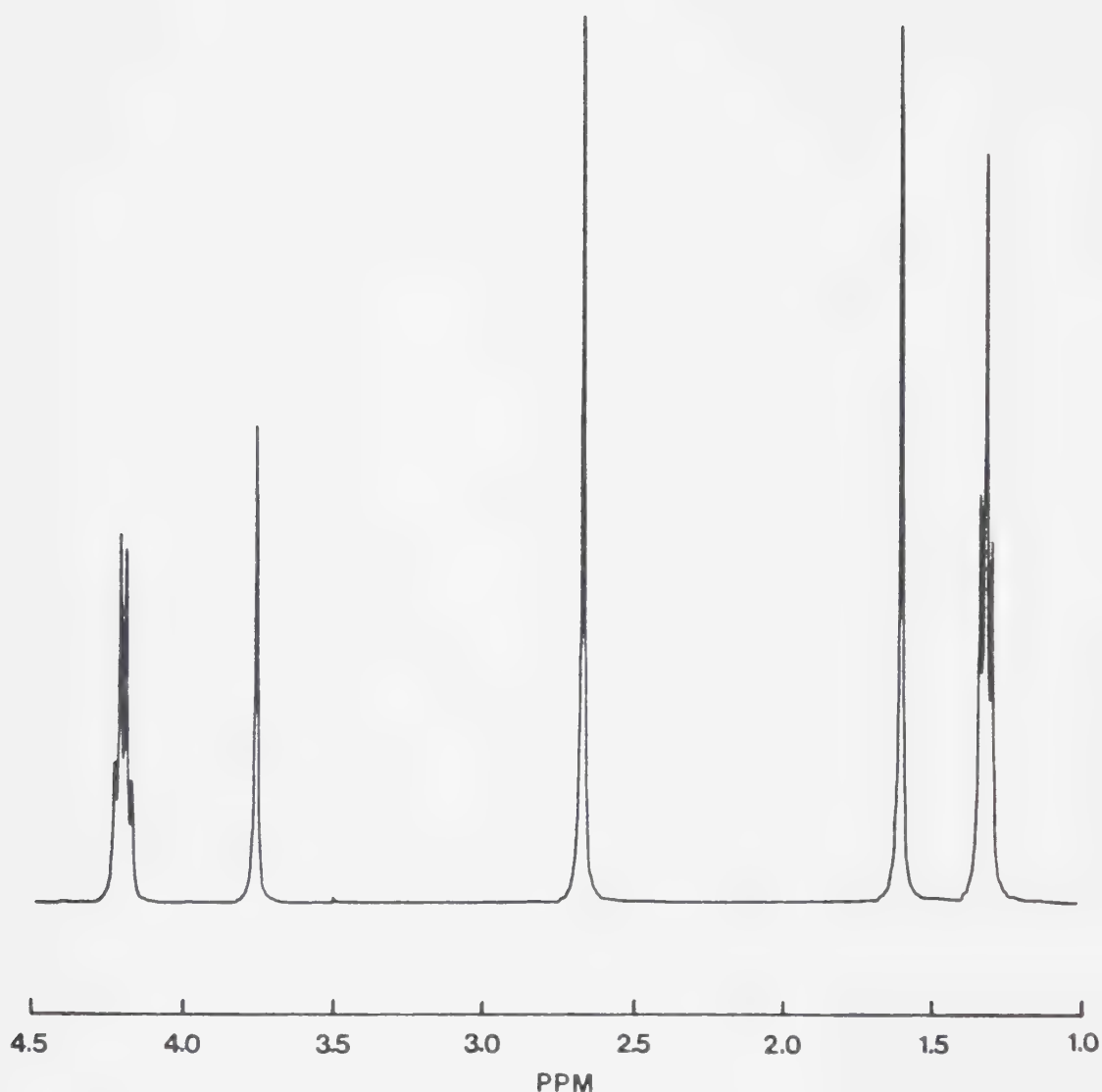


Figure 69. A single-pulse NMR spectrum of diethylsuccinate and 1,4-dioxane in CDCl_3 . The resonance at 3.75 ppm is due to 1,4-dioxane and that at 1.59 ppm to traces of water in the solution. The other resonances are due to diethylsuccinate and are identified in the text.

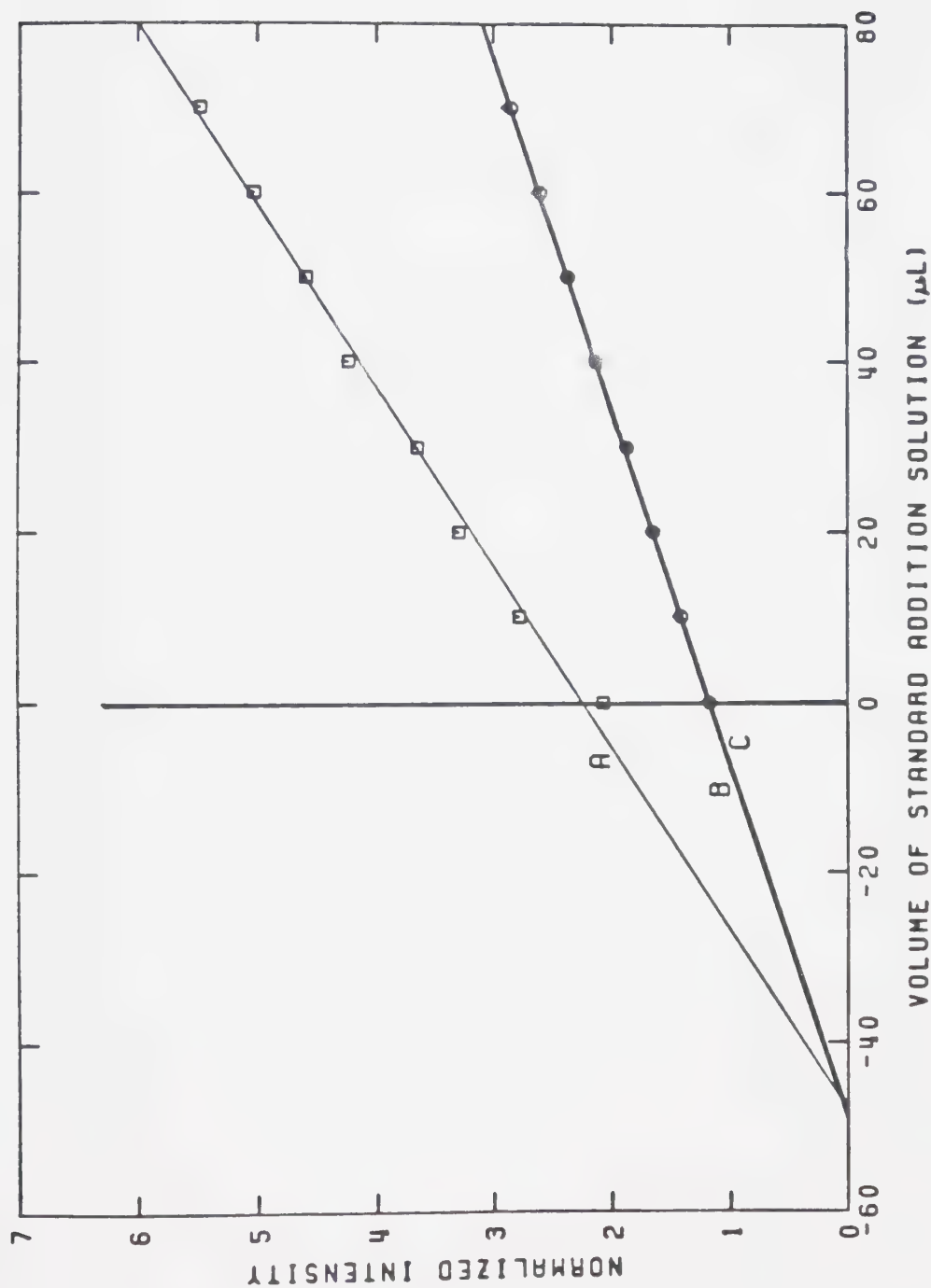


Figure 70. Plots of the results of a typical standard addition experiment conducted on a CDCl_3 solution of diethylsuccinate, the resonances for which are normalized to 1,4-dioxane. The results shown are for area measurements on single-pulse spectra. Lines A to C correspond to the triplet, quartet and singlet resonances of diethylsuccinate, respectively. The calculated X-Intercept is $-50 \mu\text{L}$.

Table 12

Volume Axis Intercepts for the Singlet of Diethylsuccinate
in NMR Standard Addition Experiments^(a)

Sample	Single-Pulse		Spin-Echo	
	Areas	Heights	Areas	Heights
1	-49.7 ± 1.6	-49.1 ± 0.6	-51.9 ± 4.1	-49.0 ± 1.0
2	-48.0 ± 1.2	-50.0 ± 0.3	-52.5 ± 2.2	-50.8 ± 1.2
3	-50.0 ± 1.8	-49.0 ± 0.4	-58.1 ± 6.4	-48.3 ± 1.4
4	-49.0 ± 1.9	-49.9 ± 0.2	-55.0 ± 3.0	-51.0 ± 0.2
5	-48.6 ± 0.4	-48.4 ± 0.4	-53.9 ± 2.3	-49.7 ± 2.4
Average	-49.1 ± 0.8	-49.3 ± 0.7	-54.3 ± 2.4	-49.8 ± 1.1

(a) In μL ± absolute standard deviations. Expected intercept is -50 μL .

Table 13

Volume Axis Intercepts for the Triplet of Diethylsuccinate
in NMR Standard Addition Experiments^(a)

Sample	Single-Pulse		Spin-Echo	
	Areas	Heights	Areas	Heights
1	-50.0 \pm 2.0	-45.2 \pm 1.2	-50.7 \pm 3.7	-48.4 \pm 1.3
2	-45.1 \pm 2.0	-45.3 \pm 0.9	-53.4 \pm 2.7	-48.4 \pm 1.3
3	-46.4 \pm 1.5	-42.6 \pm 1.9	-63.6 \pm 5.5	-50.6 \pm 2.6
4	-44.4 \pm 2.2	-45.6 \pm 0.3	-50.4 \pm 2.0	-49.1 \pm 1.4
5	-47.9 \pm 2.8	-43.0 \pm 1.3	-57.0 \pm 1.6	-51.1 \pm 2.5
Average	-46.8 \pm 2.2	-44.4 \pm 1.4	-55.0 \pm 5.5	-49.5 \pm 1.3

(a) In μL \pm absolute standard deviations. Expected intercept is -50 μL .

Table 14

Volume Axis Intercepts for the Quartet of Diethylsuccinate
in NMR Standard Addition Experiments (a)

Sample	Single-Pulse		Spin-Echo	
	Areas	Heights	Areas	Heights
1	-49.5 ± 1.5	-44.8 ± 1.3	-50.7 ± 2.8	-48.0 ± 1.3
2	-49.2 ± 1.6	-46.3 ± 1.1	-54.4 ± 1.9	-49.7 ± 0.5
3	-49.8 ± 2.4	-42.8 ± 2.3	-61.2 ± 6.1	-46.0 ± 2.5
4	-49.2 ± 2.3	-47.9 ± 0.7	-52.2 ± 2.1	-50.8 ± 0.8
5	-49.4 ± 1.1	-43.3 ± 1.1	-49.5 ± 2.6	-46.4 ± 1.3
Average	-49.4 ± 0.3	-45.0 ± 2.1	-53.6 ± 4.6	-48.2 ± 2.1

(a) In μL ± absolute standard deviations. Expected intercept is -50 μL .

deviations as obtained from linear least-squares fits of the experimental data are presented for each resonance for both the single-pulse and the spin-echo techniques using both peak areas and heights to determine if any differences between measurement modes exist. The results indicate no significant differences between the three multiplet types studied. All three gave a volume-added intercept generally within $\pm 10\%$ of the expected $-50 \mu\text{L}$. In many cases, the intercept was much closer. Generally, the spin-echo standard addition experiments gave a slightly greater volume-added intercept than the single-pulse results. The standard deviations for the volume-added intercepts obtained for normalized peak height data were usually somewhat lower than those for normalized peak area data. Several of the intercepts which were extremely far from $-50 \mu\text{L}$ were noted to have quite high standard deviations. The large standard deviations of these results can be used to indicate their inaccurate nature. The overall average of all the volume-added intercepts is $-49.5 \mu\text{L}$, which is quite close to the theoretical $-50 \mu\text{L}$ indicating no bias in the results.

In order to determine if there are changes in the T_1 or T_2 relaxation times for the singlet, triplet and quartet resonances of diethylsuccinate and for the 1,4-dioxane resonance during the course of the standard

addition experiments, the T_1 and T_2 relaxation times were measured for two samples both before and after the standard addition procedure. These measurements are shown in Table 15. No great changes were noted in any of the relaxation times after the standard addition experiments. Moderate variations were observed for several of the relaxation times but they were only a few percent of the values concerned. Since the T_1 relaxation times appeared to be relatively constant over the course of the standard addition experiments, the use of a shorter relaxation delay between successive scans than $5T_1$ values was investigated [7]. The reason for this was that a constant T_1 for a resonance over the course of the standard addition procedure would eliminate the need to wait for equilibrium to be reestablished since the resonances will relax to the same extent between scans which will affect the intensities of a resonance to the same relative degree in successive spectra. The use of waits as short as $2T_1$ values (10 seconds) were found to give as good results in terms of the volume added intercepts as the longer waits with considerable savings in time.

Having established that the NMR standard addition method of determining concentrations works well enough to give reasonably reliable answers, use will be made of it

Table 15

Determinations of T_1 and T_2 Relaxation Times(a) for Diethylsuccinate and 1,4-Dioxane Before and After Standard Addition Experiments

Resonance	Before		After	
	T_1	T_2	T_1	T_2
Singlet	2.59 ± 0.01	1.02 ± 0.01	2.47 ± 0.01	1.06 ± 0.01
	2.68 ± 0.07	1.03 ± 0.06	3.05 ± 0.09	1.02 ± 0.06
Triplet	3.41 ± 0.02	1.21 ± 0.03	3.29 ± 0.02	1.18 ± 0.06
	3.39 ± 0.11	1.06 ± 0.06	3.82 ± 0.12	1.05 ± 0.06
Quartet	4.11 ± 0.02	1.16 ± 0.01	3.94 ± 0.01	1.25 ± 0.01
	4.20 ± 0.12	0.96 ± 0.04	4.44 ± 0.07	1.03 ± 0.10
1,4-Dioxane	4.87 ± 0.04	1.22 ± 0.02	4.66 ± 0.02	1.30 ± 0.02
	4.44 ± 0.16	1.31 ± 0.10	5.05 ± 0.07	1.24 ± 0.08

(a) In seconds \pm absolute standard deviations.

to determine the concentrations of some of the free intracellular components of human erythrocytes. As Brindle and coworkers [88] noted, the signals from the same compound inside and outside cells are not necessarily equal in relative intensity. This necessitates the use of hemolyzed cells in standard addition experiments. This is to ensure that the extra intensity derived from amounts added is comparable to that already present in the sample since there will no longer be any difference in the environment of the two portions of a compound.

As Figure 71 illustrates, well resolved resonances from several compounds are observed in ^1H spin-echo NMR spectra of hemolyzed red blood cells. Some of those which are fairly intense and have been previously assigned [16,17] have been utilized in this work. They include resonances from glutathione (GSH), glycine, ergothioneine, creatine, alanine and valine, the chemical shifts of which are shown in Figure 71.

An addition solution was prepared as described in Chapter II for adding to 0.5-mL samples of hemolysate to which 5 μL of a 50 mM t-butanol solution were added as an internal standard. The addition solution was added in 10- μL increments until 50 to 70 μL were added. In order to evaluate the precision of the concentration values determined in erythrocyte samples using the standard



Figure 71. A spin-echo NMR spectrum obtained with a τ_2 delay of 0.06 second on a sample of hemolyzed erythrocytes. Several resonances used to determine the concentrations of some of the compounds in the sample by a standard addition procedure are labelled in the spectrum.

addition technique, several replicates were performed on samples from one donor obtained and analyzed on the same date. The concentrations determined from these experiments are shown in Table 16. No correction for the portion of the 0.5-mL volume of hemolyzed erythrocytes which was due to external wash solution was applied to the standard addition results on erythrocyte samples [89]. As well as evaluating the precision of the NMR standard addition procedure, an attempt was made to examine the reproducibility of the sample pretreatment procedure described in Chapter II by working up portions of the blood sample separately. The results show a fair amount of scatter for the measured concentration levels of the compounds studied due to the NMR standard addition procedure. The precision among replicates of the same workup was only fair with a range of values of up to $\pm 25\%$ from the average of the three replicates performed. No evaluation of the variations between different workups was conducted due to the lack of precision of the replicates. It should be pointed out that the concentration levels measured for valine were extremely low and that the results showed a large relative standard deviation due to the small S/N ratio of the valine resonances (see Figure 71). Because of this, the valine results should only be used as estimates of the concentration levels in erythrocyte samples.

Table 16

Concentrations of Compounds(a) in Hemolyzed Erythrocytes from Donor I Determined by
Replicate NMR Standard Addition Experiments on the Same Blood Sample

<u>Sample</u>	<u>GSH (gly)</u>	<u>Glycine</u>	<u>Ergothioneine</u>	<u>Creatine</u>	<u>Alanine</u>	<u>Valine</u>
1(b)	1.78±0.16	0.12±0.01	0.30±0.01	0.29±0.02	0.23±0.02	0.08±0.01
2(b)	2.21±0.22	0.12±0.02	0.36±0.01	0.35±0.06	0.26±0.03	0.06±0.01
3(b)	1.57±0.16	0.10±0.01	0.27±0.01	0.22±0.01	0.17±0.03	0.09±0.02
4(c)	2.23±0.28	0.11±0.01	0.36±0.02	0.32±0.07	0.26±0.05	0.04±0.02
5(c)	1.53±0.26	0.11±0.01	0.31±0.05	0.22±0.02	0.18±0.03	0.01±0.02
Average	1.86±0.34	0.11±0.01	0.32±0.04	0.28±0.06	0.22±0.04	0.06±0.03

(a) Measured in $\text{mM} \pm$ absolute standard deviations.

(b) From the same portion of sample worked up by the erythrocyte pretreatment procedure described in Chapter II.

(c) From two other separate portions of sample worked up by the erythrocyte pretreatment procedure described in Chapter II.

Next, the standard addition technique was used to determine the concentration levels of several intracellular, small molecules in human erythrocyte samples from a variety of donors. The results of these experiments are shown in Table 17. More than one value listed under a compound for a donor indicates results obtained on different dates. The range of concentration values between donors and among the values obtained for a single donor on different occasions were approximately the same. Whether these variations are meaningful cannot be accurately determined due to the lack of precision in the NMR standard addition technique. Only large variations in the levels of these compounds could reliably be identified using this technique. The average levels determined in the standard addition experiments on hemolyzed human erythrocytes agree quite well with those quoted in the literature [79,90] for several of the compounds studied. Differences can be attributed to the natural variability of the levels of these compounds coupled with the small number of donors studied in this work. The results for alanine and valine were found to be somewhat low, probably due to washing out of some of these compounds during the erythrocyte pretreatment procedure.

In order to determine if compounds are washing out of the red cells during the sample pretreatment, standard

Table 17

Concentrations of Compounds in Hemolyzed Erythrocytes Determined by

Standard Addition Measurements (a)

Donor	GSH(gly)	Glycine	Ergothioneine	Creatine	Alanine	Valine
I	2.35	0.17	0.50	0.35	0.24	0.09
	2.16	0.35	0.25	0.44	0.26	0.10
	2.35	2.22	0.45	0.43	0.24	0.20
	2.48	± 0.22	0.40	0.32	0.24	0.03
	1.86	0.15	± 0.10	± 0.07	± 0.02	± 0.07
	2.12	0.11	0.32	0.28	0.22	0.06
II	1.78	0.10	0.29	0.31	0.21	0.04
	1.96	0.32	0.24	0.58	0.11	0.09
III	2.15	0.28	0.26	0.39	0.27	0.07
	2.39	0.42	0.57	0.37	0.19	0.12
IV	1.66	0.46	0.56	0.62	0.42	0.12
	2.02	0.38	0.31	0.27	0.24	0.06
V	2.61	0.27	0.18	0.56	0.22	0.09
VI	2.06	0.29	0.32	0.38	0.11	0
VII	2.12	0.20	0.33	0.41	0.16	0.10
VIII	2.10	0.22	0.69	0.39	0.08	0.11
Average	2.10 \pm 0.28	0.29 \pm 0.09	0.38 \pm 0.16	0.42 \pm 0.09	0.19 \pm 0.08	0.08 \pm 0.04
Literature [79,90]	2.29	0.34	0.42	0.26	0.44	0.17

(a) Measured in mM. Uncertainties in the values are of the same order as those in Table 16. Multiple values for a particular donor are for experiments performed on different dates.

addition experiments were carried out on 0.5-mL portions of a sample of intact erythrocytes from Donor I taken after two, three and four washes with saline D₂O and hemolyzed prior to adding the internal standard. These results are shown in Table 18. No significant losses of any of the compounds studied are evident from the data although losses may have occurred during the first wash. This data confirms in quantitative terms the qualitative results observed in Chapter IV.

The possibility of changes in T_1 and T_2 relaxation times over the course of the standard addition experiments on hemolyzed red blood cells was investigated because such changes could give rise to erroneous concentration determinations. The results of T_1 and T_2 determinations on two samples of hemolyzed erythrocytes both before and after the standard addition procedure are presented in Table 19. T_1 determinations in red cell samples were made by using the inversion-recovery-spin-echo sequence [6] rather than just the inversion-recovery sequence [7]. Linking the inversion-recovery sequence to the spin-echo sequence allows T_1 relaxation times to be measured for the small molecules in red cells, without the interference of hemoglobin resonances which would otherwise prevent the determination of T_1 values. The results of the T_1 and T_2

Table 18

Concentrations of Compounds(a) in Hemolyzed Erythrocytes from Donor I Determined by
NMR Standard Addition Experiments on a Blood Sample After Successive Washes
with Saline D₂O

<u># Washes</u>	<u>GSH(gly)</u>	<u>Glycine</u>	<u>Ergothioneine</u>	<u>Creatine</u>	<u>Alanine</u>	<u>Valine</u>
2	2.26	0.11	0.31	0.36	0.24	0.07
3	1.90	0.09	0.28	0.31	0.20	0
4	2.22	0.10	0.27	0.27	0.19	0.05

(a) Measured in mM. Uncertainties in the values are of the same order as those in Table
16.

Table 19
Determinations of T₁ and T₂ Relaxation Times^(a) on Hemolyzed Erythrocyte Samples
Before and After Standard Addition Experiments

Compound	Before		After	
	T ₁	T ₂	T ₁	T ₂
GSH(gly)	1.39 ± 0.04	0.19 ± 0.01	1.28 ± 0.06	0.21 ± 0.02
	1.28 ± 0.02	0.21 ± 0.03	1.16 ± 0.04	0.22 ± 0.02
Glycine	2.90 ± 0.10	0.72 ± 0.03	2.51 ± 0.06	0.61 ± 0.01
	2.70 ± 0.11	1.09 ± 0.19	2.49 ± 0.04	0.70 ± 0.07
Ergothioneine	1.61 ± 0.08	0.29 ± 0.01	1.16 ± 0.09	0.26 ± 0.01
	1.61 ± 0.06	0.25 ± 0.02	1.19 ± 0.12	0.19 ± 0.01
Creatine	1.57 ± 0.04	0.27 ± 0.01	1.65 ± 0.03	0.30 ± 0.01
	1.79 ± 0.07	0.26 ± 0.02	1.80 ± 0.03	0.29 ± 0.02
Alanine	1.27 ± 0.09	0.38 ± 0.00	1.50 ± 0.07	0.41 ± 0.03
	1.38 ± 0.05	0.50 ± 0.18	1.46 ± 0.02	0.45 ± 0.11
Valine	1.60 ± 0.16	(b)	1.01 ± 0.04	0.26 ± 0.06
	0.97 ± 0.17	(b)	1.04 ± 0.04	0.24 ± 0.02
t-Butanol	1.55 ± 0.05	0.15 ± 0.02	1.46 ± 0.08	0.14 ± 0.00
	1.61 ± 0.04	0.14 ± 0.00	1.63 ± 0.06	0.14 ± 0.01

(a) In seconds ± absolute standard deviations.
(b) Signals too weak to measure accurately.

measurements before and after the standard addition procedure indicate no significant changes in relaxation times during the standard addition experiments.

E. Proportionality Constants in Concentration Determinations by NMR

Another means of determining the concentrations of intracellular compounds in samples of human erythrocytes that has been investigated in this work is the mathematical extrapolation of resonance intensities measured in the spin-echo NMR experiment at a certain τ_2 delay time back to their intensities at a τ_2 delay of zero. At this point, there has been no differential T_2 relaxation and the relative intensities of resonances are proportional to the number of nuclei giving rise to them as in the single-pulse NMR experiment.

Theoretically, this means measuring the intensity of a particular resonance as a function of time in order to determine the T_2 relaxation time as described in Chapter IV. From a knowledge of the T_2 value, the initial intensity at a τ_2 delay of zero, I_0 , can be calculated from the intensity measured at a certain τ_2 delay time, $I_{2\tau_2}$, in the spin-echo experiment by:

$$I_0 = I_{2\tau_2} e^{(2\tau_2/T_2)}$$

(22)

This is a cumbersome procedure to apply to each sample, requiring the acquisition of a whole series of spin-echo spectra at various τ_2 delay times in order to measure T_2 values. In fact, the T_2 relaxation time for a particular resonance in samples of red blood cells from different donors is found to remain fairly constant from donor to donor. Table 20 presents the results of T_2 determinations on intact red blood cells for several donors for a variety of compounds. The average relative standard deviation of the measured T_2 values is about $\pm 7\%$. This reasonably small average variation in the T_2 relaxation time of a particular resonance between donors allows the use of an average T_2 value for each of the resonances studied to calculate a proportionality constant at a certain τ_2 delay time:

$$K = e^{(2\tau_2/T_2)} \quad (23)$$

to be used in the calculation of I_0 :

$$I_0 = I_2 \tau_2^K \quad (24)$$

Table 20

T₂ Relaxation Times^(a) for Compounds in Intact Erythrocytes

<u>Donor</u>	<u>GSH(gly)</u>	<u>Glycine</u>	<u>Ergothioneine</u>	<u>Creatine</u>	<u>Alanine</u>
I	0.145 } 0.146 } 0.141 }	0.500 } 0.668 } 0.661 }	0.274 } 0.265 } 0.260 }	0.223 } 0.241 } 0.237 }	0.326 } 0.329 } 0.286 }
IX	0.155	0.521	0.201	0.227	0.305
X	0.161	0.571	0.235	0.233	0.391
XI	0.153	0.506	0.243	0.222	0.343
XII	0.154	0.547	0.263	0.231	0.352
XIII	0.150	0.550	0.276	0.220	0.319
Average	0.153	0.551	0.247	0.228	0.343
Rel. Std. Dev.	3.7%	6.7%	11.1%	2.5%	8.7%

(a) Measured in seconds.

This reduces the number of spectra that are required to determine I_0 values to one collected at the τ_2 value for which K is calculated. For a τ_2 delay time of 0.06 second the value of K in intact cells, as evaluated from the average T_2 relaxation times for the resonances in intact cells given in Table 20, is 2.19 ± 0.06 for the methylene protons of the glycine residue of GSH, 1.24 ± 0.02 for the methylene protons of glycine, 1.63 ± 0.09 for the methyl protons of ergothioneine, 1.69 ± 0.02 for the methyl protons of creatine and 1.42 ± 0.04 for the methyl protons of alanine. The values in Table 20 are for intact erythrocytes. The resonances for these compounds in hemolyzed erythrocytes generally have different T_2 values and thus different proportionality constants would be evaluated.

Initial intensity measurements obtained for resonances on the basis of peak areas, I_{0a} , are immediately comparable in terms of relative concentrations, taking into account the number of protons, n , giving rise to each resonance:

$$I_R = I_{0a}/n \quad (25)$$

where I_R represents the comparable peak intensities. In spin-echo spectra of intact human erythrocytes, peak area

measurements are often more difficult to make than peak height measurements due to uncertainties in the baseline and the partial overlap of resonances. Peak height measurements on the other hand are very easy to obtain. However, for initial intensity measurements obtained as peak heights, I_{0h} , some consideration to peak widths must be given. The peak heights are only indicative of the relative amounts of compounds as long as the peak widths at half height, $W_{1/2}$, are all the same. The $W_{1/2}$ values for the resonances studied are not all the same. They average 7.8 ± 0.8 Hz for the methylene protons of the GSH glycine residue, 4.9 ± 0.8 Hz for the methylene protons of glycine, 6.0 ± 0.6 Hz for the methyl protons of ergothioneine, 6.2 ± 0.8 Hz for the methyl protons of creatine and 6.5 ± 0.8 Hz for the methyl protons of alanine. In order to compare the initial peak heights extrapolated from spin-echo spectra of intact cells, the values must be made relative to each other. This can be accomplished by multiplying the initial intensity value by the $W_{1/2}$ value for each resonance studied and dividing this result by the number of protons giving rise to each resonance:

$$I_R = \frac{I_{0h} W_{1/2}}{n} \quad (26)$$

At this stage, the values of I_R obtained for either peak areas or heights for the various resonances are indicative of the relative concentrations of the red blood cell components. To obtain absolute concentration levels for these compounds requires knowledge of the concentration of one or more of the compounds in the erythrocyte samples. The GSH concentration was found to be fairly uniform from donor to donor for healthy individuals from the standard addition experiments, averaging about 2.29 ± 0.23 mM. By assigning the GSH concentration as 2.29 mM, concentration values can be determined for the other compounds. Results of this type are shown in Tables 21 and 22 for measurements made using peak areas and peak heights, respectively, for the resonances other than GSH studied in spin-echo spectra obtained with a τ_2 delay time of 0.06 second. In general, the results agree reasonably well with the literature [79,90] and with the results obtained from the standard addition experiments. The creatine levels given in Table 21 using peak areas are probably somewhat high due to the partial overlap of the creatine resonance at 3.01 ppm with that of the GSH β -cysteine methylene protons. Other differences can, to a large degree, be accounted for in terms of the natural variability of the levels of the various compounds and the small number of donors studied.

Table 21

Concentrations of Compounds in Intact Erythrocytes Determined Using Proportionality
 Constants and Intensity Measurements Based on Peak Areas(a)

<u>Donor</u>	<u>Glycine(b)</u>	<u>Ergothioneine(c)</u>	<u>Creatine(d)</u>	<u>Alanine(e)</u>
I	0.21	0.28	0.54	0.49
IX	0.23	0.26	0.51	0.18
X	0.38	0.41	0.68	0.37
XI	0.30	0.58	0.81	0.33
XIV	0.43	0.13	1.06	0.28
XV	0.45	0.34	0.90	0.27
Average	0.33±0.10	0.33±0.15	0.75±0.21	0.32±0.11
Literature [79,90]	0.34	0.42	0.26	0.44

(a) Measured in mM. Absolute concentrations based on [GSH] = 2.29 mM.

(b) The uncertainty in the glycine concentrations due to the uncertainty in K, determined from the average T₂, is 0.005 mM.

(c) The uncertainty in the ergothioneine concentrations due to the uncertainty in K is 0.018 mM.

(d) The uncertainty in the creatine concentrations due to the uncertainty in K is 0.009 mM.

(e) The uncertainty in the alanine concentrations due to the uncertainty in K is 0.009 mM.

Table 22

Concentrations of Compounds in Intact Erythrocytes Determined Using Proportionality Constants and Intensity Measurements Based on Peak Heights^(a)

<u>Donor</u>	<u>Glycine</u> ^(b)	<u>Ergothioneine</u> ^(c)	<u>Creatine</u> ^(d)	<u>Alanine</u> ^(e)
I	0.18 } 0.17 } 0.17 }	0.15 } 0.15 } 0.16 }	0.36 } 0.35 } 0.38 }	0.28 } 0.28 } 0.28 }
IX	0.15	0.15	0.27	0.13
X	0.19	0.22	0.36	0.15
XI	0.22	0.22	0.39	0.33
XII	0.14	0.11	0.33	0.15
XIII	0.23	0.11	0.32	0.16
Average	0.18±0.04	0.16±0.05	0.34±0.04	0.20±0.08
Literature [79,90]	0.34	0.42	0.26	0.44

(a) Measured in mM. Absolute concentrations based on [GSH] = 2.29 mM.

(b) The uncertainty in the glycine concentrations due to the uncertainty in K, determined from the average T₂, is 0.003 mM.

(c) The uncertainty in the ergothioneine concentrations due to the uncertainty in K is 0.009 mM.

(d) The uncertainty in the creatine concentrations due to the uncertainty in K is 0.004 mM.

(e) The uncertainty in the alanine concentrations due to the uncertainty in K is 0.006 mM.

F. Discussion

The results presented in this chapter indicate that acceptable values for the concentrations of compounds in solution can be determined from the intensities of resonances in spin-echo spectra using several techniques. The use of a standard addition approach yields reasonable values for the volume added intercepts in CDCl_3 solutions of diethylsuccinate as presented in Tables 12 to 14. The measured T_1 and T_2 relaxation times were noted to remain fairly constant over the course of the experiments, as shown by the results in Table 15, which validates the use of the standard addition technique with the spin-echo NMR experiment. Both general techniques described here, the standard addition method and the use of extrapolation procedures involving proportionality constants, appear to give reasonable concentration levels for compounds in samples of human erythrocytes, although neither method gives extremely accurate results. In the case of the standard addition method, the technique seems to have a fairly large imprecision, the reasons for which are not clear. For the method involving proportionality constants, some tolerable uncertainties are introduced by the use of average T_2 values in calculating the proportionality constants. The

use of peak areas rather than peak heights gives results somewhat more in line with the literature when using proportionality constants as indicated by the results of Tables 21 and 22. Both of the general methods for measuring concentrations in erythrocytes would seem to be prone to errors due to overlapping resonances from other compounds. In the case of the creatine results using proportionality constants with area measurements, some contributions from GSH are certain but there may well be unknown contributions to the other resonances studied from minor erythrocyte components.

The method of choice would seem to be the use of proportionality constants using area measurements in cases where the T_2 relaxation times are known since there is less experimental effort involved than with the standard addition method and the technique can be applied to intact or hemolyzed cells. This is in contrast to the standard addition procedure which necessitates the hemolysis of the red blood cells. However, in cases where the T_2 values are unknown or vary from sample to sample, that is the NMR matrix effects are uncertain, the standard addition approach may be simpler and thus preferred.

CHAPTER VI

DETERMINATION OF GLUTATHIONE IN ERYTHROCYTES BY TITRATION WITH t-BUTYLHYDROPEROXIDE

A. Introduction

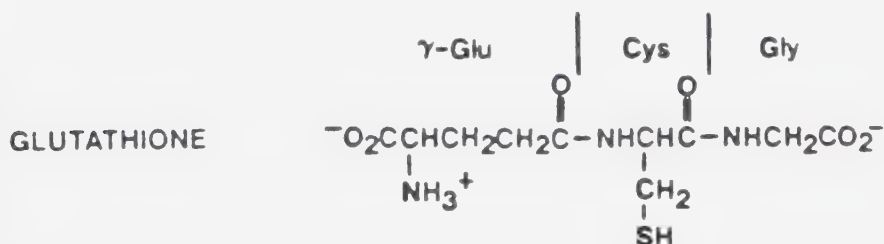
As has been shown in previous chapters, numerous small molecules in intact and hemolyzed erythrocytes can be observed selectively by ^1H spin-echo FT NMR. However, because of differential spin-spin relaxation and phase modulation effects, it is difficult to obtain quantitative information from resonance intensities. In Chapter V, generalized quantitative procedures based on standard addition titrations and the use of proportionality constants were developed. In this chapter, the use of a titration based on a selective reaction with the compound of interest in the erythrocyte is studied. Such titration procedures are commonly used in analytical chemistry to measure the amount of a compound present in a sample, however, they have been less widely used with biological samples as complex as cellular systems due to the difficulty in following the progress of the titration. It is shown in this chapter that advantage can be taken of

the high degree of selectivity possible with the ^1H spin-echo NMR technique to solve this problem.

There are several general criteria which any titration procedure must satisfy. First, the titration reaction must be selective and complete for the compound of interest. The titrant must not react with other sample components, which may pose considerable problems in a complex biological sample containing an extremely varied number of compounds. Second, the reaction must proceed fairly rapidly to completion after each increment of titrant is added. Third, there must be a systematic change in some property which can be monitored to allow the progress of the titration to be followed and the end point of the titration to be located. The changes which might occur in an NMR spectrum due to the titration reaction are a change in either chemical shift or in intensity of a resonance. One further criterion which is unique to NMR and is necessary when changes in peak intensities are involved is that spin-spin relaxation times for the monitored resonances remain essentially constant throughout the titration procedure so that changes in peak intensities during the course of the titration are due only to reaction with the titrant and not to changing spin-spin relaxation times.

A titration procedure for the determination of glutathione (GSH) is described in this chapter to illustrate the determination of a specific compound in human erythrocytes by combining a highly selective reaction with the selectivity of the ^1H spin-echo experiment. The titration procedure is based on the enzyme-catalyzed reaction of GSH with organic hydroperoxides.

Glutathione (γ -L-glutamyl-L-cysteinylglycine) is a tripeptide of glutamic acid, cysteine and glycine found extensively in cellular systems.



Its role in the red blood cell is to activate enzymes and protect hemoglobin from oxidation by keeping the sulfhydryl groups of the proteins reduced [33]. It protects the cells from oxidative damage by reacting with free radicals and peroxides present in the cells [91]. In red blood cells, about 99% of the free glutathione is normally found in the reduced form [92].

Although the reaction of GSH with peroxides proceeds spontaneously in the red cell, it is accelerated by the

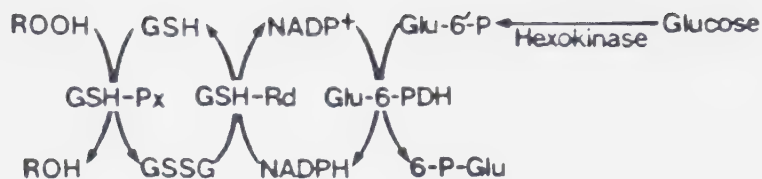
selenium-containing [93] enzyme glutathione peroxidase (GSH-Px) [91] discovered by Mills in 1957 [94]. This enzyme has a high specificity for GSH [95] and will destroy a variety of organic hydroperoxides which may be produced by cellular processes at rates similar to that for the destruction of H_2O_2 by GSH-Px [96].

The overall reaction involves the conversion of the hydroperoxide to its corresponding alcohol and water with the accompanying oxidation of GSH to the disulfide form, GSSG.



The proposed three step mechanism for GSH-Px action takes into account the similar reaction rates of different hydroperoxides [97,98]. The first step is the oxidation of the enzyme by the hydroperoxide substrate and the release of the alcohol and water molecules. The next step involves two successive additions of GSH to the enzyme. The final step is the release of GSSG from the enzyme leaving it in the reduced form.

In viable cellular systems, glutathione is maintained in the reduced form by the action of the enzyme glutathione reductase (GSH-Rd) [99].

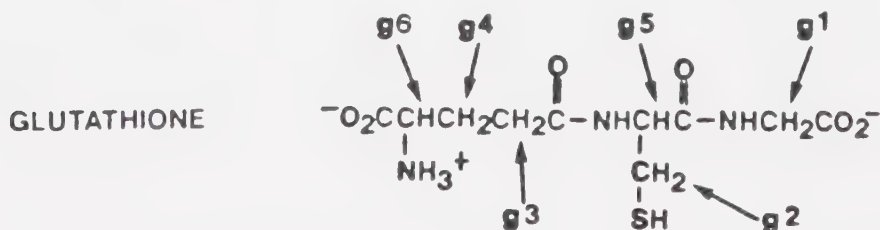


The reaction involves the reduction of GSSG by NADPH.



NADH can also take part in this reaction but is less effective than NADPH. The NADP⁺ is reduced by the action of glucose-6'-phosphate dehydrogenase (Glu-6'-PDH) on glucose-6'-phosphate (Glu-6'-P) to form 6-phosphogluconolactone (6-P-Glu). Glu-6'-P is in turn produced from glucose by the action of the enzyme hexokinase.

The enzyme catalyzed reaction of GSH with hydroperoxides readily fulfills the general criteria for titration reactions outlined above. The reaction in a cellular system is very selective and rapid. The splitting of the methylene protons adjacent to the sulfhydryl group (g2) is different in the NMR spectra of



the two forms of glutathione, changing from the AB portion of one ABX spin system in GSH (top spectrum in Figure 72) to the AB part of another ABX spin system in the oxidized form, GSSG (bottom spectrum in Figure 72). The chemical shifts of the AB portion of the ABX spin system of GSSG are somewhat different from the chemical shifts of the AB portion of the ABX spin system of GSH. Since exchange of glutathione between its reduced and oxidized forms is slow on the NMR time scale, discrete resonances are observed for both of the forms. The reduction in intensity of the cysteine β -CH₂ resonances of GSH can therefore be followed in successive NMR spectra as the titration proceeds.

There are several possible sources of error in any titration procedure for determining GSH involving peroxides as titrant. One potential source of error is that caused by catalase, another enzyme present in cellular systems, which also reduces H₂O₂ at about the same rate as GSH-Px [100]. Fortunately, however, catalase does not reduce organic hydroperoxides to any appreciable extent. The air oxidation of GSH to form the disulfide is another source of error which must be minimized. As well, the reduction of GSSG produced in the titration back to GSH by the action of GSH-Rd must be prevented.

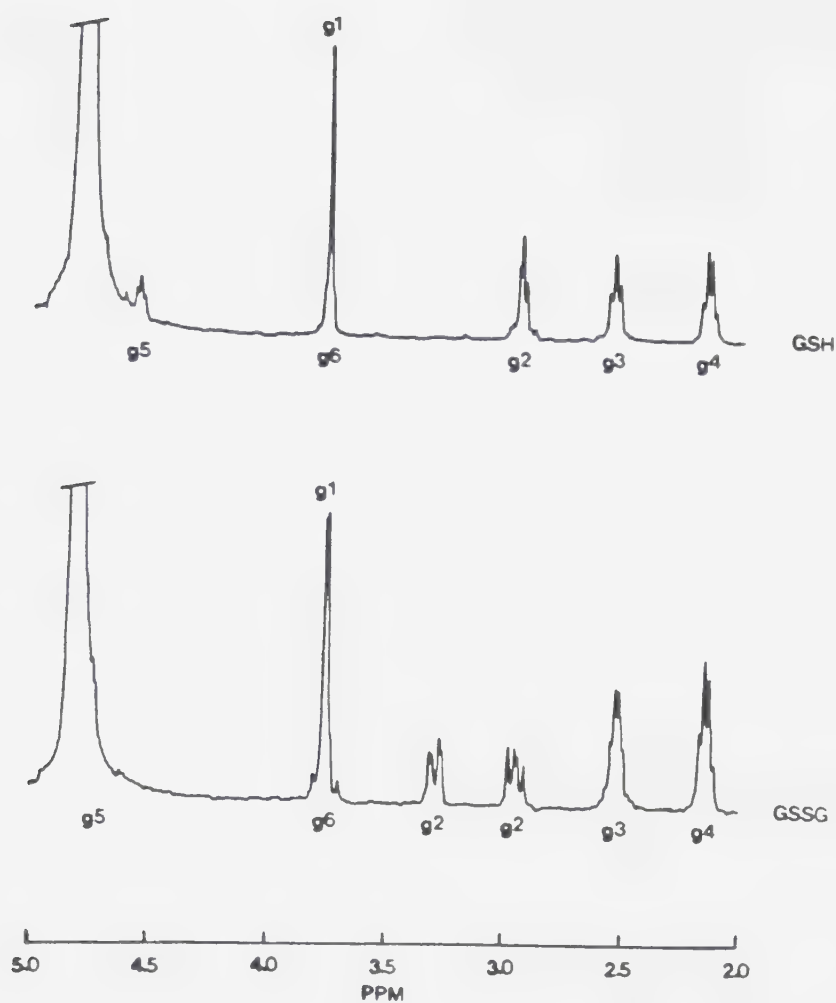


Figure 72. 360 MHz single-pulse spectrum of GSH (top) and GSSG (bottom).

B. The NMR Titration Procedure

The NMR titration procedure developed in this work makes use of the reaction of t-butylhydroperoxide (t-BHP) with GSH to form GSSG. The reaction is catalyzed by GSH-Px.



The use of an organic hydroperoxide as titrant ensures that catalase activity will be negligible and the reaction will proceed entirely via the GSH-Px pathway. Reduction of the GSSG produced during the titration process was minimized by washing the red blood cells several times with saline D₂O to remove glucose which fuels the reduction process. As discussed later, this is unnecessary if hemolyzed cells are titrated because the metabolism of glucose is prevented when the cells are hemolyzed.

The titration procedure employed involved the sequential addition of 5- μL increments of a standardized 0.014 M t-BHP titrant to samples of intact or hemolyzed red blood cells directly in an NMR tube. Each increment of titrant was added using a 10- μL syringe. For hemolyzed cells, a 0.5-mL aliquot of hemolysate was placed in an NMR

tube with a 1-mL syringe. In the case of whole cells, 0.35 mL of cells and 0.15 mL of saline D₂O were generally used to make up a 0.5-mL initial titration volume. The reason for this dilution of the whole cells was to decrease the viscosity of the packed cells by suspending them in a small volume of liquid. This facilitated the rapid mixing of the added increments of t-BHP titrant by reasonably vigorous shaking of the NMR tube for approximately one minute.

Before any t-BHP was added and after each 5- μ L addition, a spin-echo NMR spectrum was collected using a τ_2 delay time of 0.04 second. This value for τ_2 was chosen after some trial and error as giving the best signals for the cysteine methylene protons of GSH, the intensities of which were measured to monitor the course of the titration. The reaction between GSH and t-BHP produced GSSG which could be distinguished from GSH as shown in the spin-echo spectrum of Figure 73. The resonances for the cysteine methylene protons of both GSH and GSSG are indicated in the spectrum as well as the glycine resonance at 3.54 ppm, the ergothioneine resonance at 3.25 ppm and the creatine resonance at 3.01 ppm. There is extensive overlap of resonances for the two forms of glutathione in the region of 2.9 to 3.0 ppm. However, at a τ_2 delay time of 0.04 second, resonances for GSH alone,

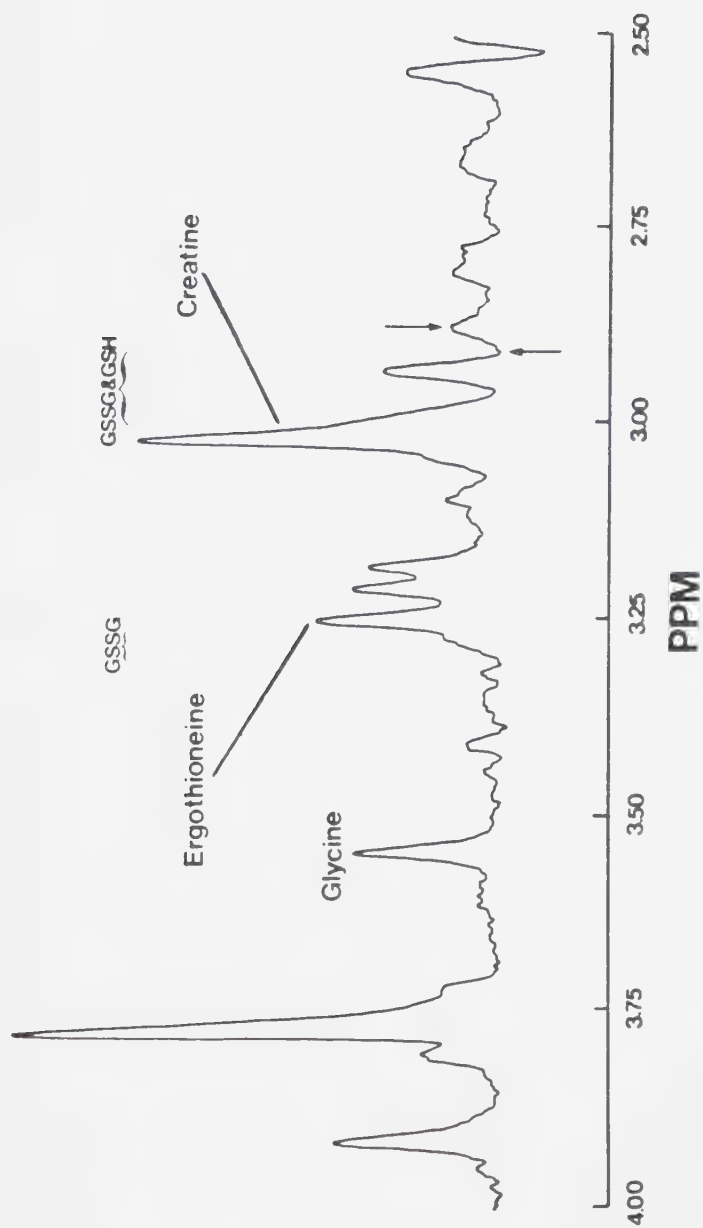


Figure 73. 360 MHz spin-echo NMR spectrum ($\tau_2 = 0.04$ second) of hemolyzed red blood cells which had been washed with saline D_2O . Several compounds are identified in the spectrum. The resonances indicated at 2.88 and 2.91 ppm are due only to GSH.

which were used to follow the progress of the titration, can be found at 2.88 and 2.91 ppm. At this τ_2 delay value, resonances from GSSG at these chemical shifts are at a null in their phase modulation cycle. The GSH resonances are phase modulated as well resulting in that at 2.91 ppm being inverted and that at 2.88 ppm being positive in intensity at the τ_2 delay time of 0.04 second employed. As the titration proceeded, the two GSH peaks decreased in intensity due to the reaction of the GSH to form GSSG as shown in Figure 74 for the titration of a sample of hemolyzed red blood cells.

The resonances for the cysteine β -CH₂ protons of GSH which were monitored in the titration decreased very linearly with increasing amounts of titrant added to the sample in a manner consistent with a direct relationship between the added titrant and the intensity of the resonances for the cysteine methylene protons of GSH. On the other hand, the resonances for glycine, ergothioneine and creatine identified in Figure 73 at 3.54, 3.25 and 3.01 ppm, respectively, remained relatively constant and were not affected in a consistent manner by the addition of titrant.

In order to add each increment of t-BHP in the titration procedure, it was necessary to remove the NMR tube from the spectrometer. When the sample was replaced

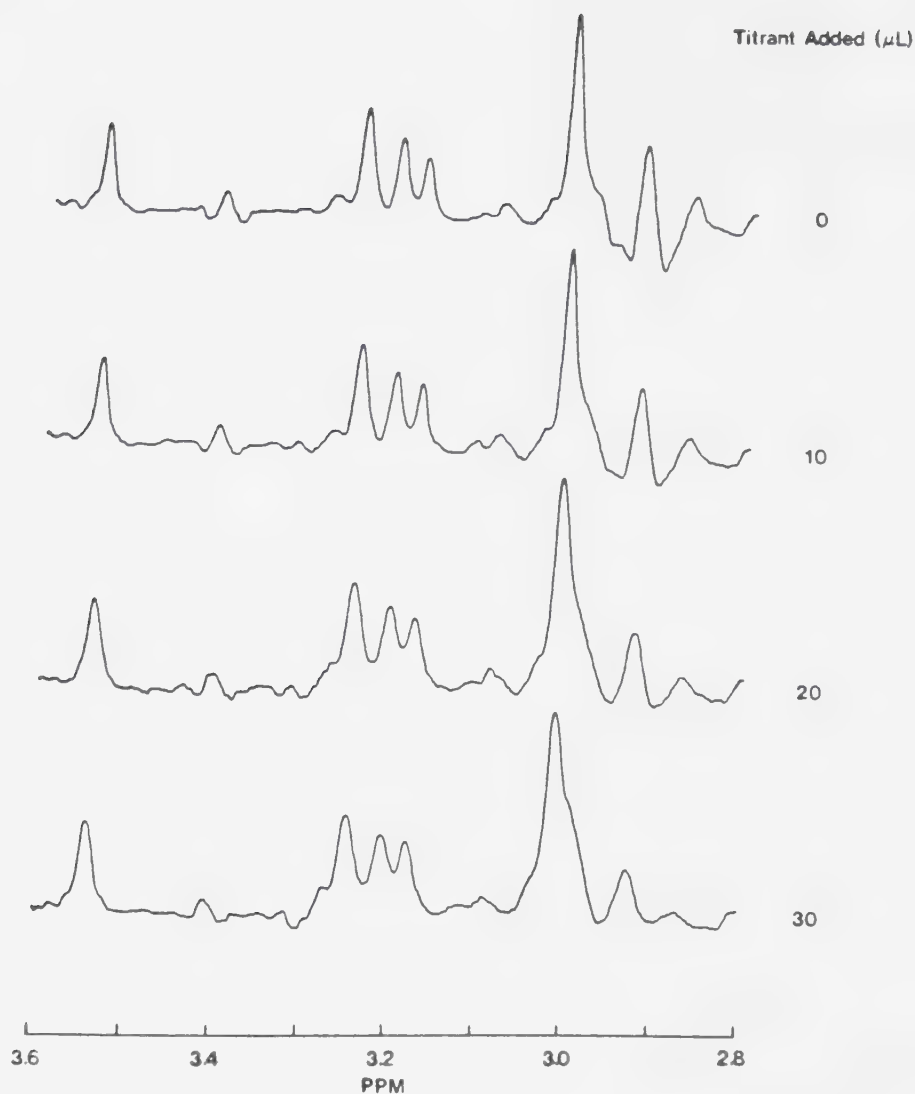


Figure 74. A series of spin-echo spectra ($\tau_2 = 0.04$ second) obtained as increments of a t-BHP solution were added to a sample of hemolyzed erythrocytes to titrate the GSH. The GSH resonances at 2.88 and 2.91 ppm are observed to decrease with the addition of t-BHP.

in the spectrometer slight reshimming adjustments were necessary to restore the resolution to an adequate level. However, there may be slight differences in the resolution of the spectra collected with this procedure which will alter peak shapes in the spectra. Since peak heights were used to determine the amount of GSH present, a normalization procedure was employed using some other resonance in the spectrum which is not involved in the titration reaction. This resonance will be affected in the same way as the GSH resonances by changes in resolution. Such a normalization procedure will also account for minor dilution effects caused by the addition of titrant to the sample and compensate for such experimental variations as the number of scans collected, the receiver gain and the vertical scaling factor of the plotted spectrum.

The resonance used as an internal standard to which the sum of the measured absolute intensities of the GSH resonances at 2.88 and 2.91 ppm was normalized was the ergothioneine signal at 3.25 ppm. In order to check the validity of using this resonance as an internal standard, the resonances from glycine (3.54 ppm) and creatine (3.01 ppm) were also normalized to ergothioneine. The titration was followed by plotting the normalized GSH peak intensities on the ordinate axis against the volume of

titrant added on the abscissa. The end point of the titration was determined as the intercept on the abscissa of the linear least-squares fit of the data, which corresponds to the disappearance of the resonances from the cysteine methylene protons of GSH. Typically, the end point was around 40 μL for the 0.014 M t-BHP titrant used. With 5- μL additions of titrant, this generally required about two hours for each titration. An example of a titration curve is shown in Figure 75 for the data obtained from the spectra in Figure 74. Also shown are the data for the normalized glycine and creatine resonances. The amount of GSH in the sample was determined as twice the amount of t-BHP titrant represented by the end point of the titration (see Equation 29). GSH concentration values reported were not adjusted to account for external fluid present in the samples of packed cells analyzed [89].

C. Hemolyzed Red Blood Cells

Spin-echo NMR spectra collected over the course of a typical NMR titration carried out on hemolyzed red blood cells (HRBC) have already been presented in Figure 74. Measurements made on these spectra resulted in the curves shown in Figure 75. There is a linear decrease in the intensity of the resonances for the cysteine $\beta\text{-CH}_2$ protons

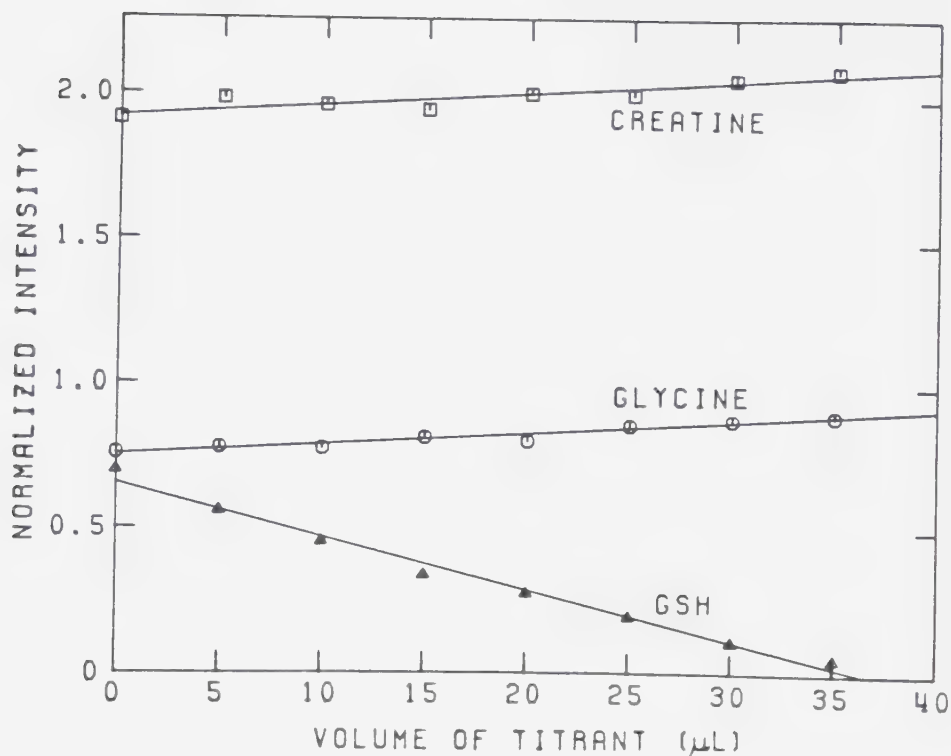


Figure 75. The titration curve for the NMR titration shown in Figure 74. The sum of the intensities of the GSH resonances at 2.88 and 2.91 ppm, normalized against the ergothioneine resonance at 3.25 ppm, is plotted as a function of t-BHP added. Also shown are the normalized glycine and creatine resonances at 3.54 and 3.01 ppm, respectively.

of GSH relative to that of ergothioneine which begins with the addition of the first increment of t-BHP (see Equation 29) and continues with subsequent additions. This gives rise to the GSH titration curve shown in Figure 75.

The results of the titrations conducted on samples of HRBC from several donors are summarized in Table 23. The average GSH level in the donors studied was found to be 2.80 mM with a standard deviation among the donors of 0.33 mM . Variations in GSH levels were found not only among the donors but also between samples from the same donor obtained on different dates. It is interesting to note that Donor IX appeared to have a reasonably high GSH level as determined by this procedure. Blood from this donor was found to have a consistently high GSH level in other studies as well.

The precision of the NMR titration technique was evaluated by conducting replicate titrations on the same sample of erythrocytes for several of the donors and was found to vary from 1 to 7% with an average precision of 3.6%. The relative standard deviation of the end point as determined from linear least-squares evaluations on several of the titrations based on the scatter in the individual points of the titrations was found to be 2.9% on average.

Table 23
Glutathione Levels in Hemolyzed Erythrocytes

Donor	[GSH] _{DTNB} (mM) (a)	[GSH] _{NMR} (mM)	
		Single Values	Average of Replicates for Donor
I	1.92(oxy)	2.50(b)	2.58
		2.60	
		2.70	
		2.49	
	--	2.67(c)	2.53(d)
	--	2.80(c)	--
	1.63(oxy) 1.99(deoxy)	2.10(c)	--
IX	--	3.14 3.10	3.12
X	--	2.51	2.51
XI	1.89(oxy) 2.14(deoxy)	2.97(e) 3.17(e)	3.07
XII	1.92(oxy) 2.15(deoxy)	3.25	3.25

Table 23 (Cont'd.)

Donor	[GSH] _{DTNB} (mM) (a)	[GSH] _{NMR} (mM)		
		Single Values	Average of Replicates	Average for Donor
XIV	1.78(oxy)	2.62	2.57	2.36
		2.52		
	1.56(oxy)	2.24	2.13	
		2.03		
XVI	1.61(oxy)	2.88	--	2.88
	2.13(deoxy)			
XVII	1.84(oxy)	2.67	--	2.67
	2.09(deoxy)			

- (a) Average of from one to six values. The standard deviation among replicates was typically ~±5%.
- (b) Replicates performed on the same day over a period of approximately 12 hours.
- (c) Single values determined on samples taken and analyzed on separate days.
- (d) Average of single values and average value for replicates.
- (e) Determined on a sample of unwashed hemolyzed red blood cells.

Samples of HRBC were analyzed using the accepted clinical method of GSH determination employing DTNB to measure their GSH levels [32,101,102] in order to evaluate the performance of the NMR titration procedure. These determinations were carried out on different portions of the same samples on which the NMR titrations were conducted. The DTNB analyses were conducted concurrently with the NMR titrations. Details of the experimental procedure used for the DTNB method are given in Chapter II. The results as shown in Table 23 were always considerably lower for the DTNB determinations as compared with the NMR titration results. Again variations between donors and among samples from the same donor obtained and analyzed on different occasions were apparent.

Differences in the GSH levels determined by the DTNB method were also noted when the analysis was performed on both oxygenated and deoxygenated blood. Deoxygenation was achieved by bubbling a solution containing 0.1 or 0.2 mL of HRBC and enough H_2O to give a volume of 2 mL with nitrogen which had been passed through an oxygen scrubber. At the same time, the protein precipitating solution was bubbled with nitrogen. After bubbling for approximately 10 minutes, the two solutions were mixed and GSH determined by the DTNB procedure. Care was taken to keep the two solutions from contacting the atmosphere

until the protein precipitation step was accomplished. The values obtained for the deoxygenated blood (Table 23) were found to be closer to those determined in the NMR titration procedure than those obtained for the oxygenated blood.

A sample of unwashed HRBC from Donor XI was titrated using the NMR method. The titration curve shown in Figure 76 which resulted from this sample had an initial plateau region where no titration of the GSH was occurring followed by the usual linearly decreasing titration curve. The titration was assigned as beginning at the intercept of the linear least-squares fit of the plateau region with the linearly decreasing least-squares fit of the rest of the data. The value for the GSH concentration obtained using this procedure agreed well with that obtained on a saline D₂O washed sample of HRBC from Donor XI drawn at the same time as the unwashed sample.

D. Whole Red Blood Cells

Spin-echo spectra collected over the course of a typical titration of intact human erythrocytes are shown in Figure 77. One distinct difference between the titrations of saline D₂O washed whole cells and saline D₂O washed hemolysate which is evident in these spectra was the appearance of a plateau for the initial two or three

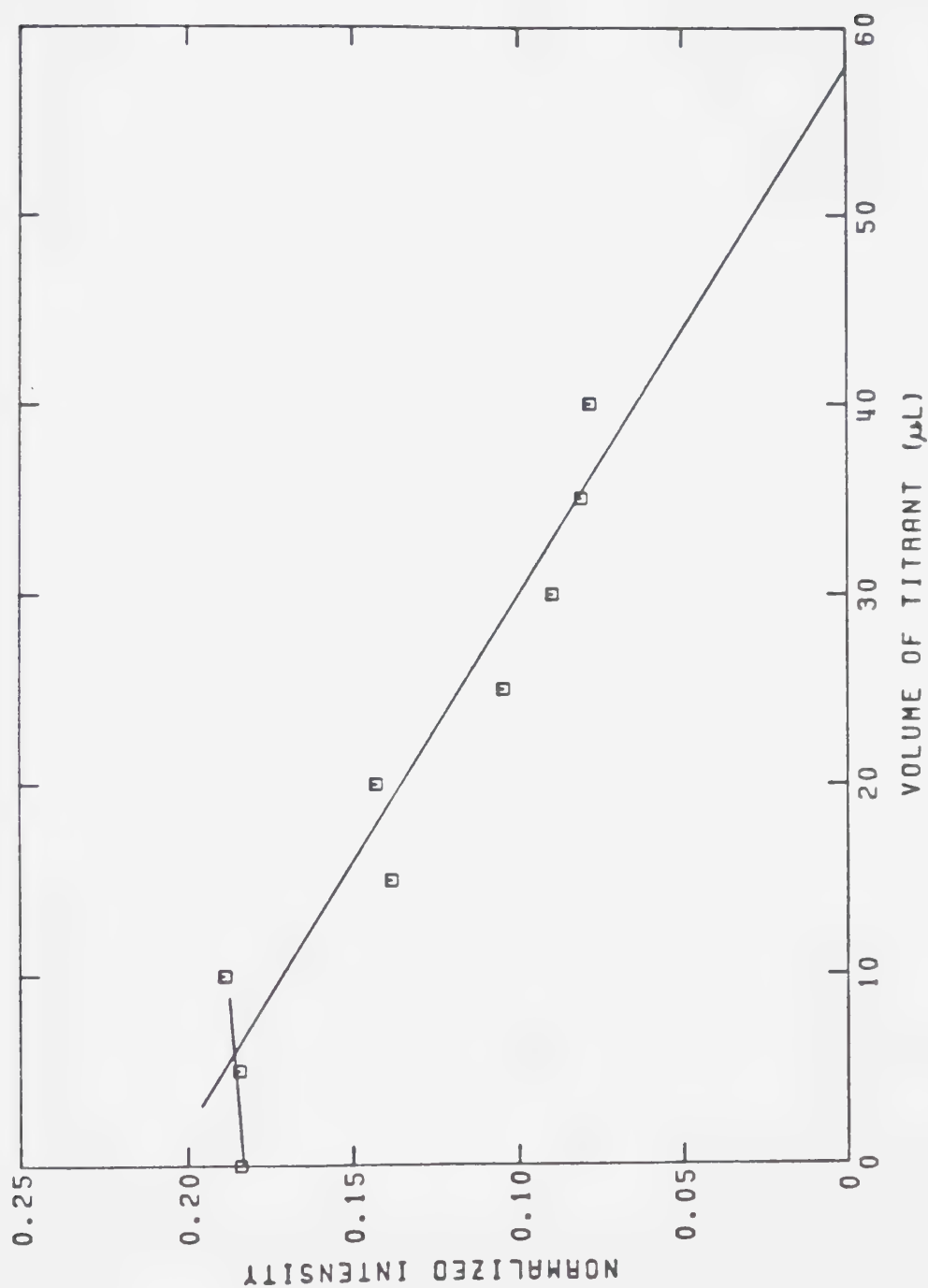


Figure 76. The titration curve for a sample of unwashed HRBC. The sum of the intensities of the GSH resonances at 2.88 and 2.90 ppm, normalized against the ergothioneine resonance at 3.25 ppm, is plotted as a function of t-BHP added. Initially, a short plateau was observed followed by a linearly decreasing titration curve.

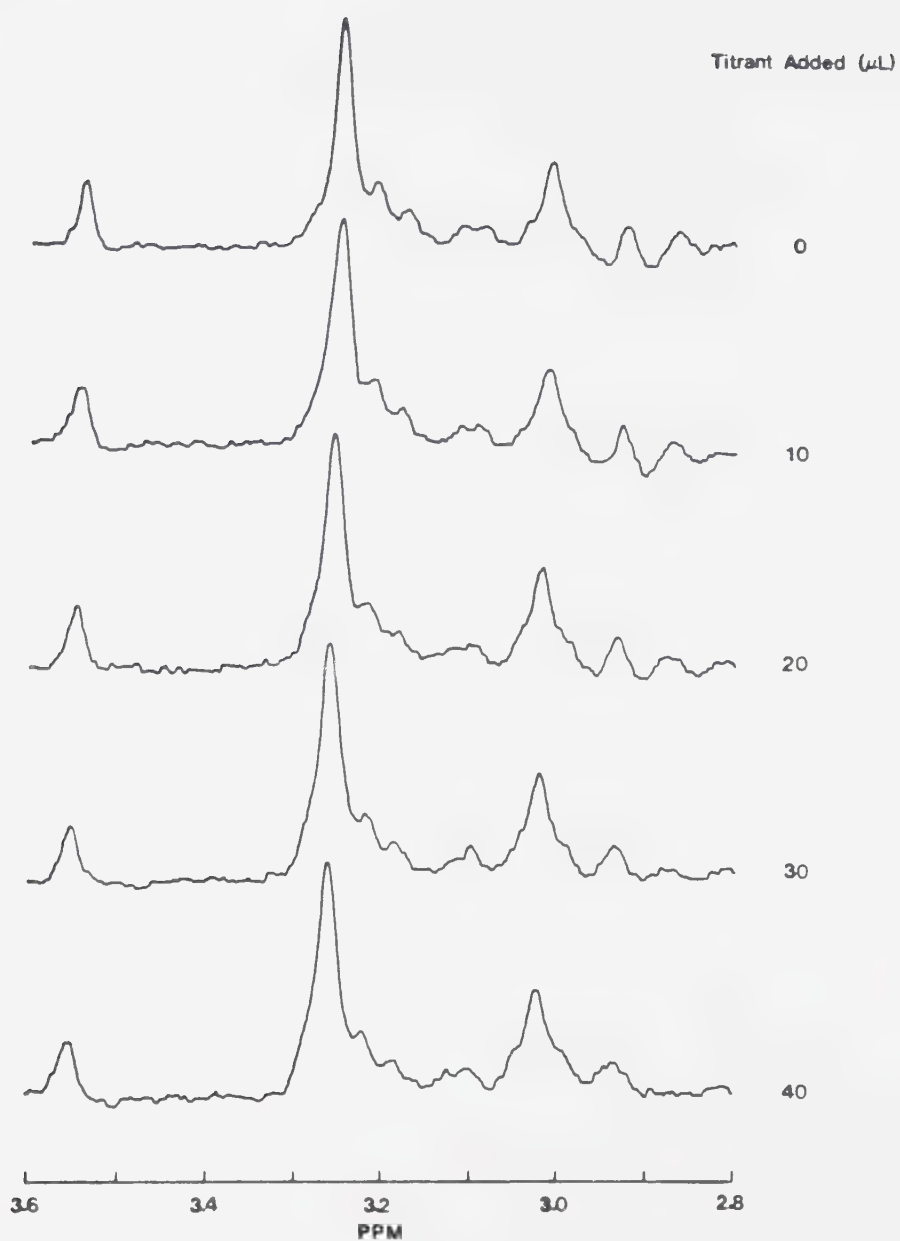


Figure 77. A series of spin-echo spectra ($\tau_2 = 0.04$ second) obtained as increments of t-BHP solution were added to a sample of intact erythrocytes.

points of the titrations (5 to 10 μ L of t-BHP added) of whole red blood cells (WRBC) which was not observed in the titrations of washed HRBC. This is illustrated in the titration curve for the results of Figure 77 which is depicted in Figure 78. This plateau was assumed to be due to NADPH and residual glucose which was not washed out of the whole cells causing the reduction of the initial amounts of GSSG formed in the titration reaction.

The plateau tends to complicate the determination of the titration volume in samples of whole cells. The intersection of the linear least-squares line derived for the plateau region, during which the concentration of GSH was being held constant despite the addition of t-BHP titrant, with that for the linearly decreasing region, during which the GSH was being actively titrated, was taken as the start of the titration. The volume of titrant added from this point until the end point was reached, as signalled by the intercept on the volume axis of the linearly decreasing line, was used as the titration volume in determining the concentration of GSH in the sample.

The results for the NMR titrations carried out to measure the GSH levels in WRBC for four donors are shown in Table 24. The GSH levels obtained were similar to those obtained for HRBC titrations with an average among

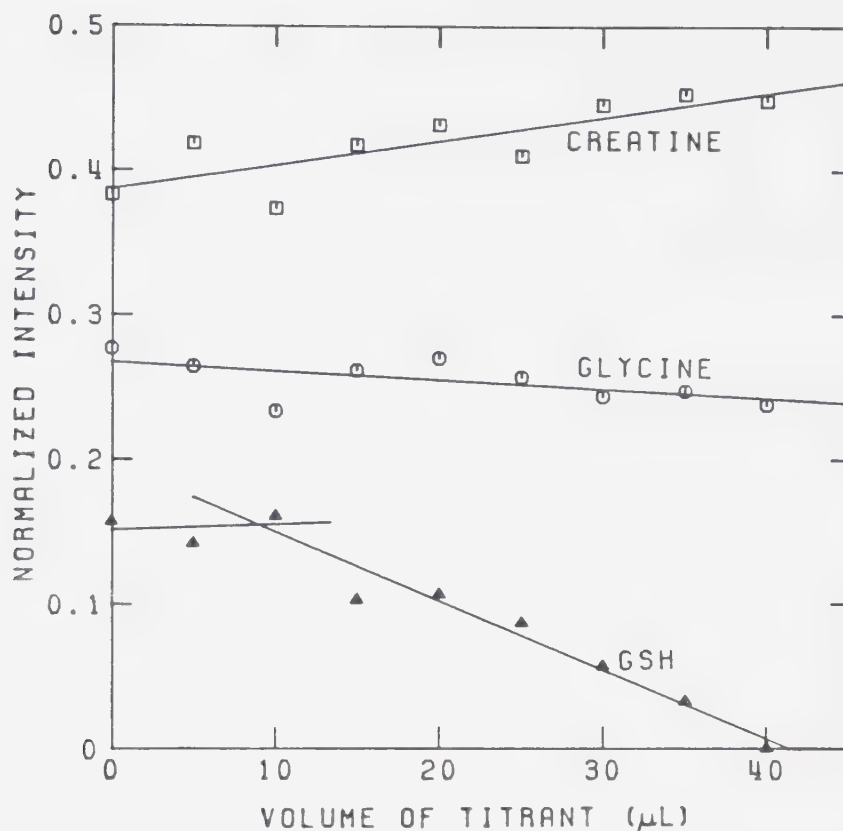


Figure 78. The titration curve for the NMR titration shown in Figure 77. The sum of the intensities of the GSH resonances at 2.88 and 2.91 ppm, normalized against the ergothioneine resonance at 3.25 ppm, is plotted as a function of t-BHP added. Initially, a plateau was observed followed by a linearly decreasing titration curve. Also shown are the normalized glycine and creatine resonances at 3.54 and 3.01 ppm, respectively.

Table 24
Glutathione Levels in Intact Erythrocytes

Donor	[GSH] _{NMR} (mM)		
	Single Values	Average of Replicates	Average for Donor
I	2.15 ^(a)	2.15	2.40
	2.07		
	2.18		
	2.20		
	2.70	2.65	
	2.61		
IX	3.36 ^(b)	--	3.36
X	2.56	2.60	2.60
	2.60		
	2.65		
XI	2.40 ^(c)	2.44	2.44
	2.50		

(a) Replicates performed on a different blood sample than that used for the replicate study in Table 23.

(b) Sample obtained at the same time as the hemolyzed sample for Donor IX in Table 23.

(c) Determination carried out on 0.5 mL packed cells rather than 0.35 mL packed cells plus 0.15 mL saline D₂O.

the donors of 2.71 mM and a standard deviation of 0.45 mM. The same types of variation among donors and between samples taken on different dates from the same donor were noted as before. Donor IX was again found to have a rather high level of GSH as in the HRBC results. Both the WRBC and HRBC samples from Donor IX were taken together on the same date.

The precision among replicates of the same erythrocyte sample was found to be about 2 to 3% and the relative standard deviation of the end point for each titration based on the scatter in the individual points of the titrations was evaluated as 6.8% on average. The somewhat larger relative standard deviation for end point precision with WRBC was due to the smaller titre required since only 0.35 mL of WRBC were generally titrated compared with 0.5 mL of hemolysate. The average absolute precisions of the end points were found to be only slightly greater for whole cells, averaging about 1.7 μ L of titrant for all the titrations carried out on both hemolyzed and whole cells.

E. Reaction of GSSG with Hemoglobin

Thiol-disulfide exchange, as represented by Equations 30 and 31, is a common reaction for disulfides.



Such a reaction involving the GSSG produced in the titration reaction with other thiols in red blood cells would give high results for GSH if the reaction occurred on the time scale of the titration experiment. Hemoglobin (HbSH) is the other major thiol containing molecule in erythrocytes [104]. An experiment was conducted to determine if any disulfide exchange between GSSG and HbSH in the red cells was affecting the titration results. Such a reaction would release GSH which would have to be retitrated giving rise to a high bias in the titration results.



An approximately 5-mL sample of HRBC, which had been titrated with 45 μL of 0.14 M t-BHP to convert all the GSH to GSSG, was dialyzed three times against 10 times this volume of saline D_2O to remove all traces of GSSG and other small molecules. The dialysis was begun immediately after titration with t-BHP and each dialysis was allowed to proceed for 12 hours. Thus, some GSSG was in contact

with the hemoglobin of the HRBC sample for the initial 12 hours. The resulting solution, which contained hemoglobin and small molecules associated with the hemoglobin, was observed to contain a trace of glycine, presumably released from the hemoglobin, in its spin-echo NMR spectrum measured with a τ_2 delay time of 0.04 second (Figure 79A). This glycine was most likely in equilibrium with that reversibly bound by the hemoglobin. No GSH or GSSG could be detected in the spectrum. A total of 30 μL of a 100 mM solution of dithioerythritol (DTE) was added to a 0.5-mL sample of the dialyzed solution in 10- μL increments in order to release any glutathione bound as a mixed disulfide to hemoglobin.



The presence of GSH was ascertained by the appearance of a resonance in the NMR spectrum at 3.76 ppm, corresponding to the methylene protons of the glycine residue of GSH (Figure 79B). No further changes were observed in the resonance for the GSH glycine residue after 20 μL of DTE solution had been added. The GSH was presumably released from the hemoglobin by disulfide exchange with the added DTE as indicated in Equation 33. A control sample of 0.5

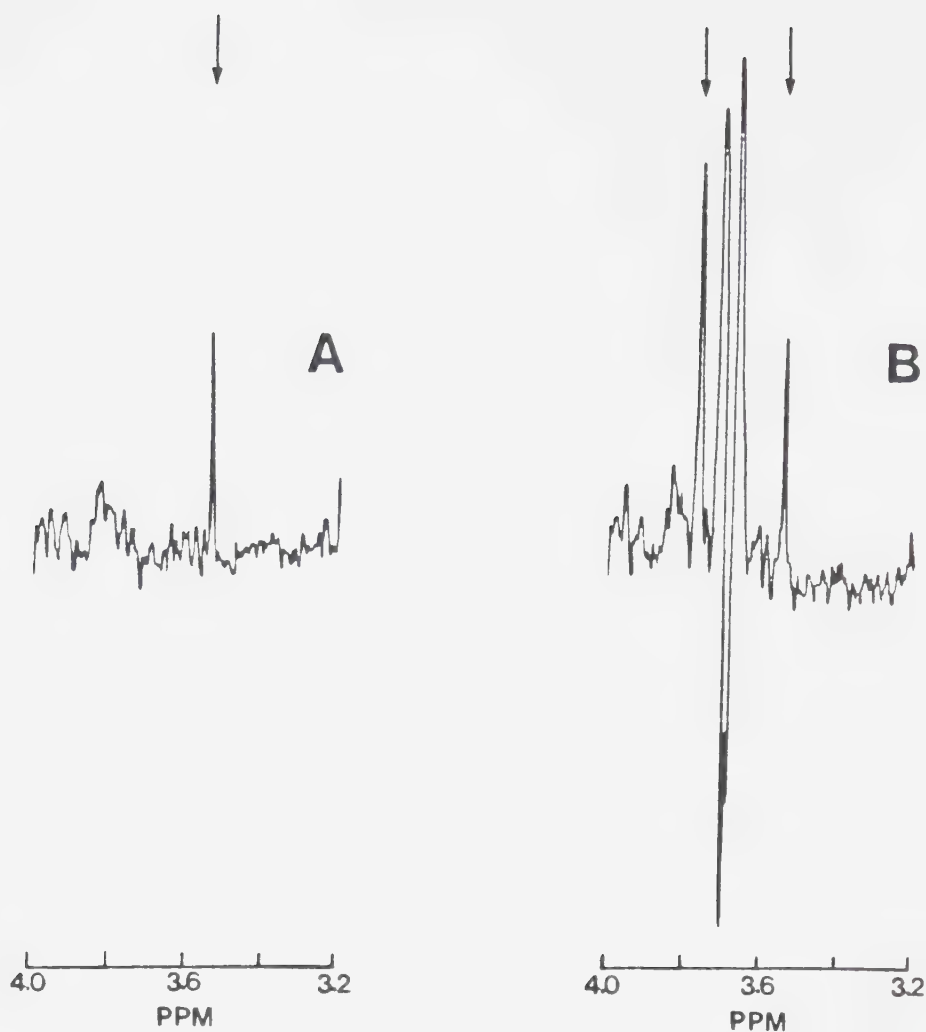


Figure 79. 360 MHz spin-echo NMR spectra ($\tau_2 = 0.04$ second) of a sample of hemolyzed erythrocytes which had been dialyzed to remove small molecules following the titration of the GSH with t-BHP. (A) is a portion of the spectrum showing a residual glycine resonance at 3.54 ppm. (B) is the same sample after the addition of DTE to release GSH (3.76 ppm) bound to hemoglobin as a disulfide.

mL of untitrated HRBC, dialyzed in the same manner as the titrated sample and treated similarly with DTE, released only a trace of GSH. The amount of glutathione bound by the hemoglobin due to disulfide exchange with GSSG in the titrated sample was determined by the standard addition of microliter amounts of a 100 mM solution of GSH using the residual glycine resonance as an internal standard to be roughly 0.25 mM.

An attempt was made to determine the rate at which the disulfide exchange between HbSH and GSSG occurs in order to evaluate its effects on the NMR titration results. 10 μ L of a 50 mM GSSG solution was added to 0.5-mL samples of both dialyzed and nondialyzed HRBC. Spectra were measured immediately after addition and at one-hour intervals for seven hours thereafter. No detectable production of GSH could be determined in either case which would indicate that the HbSH-GSSG disulfide exchange occurs slowly over longer periods of time.

F. Discussion

The NMR procedure for measuring GSH levels in samples of red blood cells by titration with t-BHP appears to work quite well as judged by the results obtained. The overall average value for the GSH concentration in human erythrocytes, including both hemolyzed and whole cell

results, was determined to be 2.76 mM with a standard deviation of 0.35 mM among the donors studied using the NMR titration procedure. The precision among replicates performed on the same sample was generally very good, in the range of 2 to 5%. The literature values for normal GSH levels in human erythrocytes as quoted by Kosower and Kosower [105] are $2.21 \pm 0.10 \text{ mM}$ for oxygenated blood and $2.76 \pm 0.10 \text{ mM}$ for blood containing deoxygenated hemoglobin. Other sources report the level of free GSH in normal red blood cells as $2.47 \pm 0.33 \text{ mM}$ [106], $1.92 \pm 0.09 \text{ mM}$ [107] and $2.24 \pm 0.22 \text{ mM}$ [108]. The results of the NMR titration procedure were significantly higher than the 1.92 to 2.47 mM reported for oxygenated blood cells but agree well with the 2.76 mM quoted for deoxygenated blood.

Approximately 0.55 mM GSH is released into the blood cells from hemoglobin when it undergoes deoxygenation, presumably because of some conformational change [105]. This hemoglobin-bound GSH is a natural reserve which may be utilized by the cells in times of oxidative stress, when GSH is being oxidized in the cells, to maintain the normal level of GSH. In clinical methods of GSH determination, including the DTNB method used in this work, the first step normally carried out is the lysis of the cells and the precipitation of the proteins, notably

hemoglobin, present in the hemolysate. Unless great care is taken to ensure deoxygenation, requiring the complete exclusion of oxygen, the hemoglobin will be in the oxygenated state and any GSH bound or otherwise associated with it will be precipitated along with the protein and lost from the analysis. This was supported by experiments on HRBC from several donors where up to an additional 0.36 mM of GSH was detected by deoxygenating the blood prior to the protein precipitation step. The absence of any oxygen in the hemolysate cannot be assured by the deoxygenation procedure employed. The actual difference in GSH concentration between the oxygenated and deoxygenated hemolysate may be somewhat higher than that measured and more in line with the 0.55 mM reported by Kosower and Kosower [105].

The NMR titration procedure appears to be measuring the total amount of GSH in the red blood cells and not just that which is free in solution. Presumably as the added t-BHP oxidizes the free GSH in the sample the hemoglobin releases some of its reserve of GSH which in turn is titrated until all the hemoglobin-associated GSH is released. This would indicate that the hemoglobin-associated GSH is not tightly bound as it behaves as if it is quite labile. Other evidence supporting this supposition was found in the experiments where DTE was

added to dialyzed HRBC to release any hemoglobin-bound GSH. Only a trace of GSH, which is known to exist naturally as HbSSG [109], was detected. The approximately 0.55 mM hemoglobin-associated GSH had dialyzed away.

The potential problem of air oxidation of GSH in blood samples appears to have been avoided. Air oxidation would be expected to be a particular problem in the case of HRBC since there is no GSH-Rd activity. However, the replicate GSH determinations conducted on a sample from Donor I (see Table 23) indicate essentially no changes with time. The fourth replicate titration was begun approximately 10 hours after the first titration and yet the GSH level found was the same for both. As well, the normalized GSH intensities for the initial spectra in all four of the replicate titrations are approximately the same indicating no changes in the relative ratio of GSH to ergothioneine as would be expected if air oxidation of GSH was occurring.

The variations in GSH level between donors and among the values obtained for one donor on different dates appear to be valid. The same trends were observed for both the DTNB results and the NMR titration results on portions analyzed from the same samples. The magnitude of the differences between donors and among samples from the same donor obtained at different times were far greater

than the precision of the measurements as evaluated from replicates performed on the same sample. Portions of the same sample from Donor IX analyzed by the NMR titration procedure gave the same result for both HRBC and WRBC indicating no difference in the GSH level of the hemolysate as compared to the whole cells.

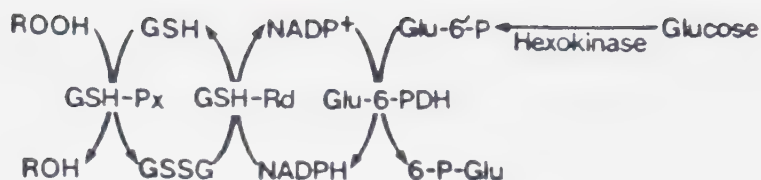
The practice of taking 0.35 mL of whole cells plus 0.15 mL of saline D₂O to make up 0.5 mL in the NMR tubes rather than simply using 0.5 mL of whole cells was based on the premise that better mixing of titrant would be achieved for the more viscous whole cell samples with the addition of some liquid to lower the viscosity. In practice, this was found to be unnecessary as adequate mixing of the titrant was achieved for 0.5 mL of whole cells, used in several of the latter titrations. In fact, the precision of the titrations was improved by using more whole cells since the S/N ratio was enhanced in the spectra collected.

The use of ergothioneine as an internal standard against which the resonances for the cysteine β -CH₂ protons of GSH were normalized was judged satisfactory based on the stability of the normalized glycine and creatine peaks over the course of the titration. In many cases, the normalized glycine and creatine resonances were noted to change in intensity in a somewhat systematic

fashion, however, the changes were much more gradual than for the cysteine β -CH₂ resonances of GSH. Furthermore, these gradual changes could be either positive or negative in direction for different samples. The volume axis intercepts for linear least-squares fits of intensity versus volume of titrant added data sets for glycine and creatine were extremely variable and could not be interpreted as having any meaningful relationship to the amount of titrant added.

The slight trends apparent in the normalized glycine and creatine peaks can be explained as minor changes in the T₂ relaxation times of the protons of either these compounds or ergothioneine. Such T₂ changes would conceivably affect the resonances for the cysteine methylene protons of GSH as well, but the magnitude of these effects was small in comparison to the change due to the titration of the GSH. Based on the precision of the titration results obtained, such effects had a negligible influence on the end points.

The initial plateau found for the first two or three points in the titration of whole cell samples was hypothesized as being due to the reduction of the titrated GSSG back to GSH through the action of GSH-Rd involving NADPH (Equation 28). Even though the red cells were washed several times with saline D₂O to remove glucose, a



small residual amount was most certainly present as well as small quantities of Glu-6'-P and NADPH. Since the cells were still intact, their metabolism was still active and the reduction of GSSG to GSH proceeded until all the available NADPH that could be generated through the metabolic pathways shown above was consumed. The length of the plateau could be taken as a measure of the amount of t-BHP necessary to oxidize all the NADPH potential remaining in the cells.

In the case of saline D₂O washed HRBC titrations, no such plateau was observed. The process of hemolysis is known to disrupt the metabolism of glucose by red blood cells [110]. In particular, it prevents the reduction of NADP⁺ and NAD⁺ to NADPH and NADH. In addition, hemolysis leads to the destruction of both NADP⁺ and NAD⁺ by the enzyme NADase [111]. Actually, it is speculated that the destruction of NADP⁺ may be caused by another similar enzyme NADPase rather than NADase. Thus, the only GSSG reducing potential which is available to HRBC is the small amount of NADPH and NADH present which generally amounts to less than 0.07 mM [112]. Because of this, it is

unnecessary to remove the glucose from red blood cell samples which are hemolyzed prior to analysis using the NMR titration procedure. The titration results for the analysis of HRBC samples would be expected to show that none of the GSSG formed on titration of the hemolysate will be reduced to GSH, causing an absence of the initial plateau seen for the whole cell titrations.

Experimentally, a small plateau is actually observed in the titration of unwashed HRBC which is attributed to a small amount of residual GSSG reducing potential not destroyed by the hemolysis of the cells.

The formation of a mixed disulfide of hemoglobin and glutathione through exchange with GSSG has the potential of causing high results for the measured levels of GSH in erythrocyte samples. This is due to the release of GSH in the exchange (Equation 32) which would have to be retitrated with t-BHP. The appearance of about 0.25 mM of GSH released from hemoglobin upon addition of DTE to a dialyzed sample of titrated HRBC compared with only a trace of GSH released from an untitrated sample similarly dialyzed substantiates the existence of this disulfide exchange reaction. The 0.25 mM of GSH represents about 10% of the total GSH present in the cells and as such could increase the measured concentration of GSH by this amount since for every molecule of HbSSG formed one

molecule of GSH is also produced. Evidence from experiments where GSSG was added to dialyzed and nondialyzed hemolysate and an increase in the GSH concentration sought failed to detect any rise over several hours. This would seem to indicate that the exchange reaction is fairly slow and occurs only upon prolonged standing such as during the dialysis experiment in which it was detected. This would therefore suggest that over the time span of the NMR titration procedure, one to two hours, very little such exchange would take place resulting in a negligible raising of the GSH level measured with this technique. The experimental data for concentrations of GSH support this premise as the levels measured agree well with literature values for GSH in deoxygenated blood [105]. There exist several standard techniques for determining GSH concentrations in red cells in the literature [32,101,102,113-116], some of which are in widespread clinical use. The most commonly employed procedure is a colorimetric assay based on the formation of a yellow anion of DTNB [32,101,102]. This work has utilized the DTNB method in establishing the validity of the NMR titration procedure. It is not to be argued that the NMR procedure is competitive with such clinical methods. In fact, the expense of a high field NMR spectrometer compared with that of a spectrophotometer as

well as the increased analysis time and demanding experimental procedure required with the NMR technique make its routine use prohibitive. However, the NMR technique does provide significantly different information from that of the clinical procedures, giving the total GSH concentration present in the cells both free and hemoglobin-bound as compared with the free GSH concentration generally determined by the DTNB procedure. One of the big advantages of the NMR technique for such determinations is that it is capable of providing this information in a noninvasive manner on intact cells.

The main value of the present work is that it demonstrates for the first time the coupling of the noninvasive character of NMR and the selectivity of an enzymatic reaction for the determination of a compound naturally present in an intact cellular system. While this will never be a routine clinical procedure, it is the type of technique which might be useful in the study of intact cellular systems by NMR, an area of research which is becoming increasingly important. The application of techniques such as described here is limited only by the ingenuity of the investigator in finding and manipulating selective reactions in cells to gain insights into cellular metabolism.

BIBLIOGRAPHY

1. E.L. Hahn, Phys. Rev., 80, 580 (1950).
2. E.M. Purcell, H.C. Torrey and R.V. Pound, Phys. Rev., 69, 37 (1946).
3. F. Bloch, W.W. Hansen and M. Packard, Phys. Rev., 69, 127 (1946).
4. J.W. Cooley and J.W. Tukey, Math. Comput., 19, 297 (1965).
5. F. Bloch, W.W. Hansen and M. Packard, Phys. Rev., 70, 474 (1946).
6. D.L. Rabenstein, Anal. Chem., 50, 1265A (1978).
7. R.L. Vold, J.S. Waugh, M.P. Klein and D.E. Phelps, J. Chem. Phys., 48, 3831 (1968).
8. R.L. Vold, R.R. Vold and H.E. Simon, J. Mag. Res., 11, 283 (1973).
9. L.W. Reeves, in "Dynamic Nuclear Magnetic Resonance Spectroscopy", L.M. Jackman and F.A. Cotton, eds., Academic Press, New York, 1975, p. 88.
10. H.Y. Carr and E.M. Purcell, Phys. Rev., 94, 630 (1954).
11. S. Meiboom and D. Gill, Rev. Sci. Instrum., 29, 688 (1958).

12. D. Shaw, "Fourier Transform NMR Spectroscopy", Elsevier Scientific Publishing Company, Amsterdam, 1976, p. 67.
13. R. Freeman and H.D.W. Hill, in "Dynamic Nuclear Magnetic Resonance Spectroscopy", L.M. Jackman and F.A. Cotton, eds., Academic Press, New York, 1975, p. 131.
14. I.D. Campbell, C.M. Dobson, R.J.P. Williams and P.E. Wright, FEBS Lett., 57, 96 (1975).
15. D.L. Rabenstein and T.T. Nakashima, Anal. Chem., 51, 1465A (1979).
16. F.F. Brown, I.D. Campbell, P.W. Kuchel and D.L. Rabenstein, FEBS Lett., 82, 12 (1977).
17. D.L. Rabenstein and A. Isab, unpublished results.
18. G. Bodenhausen, R. Freeman, R. Niedermeyer and D.L. Turner, J. Mag. Res., 26, 133 (1977).
19. L. Müller, A. Kumar and R.R. Ernst, J. Mag. Res., 25, 383 (1977).
20. R.R. Ernst, J. Chem. Phys., 45, 3845 (1966).
21. M.R. Bendall, D.M. Doddrell and D.T. Pegg, J. Am. Chem. Soc., 103, 4603 (1981).
22. D.W. Brown, T.T. Nakashima and D.L. Rabenstein, J. Mag. Res., 45, 302 (1981).
23. R. Benesch and R.E. Benesch, Biochim. Biophys. Acta, 23, 643 (1957).

24. R.S. Reid, Ph.D. Thesis, University of Alberta, p. 42 (1981).
25. R.E. Benesch and R. Benesch, J. Am. Chem. Soc., 77, 5877 (1955).
26. G. Jung, E. Breitmaier and W. Voelter, Eur. J. Biochem., 24, 438 (1972).
27. N.W. Pirie and K.G. Pinhey, J. Biol. Chem., 84, 321 (1929).
28. R.D. Mair and A.J. Graupner, Anal. Chem., 36, 194 (1964).
29. C.D. Wagner, R.H. Smith and E.D. Peters, Ind. Eng. Chem., Anal. Ed., 19, 976 (1947).
30. W.E. Harris and B. Kratochvil, "An Introduction to Chemical Analysis", Saunders College Publishing, Philadelphia, 1981, p. 261.
31. R.G. Bates, "Determination of pH: Theory and Practice", 2nd edition, John Wiley and Sons, New York, 1973, p. 375.
32. E. Beutler, O. Duron and B.M. Kelly, J. Lab. Clin. Med., 61, 882 (1963).
33. E.S.G. Barron, Arch. Biochem. Biophys., 59, 502 (1955).
34. J.L. Dye and V.A. Nicely, J. Chem. Educ., 48, 443 (1971).
35. W.E. Wentworth, J. Chem. Educ., 42, 96, 162 (1965).

36. F.J. Weigert, M. Jautelat and J.D. Roberts, *Proc. Nat. Acad. Sci. USA*, 60, 1152 (1968).
37. J.R. Blunt and J.B. Stothers, *Org. Mag. Res.*, 9, 439 (1977).
38. H. Eggert and C. Djerassi, *J. Org. Chem.*, 38, 3788 (1973).
39. R.A. Dwek, "Nuclear Magnetic Resonance in Biochemistry: Applications to Enzyme Systems", Clarendon Press, Oxford, 1975, p. 363.
40. H.J. Reich, M. Jautelat, M.T. Messe, F.J. Weigert and J.D. Roberts, *J. Am. Chem. Soc.*, 91, 7445 (1969).
41. L.F. Johnson, 10th Experimental NMR Conference, Pittsburgh, 1969.
42. J.B. Grutzner, *J. Chem. Soc. Chem. Commun.*, 64 (1974).
43. E.W. Hagaman, *Org. Mag. Res.*, 8, 389 (1976).
44. H.-J. Schneider and W. Freitag, *J. Am. Chem. Soc.*, 98, 478 (1976).
45. M.R. Bendall, D.M. Doddrell and D.T. Pegg, *J. Am. Chem. Soc.*, 103, 4603 (1981).
46. J.B. Stothers, "Carbon-13 NMR Spectroscopy", Academic Press, New York, 1972, p. 311.
47. C. LeCocq and J.-H. Lallemand, *J. Chem. Soc. Chem. Commun.*, 150 (1981).

48. S.L. Patt and J.N. Shoolery, *J. Mag. Res.*, 46, 535 (1982).
49. V. Rutar, *J. Mag. Res.*, 48, 155 (1982).
50. D.M. Doddrell and D.T. Pegg, *J. Am. Chem. Soc.*, 102, 6388 (1980).
51. D.P. Burum and R.R. Ernst, *J. Mag. Res.*, 39, 163 (1980).
52. M.R. Bendall, D.T. Pegg and D.M. Doddrell, *J. Mag. Res.*, 45, 8 (1981).
53. G.A. Morris and R. Freeman, *J. Am. Chem. Soc.*, 101, 760 (1979).
54. G.A. Morris and R. Freeman, *J. Am. Chem. Soc.*, 100, 6763 (1978).
55. M.H. Levitt and R. Freeman, *J. Mag. Res.*, 39, 533 (1980).
56. W.P. Aue and R.R. Ernst, *J. Mag. Res.*, 31, 533 (1978).
57. R. Freeman, S.P. Kempell and M.H. Levitt, *J. Mag. Res.*, 35, 447 (1979).
58. S.J. Opella and T.A. Cross, *J. Mag. Res.*, 37, 171 (1980).
59. L. Müller, A. Kumar and R.R. Ernst, *J. Chem. Phys.*, 63, 5490 (1975).
60. P.H. Bolton, *J. Mag. Res.*, 46, 343 (1982).

61. M.R. Bendall, D.T. Pegg, D.M. Doddrell and D.M. Thomas, *J. Mag. Res.*, 46, 43 (1982).
62. G. Bodenhausen, R. Freeman and G.A. Morris, *J. Mag. Res.*, 23, 171 (1976).
63. R. Freeman, G.A. Morris and M.J.T. Robinson, *J. Chem. Soc. Chem. Commun.*, 754 (1976).
64. G.T. Andrews, I.J. Colquhoun, B.R. Doggett, W. McFarlane, B.E. Stacey and M.R. Taylor, *J. Chem. Soc. Chem. Commun.*, 89 (1979).
65. D.G. Gadian, "Nuclear Magnetic Resonance and Its Applications to Living Systems", Oxford University Press, London, 1982, p. 111.
66. Reference 39, p. 26.
67. Reference 65, p. 110.
68. A. Daniels, R.J.P. Williams and P.E. Wright, *Nature*, 261, 321 (1976).
69. L.C. Craig, in "A Laboratory Manual of Analytic Methods of Protein Chemistry Including Polypeptides", P. Alexander and R.J. Block, eds., Vol. 1, Pergamon Press, London, 1960, p. 103.
70. A. Loewenstein and J.D. Roberts, *J. Am. Chem. Soc.*, 82, 2705 (1960).
71. E. Grunwald, A. Loewenstein and S. Meiboom, *J. Chem. Phys.*, 27, 641 (1957).

72. D. Chapman, D.R. Lloyd and R.H. Prince, J. Chem. Soc., 3645 (1963).
73. A.L. Lehninger, "Biochemistry", Worth Publishers, Inc., New York, 1972, p. 90.
74. D.L. Rabenstein and T.L. Sayer, Anal. Chem., 48, 1141 (1976).
75. "Stability Constants of Metal-Ion Complexes", L.G. Sillén and A.E. Martell, compilers, Alden Press, Oxford, 1971, p. 264, 343, 459, 559.
76. M. Kunitz and J.H. Northrop, J. Gen. Physiol., 19, 991 (1936).
77. K. Brew, T.C. Vanaman and R.L. Hill, J. Biol. Chem., 242, 3747 (1967).
78. D.L. Rabenstein, A.A. Isab and D.W. Brown, J. Mag. Res., 41, 361 (1980).
79. H. Behrendt, "Chemistry of Erythrocytes: Clinical Aspects", Thomas Books, Springfield, 1957, p. 56.
80. Reference 73, p. 210.
81. T.M. Shaw and R.H. Elsken, J. Chem. Phys., 18, 1113 (1950).
82. R.B. Moon and J.H. Richards, J. Biol. Chem., 248, 7276 (1973).
83. M.J. Dawson, D.G. Gadian and D.R. Wilkie, J. Physiol., 267, 703 (1977).

84. M.L. Martin, J.-J. Delpuech and G.J. Martin,
"Practical NMR Spectroscopy", Heyden and Sons,
Philadelphia, 1980, p. 364.
85. J.P. Franke and R.A. deZeeuw, Anal. Chem., 50, 1374
(1974).
86. B.W.H. Saxberg and B.R. Kowalski, Anal. Chem., 51,
1031 (1979).
87. R. Klein and C. Hach, Amer. Lab., 9(7), 21 (1977).
88. K.M. Brindle, F.F. Brown, I.D. Campbell, C.
Grathwohl and P.W. Kuchel, Biochem. J., 180, 37
(1979).
89. Reference 79, p. 25.
90. I.N. Kugelmass, "Biochemistry of Blood in Health and
Disease", Thomas Books, Springfield, 1959, p. 57.
91. A.A. Voetman, J.A. Loos and D. Roos, Blood, 55, 741
(1980).
92. S.K. Srivastava and E. Beutler, Anal. Biochem., 25,
70 (1968).
93. J.T. Rotruck, A.L. Pope, H.E. Ganther, A.B. Swanson,
D.G. Hafeman and W.G. Hoekstra, Science, 179, 588
(1973).
94. G.C. Mills, J. Biol. Chem., 229, 189 (1957).
95. G.C. Mills, J. Biol. Chem., 234, 502 (1959).
96. C. Little and P.J. O'Brien, Biochem. Biophys. Res.
Commun., 31, 145 (1968).

97. L. Flohé, G. Loschen, W.A. Günzler and E. Eicheie, Hoppe Seyler's Z. Physiol. Chem., 353, 987 (1972).
98. L. Flohé and W.A. Günzler, in "Glutathione", L. Flohé, H.C. Benohr, H. Sies, H.D. Waller and A. Wendel, eds., Academic Press, New York, 1974, p. 133.
99. T.W. Rall and A.L. Lehninger, J. Biol. Chem., 194, 119 (1952).
100. B. Chance, H. Sies and A. Boveris, Physiolog. Rev., 59, 527 (1979).
101. G.L. Ellman, Arch. Biochem. Biophys., 82, 70 (1959).
102. E. Beutler, "Red Cell Metabolism - A Manual of Biochemical Methods", 2nd edition, Grune and Stratton, New York, 1975, p. 112.
103. P.C. Jocelyn, "Biochemistry of the SH Group", Academic Press, New York, 1972, p. 121.
104. Reference 103, p. 240.
105. N.S. Kosower and E.M. Kosower, in "Glutathione: Metabolism and Function", I.M. Arias and W.B. Jackoby, eds., Raven Press, New York, 1976, p. 159.
106. D.L. Rabenstein and R. Saetre, Clin. Chem., 24, 1140 (1978).
107. J.C. Banford, D.H. Brown, A.A. McConnell, C.J. McNeil, W.E. Smith, R.A. Hazelton and R.D. Sturrock, Analyst, 107, 195 (1982).

108. F.A. Ibbott, in "Clinical Chemistry: Principles and Techniques", 2nd edition, R.J. Henry, D.C. Cannon and J.W. Winkelman, eds., Harper and Row, Hagerstown, 1974, p. 618.
109. T.H.J. Huisman and A.M. Dozy, J. Lab. Clin. Med., 60, 302 (1962).
110. J. Runnström and L. Michaelis, J. Gen. Physiol., 18, 717 (1935).
111. G.J. Brewer, in "The Red Blood Cell", 2nd edition, D.M. Surgenor, ed., Vol. 1, Academic Press, New York, 1974, p. 408.
112. R.B. Pennell, in "The Red Blood Cell", 2nd edition, D.M. Surgenor, ed., Vol. 1, Academic Press, New York, 1974, p. 127.
113. W.E. Knox, in "The Enzymes", P.D. Boyer, H. Lardy and K. Myrbäck, eds., Vol. 2, Academic Press, New York, 1960, p. 253.
114. L. Lack and M. Smith, Anal. Biochem., 8, 217 (1964).
115. P. Klein and E. Robbins, J. Cell Biol., 46, 165 (1970).
116. M. Koivusalo and L. Uotila, Anal. Biochem., 59, 34 (1974).

B30391